SPRAY DRIER SIMULATION AND AIR FLOW PATTERN STUDIES

BY

SANJEEV SHARMA

DOCTOR OF PHILOSOPHY

DEPARTMENT OF CHEMICAL ENGINEERING

THE UNIVERSITY OF ASTON IN BIRMINGHAM

APRIL 1990

The University of Aston in Birmingham

SPRAY DRIER SIMULATION AND AIR FLOW PATTERN STUDIES

By

SANJEEV SHARMA

Doctor of Philosophy 1990

SUMMARY

The literature pertaining to the key stages of spray drying has been reviewed in the context of the mathematical modelling of drier performance. A critical review is also presented of previous spray drying models.

A new mathematical model has been developed for prediction of spray drier performance. This is applicable to slurries of rigid, porous crust-forming materials to predict trajectories and drying profiles for droplets with a distribution of sizes sprayed from a centrifugal pressure nozzle. The model has been validated by comparing model predictions to experimental data from a pilot-scale counter-current drier and from a full-scale co-current drier. For the latter, the computed product moisture content was within 2%, and the computed air exit temperature within 10°C of experimental data.

Air flow patterns have been investigated in a 1.2m diameter transparent counter-current spray tower by flow visualisation. Smoke was introduced into various zones within the tower to trace the direction, and gauge the intensity, of the air flow. By means of a set of variable-angle air inlet nozzles, a variety of air entry configurations was investigated. The existence of a core of high rotational and axial velocity channelling up the axis of the tower was confirmed. The stability of flow within the core was found to be strongly dependent upon the air entry arrangement.

A probe was developed for the measurement of air temperature and humidity profiles. This was employed for studying evaporation of pure water drops in a 1.2m diameter pilot-scale counter-current drier. A rapid approach to the exit air properties was detected within a 1m distance from the air entry ports. Measured radial profiles were found to be virtually flat but, from the axial profiles, the existence of plug-flow, well-mixed-flow and some degree of air short-circuiting can be inferred.

The model and conclusions should assist in the improved design and optimum operation of industrial spray driers.

Key words: Spray Drying, Mathematical Modelling, Simulation, Air Flow Patterns.

Dedication

To my family, especially my Parents for continual encouragement, and my wife Priti for invaluable support and inspiration.

Acknowledgements

The Author would like to express his gratitude to the following people :

Dr C.J. Mumford for his valued guidance throughout the course of this research programme.

Mrs W. Overton for her patience and expertise in the transcription of this thesis.

Mr C. Sudlow for his valued assistance with the graphics.

Procter & Gamble Limited for supporting the research into air flow patterns and kindly giving permission for its publication.

Mr G Bains for his assistance with the operation of the transparent spray tower described in Section 7.1.

Contents

List of Figures

List of Plates

List of Tables

Chapter 1

Introduction

Spray drying involves the transformation of a feed which can be a solution, slurry or paste, into dried particulate form in a single continuous drying process. This is achieved by spraying the feed as fine droplets into a hot drying medium, normally air.

Spray drying has found extensive applications in a wide variety of industries ranging from the delicate processing conditions required for food and pharmaceutical manufacture to the high tonnages associated with the manufacture of bulk chemicals and detergent powders.

The spray drying operation essentially consists of four inter-related process stages. These are:

1. Atomisation of the liquid feed into a spray.
2. Spray-air contact (the essential features being droplet motion and the air-flow pattern within the drier).
3. Drying of the spray.
4. Separation of dried product from air

One of the most important reasons for the application of spray drying is the control it provides over dried product form. In many cases the product is heat-sensitive and expensive, and quality, in terms of physical and other characteristics, predominates over thermal efficiency considerations. The spray drying process has, in fact, been developed to such a fine art that drier designs are available for a variety of powder forms e.g. dust-free; agglomerated; low or high bulk density (typically in the range 0.5 - 0.6 g/cm^3). Even

if the spray drier cannot achieve the powder specification alone, it can be combined with other drying techniques such as fluid-bed drying in two-stage processes.

Now the properties of a spray-dried material are a function of the feed condition, the atomiser type, the operating conditions of the drier and the residence times of the droplets. The last factor is determined by their trajectories. Hence the prediction of the paths taken by droplets following release from an atomiser is of considerable importance in the design of a spray drier and in the optimisation of performance. The trajectory of a droplet determines its residence time and hence the extent of drying. In addition, a knowledge of droplet motion can facilitate the prediction of wall and/or inter-drop impingement which are critical considerations in drier design and operation. For example, a drop which impinges on the wall before it has been dried sufficiently to form a crust which does not rupture on impact, may contribute to undesirable wall build-up; this may create a fire hazard or if over-heated material is displaced, result in off-specification product. Similarly inter-drop impingement in a multi-nozzle drier may result in uncontrolled agglomeration and a greater spread in dried particle size distribution.

Within a spray there is, of-course, a distribution of drop sizes (e.g. in the range 20 to 500 microns), so that a wide spectrum of trajectories will be involved. Combined with interactions with the prevalent air-flow pattern, this creates a complex spray-air contact situation, making spray drier design and performance optimisation an arduous task. In this respect, the objectives of this study were:

(i) To develop a mathematical model for the prediction of the trajectories of various-sized droplets sprayed from a pressure nozzle atomiser, and the dryness of the droplets during their travel.

(ii) To validate the mathematical model by comparing model predictions to experimental data.

(iii) To investigate the air-flow patterns in counter-current drying via smoke visualisation studies and by the measurement of air temperature and humidity profiles in a pilot scale drier.

(iv) To carry out a preliminary study on the phenomena of in-spray droplet agglomeration in counter-current drying.

In combination, the above objectives should lead to operational improvements in spray drying and also facilitate efficient drier design.

In the development of any theoretical or empirical analysis of spray drying, a fundamental knowledge of the principal process stages is a necessity. Hence in Chapters 2, 3 and 4, the literature pertaining to the key features of spray drying, namely (a) atomisation, (b) droplet motion and air-flow patterns, and (c) drying of the spray, is reviewed. A critical review of past spray drying mathematical models is presented in Chapter 5.

The model developed in this study, and the experimental investigations are then detailed in Chapters 6 and 7 respectively. The results of the study are presented in Chapter 8 and discussed in Chapter 9. Finally conclusions are given, together with recommendations for further work, in Chapter 10.

The study is believed to present a novel approach to the simulation of the spray drying of slurries, and to the understanding of air flow patterns in counter-current drying. It should therefore be of assistance in the improved design and optimum operation of industrial spray driers.

Chapter 2

Atomisation

The first stage in spray drying involves disintegration of the liquid feed into numerous individual droplets and their dispersion as a spray. This process of atomisation is also employed extensively in other areas of Chemical Engineering e.g. in liquid burners, humidifiers and scrubbers. In such processes, although the production of a large surface area is often a key requirement, the size range and uniformity of the drops produced by the atomiser may also be critical. For example in spray drying, an ideal atomiser would be one that produced small, discrete drops of identical size. The droplet trajectories, residence times and hence drying rates would then be essentially similar, ensuring a final dried product of uniform characteristics. This scenario would in addition considerably simplify the design of drying equipment and would result in more satisfactory operation.

However, whilst a succession of equal-sized single droplets can be produced[1], homogeneous sprays cannot yet be obtained at industrial feed rates, and droplets with a distribution of sizes, typically in the range 20 to 500μm, always emerge from the atomiser. These droplets then follow a wide spectrum of trajectories and experience a range of residence times within the drying chamber. This can lead to the production of undesirable fines, and to the smaller droplets becoming over-dried with associated thermal degradation. It can also lead to the larger droplets impinging upon the walls of the drying chamber causing build-up, or leaving the drier before the desired level of moisture content has been attained. In the latter case the fact that the average moisture content is within limits may not result in an acceptable product since moisture migration may subsequently cause stickiness, agglomeration or corrosion.

The spray drying process is thus critically dependent on the droplet size distribution, and off-specification product can easily result if the distribution is not controlled. The selection of the correct atomiser to cope with the particular physical properties of a feed, especially viscosity at the applied rate of shear and total solids, is thus critically important. The different atomisation techniques available can be classified in relation to the different forms of energy employed to break-up the bulk liquid. Pressure energy, centrifugal energy and kinetic energy are the commonly employed forms. Less common are atomisers employing sonic or vibrational energy although, provided limitations on throughput can be overcome, their use may become more widespread in the future. A classification of liquid atomisers used in spray drying is shown in Table 2.1.

The principal types are

(i) Rotary atomisers which feature high velocity discharge of liquid from the edge of rotating wheel or disc;

(ii) Pressure nozzles which feature the discharge of liquid under pressure through an orifice;

(iii) Pneumatic, or twin-fluid nozzles which feature break-up of liquid on impact with high velocity air or other gas; and

(iv) Sonic nozzles which feature break-up of fluid through sonic excitation. These will not be discussed further in view of their current limited application in spray drying[2].

Before the different atomiser types are described in detail, the fundamental mechanisms which bring about disintegration of a liquid feed are outlined below.

2.1 THE MECHANISMS OF DROPLET ATOMISATION.

The fundamental principle of disintegration of a liquid consists of increasing its surface area until it becomes unstable and disintegrates. In practice a rod, or thread, of liquid is first formed which then proceeds to break down into droplets. The process by which these droplets are produced depends upon:

(a) The nature of flow in the atomiser, i.e. whether it is laminar or turbulent.

(b) The type of energy employed in the atomiser, i.e. rotary, pressure or pneumatic. (Sonic atomisers are not considered here).

(c) The physical properties of the liquid, and

(d) The physical properties of the ambient atmosphere.

However, the fundamental mechanism of the break-down of unstable threads of liquid into rows of drops is independent of the above factors and conforms to the classical theory of Rayleigh[3]. This theory states that a free column of liquid becomes unstable when its length is greater than its circumference, and that for a non-viscous liquid, the wavelength of the disturbance which will grow most rapidly in amplitude is 4.5 times the diameter. A uniform thread will break down into a series of drops of uniform diameter, each separated by one or more satellite drops. However, because of the irregular character of the atomisation process, non-uniform threads are produced which result in a wide range of droplet sizes.

For spray sheets three modes of disintegration have been established[4]. These are termed

(a) Rim disintegration

(b) Perforated sheet disintegration and

(c) Wave disintegration.

Each of these modes is explained below.

Table 2.1 *Classification of Atomiser Types*

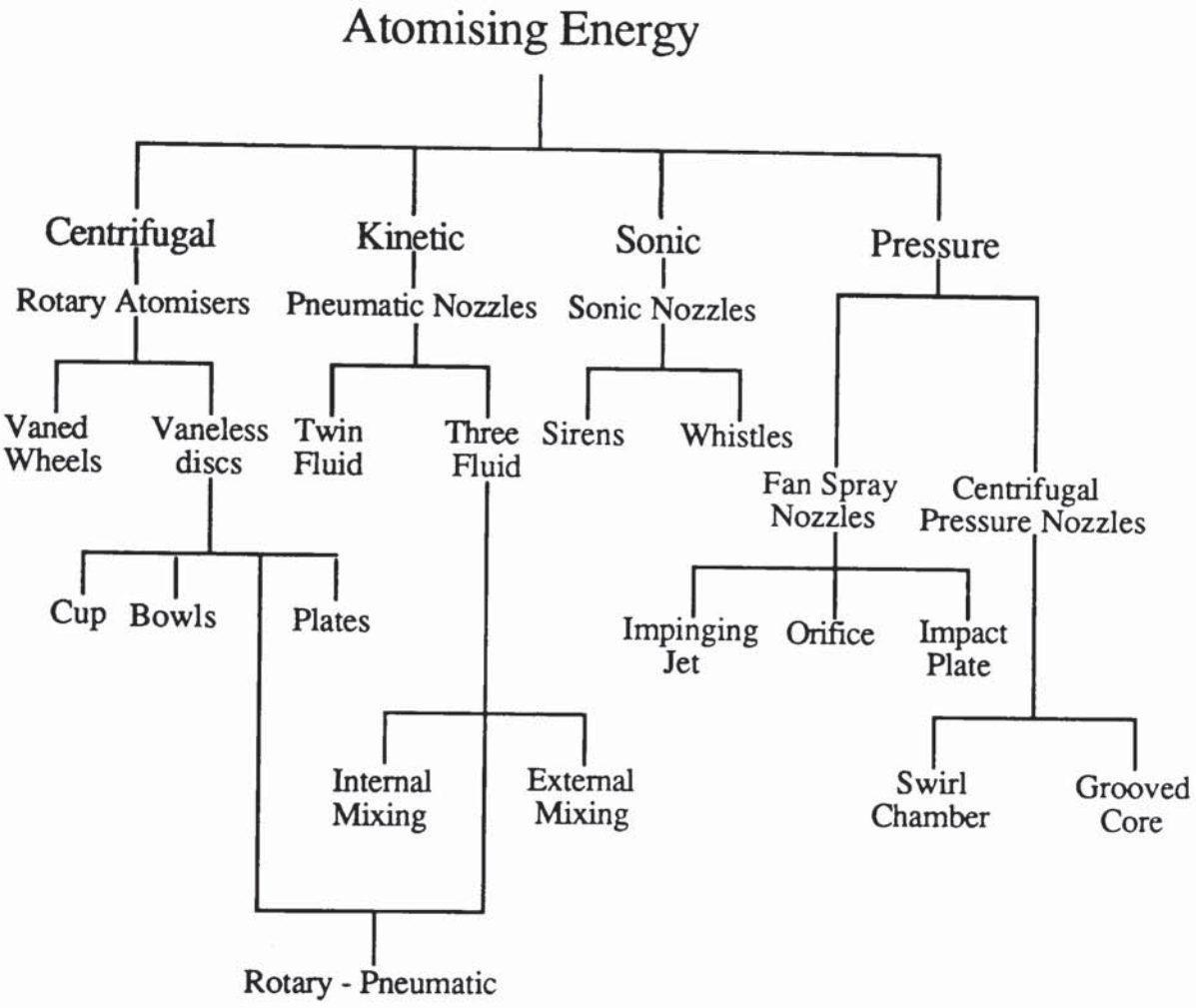

(a) Rim Disintegration

Because of surface tension, the free edge of any sheet contracts into a thick rim and rim disintegration occurs as it breaks up by instabilities analogous to those of free jets. In the case of a fan spray sheet, liquid threads pulled out from the rim during contraction, rapidly disintegrate into a stream of drops. For a spinning disc or cup, the free edge of liquid formed at the rim can be controlled by the liquid flowrates together with rotational speed. At very low flowrates discrete drops are formed producing a near mono-disperse spray, whilst at higher flow rates long jets are formed which break down into a string of drops of much smaller size. With further increase of flowrate a sheet is formed which

extends from the edge until a position of equilibrium is formed. Threads are formed irregularly resulting in a wide spectrum of drop sizes.

(b) Perforated Sheet Disintegration

In perforated sheet disintegration, small holes appear in the sheet as it advances into the atmosphere. These holes rapidly grow in size until the thickening rims of adjacent holes coalesce to form threads of varying diameter, which subsequently break down into drops.

(c) Wave Disintegration

Disintegration can also occur through the superimposition of a wave motion on the sheet. Sheets of liquid corresponding to half or full wave lengths of liquid are torn off and tend to draw up under the action of surface tension, but may suffer disintegration by air action or liquid turbulence before a regular network of threads can be formed.

Which of these mechanisms predominates in the disintegration of a liquid sheet, depends upon the ambient atmosphere and on the liquid physical properties as described below.

Effect of Ambient Atmosphere on Sheet-Disintegration

The following generalisations apply to the influence of ambient condition on sheet disintegration.

(i) Under atmospheric pressure, and for spraying at high, turbulent, flow rates, the main cause of sheet instability is aerodynamic forces acting on the interface, causing exponentially propagating waves to be imposed on the sheet i.e. wave disintegration.

(ii) Above an ambient temperature of 300°C, it has been found that the disintegration occurs by a combination of waves and perforations, the

contribution of the latter predominating with increasing temperature [5]. Such high temperatures can occur in the vicinity of the nozzle in a co-current drier.

(iii) For subatmospheric pressures sheet disintegration will result through a perforated sheet mechanism [6, 7].

Effect of Liquid Properties on Sheet-Disintegration.

The influence of liquid properties on sheet- disintegration may be summarised as,

(i) Liquid viscosity resists drop formation in all stages; an increase in viscosity will therefore prolong the sheet.

(ii) Surface tension will resist deformation of the sheet but will assist drop formation after the sheet has broken down.

(iii) Density has little influence on atomisation, and for the small range encountered in spray drying its effect may be ignored.

Of particular interest in spray drying are the atomisation characteristics of solutions and slurries. It was found [7] that in low concentration, e.g. 0.05%, wettable particles had no influence on the mode of the sheet disintegration. However when the concentration was increased to form a slurry, by adding up to 20% clay to water, the process of disintegration changed markedly. For the lower concentration, wave disintegration occurred, but for the slurry, the sheet disintegrated closer to the nozzle by tears and holes i.e. perforated sheet disintegration. This was accompanied by the formation of larger droplets.

The general theory on disintegration mechanisms given above is applicable to any sheet or ligament of liquid, regardless of how it is formed, i.e. it is atomiser independent. The exact mode of disintegration will of course be a function of the particular liquid and air properties and the atomiser type.

The characteristics of the principal types of atomiser employed in spray drying are described in the next section. As this study is specifically concerned with spray drying with pressure nozzle atomisation, this review will be biased in this direction.

2.2 CENTRIFUGAL PRESSURE NOZZLE ATOMISATION

In pressure nozzle atomisation, the liquid feed is forced under pressure through an orifice, transposing pressure energy within the liquid bulk into kinetic energy of thin moving liquid sheets [8, 9]. Liquid sheets range in thickness from 1 to 5 μm [10] and rapidly disintegrate under the influences of the liquid physical properties and frictional effects with the surrounding air. Conversion of pressure energy occurs in such a way that the liquid acquires a rotary motion upstream of the orifice. This arrangement permits greater energy transfer, leading to improved atomisation.

Methods of imparting rotary motion within a pressure nozzle include the use of

(a) Inclined slotted inserts,

(b) Swirl inserts,

(c) Spiral grooved inserts, and,

(d) Tangential flow.

The three types of insert are shown in Figure 2.1

The rotary motion inside a pressure nozzle also results in a conical sheet issuing from the orifice. The velocity of the sheet will be constant and the thickness of the sheet will diminish as the core develops. For any given pressure there is a maximum sheet length. Increase in pressure reduces the sheet length. As discussed earlier, increase in viscosity acts to lengthen the sheet, whereas increase in surface tension has the opposite effect; increase in sheet velocity and increased turbulence caused by frictional effects with

the air reduces sheet length. A few correlations for prediction of sheet length have been published [11, 12, 13] but commercial-sized atomisers operating in spray driers hardly exhibit any visible sheet due to the immense turbulence associated with the process.

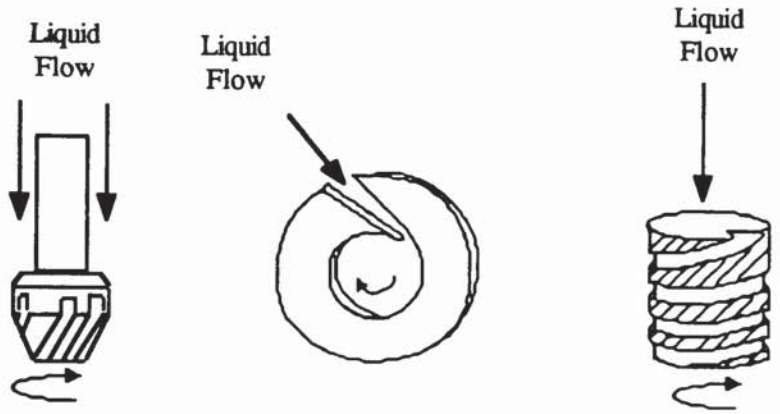

Figure 2.1 *Inserts for Centrifugal Pressure Nozzles*

2.2.1 Spray Patterns from Centrifugal Pressure Nozzles

The conical spray that emerges from the orifice is usually hollow and symmetrical with respect to the axis of the nozzle; the spray droplets are concentrated entirely in the periphery of the cone, leaving the centre virtually free of spray. However, solid cone sprays can be formed if some of the liquid is allowed to flow axially through the orifice; the whole volume of the spray cone is then filled with an almost evenly-distributed mass of droplets. The droplet population spread for solid and hollow cone nozzles is shown in Figure 2.2. In low throughput nozzles, up to about 15 cm^3/s, the hollow cone characteristics rapidly merge to the full cone state as drops are entrained by air induced into the spray cone [1].

Hollow-cone sprays are characterised by an air core at the centre of the orifice formed as a result of liquid rotation within the nozzle. If the air core is not stable, hunting may occur and the conical sheet rapidly opens and closes. Under these conditions the

spray characteristics are again effectively those of a full cone spray. The form of the conical sheet depends upon the working pressure and passes through a number of stages as the pressure is increased. At low pressures the liquid first forms a bubble. With increase in pressure the bubble opens to form a hollow cone with a curved surface. As the pressure is further increased the curved surface straightens and the region of disintegration moves towards the orifice. The pressures at which each stage occurs depends upon nozzle design and liquid properties, but are generally in the range 10 - 50 psi.

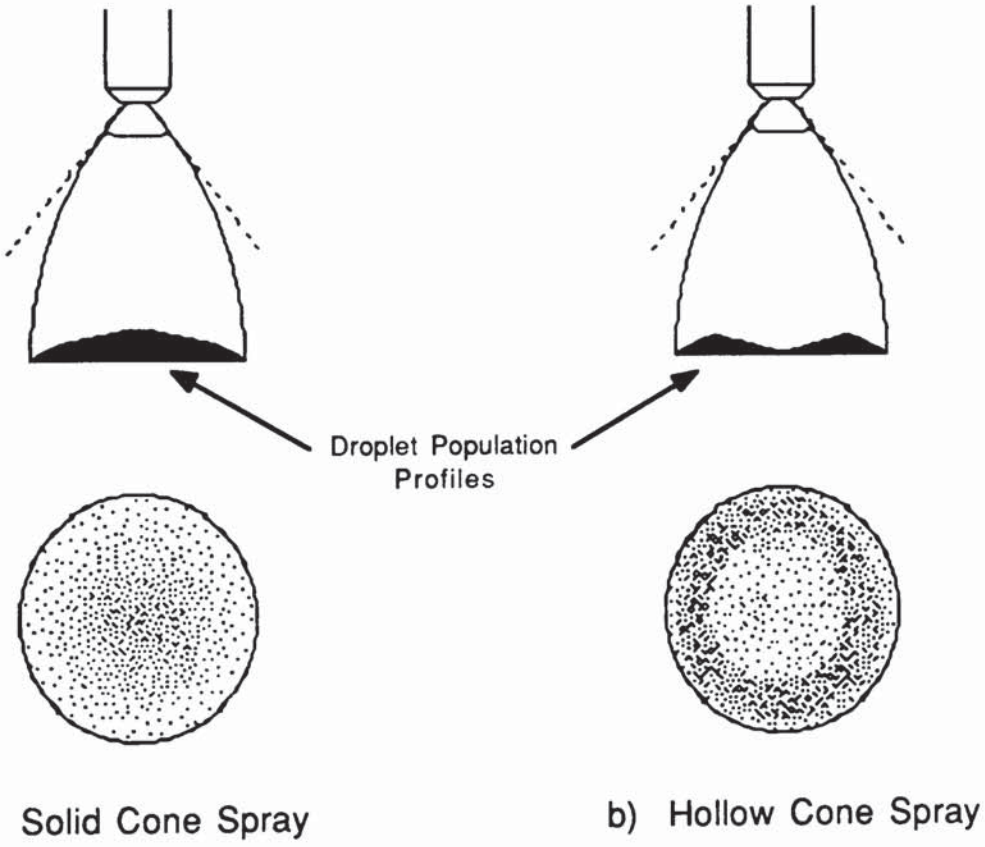

Figure 2.2 *Droplet Population in Solid and Hollow Cone Sprays*

Nozzles producing solid and hollow cones can be used in any of the co-current, counter-current or mixed-flow driers described in Chapter 3. Nozzles forming hollow cone sprays are particularly suited for operation in co-current driers, since the majority of the droplets are dispersed in the periphery of the cone and therefore readily contacted with

the drying air. Solid cone sprays are not as effective in co-current driers because the droplet population density is greatest at the core of the cone; hence these droplets are subjected to an atmosphere of high humidity for an extended period. i.e. a longer time is required for the spray dispersion to expose the central drops to the drying air.

Solid cone sprays are more suited for counter-current spray drier operation as the full face of the cone is then exposed to the drying air. In addition, because the larger droplets in the centre of the cone will be moving mainly in the axial direction, the chance of a semi-wet droplet hitting the walls of the drier will be reduced. Furthermore, although they possess a radial velocity component, the smaller droplets at the periphery of the cone would have sufficient contact with the drying air to reach an adequate degree of dryness before arrival at the wall. If hollow cone sprays are applied to counter-current operation, greater wall deposition can be expected. This will occur because of the high population density at the extremity of the cone, and the fact that the droplets possess radial velocity results in the need for increased drying time if all drops are to be sufficiently dry before impaction on the wall.

2.2.2 Fluid Flow from Pressure Nozzles.

The flow of liquid from the orifice of a centrifugal pressure nozzle is shown schematically in Figure 2.3. Once the liquid leaves the confines of the orifice, it ceases to spin or swirl and the particles of liquid move outward in a straight line with components of velocity, V_z, in the axial and, V_r, in the radial direction only. From basic geometry the liquid leaving the orifice will travel rectilinearly at an angle of $\tan^{-1}(V_z/ V_r)$ to the nozzle axis.

The resultant velocity of the liquid sheet is given by:

$$V = (V_z^2 + V_r^2)^{0.5} \qquad 2.1$$

Now from the conservation of energy:

$$\frac{P_o}{\rho_L} + \frac{(V_o')^2}{2} = \frac{P}{\rho_L} + \frac{V^2}{2} \qquad 2.2$$

where P_o and V_o' are the atomisation pressure and upstream liquid velocity respectively.

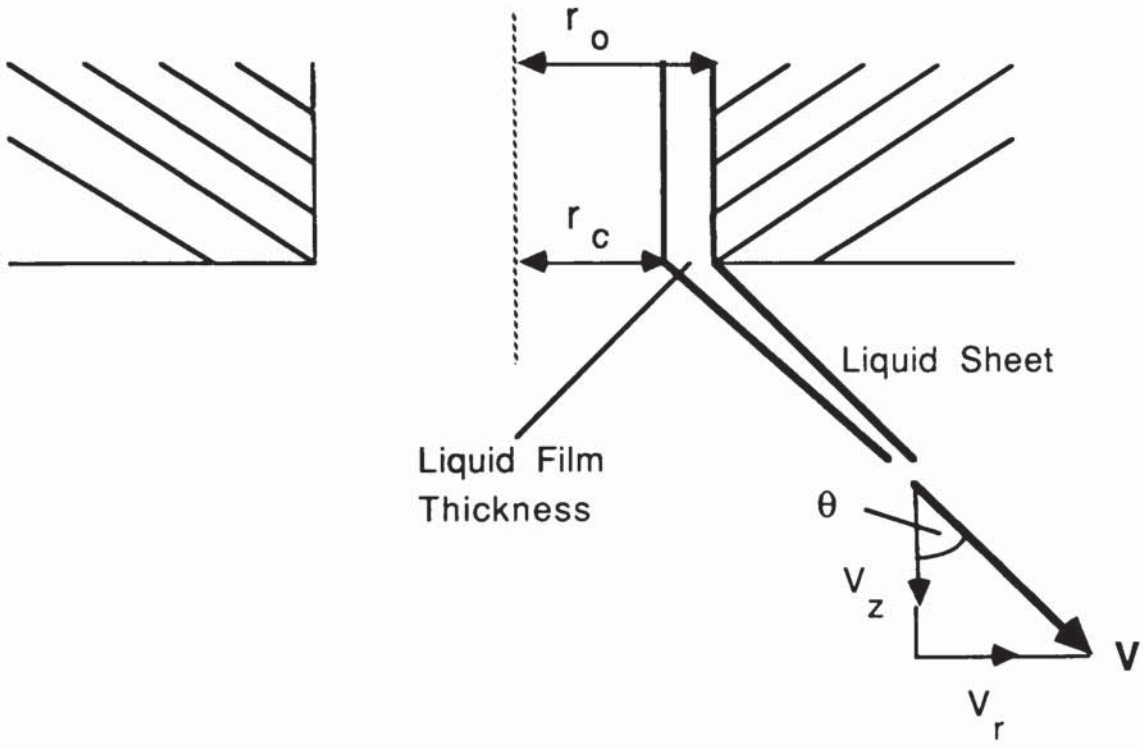

Figure 2.3 *Liquid Flow from a Pressure Nozzle*

Neglecting the upstream velocity:

$$V = \left[\frac{2\,(P_o - P)}{\rho_L}\right]^{0.5} \qquad 2.3$$

However, in reality some of the energy is dissipated in overcoming friction within the nozzle. The velocity is therefore corrected as follows:

$$V = C_v \left[\frac{2\,(P_o - P)}{\rho_L}\right]^{0.5} \qquad 2.4$$

Where C_v is the velocity coefficient.

Now from continuity, the volumetric flowrate of liquid from the nozzle is given by:

$$Q_v = \pi r_o^2 \left[1 - \left(\frac{r_c}{r_o}\right)^2 \right] V_z \qquad 2.5$$

where r_o r_c are the orifice and air core radii respectively.

Also, $$V_z = V\text{Cos}\theta \qquad 2.6$$

Combining equations 2.4, 2.5 and 2.6

$$Q_v = \pi r_o^2 \left(1 - \frac{r_c^2}{r_o^2}\right) C_v \left[2 \frac{(P_o - P)}{\rho_L} \right]^{0.5} \text{Cos}\theta \qquad 2.7$$

or,

$$Q_v = C_d \pi r_o^2 \left(\frac{2\Delta P}{\rho_L}\right)^{0.5} \qquad 2.8$$

where

$$C_d = C_v \left(1 - \frac{r_c^2}{r_o^2}\right) \text{Cos}\theta \qquad 2.9$$

and $$\Delta P = P_o - P$$

The discharge coefficient, C_d, is dependent upon the orifice size and varies with dimensions of each nozzle design. Thus C_d is a constant for a particular liquid and nozzle. From equation 2.8 it follows that a plot of flowrate versus the square root of the total pressure drop is a straight line, the gradient being a measure of $C_d \pi r_o^2 (2/\rho_L)^{0.5}$. It also follows from the same equation that the flowrate is directly proportional to the square root of pressure and varies inversely with square root of liquid density.

Hence,

$$\frac{Q_{v2}}{Q_{v1}} = \left(\frac{P_2}{P_1}\right)^{0.5} = \left(\frac{\rho_{L1}}{\rho_{L2}}\right)^{0.5} \qquad 2.10$$

To describe the atomisation process quantitatively for use in spray drier modelling, the variation of key parameters, with atomisation pressure and nozzle design needs to be

evaluated for the specific liquid feed. The parameters of interest for this study are the air core diameter, for prediction of liquid sheet velocity and thickness, and the cone angle.

(a) Air Core Diameter

Darnell [14] and McIrvine [15] measured air core diameters at the orifice of transparent plastic nozzles under various conditions. Darnell showed that for pressures where the cone- angle was independent of pressure change, the air core diameter was also unaffected by pressure change. The data of McIrvine for the viscosity range 1 to 10 cp suggested that viscosity does not appreciably affect nozzle capacity, cone angle or air core diameter. For higher viscosities the size of the air core decreased with increase in viscosity.

Nelson and Stevens [16] performed dimensionless analysis to correlate the data of Darnell and McIrvine for air core diameter. Based upon the above findings they concluded that the ratio of air core diameter to orifice diameter D_c/D_o was independent of the Reynolds number at the orifice, and a function only of the spray cone angle θ. The latter was in turn dependent only on nozzle dimensions. A plot was thereby presented of D_c/D_o versus θ for θ ranging between 20° and 120°.

(b) Spray Cone Angle

A minimum pressure of approximately 20 psi is required to develop any form of spray angle [17], but once the conical sheet is fully developed the angle θ of the conical sheet is practically independent of the pressure. However away from the orifice, the angle of the spray curtain varies with distance from the nozzle, atomisation pressure, ambient density and flowrate, as a result of air entrainment effects. Viscosity has a pronounced effect in that an increase produces a narrower spray angle. At very high viscosities the spray angle is so reduced that a plug stream of liquid results, and atomisation ceases.

2.2.3 Application of Pressure Nozzles and Industrial Practice

Centrifugal pressure nozzles are used extensively in many industries especially where coarse, free-flowing, spray-dried products of mean particle size 150-300 μm are required. Typical operating pressures range from 100 psi to as high as 7000 psi for products as diverse as milk, coffee, detergents, soaps, ceramics and many inorganic salts. The appeal of pressure nozzle atomisers lies essentially in: (a) their low cost resulting from the relatively simple construction, (b) their ease of removal and replacement, and (c) their simple maintenance. However set against these there are: (a) the unfavourable need for high pressure pumping, (b) the need for effective in-line straining of the feed to avoid orifice clogging, and (c) severe restrictions on the type of material which can be handled without undue nozzle wear. Pressure nozzles are prone to erosion as a result of the high liquid velocities generated at the swirl chamber and the orifice. They are thus unsuitable for abrasive feeds unless special materials of construction, e.g. tungsten carbides, are employed. However the greatest disadvantage of pressure nozzles is probably the fact that atomisation and feed flowrate cannot be controlled independently; the capacity of each nozzle can only be changed by changing the operating pressure or the orifice size, both of which will lead to a change in the spray quality.

Whenever capacity and particle size distribution requirements permit, a single centrally-located nozzle should be used within the drier . This simplifies the operation by ease of its control and ease of nozzle observation. Invariably however, the large capacities demanded by industry will result in the need for multi-nozzle assemblies. In such installations several nozzles are either connected to a ring main around the periphery of the tower or a cluster of several nozzles, connected to a feed pipe, is located centrally at the top of the tower. Both of these arrangements are utilised in conjunction with co-current drying. The ring-main design permits ease of access to the nozzles via the drier wall, thus facilitating nozzle observation, replacement and maintenance. However greater care has to be taken to ensure uniformity of flow to each nozzle, especially if slurries are

being atomised which may have a tendency to settle out inside the ring main. The nozzle cluster assembly results in improved evaporation conditions by locating the nozzle in the centre of the air disperser for optimum spray- air contact. In counter-current drying the ring-main design is employed almost exclusively, thereby allowing a wide spray coverage over the drier cross-section.

Although high capacities are achievable with multi-nozzle operation, there will inevitably be an increase in the concentration of droplets within the drying chamber. As a consequence, spray and droplet impingement is likely to occur resulting in the formation of agglomerates. Such agglomeration is generally undesirable as it will result in a non-uniformly dried product of wide particle size distribution. Hence there is a critical limit to the total number of nozzles that can be used, and to the proximity of adjacent nozzles, if excessive agglomeration is to be avoided. In the drying of detergents, methods which can be employed to prevent excessive agglomeration without sacrificing capacity, include use of single large- orifice-diameter nozzles [18] and multi-stage drying methods [19]. When a single nozzle is employed, an adequately large spray angle will need to be developed in order to avoid excessive spray by- pass of the drying air. In the multi-stage drying method a second set of nozzles is installed at some predetermined level in the drier. This level is selected on the basis that the air temperature around the spray is sufficiently high, and that the droplets from the upper set of nozzles have been dried to an adequate moisture, and hence 'stickiness', level.

Operating Conditions.

The typical range of operating conditions for pressure nozzles is given below [20],

1. Pressure: up to 10,000 psi
2. Capacity: up to 4,500 kg/h through a single nozzle
3. Types of Feed: solutions, suspensions and slurries

4. Feed Viscosity: up to several hundred centipoises depending on the pressure, capacity and orifice size.

2.3 ROTARY ATOMISATION

In rotary atomisation, liquid is fed onto a rotating cup, wheel or disc where it is centrifugally accelerated to a high velocity before being discharged. Since the accelerating force can be independently controlled, this type of atomiser is extremely versatile and can successfully handle a wide range of feed rates with liquids having a wide range of properties. There are a wide variety of existing designs, and these can be classified into three groups

(i) Flat discs,

(ii) Bowls or Saucers, and,

(iii) Vaned discs or Slotted wheels.

For each type, the diameter may vary from 2.5 cm to 46 cm with rotary speeds of up to 60,000 rpm [21].

The extent of atomisation achieved by each of these will depend upon [22]:

(a) the peripheral speed of wheel, cup, or disc,

(b) the rate of liquid feed,

(c) the liquid properties, and

(d) the atomiser design.

Maximum centrifugal energy is imparted to the liquid when it acquires the peripheral speed of the rotating surface prior to discharge. If a flat, smooth disc is used, severe slippage occurs between the liquid and the surface of the disc. Hence the liquid is discharged from the edge of the disc with a much lower velocity than the peripheral speed of the disc. Slip can be prevented in commercial atomisers if radial vanes are used. The liquid is then confined to the surface of the vane and the maximum release velocity is attained at the periphery. Alternatively, slippage can be considerably reduced by increasing friction

between the liquid and the rotating surface. This is commonly achieved by feeding the liquid onto the lower surface of a disc shaped as an inverted plate, bowl or cup, so that as the liquid is forced outwards due to the centrifugal force, it is pressed against the surface of the disc. Both of the above techniques are employed to handle commercial feed rates, with the vaned disc atomiser being employed for fine spray requirements.

2.3.1 Droplet Flow Pattern from Rotary Atomisers

Atomisation occurs when the surface tension and viscous forces acting on the liquid feed are overcome by centrifugal forces. The manner in which droplets are produced from a rotary atomiser depends upon

(a) the viscosity and surface tension of the liquid;

(b) the inertia of the liquid at the periphery of the disc;

(c) frictional effects between the liquid droplets and surrounding air; and

(d) the disc diameter and speed.

Three patterns of drop formation can be distinguished [23]:

(i) At low disc peripheral speed and low feed rates, the liquid viscosity and surface tension control the mechanism of atomisation and sprays are formed by discrete drop formation and release of droplets from the edge of the disc, as shown in Figure 2.4a. The droplets are initially attached by a fine attenuating thread.

(ii) At higher feed rates and disc speeds, e.g.around 700 rpm, the retaining threads grow in thickness and because of the longer time of break- up, form ligaments which subsequently disintegrate into a spray of parent and satellite droplets as shown in Figure 2.4b

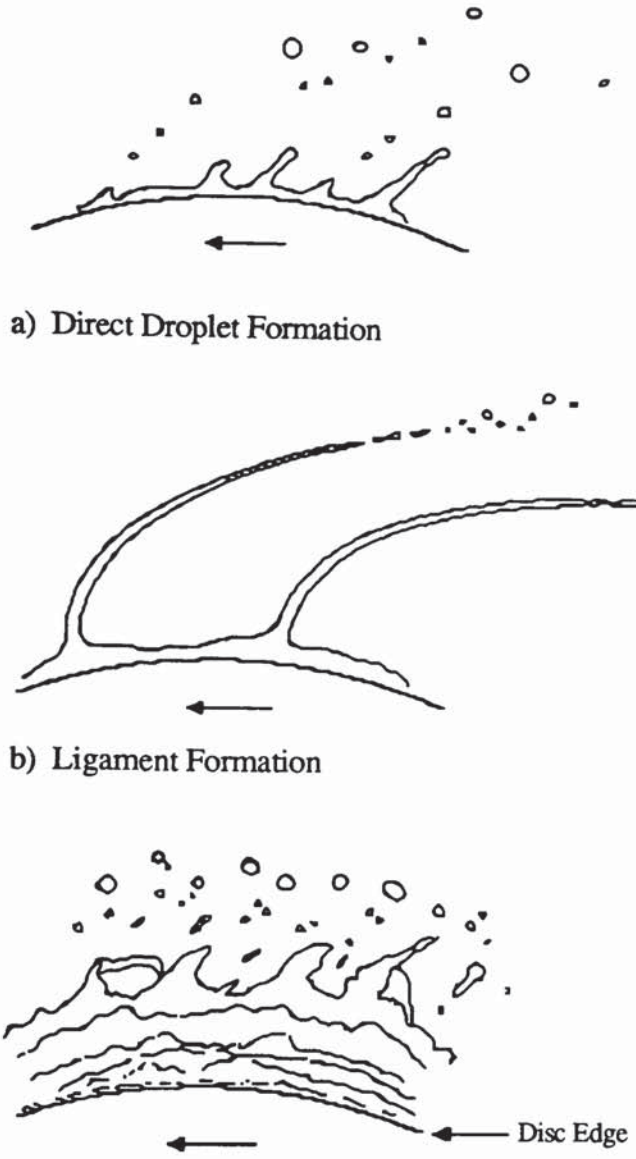

Figure 2.4 *Mechanisms of Drop Formation from Rotary Atomisers*

(iii) With further increase of flowrate and disc speed, to levels typical of commercial atomisers, e.g. around 3,000 rpm, ligaments are unable to carry-away all the liquid and a thin sheet extends around the disc as shown in Figure 2.4c. The mechanism by which the sheet breaks-apart as described in section 2.1, results in the formation of a heterogeneous spray.

This is in contrast to the first two drop formation patterns which can result in a spray of reasonably uniform drop size.

2.3.2 Liquid Flow in Rotary Atomisers.

Liquid fed onto the centre of a rotating surface spreads outwards due to centrifugal forces and simultaneously moves across the surface. Figure 2.5 shows droplet travel from a rotary atomiser. The liquid film on leaving the edge of the atomiser has a radial velocity V_r and tangential velocity V_t giving a resultant V. The angle of release is less than 45°. In fact under normal operating conditions the radial velocity is much less than the tangential velocity and the liquid is discharged almost tangentially from the periphery.

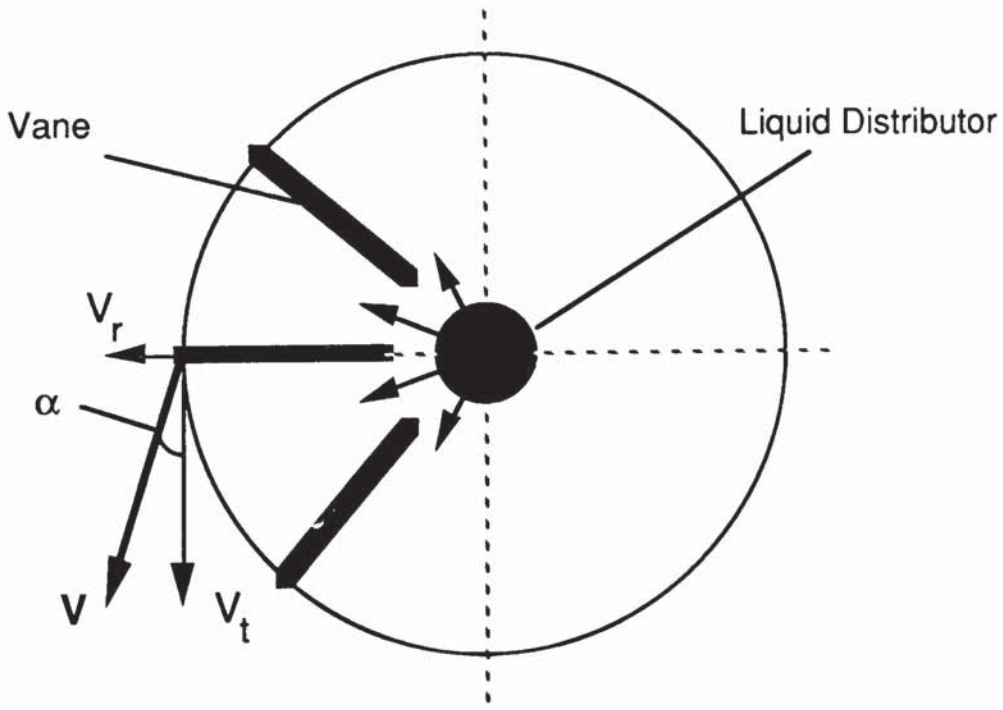

Figure 2.5 *Liquid Flow from a Rotary Atomiser*

Estimation of Radial Discharge Velocity

The radial velocity at the periphery of the disc is given by the relation

$$V_r = 0.0024 \left(\frac{\rho_L N^2 Q_v^2}{\mu_L D_o}\right)^{0.33} \quad \text{for bowls} \qquad 2.11$$

and,

$$V_r = 0.0024 \left(\frac{\rho_L \pi^2 N^2 D_o Q_v^2}{\mu_L b^2 n_v^2}\right)^{0.33} \quad \text{for vaned discs} \qquad 2.12$$

where the symbols are as defined in the Nomenclature.

Tangential Discharge Velocity

On the assumption that no slippage occurs, then the liquid acquires the peripheral velocity of the wheel upon discharge

$$V_t = \pi D_o N \qquad 2.13$$

Resultant Discharge Velocity and Angle

From the tangential and radial components the resultant release velocity is

$$V = (V_t^2 + V_r^2)^{0.5} \qquad 2.14$$

and the angle of liquid release from basic geometry is

$$\alpha = \tan^{-1} \left(\frac{V_r}{V_t}\right) \qquad 2.15$$

2.3.3 Application of Rotary Atomisers.

Applications of atomiser wheels are found in many major industries including ceramics, dairy products, organic chemicals and pharmaceuticals, where they are used to produce droplets of mean size 30 - 120 μm. The main benefits of rotary atomisers [24] are that

(a) they rarely plug;

(b) erosion is seldom serious, and even if it occurs it seldom changes the operating characteristics of the atomiser;

(c) a gravity or low pressure feed can normally be employed, and,

(d) changes in particle size from the atomiser caused by changes in feed-stock characteristics can usually be compensated for by change in disc speed.

However set against these, there are the following disadvantages:

(a) The atomiser disc, wheel or cup as well as the drive mechanism is expensive.

(b) The spray pattern is not suited for counter-current driers or for multi-atomiser units. The latter would result in the need for an extremely large drier diameter.

(c) Rotary atomisers are not well suited to handle viscous feeds.

Operating Conditions

The typical range of operating conditions for rotary atomisers is,

1. Rotary speed: From 500 to 30,000 rpm
2. Disc diameter: From 5 to 25 cm
3. Feed rate: From 0.025 to 7,000 kg/h
4. Types of Feed: All pumpable liquids, solutions, slurries, pastes etc.
5. Feed Viscosity: Up to a few hundred centipoises.

2.4 PNEUMATIC ATOMISERS

Pneumatic or two-fluid atomisation involves the use of a high velocity gas stream to impact the liquid surface. The frictional forces so produced will induce liquid disintegration. The liquid feed and the atomising gas (normally air) are passed separately to the nozzle head where impact and consequently disintegration of liquid takes place. A high relative velocity between the liquid and the atomising gas must be generated so that optimum frictional conditions can be attained. These conditions are achieved by either accelerating the gas to sonic or supersonic velocities prior to impact or by impacting the gas on to unstable thin liquid sheets, formed by rotating the liquid in the nozzle. For low feed rates, rotation of liquid within the nozzle is not completely necessary for atomisation. However it is essential when handling high liquid feed rates.

Various design techniques are available to produce optimum conditions of liquid-air contact. All involve pre-filming and air annulus sizing to attain adequate relative velocity between air and liquid at the nozzle head. The designs are as follows:

(a) Internal mixing: liquid-air contact within the nozzle head.

(b) External mixing: liquid-air contact outside nozzle head.

(c) Three Fluid nozzle: combined internal and external mixing utilising two air flows within nozzle.

(d) Pneumatic Cup atomiser: liquid-air contact at the rim of the rotating nozzle.

More efficient energy transfer is achievable with the internal mixing design than with external mixing. However, the latter enables greater control of atomisation since the air and liquid streams can be independently controlled.

The three-fluid design combines the advantages of both internal and external designs, thus obtaining a high degree of energy transfer together with good control of the spray characteristics. This design provides greater available kinetic energy and is therefore

used in the atomisation of high viscosity liquids, where the advantage of being able to handle difficult liquids offsets the low nozzle efficiencies.

Pneumatic cup atomisers are used for high viscosity liquids. They are capable of producing small mean droplet sizes over a wide range of feed rates. With low viscosity fluids, droplets of a low mean drop size (15-20 microns) are produced with a high degree of homogeneity. The higher the liquid viscosity, the larger the mean droplet size and the lower the homogeneity of the spray.

Even the smallest droplets produced from a pneumatic atomiser can be expected to travel significant distances into the drying chamber before attaining their terminal velocities owing to the momentum of the spray and the expanding atomising gas.

Masters [17] provides an in-depth review of the extensive work that has been carried out on the effect of operating variables on pneumatic atomisation.

2.5 ATOMISER SELECTION GUIDELINES

Selection of the mode of atomisation has a considerable bearing on the dimensions of the spray tower. For example a disc atomiser, because of its horizontal trajectories, usually requires a tower with a larger diameter, but less height, than would be required with a pressure or pneumatic nozzle. In many cases there is no clear-cut choice between rotary or nozzle atomisers, as frequently the required product size can be obtained with either type.

The following general guidelines can be applied to assist the selection of an atomiser for a given drier application:

(1) *Spray homogeneity:* Droplet size-distributions from rotary or nozzle atomisers can have similar characteristics at low to intermediate feed rates. At high feed rates spray homogeneity is generally greater with rotary atomisers.

(2) *Particle size range:* Vaned atomiser wheels, two-fluid nozzles and pneumatic-cup atomisers are preferred for the finest spray requirements, e.g. 50 - 100 μm; vaned atomiser wheels and pressure nozzles are preferred for intermediate size ranges, e.g. 150 μm, and pressure nozzles, for coarse sprays, e.g. 150 - 300 μm. Note that the droplet size range required in a given process will depend upon the dried product size required after allowing for shrinkage or swelling.

(3) *Operational Flexibility:* Atomisation by rotary atomisers is more flexible than nozzle atomisation, since atomisation characteristics and feed flowrate can be independently controlled.

(4) *The physical properties of the feed material:* In general, for materials that are abrasive, prone to clogging or that are difficult to pump to high pressure, rotary atomisers are preferred.

(5) *The drying chamber design::* Nozzles are more adaptable to the particular design of a drying chamber. The confined nature of the spray facilities positioning in either co-current, counter- current or mixed flow driers with either rotary or parallel air flow. Rotary atomisers are generally limited to co-current driers with rotary air flow.

2.6 REPRESENTATION OF SPRAYS FROM ATOMISERS

From the analysis presented in this Chapter it is clear that there are three main factors which affect drop size. These are:

(i) the atomiser design, which determines the manner of liquid discharge,

(ii) the liquid properties which influence the behaviour of the disintegrating sheet, and,

(iii) the spraying atmosphere, which affects the mode of disintegration.

Furthermore, due to the random nature of the process, the droplets produced by atomisation are not uniform but cover a range of sizes. Nozzle manufacturers frequently report a single parameter as an indication of droplet size, usually the volume surface mean diameter. However a single parameter does not provide adequate definition of the entire spray, and the application of continuous distribution functions is preferred. Some of the most frequently used distribution functions for droplets are given below since they are commonly encountered in spray drying analysis and research.

The Rosin Rammler Volume Distribution

This function [25] was derived for disintegration of friable materials such as coal but is widely applied to express distributions, especially for nozzle sprays. Its mathematical form is given in Table 2.2, equation 2.16. If this function is applicable to a particular spray, a plot of $\log(100/V_D)$ against D will give a straight line on log-log paper, the slope of which will be q.

The value of q will lie between 2 and 4, the higher values indicating a more uniform distribution. The Rosin-Rammler mean can also be obtained from such a plot, as it is the drop diameter above which 36.8% of the total volume lies.

The Nukiyama - Tanasawa Distribution

This function has been empirically derived for spray distributions from pneumatic or twin-fluid atomisers [26]. Its mathematical form is given by equation 2.17. For the distribution to apply, a plot of $\log(d(N)/D^2)$ against D^q will give a straight line. The dispersion coefficient q is a constant for a given nozzle and can vary from 1/6 to 2.

The Log-Normal Distribution.

The log-normal distribution has a theoretical relation to droplet formation; its mathematical form is given by equation 2.18 in Table 2.2. This distribution gives a straight line on a plot of size D against the number-percent oversize on log probability paper.

Table 2.2 *Common Distribution Functions*

Distribution	Form	Equation Number
Rosin-Rammler	$V_D = 100 \exp [-(D/D_R)^q]$	2.16
Nukiyama-Tanasawa	$\frac{d(N)}{d(D)} = BD^2 \exp(-CD^q)$	2.17
Log-Normal	$\frac{d(N)}{d(D)} = \frac{1}{DS_G\sqrt{2\pi}} \exp\left[-\frac{(\log D - \log D_{Gm})^2}{2S_G^2}\right]$	2.18
Square-Root Normal	$\frac{d(N)}{d(D)} = \frac{1}{2\sqrt{2\pi}\, D\, S_G} \exp\left[-\frac{(\sqrt{D} - \sqrt{D_{Gm}})^2}{2S_G^2}\right]$	2.19
Upper-Limit	$\frac{d(N)}{d(D)} = \frac{1}{DS_G\sqrt{2\pi}} \exp\left[-\frac{\log [(D_{max} - D)/D_{Gm}]^2}{2S_G^2}\right]$	2.20

The Square-root Normal Distribution

This has been applied extensively to the drop sizes obtained from swirl spray nozzles [27]. The equation is similar to that for the log-normal distribution except that log D is replaced by $\sqrt{D}$ as shown in Table 2.2, equation 2.19.

Upper Limit Distribution

This is a development of the log-normal distribution and is expressed by equation 2.20. Proposed by Mugele and Evans [28] it contains a third parameter, the stable maximum droplet size which gives greater flexibility in fitting experimental data. This function has been shown to approximate typical experimental droplet data for a centrifugal pressure nozzle.

In conclusion, the atomisation process is obviously the starting point for any study on droplet motion and drying in a spray drier. The liquid flow characteristics and droplet size-distribution from an atomiser will, together with the prevalent air-flow-pattern, dictate droplet trajectories, residence times and hence moisture levels. Therefore in the development of any theoretical analysis of the spray drying process the fundamental information presented in this Chapter must be taken into consideration.

Chapter 3

Droplet Motion and Air Flow Patterns

A knowledge of the manner in which droplets produced from the atomiser interact with the drying air is a pre-requisite for the sound design and efficient operation of a spray drier.

The motion of a drop will, to a very large extent, be dictated by the air-flow patterns in the drying chamber. Hence the chamber and air-disperser design must create a flow pattern which will

(a) enable sufficient residence time for droplets to be dried to the desired average moisture content; and

(b) prevent partially-dried particles impinging upon the walls of the drying chamber or the atomiser.

Wall deposits result from particles travelling too rapidly to the wall and thus not experiencing sufficient drying time for the formation of a rigid crust. Wall deposits should be minimised since on displacement they could result in an off-specification product and on accumulation as layers, may even pose a fire hazard [29]. Atomiser deposits result from entrainment of drops in local eddies. Eddies can result in particles becoming over-dry, and possibly scorched e.g. by causing recirculation of particles into the hotter regions near the air inlets of the drier.

Spray-air contacting patterns can be classified according to the position of the atomiser in relation to the air inlet, and the type of arrangement employed, is of considerable importance since it has great bearing on dried product properties. There are three alternative contacting patterns [20, 32, 33] which can be termed

(a) co-current contact;

(b) counter-current contact; and

(c) mixed-flow contact.

These arrangements are illustrated in Figures 3.1 and 3.2.

It should, however, be stressed that the above classification is a vast oversimplification of the real situation where any simple unidirectional flow pattern would be destroyed by turbulence within the spray drying chamber. The different drier arrangements are described below.

(a) Co-current Contact

With reference to Figure 3.1a, if the air and the spray pass through the drier in the same direction then this is termed co-current contact. This arrangement is widely used in industry especially for the drying of materials which are heat degradable [30, 31] e.g. coffee, fruit juices and pharmaceuticals. In this type of flow arrangement, the spray from the atomiser immediately contacts the hottest air resulting in rapid evaporation. The droplets in the spray fall to a temperature approaching the wet-bulb temperature of the air, seldom > 70°C, and the high evaporation rate brings about a rapid decrease in air temperature. Even when the critical moisture content is reached and crust formation begins, the droplet temperature does not rise substantially since the droplet is then in contact with much cooler air. Hence low temperature conditions prevail and no heat degradation takes place.

(b) Counter-current Contact

Alternatively if the spray and the air travel in opposite directions through the tower, this is termed counter-current contact (Figure 3.1b). This arrangement offers excellent heat utilisation [34, 35] but it does subject the driest particles to contact with the hottest air stream. Therefore it is unsuitable for drying materials which are heat-sensitive. Counter-current flow is used with nozzle atomisers since the upward force of the air reduces the axial velocities of the large droplets, hence permitting sufficient residence time in the

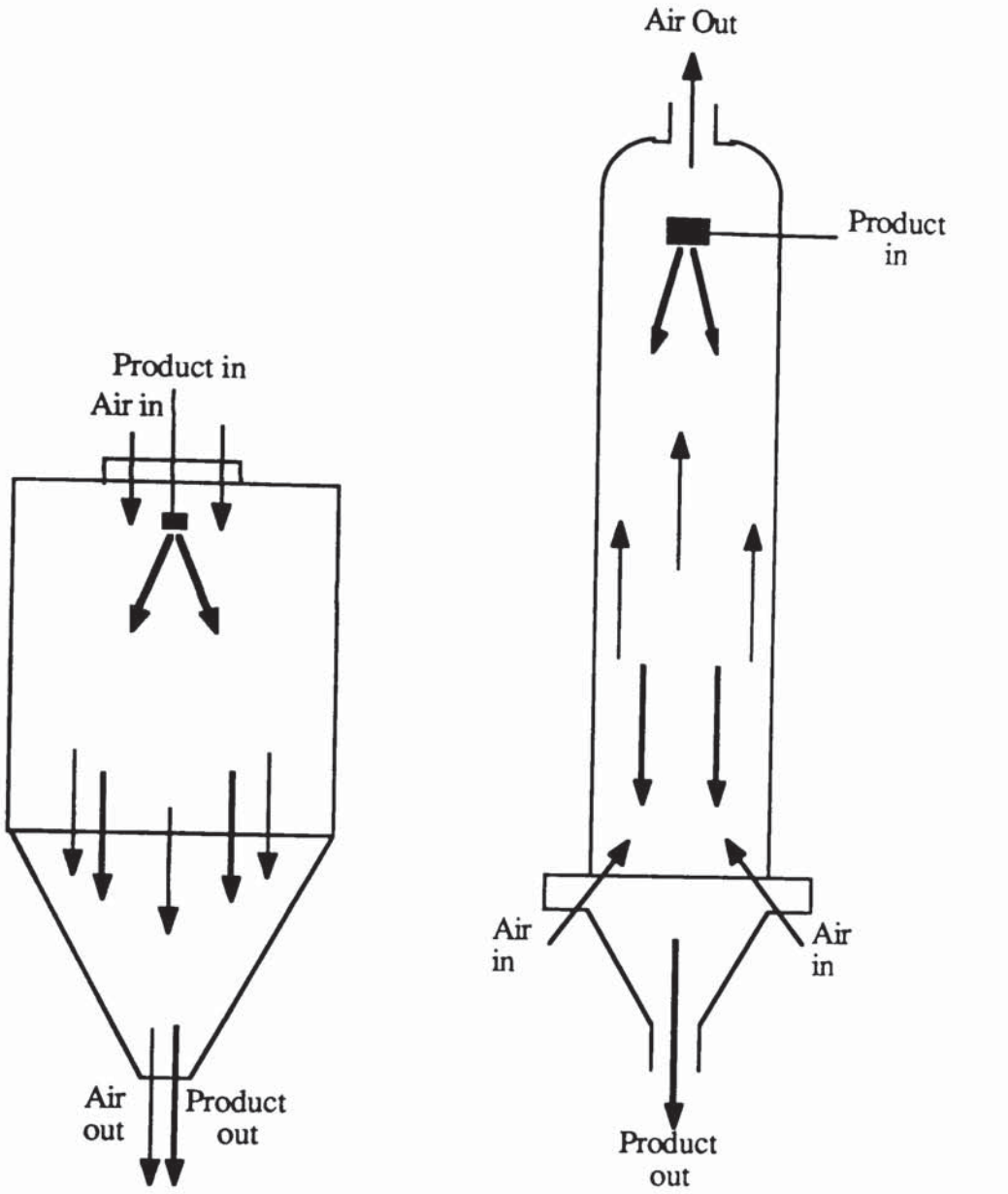

a) Co-current Air Flow b) Counter-current Air Flow

Figure 3.1 *Co-current and Counter-current Contacting Patterns*

drying tower for completion of drying. The upward force of the air, however, also results in increased agglomeration of particles in counter-current driers. This is because, as the particles dry, some may be entrained with the upward flow of air and thus may collide with and adhere to the wetter particles. Alternatively the downward velocities of the smaller particles may be so reduced that heavy, wet particles of higher velocity may collide with them [36]. Thus it is important that the air velocity in the drier is kept sufficiently low if

excessive entrainment or agglomeration of particles is to be avoided [37, 38]. Counter-current contact is used almost exclusively for the drying of soaps and detergents where a popular variation is to introduce the drying air tangentially into the tower so that it possesses a swirling motion within the drier. The merits of imparting swirl to the air are considered in Section 3.2.

(c) Mixed-flow Contact

Finally there are drier designs which offer a combination of both co-current and counter-current contacting as shown in Figure 3.2. This is termed mixed-flow contact and is characterised by complex flow patterns with a high degree of turbulence and mixing within the drying chamber. This type of drier can be used for the production of coarse, free-flowing powder in a drying chamber of limited size and volume. However high temperature conditions prevail in the drier and therefore this arrangement cannot be used with heat sensitive materials.

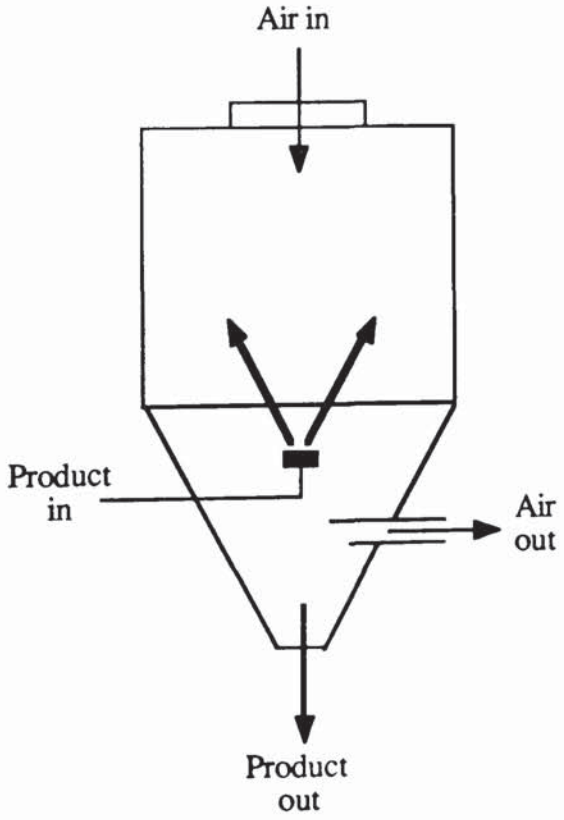

Figure 3.2 *Mixed-Flow Contacting Patterns*

The contacting pattern most-suited to a particular spray drier installation depends upon the nature of the product involved. Specifically, it depends upon the required dried particle form and upon the temperature to which the product can be subjected. For example, if a co-current drier is selected, then the very high initial evaporation rates, in addition to maintaining low droplet temperatures, will increase the tendency of the droplets to expand or fracture to give a dried product comprising of non-spherical, porous particles of low bulk density. Conversely if the product is not heat-sensitive and a counter-current drier is selected, the droplets will initially contact cooler air and the subsequently lower evaporation rate will result in a reduced tendency for the droplets to expand or fracture during drying. A low porosity, high bulk density product is thus characteristic of counter-current driers.

Regardless of the type of flow arrangement, the droplets released from the atomiser possess velocities greatly in excess of the drying air velocity e.g. 30 to 100 m/s compared with generally less than 2 m/s. Rapid deceleration therefore occurs. In order to predict spray movement within the spray drier the fundamentals of aerodynamic drag on the droplets must therefore be considered.

3.1 DROPLET MOTION : THE MOMENTUM TRANSFER PROBLEM

The phenomena of momentum transfer arising from particulate motion in a fluid is the pre-determining factor in any hydrodynamic analysis of spray drying. Essentially, determination of particle trajectories and residence times is dependent upon evaluation of the drag force exerted by the fluid on the particle. The following section describes the mechanism of momentum transfer to a submerged object, the representation of drag data, and the application of such data to spray drying operations. For this analysis the droplet and dried particle are assumed to be perfectly spherical.

3.1.1 Mechanism of Drag on Submerged Objects

When a fluid flows over a submerged object, in this case a sphere, the fluid which is in direct contact with the surface is brought to rest and because of viscous forces acting within the fluid, a velocity gradient is set up, perpendicular to the direction of flow. The drag force resulting from the retardation at the surface is transmitted through the fluid, the effect of the drag diminishing at increasing distances from the surface. The velocity gradient can therefore be considered to be confined to the fluid in the immediate vicinity of the surface called the boundary layer.

Consider the flow of fluid over a submerged sphere as shown in Figure 3.3. The velocity of the fluid drops to zero at the centre of the leading face, whilst the fluid is accelerated around the sides of the sphere. So, referring to Figure 3.3 as the fluid passes from A to B, its kinetic energy will increase at the expense of its pressure energy, resulting in the development of a negative pressure gradient around the surface of the sphere from A to B. Now from B to C the velocity of the fluid just outside the boundary layer will decrease resulting in an increase in pressure and a positive pressure gradient from B to C. The fluid moving in the immediate vicinity of the surface of the sphere, in the boundary layer, will be under the influence of the same pressure field as that existing outside.

Thus the fluid in the boundary layer flowing from B to C will be influenced by 3 forces:

(i) Viscous forces acting in a downstream direction,

(ii) frictional forces causing retardation,

(iii) pressure gradient causing retardation.

Owing to the large dissipation of kinetic energy in overcoming frictional forces within the boundary layer, the fluid may be unable to surmount the pressure rise between B and C. When this occurs, the fluid cannot move far between points B and C and is eventually brought to rest. The external pressure may then cause the fluid to flow in the opposite direction [39]. The boundary layer will then separate from the sphere resulting in the formation of a vortex in the wake of the droplet. The pressure in the wake is

substantially that of the surrounding fluid which is at a low pressure since separation occurred at a point of low pressure. Thus that part of the sphere in contact with the wake will be subjected to a low pressure which, in conjunction with the high pressure on the leading face, will exert an additional force termed the pressure or form drag [40]. The total force on the sphere is thus made up of two components, the viscous drag or skin friction and the form drag. At low Reynolds numbers <24, no separation occurs [41] and most of the drag results from skin friction. At higher Reynolds numbers separation of the boundary layer results in the form drag being the major component of the total drag.

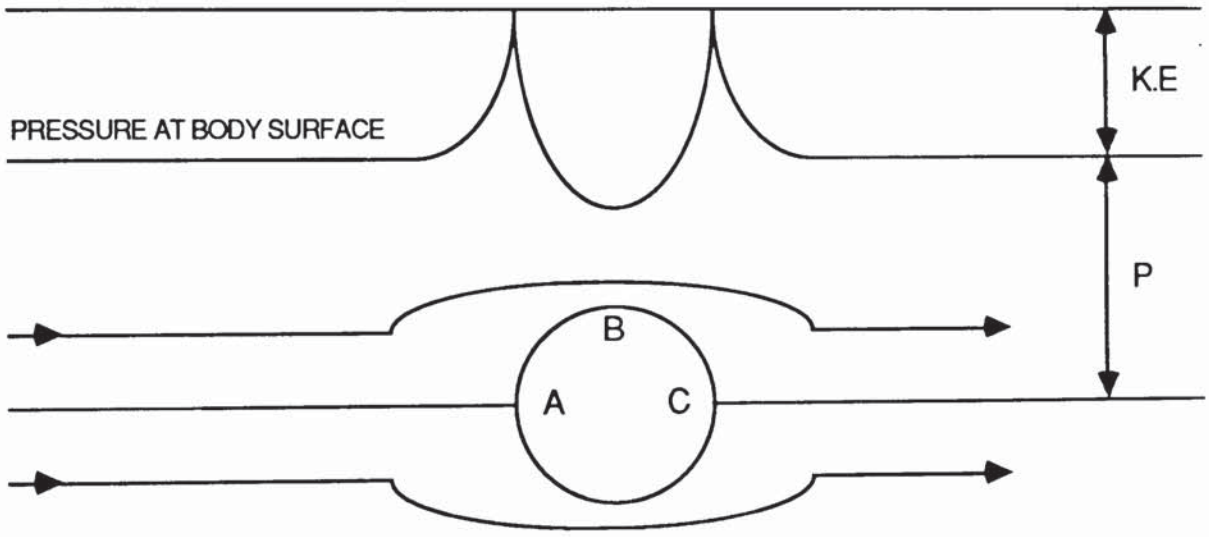

A, B, C = Arbritrary Points

K.E = Kinetic Energy

P = Pressure

Figure 3.3 *Pressure Distribution Around a Submerged Sphere*

3.1.2 Representation of Drag Data

Numerous investigations have been conducted with the aim of determining and correlating the drag force exerted when a spherical particle travels through a fluid. However, owing to the complexity of the phenomena of fluid resistance, the results of measurements on the drag force have been contradictory and this has sometimes resulted in conflicting experimental data being reported. An extensive review of the work carried out in this respect has been given by Torobin and Gauvin [42 - 46] dealing with various aspects of solids-gas flow. The results obtained from investigations on the drag force are normally represented by the standard drag coefficient curve which expresses the relation between the coefficient of drag C_D defined by:

$$C_D = \frac{F_D}{A\rho_a V_R^2/2} \qquad 3.1$$

and the particle Reynolds number,

$$Re = \frac{DV_R\rho_a}{\mu_a} \qquad 3.2$$

The conditions normally stipulated in the development of the standard drag coefficient curve are that the sphere is:

(i) smooth, rigid and non-rotating,

(ii) moving at a constant relative velocity,

(iii) in an unbounded fluid free from any disturbance.

The standard drag curve has been plotted extensively [47 - 51]. A typical curve is shown in Figure 3.4.

Many empirical or semi-empirical equations have been proposed to approximate the standard drag curve. Some of the more popular are given by Clift et. al., [49]. The same

authors also give a new correlation for the whole range of Reynolds numbers based on a review of the available data for spheres. This is reproduced in Table 3.1.

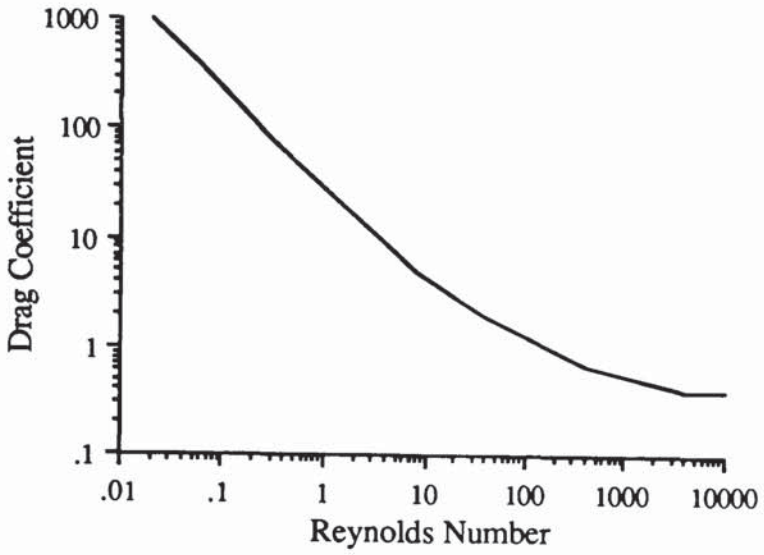

Figure 3.4 *Typical Drag Coefficient Curve for Spherical Particles*

3.1.3 Applicability of Drag data to Spray Trajectory Calculations

The highly idealised conditions under which the standard drag coefficient curve is derived are seldom met in Chemical Engineering practice. Therefore data obtained from the standard drag curve may in some instances be extremely inaccurate. To apply such data in an analysis of droplet behaviour in a spray drying chamber therefore requires consideration of complicating factors which may influence the total drag force on a particle.

These are:

(a) the effect of deceleration of the droplets,

(b) the effect of particle rotation,

(c) the effect of mass transfer.

Table 3.1 *Drag Coefficient Correlations* [49]

Range	Correlation
$Re < 0.01$	$C_D = 3/16 + 24/Re$
$0.01 < Re \leq 20$	$C_D = \frac{24}{Re} [1 + 0.1315\, Re^{(0.82 - 0.05 \log Re)}]$
$20 \leq Re \leq 260$	$C_D = \frac{24}{Re} [1 + 0.1935\, Re^{0.6305}]$
$260 \leq Re \leq 1500$	$\log C_D = 1.6435 - 1.1242 (\log Re) + 0.1558 (\log Re)^2$
$1500 \leq Re \leq 1.2 \times 10^4$	$\log C_D = - 2.4571 + 2.5558 (\log Re) - 0.9295 (\log Re)^2 + 0.1049 (\log Re)^3$

(a) The Effects of Acceleration/Deceleration

When the relative velocity between a particle and fluid changes with time the drag coefficient may differ considerably from the standard value at the appropriate instantaneous velocity [43, 48, 49, 52]. Early work on the effect of acceleration on drag produced some conflicting results [53, 54], but it is now generally accepted that the effect of unsteady motion is to increase the fluid resistance.

As for steady motion, analytic solutions for unsteady motion are only available in creeping flow when the convective terms in the Navier-Stokes equation can be neglected. The solution was developed by Basset [55] for a fluid at rest but extended by Tchen [56] to the case of a fluid moving with a variable velocity, as shown below:

$$\frac{\pi D^3}{6}\rho_p\frac{dV}{dt} = 3\pi\mu_a D(V_a - V) + \frac{\pi D^3}{6}\rho_a\frac{dV_a}{dt} + \frac{1}{2}\frac{\pi D^3}{6}\rho_a\left(\frac{dV_a}{dt} - \frac{dV}{dt}\right)$$

A B C D

$$+ \frac{3}{2}D^2\sqrt{\pi\rho_a\mu_a}\int_{t_o}^{t}\frac{\frac{dV_a}{dt'} - \frac{dV}{dt'}}{\sqrt{t - t'}}dt' \qquad 3.3$$

E

The significance of the various terms comprising this equation will now be explained. Term A represents the force required to accelerate the particle. Term B is the Stokes drag for steady motion at the instantaneous velocity. Term C is the pressure gradient term which represents the force required to accelerate the fluid which would occupy the volume of the particle in its absence. Term D is the 'added mass' which arises because acceleration of the particle requires acceleration of the fluid entrained in its wake. Finally, term E is the Basset history integral which represents the effect of past accelerations, where (t-t') is the time elapsed since the previous acceleration. This equation has been shown to accurately predict the motion of spheres accelerating from rest in various viscous fluids [57].

For rectilinear acceleration at higher Reynolds numbers there have been two distinct approaches to the calculation of drag. The first is an extension of the added mass concept, with empirical coefficients to account for departure from creeping flow. The second approach is the use of an instantaneous drag coefficient which is dependent both upon the instantaneous Reynolds number and upon an acceleration modulus, a displacement modulus and upon the solid/fluid density ratio [52].

Odar and Hamilton [58] adopted the first approach and suggested that the creeping flow equation be extended to higher Reynolds numbers as follows:

$$-F_D = C_D \frac{\pi D^2}{8} \rho_a V_R |V_R| + C_A \frac{v\rho_a \, dV}{2 \, dt} + C_H \frac{3D^2}{2} (\pi \rho_a \mu_a)^{1/2}$$

$$+ \int_0^t \frac{d\,V}{dt'} \frac{dt'}{(t - t')^{1/2}} \qquad 3.4$$

The empirical coefficients C_A and C_H were correlated from measurements of the drag on a sphere executing simple harmonic motion. The coefficients were later shown to be applicable for rectilinear motion of a sphere in free fall [59] and thought to be applicable to all rectilinear accelerations. C_A and C_H were found to be functions of the acceleration modulus only:

$$C_A = 2.1 - \frac{0.132 M_A^{\,2}}{1 + 0.12 M_A^{\,2}} \qquad 3.5$$

$$C_H = 0.48 + \frac{0.52 M_A^{\,3}}{(1 + M_A)^3} \qquad 3.6$$

Where the acceleration modulus is:

$$M_A = \frac{V^2}{d(\frac{dV}{dt})} \qquad 3.7$$

For a sphere travelling in a circular as opposed to a rectilinear path, which may be the case in spray driers incorporating swirling air flow, it may be necessary to consider additional forces. Odar [60, 61] measured the drag on a sphere moving in a circular path and found that if the path diameter was at least 7 times the particle diameter, the drag coefficient was unaffected by the curvature. The corrective terms for the added mass and history effects were however dependent upon the curvature of the trajectory.

Examination of equation 3.3 has shown that the second, third and fourth terms on the right hand side become important only when the density of the fluid becomes comparable to, or higher than, the density of the particle [62]. Hence for the case of particle motion in a gas such as in a spray drier, the equation of particle motion reduces to:

$$F_D = - C_D \frac{\pi D^2}{8} \rho_a V_R |V_R|$$

A force balance on the droplet then gives:

$$m \frac{dV}{dt} = F_g - \frac{\pi D^2}{8} \rho_a C_D V_R |V_R| \qquad 3.8$$

where F_g contains body forces e.g. gravity, the pressure gradient term (zero for steady fluid motion) and any lift terms.

The resultant motion of a particle can then be resolved into component velocities along mutually perpendicular axes, and by assuming the equation of linear motion, equation 3.8, applies to each component, the particle trajectory can be calculated. Strictly this approach is only accurate for laminar motion when the drag force is directly proportional to the velocity. When the drag is a function of the velocity to a power greater than one, the resolution of drag into components does not coincide with the resolution of velocities. However, the error in applying this method is generally considered to be less than 10% in most cases [63].

Despite the absence of added mass and history effects for particulate motion in a gas, deviations from the standard drag curve have been found in some studies. Hughes and Gilliand [48] suggest unsteady state drag coefficients 10 - 20% higher than the standard values and Marchildon [64] and Gauvin and Marchildon [65] found that drag coefficients for decelerating spheres increased by up to 10% over the standard values. Thus, in

conclusion,the present body of knowledge does not appear to enable any quantitative corrections for deceleration effects on drag to be made. It is believed that neglect of these effects however will result in the over-prediction of trajectories and hence over-design rather than under-design of equipment.

(b) The Effect of Particle Rotation

In a spray drier, particle rotation may occur as a result of a collision between two particles or a collision between a particle and the wall of the drying chamber. Rotation can also occur as a result of a non-uniform air velocity profile in the drier causing a fluid shear effect. This may occur, for example, at the walls of the drying chamber. The resultant rotation in these instances may be termed top spin and the particle will rotate about an axis normal to the direction of relative motion. Because of such rotation and/or shear the particle will experience a force perpendicular to its relative velocity with respect to the air. This is shown in Figure 3.5.

The magnitude of this lift is dependent upon the particle Reynolds number. For low Reynolds numbers, <1, for both spin and shear Saffman [66] showed that the drag on the particle is slightly increased and the lift is given by:

$$F_{L_1} = 1.615\, \mu_a\, D V_R \sqrt{Re_g} \qquad 3.9$$

where Re_g is a shear Reynolds number. In an earlier study Rubinow and Keller [67] found that spin did not affect the drag force and calculated the lift force in a non-shear fluid for low values of Reynolds number as:

$$F_{L_2} = \frac{\pi\, V_R\, \Omega\, D^3}{8}\, \rho_a \qquad 3.10$$

Boothroyd [68] compared the relative values of these lift forces, with and without fluid shear, and concluded that $F_{L_1} >> F_{L_2}$. Since the angular velocity at any point in the flow

is much harder to predict than the fluid shear rate, calculations are vastly simplified. In addition, the magnitude of any lift force is likely to be much smaller than the drag force, except very near the wall, where there is likely to be a strong tendency for a particle to be moved at right angles to the wall.

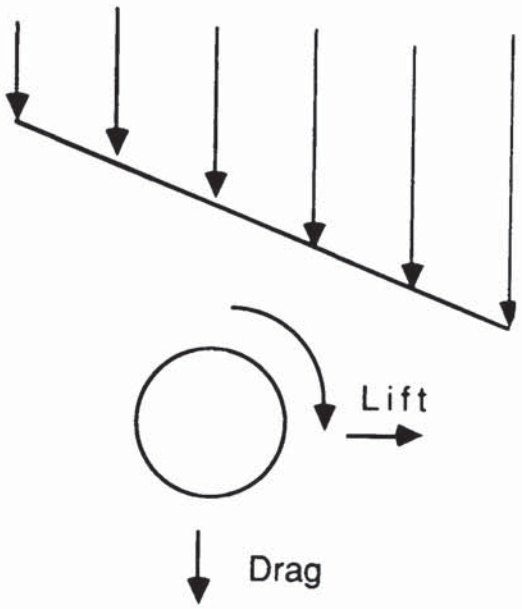

Figure 3.5 *Sphere Rotating in Simple Fluid Shear*

At higher Reynolds numbers, rotation results in a significant lift in the absence of fluid shear. This is termed the Magnus effect and the lift acts in the direction shown schematically in Figure 3.6. At the upper face of the sphere the fluid and the sphere are moving in the same direction but at the lower face they are moving in opposite directions. The fluid above the sphere is therefore accelerated resulting in a decrease in pressure, whilst the fluid below the sphere is retarded resulting in an increase in pressure. An upward lift is therefore exerted. Measurements of this lift force have generally been confined to very high Reynolds numbers, typically in excess of 2000 [49]. In spray driers, droplet Reynolds numbers in some instances may initially be of this order of magnitude, but rapid deceleration results in the droplet Reynolds number falling well below this value

almost instantaneously. Hence the Magnus effect is not likely to have a significant effect on droplet motion within a spray drier and can therefore be neglected in the computation of particle trajectories.

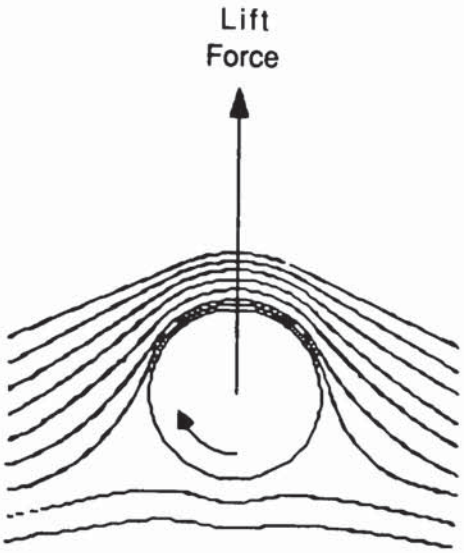

Figure 3.6 *The Magnus Effect*

(c) Effect of superimposed mass transfer

The standard drag coefficient curve applies to solid spheres which are not undergoing mass transfer. In spray drying, this condition is obviously not satisfied and the drag coefficient may therefore be expected to differ from the standard value. Evaporation may be expected to reduce skin friction due to a thickening of the boundary layer and may also affect the position of the boundary layer separation [69].

At low rates of mass transfer there is evidence that the drag coefficient is not substantially different from the standard value. Ingebo [70] found that a single curve could express drag coefficient data for both evaporating and non-evaporating particles and Eisenklam and Arunchalam [69] measured the drag coefficients of water droplets falling in air at room temperature to within 10% of the standard value.

At larger rates of mass transfer as might be experienced in a spray drier, there is evidence that the effect of superimposed mass transfer is to bring about a reduction in the drag coefficient. Hamielec et. al., [71] solved the Navier-Stokes equation numerically using a finite difference method. Two cases were considered, flow around a sphere with and without mass transfer. Their results indicated that mass transfer reduces skin friction and has little effect on the pressure distribution around the sphere. This reduction in drag was also noted by Eisenklam and Arunchalam [69] who measured, drag coefficients for burning and evaporating drops of the order 25 microns, in high temperature air. In this study, mass transfer was expressed by the transfer number B_H, defined for evaporation as:

$$B_H = \frac{C_p \Delta T}{\lambda} \qquad 3.11$$

The range of transfer numbers covered in the study was 0.092 to 3 for evaporating droplets, and as high as 36 for burning droplets. A typical value of the transfer number for a droplet in spray drier may be 0.1 to 0.2 for the initial high rates of evaporation characteristic of co-current driers. The results of the investigation showed a considerable decrease in the drag coefficient with increasing values of B_H. The major cause of the reduction in drag was attributed to the momentum of the effusing vapour, and the drag coefficient was correlated with the transfer number as follows:

$$C_{DM} = \frac{C_D}{(1 + B_H)} \qquad 3.12$$

However the transfer number as defined in equation 3.11 can only express the rate of mass transfer for pure liquid droplets or for solutions in the constant rate period, i.e. when there is no internal resistance to mass transfer. In spray drying as soon as a crust appears on the droplet surface, the rate of mass transfer is not generally controlled by the temperature driving force but by the rate of transfer of vapour e.g. by vapour diffusion through the pores in the crust. The correction for the drag coefficient given in equation

3.12 can therefore only be applied to pure liquid droplets or to droplets of solution in the constant rate period.

Renkzibulut and Yuen [72] arrived at a similar correlation in their recent numerical and experimental approach to determining the drag coefficients of evaporating liquid drops in high temperature air flow:

$$C_{DM} = \frac{C_D}{(1 + B_H)^{0.2}} \qquad 3.13$$

Chuchottaworn et. al., [73, 74] solved the Navier-Stokes equation numerically in a manner similar to Hamielec et. al., [71] and proposed the following correlations for drag coefficients of evaporating or condensing droplets:

a) In terms of a correlating parameter (φ/C_D):

$$\left(1 + \frac{C_{DM}}{C_D}\right) = \frac{Re^{0.257}}{(3.83 + 1.1\ (\varphi/C_D))} \qquad 3.14$$

where φ was defined as a surface mass injection ratio.

b) in terms of the mass transfer number B_M

$$\frac{C_{DM}}{C_D} = (1 + B_M)^{-0.19} Sc^{-0.74} (1 + B_m)^{-0.29} \qquad 3.15$$

where $$B_M = \frac{(x_{vs} - x_{vo})}{(1 - x_{vs})} \qquad 3.16$$

and x_{vs} and x_{vo} are the mass fractions of the vapour at the droplet surface and in the fluid respectively.

In a further experimental investigation, Chuchottaworn et. al., [75] determined drag coefficients of evaporating droplets and confirmed that at low rates of mass transfer the drag coefficient followed the standard curve, whilst at higher rates of mass transfer, equation 3.15 gave a good fit to the experimental data.

3.2 AIR FLOW PATTERNS

The air flow pattern in the spray drying chamber is a major consideration in drier design and performance. The movement of air in the drying chamber predetermines the rate and degree of evaporation by influencing (a) the residence time of the droplets in the drying zone, (b) the concentration of product near the walls of the drying chamber, (c) the extent that particles re-enter the hot areas around the air disperser by back-eddying, and (d) the extent of any hot air by-passing or channelling.

The air flow pattern established in a drying chamber is dependent upon the spray drier design features, in particular the air inlet and outlet arrangements, and upon phenomena resulting from the drying process itself (e.g. temperature gradients). Air disperser designs are available that create parallel flow or swirling flow. Figure 3.7 illustrates some available for co-current driers.

In Figure 3.7a the air enters as a jet and expands to the drier diameter at some distance below the atomiser. This arrangement will result in considerable back-mixing which may be undesirable if the product is heat sensitive. If this is the case, then an arrangement of the type shown in Figure 3.7b may be desirable. Perforated plates or straightening vanes are used to eliminate eddying and to produce parallel (streamline) flow. Figures 3.7c and 3.7d show arrangements which result in swirling air flow in the drying chamber by means of a tangential wall inlet, or a ceiling air disperser with air rotation controlled by angled vanes.

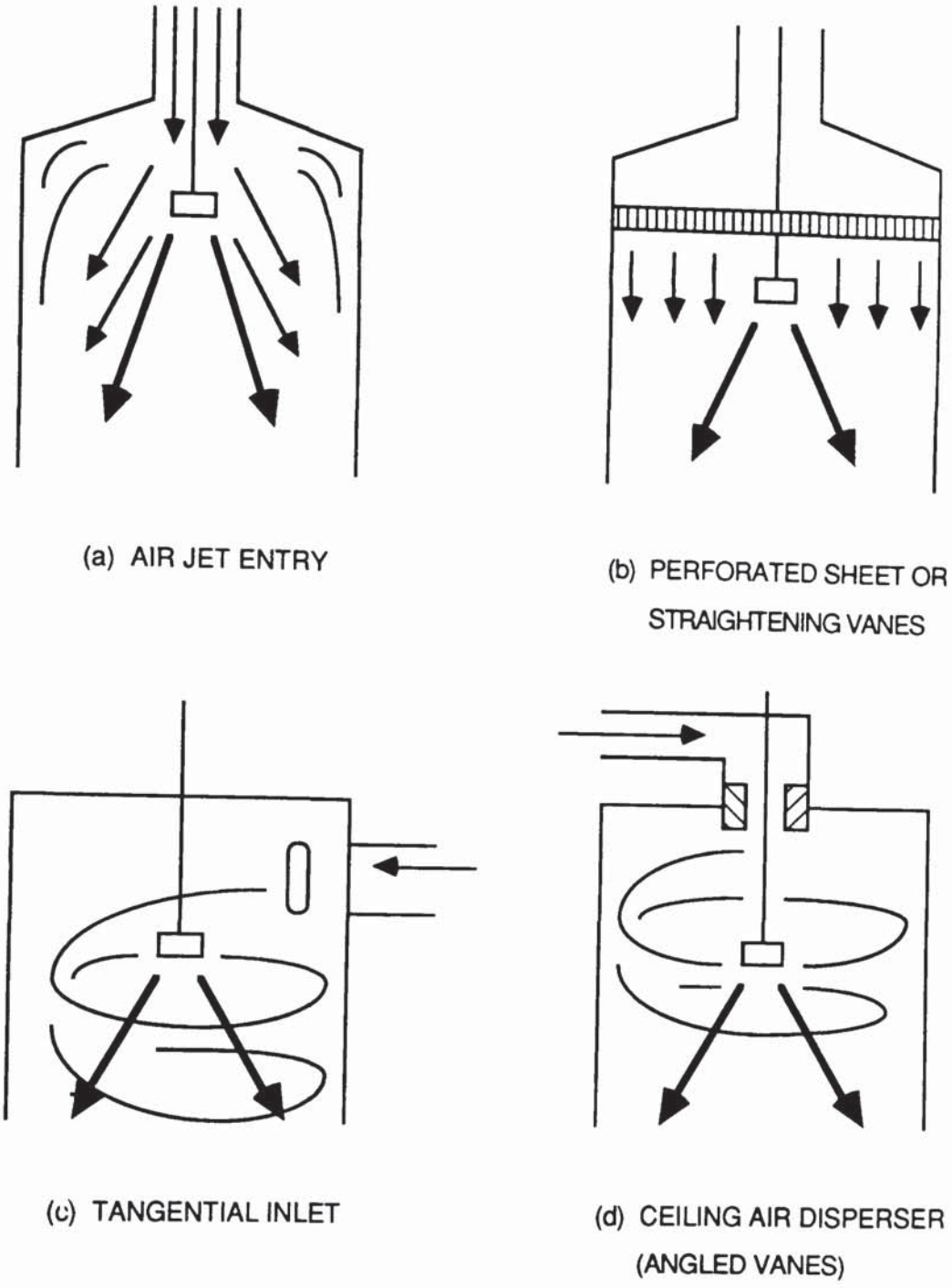

Figure 3.7 *Air Disperser Designs for Co-current Flow*

Air disperser arrangements for counter-current driers most frequently consist of a wall bustle or plenum chamber located at the base of the tower supplying air through four or more nozzles. These nozzles can be set at 90 degrees to each other as in Figure 3.8a in which case the air enters the drier radially, mixing turbulently at the base of the tower before ascending towards the air exit duct. Alternatively the air inlet nozzles can be set at

an angle both to the radial and horizontal directions in which case the air possesses a rotary or swirling motion within the drier as shown in Figure 3.8b. Designs involving a single tangential inlet at the wall of the tower or an inlet at the centre of the tower are also available but are less common.

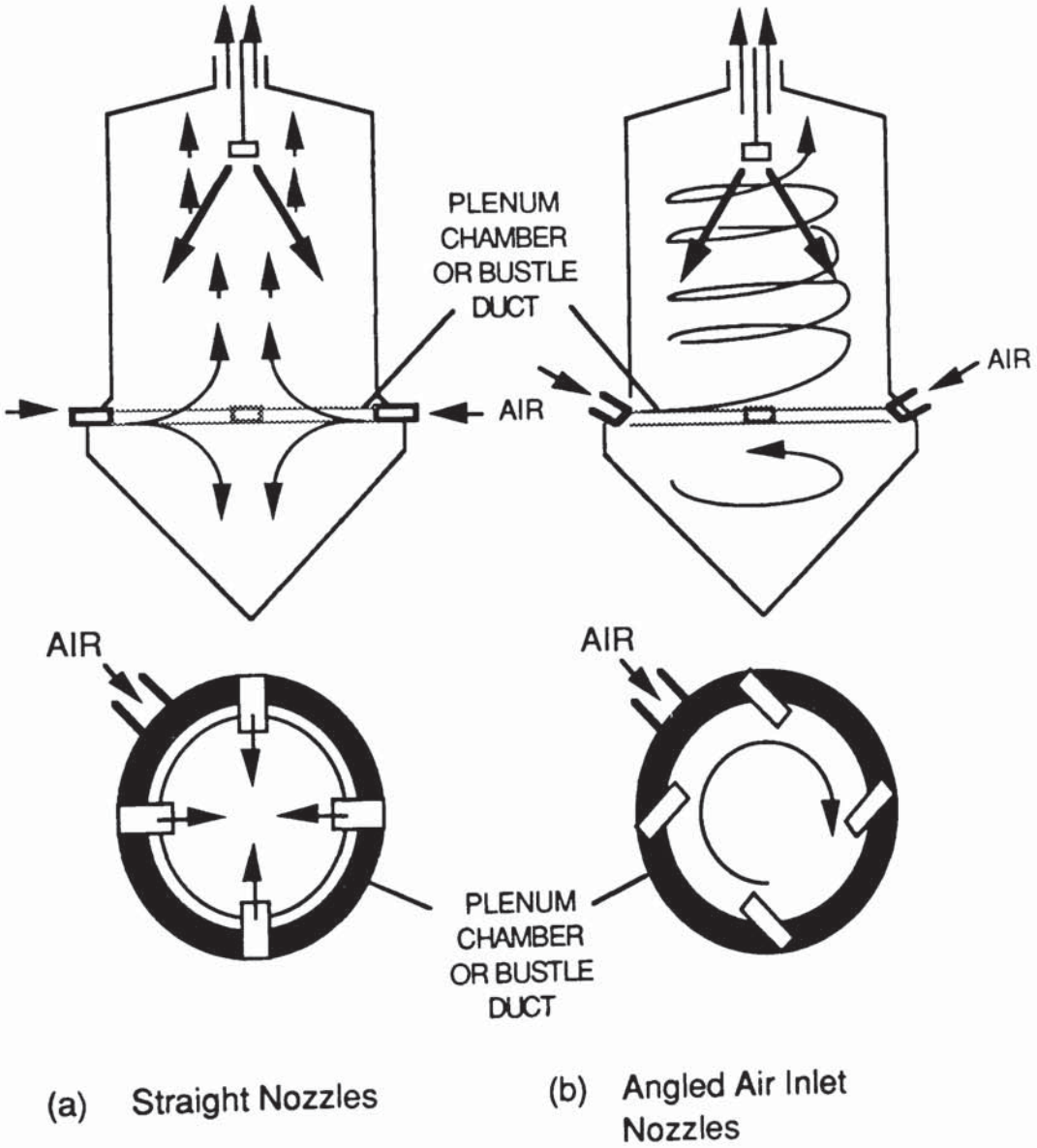

Figure 3.8 *Air Disperser Design for Counter-current Flow*

The principal advantage of imparting swirl to the air is that it increases the relative velocity between droplets and air and hence increases the heat and mass transfer coefficients and brings about more efficient drying. It has also been reported [76] that swirl results in good mixing along the axis of the tower and thereby reduces the difference in temperature between the top and bottom of the tower which may be advantageous in certain instances. However, set against these advantages is the risk of hot air channelling up the centre of the drier, and centrifugal action within the drier resulting in product being thrown to the walls of the drying chamber causing increased wall deposition.

Relatively little experimental work has been carried out on air flow patterns in spray driers due largely to the lack of a suitable experimental technique. The techniques that are commonly described for the inference of flow patterns are:

(a) velocity measurements,

(b) gas residence time analysis,

(c) temperature and/or humidity measurements,

(d) flow visualisation.

Thordarson [77] qualitatively investigated flow patterns in a 0.61m diameter transparent plastic co-current tower by injecting balsa dust into the air stream for various inlet arrangements. In almost all cases he reported the existence of swirl and back eddies.

Thomas [78] measured the residence time of dust particles in vortex flow in a co-current spray drier and reported that two distinct times of passage occurred. The shortest was associated with flow down a central core, and the longest was associated with flow adjacent to the walls of the drying chamber.

Buckham and Moulton [79] measured temperatures and humidities in a 1.2m diameter co-current drier incorporating a fixed-8-vane air distributor. The measured temperature and humidity profiles were compared with theoretical predictions assuming no

vertical mixing (i.e. plug flow) and complete mixing. From this analysis the authors concluded that the extent of vertical mixing approached 75% of complete mixing. This was attributed to the jet effect of the high velocity inlet air stream, and to localised volume contractions due to cooling by the spray and heat losses through the chamber walls.

Arni [80] investigated the effect of air inlet arrangements on flow patterns in two co-current driers. The approach adopted was to measure air velocity profiles using hot wire anemometry in the absence of spray. The first drier was identical to that used by Buckham and Moulton. In the second drier the air was distributed by means of two 60 mesh stainless steel wire screens. The velocity profiles for the Buckham drier suggested that jetting action persisted for a major fraction of the drier volume. However this implies minor mixing which is at variance with the conclusions of Buckham and Moulton. Furthermore the study suggested that vane distribution of the type used, was totally ineffective for uniformly distributing the air. In contrast, data for the second drier suggested that the mesh distributors were much more effective and resulted in a relatively uniform velocity distribution.

Velocity profiles have also been reported by Chaloud et. al., [76] for the case of a counter-current detergent spray drier incorporating swirl flow. The measured tangential and axial velocities were indicative of a core of air with high rotational and axial velocity rising through the centre of the tower. The tangential velocity profile suggests that the core rotates as a forced vortex (i.e. rigid body rotation) whilst the air outside the core behaves like a free vortex, with the tangential velocity falling with increasing radius. The vertical velocity profile suggests that the core ascends the tower with several times the mean vertical velocity of the air. Outside the core the vertical velocity drops to a minimum in an intermediate zone and then rises slightly in an outer zone adjacent to the wall. This core, if present, would be detrimental to efficient spray drier operation. It would lead to unduly hot, dry air leaving the tower without taking part in the drying process and also result in the possible entrainment of large quantities of powder out of the drying chamber.

Place et. al., [81] investigated air-flow patterns in a similar spray drier using tracer techniques. The drier was 6.4 metres in diameter and 15.25 metres in length. A helium tracer was injected at a succession of points and the subsequent variation in the tracer concentration in the air outlet was observed. From their response analysis the authors calculated average residence times or "50% exit times" (i.e the time taken for 50% of the tracer to pass out of the system). They expressed their results as contours of equal average exit-times. In addition they formulated contours of equal spreads (5% exit time - 50% exit time). Their results showed wide scatter, indicative of instability of flow within the drying chamber. The contour map identified three zones in the spray drier: a central zone and an outer peripheral zone where the flow was upward and had the same mean velocity, and an intermediate zone located in between these two, where the flow was slower or even downward. This third zone was attributed to being the main mechanism of back-mixing in the drier. The study gave no indication of significant channelling up the centre of the drier, in contrast to the earlier work of Chaloud et. al., [76]. However Place et. al., were able to detect a central core on a 1/80 scale model spray drier, during the same investigation. Using water as the fluid and coloured solutions as tracer, it was noticed that tracer injected near the axis moved vertically upwards at several times the mean vertical velocity in a coherent core, thus indicating undesirable short-circuiting of fluid. However, the feasibility of using water to accurately simulate air flow patterns is questionable.

Paris et. al., [82] developed a model for the air flow in a drier similar to that used in the studies by Place et. al., [81] and Chaloud et. al., [76]. In these former studies, flow patterns were investigated in the absence of the spray. In contrast Paris et. al., measured the residence time distribution of the air in the spray drier during normal operation. They then fitted a model comprising a combination of ideal flow regions to the measured residence time distribution. This model simulated flow in the drier by two stirred tanks in parallel with a plug flow by-pass, to represent the rapidly ascending central stream and the annular zone of intense turbulence. (As was observed by Place et. al., [81] and Chaloud

et. al., [76]). A third stirred tank which was initially conceived to represent relative stagnation at the lower cone of the drier also appeared in the model. The components of the model were described by a set of differential equations, the parameters of which were adjusted until the model distribution function best matched the experimental residence time distribution function. This was carried out via digital simulation. The parameters thus obtained led to the conclusion that the additional stirred tank should represent a highly turbulent region at the top of the tower where the spray is atomised, rather than the stagnant region first envisaged.

In a more recent investigation Ade-John and Jeffreys [83] conducted residence time distribution studies and flow visualisation experiments to identify the drying zones in a spray drier and to ascertain the volumes of these zones. The research was carried out in a transparent counter-current spray drier of 1.22m diameter, using water and sodium carbonate slurry feeds. The drying tower was fitted with a number of probes which were used both for injecting tracer and smoke, and for sampling tracer. Smoke was employed to identify the zones in the tower and to characterise the type of flow in the zones. In their experiments they observed a by-pass zone adjacent to the tower walls and determined its volume, both by smoke visualisation and by CO_2 tracer experiments. The smoke pulse experiments also revealed the existence of an intensely turbulent zone in the vicinity of the air entry ports, and a turbulent zone around the spray nozzle. These two regions were connected by a cylindrical plug flow zone. The volumes of these zones varied with operating conditions and were correlated via dimensionless analysis. A model was also developed which simulated the overall flow pattern through a combination of well-defined flows. The model predictions showed good agreement with experimental data.

Keey and Pham [84] investigated the air flow pattern in a co-current drier, 0.4m in diameter and 2m in length, by conducting smoke visualisation tests and by residence time distribution (RTD) analysis. The air inlet arrangement in the drier was of the air jet entry type (Figure 3.7a). The tracer used for the RTD analysis was Freon-12 and the data was

fitted best by a Tanks-in-Series-with-Plug-Flow model. The model was also shown to be physically realistic by smoke tests which indicated two distinct flow regimes in the chamber, a turbulent region of intense mixing above a zone where plug flow appeared to predominate. This flow pattern was claimed to be desirable for the drying of thermally sensitive materials, the well mixed region ensuring initially rapid evaporation and the parallel flow region then ensuring no heat degradation takes place when the particles are nearly dry and most at risk.

Recently Usui et. al., [85] experimentally analysed turbulent flow and mixing in a 0.94m diameter co-current spray drying chamber in the absence of spray. Data on both the radial and axial velocity distribution were obtained using a hot-wire anemometer. It was found that the turbulent fluctuations in the spray drier were considerably larger than the usual level of turbulence in free jet or tube flow. This was attributed to the unsteady nature of the downward jet of air entering the drying chamber.

Chapter 4

Drying of Droplets and Sprays

Drying of the droplets commences as soon as the spray emerging from the atomiser contacts the air. Moisture is removed via a simultaneous process of heat and mass transfer. Heat is transferred by convection from the drying air to the droplet surface and then, following the formation of a dried layer, by conduction to the core of the droplet. Heat transfer by radiation is seldom of importance within a spray drier, being largely a wall-effect with a limited depth of penetration. Furthermore as the majority of the droplets will most probably be screened by other droplets and since the temperature driving force between any radiating surface and the droplets is unlikely to be significant, detailed consideration of radiation effects does not appear to be warranted.

Simultaneously with the heat flow into the droplet, moisture is transferred from the interior of the droplet to its surface; the mechanism of mass transfer will be dictated by the nature of the crust or skin that is formed. For example, for a porous crust-forming material, the mass transfer mechanism will probably be one of vapour diffusion through the pores, whereas for a skin-forming material, the resistance to diffusion may be such that a different moisture release mechanism, for example continuous skin bursting and reformation, predominates.

The drying history of a droplet can be followed by a drying-rate curve of the type shown in Figure 4.1. The drying rate is established the instant the droplets contact the drying air, with evaporation initially taking place from the saturated surface of the droplet. Assuming a cold feed, the droplet surface temperature therefore rises to the wet-bulb temperature of the drying air, accompanied by a slight increase in drying rate, shown as Phase AB. There are two stages of moisture evaporation. Initially moisture migration

from within the droplet to its surface is sufficient to maintain surface saturation and evaporation proceeds at a nearly constant rate. This is termed the constant rate period and represents conditions of dynamic equilibrium. It is shown as Phase BC on the drying rate curve.

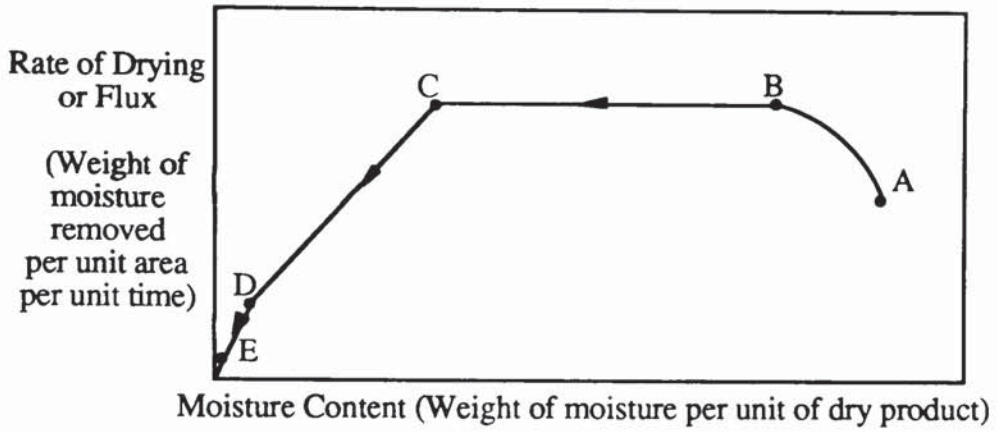

Figure 4.1 *Drying Rate Curve*

When the moisture level in the droplet can no longer maintain saturated conditions, the critical point is reached and a dried layer forms on the droplet surface. This dried layer presents a barrier to moisture transfer and acts to retain moisture within the droplet. The thickness of the dried layer increases with time, resulting in a steady fall in the evaporation rate. This is the falling rate period, shown as Phase CD. The rate of mass transfer is now dependent on the rate of moisture migration through the dried layer. This steady fall in evaporation rate will continue until no local areas of wetness remain on the droplet surface. The major resistance to mass transfer will then be in the solid layer and evaporation will continue at a decreasing rate, Phase DE, until the droplet acquires a moisture content in equilibrium with the surrounding air. During the falling-rate period of drying, the rate of heat transfer to the droplet will exceed the rate of mass transfer and this will result in a rapid rise in droplet temperature. As a consequence, it is during this mode of drying that thermal degradation may occur.

The point at which the falling-rate period of drying commences is dependent upon the properties of the droplet and upon the temperature at which drying is effected. For example in the drying of droplets of a slurry or a concentrated solution, the constant-rate period will be virtually non-existent and a dried layer will form on the droplet surface almost immediately. Similarly if drying is carried out under conditions of high air temperature, the temperature driving force may permit evaporation to commence at a rate at which migration of moisture cannot maintain surface wetness. The droplet will then experience little constant rate drying, with a dried layer, again being formed instantaneously.

In the subsequent analyses of heat and mass transfer to and from spherical droplets, a number of dimensionless groups are used to characterise the properties of the droplet and the flow conditions. These are given in Table 4.1.

Table 4.1 *Dimensionless Groups for Droplet Heat and Mass Transfer*

Group	Meaning
Reynolds (Re)	$\frac{DV_R \rho_a}{\mu_a}$
Prandlt (Pr)	$\frac{C_p \mu_a}{k_a}$
Schmidt (Sc)	$\frac{\mu_a}{D_v \rho_a}$
Nusselt (Nu)	$\frac{h_g D}{k_a}$
Sherwood (Sh)	$\frac{k_g D}{D_v}$

4.1 EVAPORATION FROM PURE LIQUID DROPLETS

For a single spherical droplet moving in a fluid, it can be expected from dimensionless analysis that the heat and mass transfer process can be described by

$$Nu = f(Re, Pr) \qquad 4.1$$

$$Sh = f(Re, Sc) \qquad 4.2$$

Much work has been done to determine the exact form of these relationships. In one of the earliest investigations Frössling (86) proposed equations of the form,

$$Nu = 2.0 + \psi\, Re^{0.5}\, Pr^{0.33} \qquad 4.3$$

$$Sh = 2.0 + \psi\, Re^{0.5}\, Sc^{0.33} \qquad 4.4$$

Various values have been experimentally determined for the constant ψ [87,88], but the most widely applied is that due to Ranz and Marshall [89] who suggested that $\psi = 0.6$ For evaporation in still air conditions, or when the relative velocity between droplet and the air is negligible, Re = 0 and the above equations reduce to

$$Nu = Sh = 2.0 \qquad 4.5$$

The actual heat and mass transfer rates in a spray drier may be expected to differ from those obtained by equations 4.3 and 4.4, because a number of simplifications have been introduced in the development of these equations These are,

(i) Any heat transfer to the vapour diffusing out of the droplet is neglected; for spray driers operating under high temperature conditions this is not valid, since a significant enthalpy is associated with the vapour as it leaves the droplet surface [90].

(ii) The droplet internal structure is assumed to be stable; in reality internal circulation, oscillation or surface distortion will increase heat and mass transfer rates.

(iii) The droplets are assumed to be non-rotating; in practice inter-droplet, or wall-droplet collisions, or the effects of fluid shear may result in droplet rotation, thus increasing evaporation rates.

4.2 SPRAYS OF PURE LIQUID DROPS

The evaporation characteristics of droplets within a spray differ from those of single drops. Although the same basic theories apply in both cases, any analysis of spray evaporation must consider (a) the relative velocities between the air and droplets (if

significant), (b) the particle trajectories, (c) the droplet population density, and (d) the representation of the spray by a mean diameter and/or drop size-distribution.

Dloughy and Gauvin [91] conducted an investigation on evaporation rates in spray drying, by progressively following evaporation of a spray of water droplets down a purpose-built co-current spray drier. They considered the drying chamber to consist of three distinct zones: the nozzle zone, in which droplets decelerate from their initial release velocity to their terminal settling velocity, the evaporation zone, where the mechanism of evaporation is the same as that from a free liquid surface (i.e. the constant rate period) and finally the drying zone in which moisture diffusion through the crust becomes the controlling factor (i.e. the falling rate period). To calculate the rates of heat and mass transfer in the evaporation zone, samples of air and water droplets were taken at a succession of points down the tower and instantaneous heat and mass transfer coefficients were calculated from energy and material balances. They concluded that the presence of the droplets as a spray had no influence on the rate of evaporation. Furthermore, for the range of droplet size considered in the study, 11.5 - 38.5 microns, the heat and mass transfer coefficients were the same as for single stationary droplets evaporating in still air, i.e. Nu = Sh = 2.0. This was attributed to equal eddy diffusivities of the droplets and the surrounding air, resulting in a negligible relative velocity. Although the evidence presented appears to be conclusive, it is doubtful whether it can be extended to the much larger droplets i.e. up to 500 microns, that may be present in industrial driers.

The conclusions drawn by Dloughy and Gauvin were in fact contradicted by Bose and Pei [92] in a later study. Both of these studies were similar in nature but a larger range of drop size, 40 - 125 microns, was considered in the latter investigation. Repeating the procedure of Dloughy and Gauvin [8], Bose and Pei [9] found that their experimentally determined values of heat and mass transfer coefficients could not be adequately correlated by Nu = Sh = 2.0. They therefore proceeded to evaluate droplet relative velocities and compare their experimental coefficient values with the Ranz and Marshall correlation. A

much better agreement was obtained, suggesting that the relative velocity existing between droplet and surrounding air is not negligible . They concluded that for industrial applications, where the droplet diameters are of a larger range, relative velocities between air and particle must be taken into consideration in the calculation of the heat and mass transfer effects.

Dickinson and Marshall [93] conducted a computational study on the rates of evaporation of sprays of non-uniform drop size distributions. They considered the cases of negligible and appreciable relative velocities with respect to the evaporation rates. Certain assumptions were made in order to simplify the modelling. These included an ideal air flow, i.e no back-mixing and more importantly that the spray comprised drops of pure liquid, implying that the droplet temperatures remained constant at the wet-bulb temperature. Nevertheless, the study did highlight several significant phenomena. For sprays moving at negligible relative velocity the investigation showed that

(a) The drying air temperature falls as the spray evaporates, resulting in a decrease in evaporation rate.

(b) Sprays with less uniform drop size distributions evaporate more rapidly at first than more homogeneous sprays with the same mean diameter. This is because the smaller droplets present, evaporate at higher rates. However the less uniform sprays take much longer to effect complete drying because of the larger droplets that are present.

(c) No mean diameter can adequately characterise a spray with respect to evaporation; two sprays with the same mean diameter but with different drop size distributions will almost certainly take different lengths of time to evaporate. Hence the drop size distribution must be taken into account.

(d) The size distribution of droplets changes during evaporation: for non-uniform sprays the mean diameter first increases initially and then decreases until completion of evaporation.

For sprays moving with significant relative velocity the study highlighted additional features:

(a) To achieve a given degree of evaporation the spray must travel a far greater distance. This is obviously because the residence time of such sprays in a given length of tower is less than for droplets travelling at their terminal velocities.

(b) The effect of relative velocity is more significant at higher initial velocities and at higher drying temperatures.

(c) For high initial velocities, the relative error in neglecting drop velocity is greatest for small drops. This is because such drops evaporate extremely rapidly and a large proportion of the evaporation occurs during droplet deceleration.

4.3 EVAPORATION FROM DROPS CONTAINING SOLIDS

The presence of dissolved solids in a droplet will result in a lowering of the vapour pressure of the solvent so that the surface temperature of the droplet will increase above the wet bulb temperature. Initially a free liquid interface exists between the drying air and the solution being dried and evaporation proceeds as for a pure liquid. When the solution is concentrated beyond saturation, a crust forms to separate the air and liquid interface and a particle with a core of saturated solution results. (This may be preceded by porous skin formation with some materials, e.g. coffee, skimmed milk).

Once the crust has formed, the subsequent mechanism of drying will depend upon the nature of the crust, i.e. the porosity and rigidity, and upon the operating conditions. If the air temperature is above the boiling point of the droplet solution, the liquid inside the droplet will reach its boiling point and vapour will be formed. This can lead to pressure forces being set up within the drop. The consequences of this will depend upon the nature of the crust. If the crust is sufficiently porous the vapour will diffuse out. If the crust is

non-porous the droplet may rupture or even disintegrate releasing jets of steam and resulting in fragmented shells and fines. If the residence times of the droplets in the hotter zones of the drier are sufficiently small, the liquid will not reach its boiling point and moisture will be removed via diffusion through the pores and then by convection into the air stream. The formation of a non-porous film or skin prior to crust formation has been observed with certain materials. If this is the case then the only mechanism whereby moisture can be transferred to the drying air is by the continuous rupturing of this film.

The effect of crust properties on droplet drying time is shown in Figure 4.2. If the droplet forms an impervious skin or film at its critical moisture content, then the drying rate falls sharply and the evaporation time for complete moisture removal is greatly extended. Alternatively if a porous crust is formed, vapour diffusion is hindered to a far lesser degree and the drying rate only falls gradually from that established during the constant-rate period of drying.

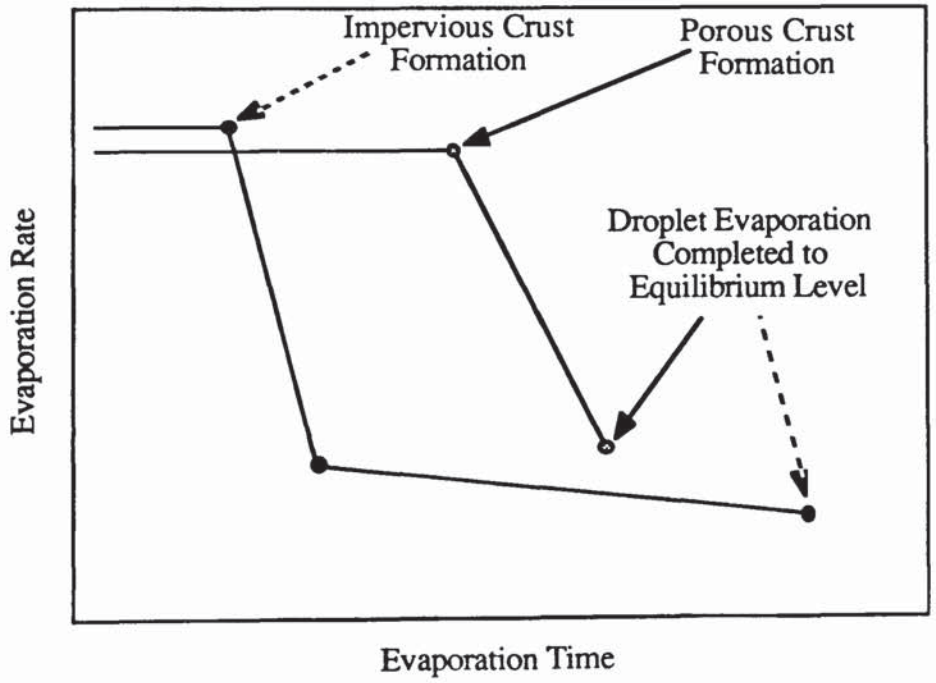

Figure 4.2 *Effect of Crust Properties on Evaporation Rate*

Charlesworth and Marshall [94] studied the evaporation characteristics of single stationary drops containing dissolved solids. They presented illustrations for the appearance changes of different crust-forming materials. Different phenomena were observed depending on whether the drying air temperature was above or below the boiling point of the droplets. Figure 4.3 demonstrates that non-porous crust forming droplets will experience shape changes. Such droplets may inflate or shrivel depending on air temperature.

Audu and Jeffreys [95] studied the drying of droplets and particulate slurries in a horizontal wind tunnel. They correlated the coefficient of mass transfer through the crust in terms of the diffusion coefficient, crust porosity and thickness as follows

$$k_c = \frac{D_v \varepsilon^{1.5}}{\beta} \qquad 4.6$$

where ε is the porosity and β is the crust thickness.

Equation 4.6 can be used together with a correlation for the gas film mass transfer coefficient e.g. of the form of equation 4.4, to calculate the overall mass transfer coefficient. The variation in droplet velocity and drying conditions down a spray drier and the fact that the crust increases in thickness as drying proceeds, means that the value of the overall mass transfer coefficient for a droplet will continuously change throughout drying. The calculation of this parameter will therefore only be useful in an overall simulation of the spray drier, where such variations can be predicted.

Cheong [96] recently developed a model based on a receding evaporation interface to predict the simultaneous heat and mass transfer rates in the drying of single drops of slurries of sodium sulphate decahydrate. Predicted wet core temperatures and droplet weights showed good agreement with experimental data.

(a) The temperature of the drying air below the boiling point of the liquid

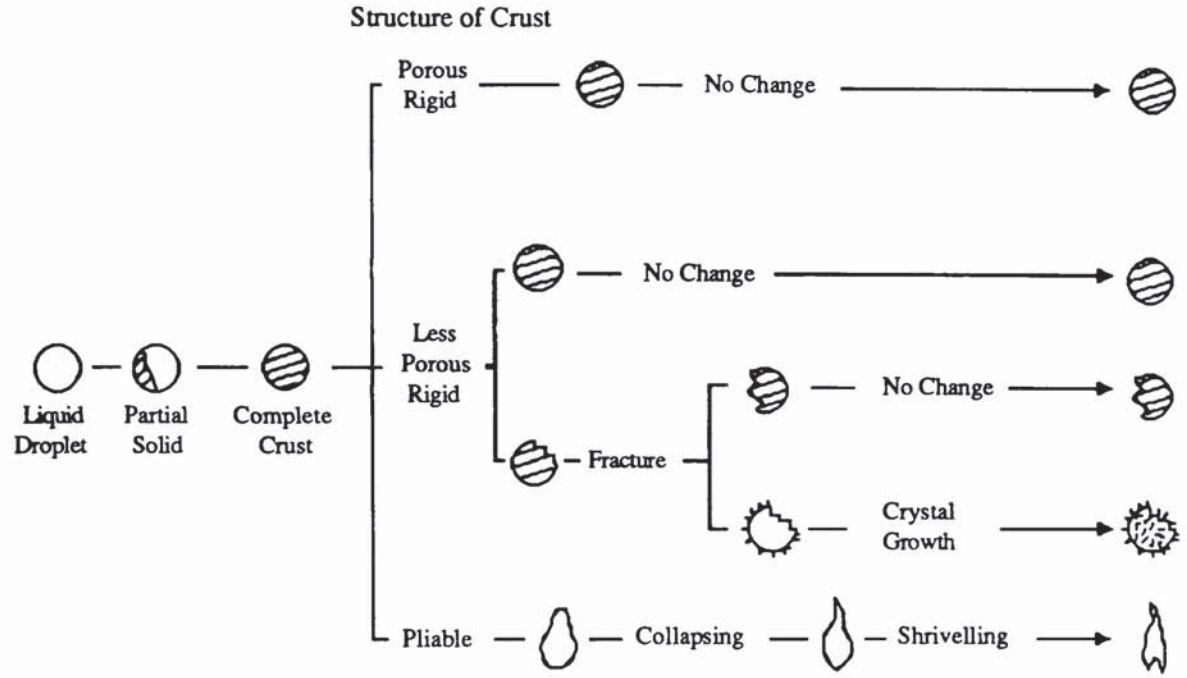

(b) The temperature of the drying air above the boiling point of the liquid

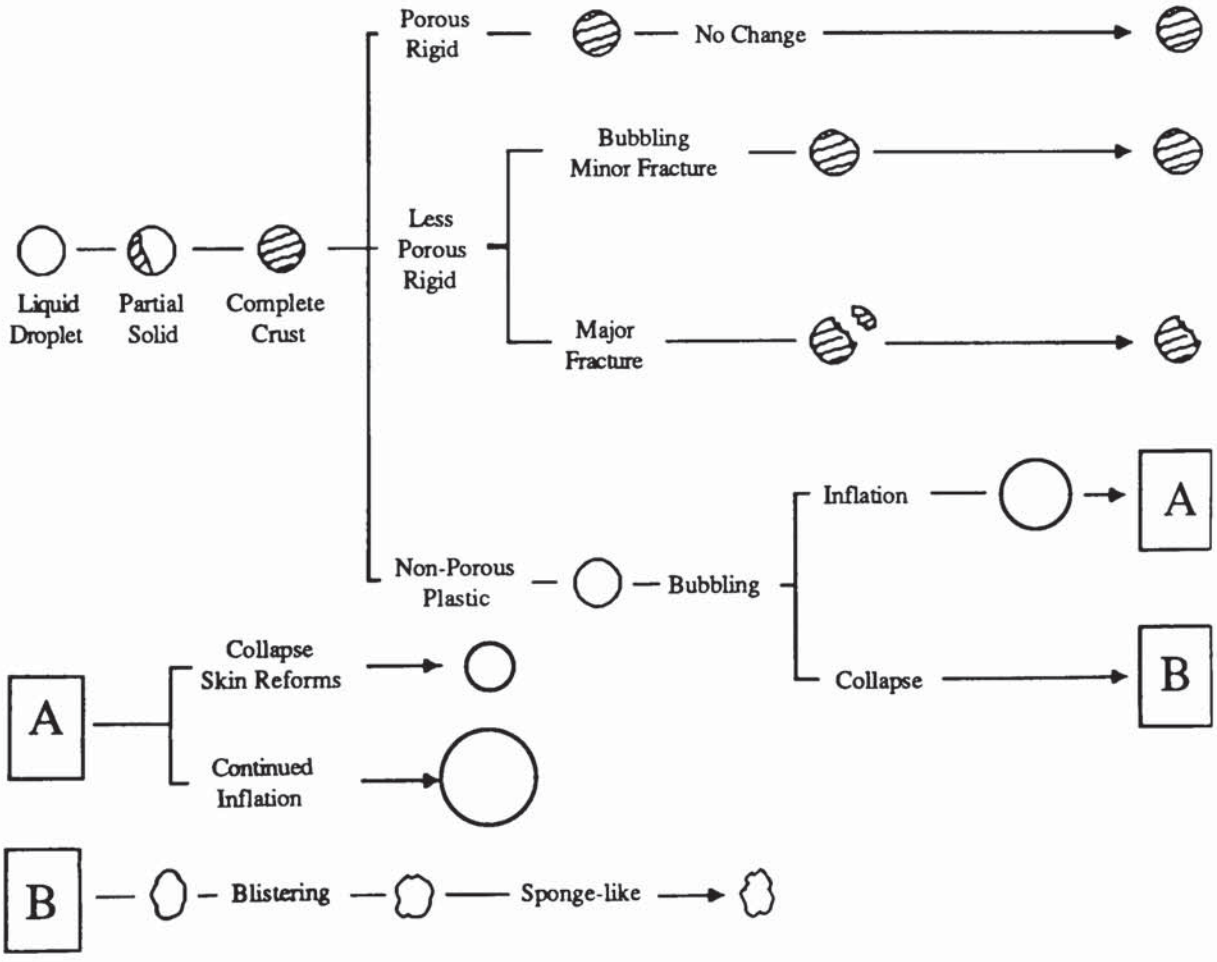

Figure 4.3 *Characteristics of Droplets Undergoing Drying*

4.4 SPRAYS OF DROPS CONTAINING DISSOLVED SOLIDS

The theoretical considerations of heat and mass transfer of single droplets also apply to sprays of droplets. The extent of vapour- pressure lowering will depend on droplet size and thus the onset of crust formation will not appear simultaneously throughout the spray distribution.

Dloughy and Gauvin [97] were among the few workers to study specifically the evaporation of sprays containing dissolved solids. They showed that a step-wise method could be employed to calculate the total spray evaporation time with a fair degree of accuracy.

Baltas and Gauvin [98] employed a computational study but considered only a simple system of spray movement at terminal velocity in the free-fall zone of a single nozzle drier. They suggested that the difficulties in accurate prediction of spray evaporation were due to the lack of representative data regarding air flow, temperature gradients and chamber shape.

Duffie and Marshall [99] studied the effect of air temperature, feed concentration and feed temperature on the bulk density of several spray dried materials but they presented data which was inconclusive.

Crosby and Marshall [100] attempted to relate wet drop sizes to the final dried particle size but, not surprisingly, found their results dependent on the type of material being spray dried. The dried particle properties could be varied within a limited range by control of operating parameters. The dried particle size however, was found to rarely exceed that of the wet spray. However in some practical drying operations the drops are required to 'puff-out', e.g. detergents to give a low bulk density product.

4.5 FACTORS INFLUENCING THE PROPERTIES OF SPRAY DRIED PRODUCTS

Spray drying produces particles which are approximately spherical and more or less hollow, depending on the type of material and the drier operating conditions. Spray drying is not well-suited for the production of solid spherical particles;hollow particles are the rule and solid particles the exception. There are four main causes of hollowness in spray dried materials:

(i) Hollow particles may result from the rapid formation of a surface layer which is semi-impervious to vapour flow. This will lead to puffing or ballooning of the particle due to the pressure of the vaporised moisture trapped within the particle.

(ii) If the rate of moisture evaporation exceeds the rate of diffusion of solids back into the drop, then upon completion of drying,air voids will be present resulting in a hollow particle.

(iii) Hollow particles may form in the drying of drops of suspended solids as a result of capillary action, drawing liquid and solids to the droplet surface, leaving behind a void at the centre of the drop.

(iv) Hollowness or porosity may result from air entrained in the feed, or during atomisation, which cannot escape during drying. If excessive, this will result in a spray dried product with a honeycomb type structure. Thus the feed mixing conditions and the presence of foaming agents, or anti-foam additives, are important considerations.

The degree of voidage in the particles of a spray dried material will obviously have a large impact on the product bulk density; this being probably the most important single property of a spray dried product. Bulk density influences the size and cost of storage containers, and of cartons in which a given weight of the product is marketed.

The bulk density of a spray dried product can be controlled, to a certain degree, by the operating conditions of the drier. The influence of various drier parameters on product bulk density can be established by carrying out a systematic, logical analysis on the drying process as shown in Table 4.2. This analysis is based upon the assumption that an increase in the drying temperature will result in an increase in the porosity or hollowness of a droplet. Whilst in general this will be true, the degree to which it occurs will be specific to the nature of the feedstock; in particular the permeability of any skin that is formed.

The nature of the feed material is, in fact, critical, in controlling particle morphology, independent of drying conditions. For example if the feedstock contains a high proportion of dissolved solids particularly of an organic nature e.g. dyes and surfactants, then the dried particles will consist of smooth-walled hollow spheres; the density being dependent on the wall thickness and whether any pores exist in the sphere walls [101]. If the feedstock contains no dissolved solids then the spheres are likely to be thin-walled and consequently a low bulk density product will result.

In the drying of dispersions the structure of the dried product will be dictated by the size and shape of particles in the feed material. For example, for large-sized particles, the dried product will consist of predominantly single or aggregates of few of the particles that were originally dispersed in the feed. If the dispersed particle size is reduced, the dried product will form spheres made up of clusters of larger numbers of the primary particles.

Table 4.2 *Effect of Drier Operating Variables on Product Bulk Density*

Operating Variable	Effect on Bulk Density
1. Feed Rate	Increase in feed rate → Higher residual moisture content / More drying → Lower tower temperature → Less drop puffing → Higher bulk density
2. Droplet Size	Increase in drop size → Less surface area → Less evaporation → Higher tower temperature → More drop puffing → Lower bulk density
3. Air Inlet Temperature	Increase in air inlet temperature → Higher tower temperature → More drop puffing → Lower bulk density
4. Air Flowrate	Increase in air flowrate → Higher tower temperature → More drop puffing → Lower bulk density
5. Turbulence	Increase in turbulence → Higher relative velocity → Higher transfer coefficients → More drying → Lower tower temperature → Less drop puffing → Higher bulk density
6. Tower Height	Increase in tower height → Longer drop residence time → More drying → Lower tower temperature → Less drop puffing → Higher bulk density

Chapter 5

Review of Spray Drying Models

Numerous models have appeared in the literature for the purpose of predicting the movement and/or drying of spray in a spray drier. In the modelling of spray-air contact, three transfer mechanisms must be considered; namely mass transfer, heat transfer and momentum transfer. Each mechanism comes into operation the instant the droplets contact the drying air. Mass transfer occurs due to the difference between the concentration of water vapour at the droplet surface and in the air. Heat transfer to the droplet results from the difference in droplet temperature and the local air temperature. The droplet's drying behaviour is dictated by the rates of both heat and mass transfer, which in turn are themselves dependent upon the rate of momentum transfer between the droplets and air. This last transfer mechanism, in the form of aerodynamic drag, acts to establish the trajectory and residence time of a droplet, and its velocity relative to the air stream. Thus all three transfer mechanisms are interactive and are functions of the drop size, and of the properties of the liquid feed and the drying air.

Early models were developed upon the assumption that the condition of the drying air was unaffected by the evaporating droplets. With such "One-way Coupling", although the droplet properties change as a result of the drying process, the properties of the drying air were assumed to remain unaltered. This oversimplification may have some justification for regions in a spray drier which can be assumed to be perfectly mixed, as described in Chapter 3. In such regions the properties of the drying air would remain constant corresponding to the exit value of the well-mixed zone.

Clearly models which take into account transfer between both phases in the spray drier are more realistic and are therefore more likely to accurately mimic spray drier

performance. This second approach is termed "Two-way Coupling" and represents a significant increase in modelling complexity.

In addition to the degree of phase coupling, spray drying models can be further subdivided according to their geometry [102]. Models can be classified as one-dimensional, quasi-one dimensional or axisymetric. A one-dimensional model involves an assumption that changes occur in one direction only, usually the axial flow direction. A quasi-one dimensional model allows for variations cross-sectionally, but assumes that the properties of both the liquid feed and the heating gas are uniform over a given cross-section. This approach may be particularly useful in describing the region near the atomiser, since the drier area can be subdivided into a droplet spray area and an annular droplet - free area. Finally the axisymetric model allows for property changes in both the radial and axial directions, but assumes no change occurs in the circumferential direction.

The system of model classification described above can now be used, as shown in Table 5.1, to describe the various types of model appearing in the literature.

5.1 ONE-WAY COUPLING, ONE DIMENSIONAL MODELS

In 1950, Seltzer and Marshall [103, 104] developed equations for the lifetime of a pure liquid drop evaporating in a hot air stream. Based upon a constant temperature driving force between air and droplet and a zero relative velocity, the following equation was proposed:

$$t = \frac{\rho_L \lambda}{2\Delta T} \int_o^{D_I} \frac{dD}{h_g} \qquad 5.1$$

The correlation suggested by Frossling [86], equation 4.3, was also applied to give the following more general equation:

Table 5.1 *Classification of Spray Drying Models*

	One-way	Two-way
One-dimensional	Seltzer and Marshall [103, 104] Sjenitzer [105] Duffie and Marshall [106] Kerkhof and Schoeber [107] Masters [17] Holland-Batt [108] Janda [109] Janda [110]	Marshall [117] Dickinson and Marshall [93] Parti and Palancz [121] Topar [122] Goffredi and Crosby [118] Yuan et. al., [119] Miura et. al., [120] Keey et. al., [123]
Quasi-one-dimensional	Gluckert [111]	Pham and Keey [124] Keey and Pham [125, 126] Katta and Gauvin [127, 128] Gauvin, et. al., [129]
Axisymetric	Lapple and Shepherd [47] Masters [17] Coulson and Richardson [51] Edeling [113] Rawson et. al., [114] Holland-Batt [115] Bailey et. al., [116] Cheng-yi [112] Kerkhof and Schoeber [107]	Baltas and Gauvin [131] Crowe et. al., [132,133]

$$t = \frac{\rho_L \lambda}{4\Delta T k_a} \int_0^{D_I} \frac{DdD}{1 + 0.276\, Pr^{0.33}\, Re^{0.5}} \qquad 5.2$$

where D_I was the initial droplet diameter.

The above equations were used to compare lifetimes of pure liquid drops for zero relative velocity conditions, with their lifetimes if they were moving throughout at a terminal velocity in accordance with Stokes law. It was concluded that for droplets travelling at their terminal velocities, the effect of the relative velocity between the droplet and the air was negligible for initial drop diameters of 300 μm or less.

Sjenitzer [105] considered the evaporation of pure liquid drops and presented charts for the determination of "braking times" and "braking distances" for droplets to decelerate from a high initial velocity to their terminal velocity. The effect of gravity was ignored in the analysis. The correlation suggested by Frossling [86] was used to calculate the fractional evaporation occurring in the deceleration period and in the free-fall period. It was concluded that for droplets of diameter 100μm or less, the evaporation during the deceleration period could be ignored.

Duffie and Marshall [106], in 1953, extended the work of Seltzer and Marshall and developed equations for the lifetime of a pure liquid drop in the intermediate region of Reynolds number, 0.2 - 500, where Stokes law is not applicable. In addition, equations were developed similar to those of Seltzer and Marshall but based on the Ranz-Marshall correlation.

Kerkhof and Schoeber [107] used a third order Runge-Kutta method to simultaneously solve the equations of motion, heat and mass transfer for the case of water droplets moving vertically in still air. Constant air properties were assumed for the analysis. The results so obtained were compared to those predicted by the method of Sjenitzer [105]. It was concluded that the latter method was only valid for smaller sizes of droplet, typically less than 100μm.

Masters [17] used the equations of Lapple and Shepherd [47] to show how the deceleration time of drops injected vertically downward into a drying gas stream can be predicted. However the analysis of Lapple and Shepherd is based upon unchanging particle mass and therefore has limited value in spray drier computations.

Holland-Batt [108] described a system of equations for determining the accelerations, velocities and distances travelled by solid particles of constant mass experiencing unsteady linear motion in a fluid. This method was based upon the use of four different Reynolds numbers to describe particle-behaviour.

Janda [109] presented equations for the prediction of horizontal droplet trajectories and droplet drying times within rotating disc spray driers incorporating swirl flow, counter-current to the direction of disc rotation. The tangential velocity profile was given by an equation of the form:

$$V_{at} = \frac{a}{r^b} \qquad 5.3$$

The droplet trajectory was considered in two parts. Droplet motion in the horizontal plane was initially considered to be counter-current to the air flow. The droplet was therefore progressively decelerated until it was eventually entrained. The droplet was then assumed to take on the velocity of the air stream. Droplet motion in this second co-current region was predicted using a modified form of the equations presented by Lapple and Shepherd. The equations of droplet motion were combined with a prediction of droplet drying time to estimate the chamber diameter required to dry a given size particle. However in the estimation of drying time it was assumed that the drying of particles of diameter less than 300 μm occurred entirely in the constant rate period.

In a further study, Janda [110] developed a computer model to calculate the minimum height of a spray drying tower fitted with a pressure nozzle. In this study it was again assumed that drying of particles up to 300μm in diameter occurs entirely within the

constant rate period, such that all the heat supplied to a droplet is accounted for by evaporation. Equations for prediction of vertical droplet movement and drying time were presented and solved by digital computer for various flow arrangements. No comparison with experimental data was reported. The basic assumption restricts application of the model to low solids concentration solutions and excludes slurries where a constant rate period is practically non existent.

5.2 ONE-WAY COUPLING, QUASI-ONE DIMENSIONAL MODELS

Gluckert [111] in a theoretical correlation of spray drier performance, developed equations to predict the maximum heat transfer rate obtainable if the largest particles in a spray were to be dry before striking the walls of the drying chamber. The analysis considered pneumatic, pressure nozzle and centrifugal atomisers and was based upon the assumption that the time of flight of the largest droplets to the chamber wall could be determined by integrating the equation for velocity decay in a free jet. Further assumptions included negligible relative velocity between droplets and air, constant droplet diameter, and extensive recirculation of air within the drying chamber such that well-mixed conditions prevailed. The validity of ignoring the relative velocity is however extremely doubtful in light of the large droplets characteristic of spray driers e.g. up to 500μm. For pneumatic atomisers the following equation for the maximum heat transfer rate was obtained:

$$q_m = \frac{6.38 k_a v^{2/3} \Delta T G_L}{(D_{max})^2 \rho_L} \sqrt{\left(\frac{\rho_a}{G_a V_a}\right)\left(\frac{G_a + G_L}{G_a},\right)} \qquad 5.4$$

For pressure nozzle atomisers the trajectory of the spray was computed from measurements of the velocity of the air entrained into the spray cone. The velocity was assumed to approximate to the spray velocity. The axial decay of the air velocity was found experimentally to follow the relationship:

$$\frac{V_{az}}{V_o} = 3.2 \left(\frac{D_o'}{Z}\right) \qquad 5.5$$

where

$$D_o' = D_o \left(\frac{\rho_L}{\rho_a}\right)^{1/2}$$

The maximum heat transfer rate was then found to be:

$$q_m = \frac{10.98\ k_a\ v^{2/3}\ \Delta T}{(D_{max})^2} \quad D_o \sqrt{\frac{\rho_a}{\rho_L}} \qquad 5.6$$

For centrifugal atomisers the following expression was developed:

$$q_m = \frac{4.19\ k_a\ (R_{ch} - \frac{r_o}{2})\ \Delta T}{(D_{max})^2\ \rho_L} \sqrt{\frac{G_L\ \rho_a}{r_o\ N}} \qquad 5.7$$

Experimentally measured rates of heat transfer for the drying of sodium sulphate and calcium carbonate solutions in co-current driers of diameters 0.3, 0.6 and 0.9m on average fell 52% above the theoretical minimum heat transfer rate at capacity conditions. However, Gluckert concludes that because the chamber diameter varies approximately as the square root of the heat transfer rate, the theory could be used to specify drier diameter to within about 20%.

5.3 ONE-WAY COUPLING, AXISYMETRIC MODELS

When droplets are released from an atomiser with significant radial velocity, the flow pattern cannot be accurately modelled using a one-dimensional model. In such cases two-dimensional models are preferred.

Lapple and Shepherd [47] developed equations for the motion of spherical particles of constant mass. They considered the cases of two dimensional motion in a gravitational field and two dimensional motion in a centrifugal field. Masters [17] has presented a step-wise procedure for solving equations developed for the first case and given examples for the cases of droplet release from a rotary atomiser in still air conditions and from a nozzle atomiser with air flow.

Coulson and Richardson [51] presented a system of equations and a solution scheme for particles of constant mass travelling radially and dropping axially due to gravity. However the analysis was not applied to spray drying systems.

Cheng-Yi [112] developed an analytical solution to the two-dimensional motion of a droplet in a spray drier. However, once again the droplets were assumed to be of constant mass.

Edeling [113] proposed a design procedure for estimating the diameter of a co-current spray tower from predicted spiral trajectories. In his study the tower was divided into two regions, the spray penetration zone and the zone of free-fall. The boundary between the zones was assumed to be the point at which the droplets attained their terminal velocity and became influenced by the swirling air flow pattern. As a result of the centrifugal force, the droplets spread towards the wall of the drying chamber. Edeling developed the following simple expression for the ratio of particle radial velocity to the terminal velocity.

$$\frac{V_r}{V_f} = \frac{g}{(V_{to})^2} \Big/ R_{ch} \qquad 5.8$$

where V_{to} is given by the following approximate relationship for the tangential velocity,

$$V_t = (V_{to}) \Big/ \sqrt{r/R_{ch}} \qquad 5.9$$

where V_{to} is the tangential velocity at the wall.

It was proposed that equation 5.9 could be used, in combination with an estimate of the drying time to predict the required tower diameter.

Rawson [114] et. al., developed a model relating the velocity temperature composition, radius and position of an evaporating liquid drop falling through a heated environment. The equations of motion, heat and mass transfer were solved using an

integrative step-by-step finite difference procedure. However, again the model was not applied to droplets in a spray drier.

Holland-Batt [115] in an extension of an earlier study, demonstrated a technique for predicting the two-dimensional trajectories of particles experiencing unsteady motion. Analytical solutions were obtained for motion in the laminar and turbulent regimes whilst for the transitional regime, $1<Re<1000$, a numerical integration was employed using a suitable relationship between the drag coefficient and Reynolds number.

Bailey et. al., [116] solved equations of motion and heat and mass transfer for pure liquid droplets evaporating in a co-current rotating hot air flow. The tangential velocity flow field of the air was assumed to consist of a 'forced vortex' i.e. solid body rotation, in a central core of radius 1/5 the radius of the drying chamber, with the annulus being in 'free vortex' flow. The effects of mass transfer on the drag and heat transfer coefficients were taken into account in the analysis. The examples described to show application of this technique were however related to spray reactors rather than spray driers. No comparison with experimental data was reported.

Kerkhof and Schoeber [107] used a third order Runge-Kutta method, with a variable step size, to integrate equations to predict the three-dimensional trajectories of evaporating water droplets in rotating air flow. The air velocity was assumed to consist of a tangential velocity component dependent upon the radial position, as was given by Bailey et. al. [116], and a uniform vertical component. Constant air properties were assumed in the analysis and no experimental verification of the model predictions was reported.

5.4 TWO-WAY COUPLING, ONE DIMENSIONAL MODELS

The studies reviewed so far have neglected any effects which the droplets may have on the gaseous phase. Furthermore the amount of validation of model predictions was

minimal. The models that will be discussed in the following sections incorporate transactions between the phases for at least one transfer mechanism.

In 1955 Marshall [117] suggested a procedure for estimating the influence of droplet size distribution on spray drier performance. The analysis involved a step-wise procedure whereby the size distribution of a pure liquid spray was divided into small size increments each represented by an average diameter. The evaporation of each size of droplet was then considered independently by applying the equations of Duffie and Marshall [106] over small time increments. At the end of each time interval a new drop size distribution was drawn-up and the fractional evaporation and fractional drop in air temperature calculated. The procedure was repeated for the new drop sizes and temperature driving force until complete evaporation had been effected.

Dickinson and Marshall [93] later extended this computational scheme to include an energy term to account for the change in temperature of humid air as a result of droplet evaporation.

Goffredi and Crosby [118] developed a model for a prediction of spray drier performance based upon the analytical solution of differential forms of overall spray drier mass and energy balances. In this study, a homogeneous drop size distribution of less than 100μm in diameter was assumed, presumably to permit the assumption of no relative velocity between the droplets and the drying gas. Design equations were presented for co-current plug flow and co-current mixed flow operation for both pure liquid and solid-containing feeds. Although no comparison with experimental data was reported, the application of these equations for the prediction of existing spray drier performance was exemplified.

Yuan et. al., [119] developed a one-dimensional mathematical model for a co-current spray drier which took into account the droplet size distribution by means of a volume-frequency function. It was assumed that the droplets had negligible relative velocity to the

drying gas, with the absolute velocity given by the centre-line velocity of a jet. The vertical velocity difference between the drying droplets was also assumed to be negligible, so that droplet residence time could be assumed to be a drop-size-independent variable in the analysis. The differential equations that were formulated were solved using a numerical method and the model was tested by comparing the predicted air temperature profile to that measured in a pilot scale spray drier, 4.8m in height and 1.6m diameter, whilst spraying a mixed solution of Na_2HPO_4 and NaH_2PO_4. The measured air temperature profile consisting of 3 data points agreed almost exactly with the predicted profile, and this was used to verify the adequacy of the model for drier design. However, this limited experimental verification is unlikely to be sufficient to adequately assess the reliability of the model.

Miura et. al., [120] numerically computed the drying histories of droplets, together with the resulting changes in air temperature and humidity, for a laboratory co-current spray drier with pneumatic atomisation. In the computation the initial drop size distribution was given by the Nukiyama - Tanasawa equation [26] and the axial air velocity in the spray was assumed to be that in a free jet. The additional resistance to mass transfer arising upon formation of a solid crust was ignored in this analysis and the equation proposed by Charlesworth and Marshall [94] to predict solid crust formation was used to establish completion of drying. The predicted air temperatures and humidities for evaporation of water and sodium sulphite sprays were compared to experimentally-determined data. Almost exact agreement was reported.

Parti and Palancz [121] developed a general mathematical model which was applicable to co-current and counter-current drying. It was assumed that the particles were all of uniform size and that their velocities were in the vertical direction only. The model incorporated mass and heat transfer coupling between the air and the droplets. No comparison of model predictions with experimental data was reported. Topar [122] later modified the model to cope with droplets with a distribution of sizes.

Keey et. al. [123] developed a computer-aided design program for evaluating spray driers. The computer program was applicable to co-current driers and used an empirically-determined relative drying factor to predict droplet evaporation in the falling-rate period. The program employed a step-wise procedure, with the assumption of a uniform drop size distribution, to determine the average evaporation rate and hence the required particle residence time. An empirical chamber effectiveness factor was then introduced, defined as the ratio of the particle to gas residence time, and this was used to yield the required chamber volume. Validation of the model was not reported.

5.5 TWO-WAY COUPLING, QUASI-ONE DIMENSIONAL MODELS

Pham and Keey [124] modelled a co-current spray drier by dividing the chamber into two zones: a jet zone, in which the aerodynamic conditions are governed by the characteristics of the nozzle and a main zone in which the particles fall at their terminal velocity. In the jet zone the temperature and velocity vary axially as well as radially. In order to simplify the problem of predicting heat, mass and momentum transfer in this zone, these complex profiles were replaced by "equivalent flat" profiles. The problem thus became quasi-one dimensional and was numerically solved. The transition from the jet zone to the main zone in the spray drier was determined empirically. Computer-predictions of droplet velocity and evaporation for a water spray were compared to experimental data. Satisfactory agreement was reported.

In a further study, Keey and Pham [125, 126] applied the same model to the drying of skimmed milk concentrate in a co-current drier. In this instance, drying in the falling-rate period was estimated by the use of a relative drying factor, defined as the ratio of the actual drying rate to the drying rate of a pure liquid drop under the same external conditions. This factor was determined from experimental single droplet studies. The computed average moisture content was compared to limited experimental data and found to agree to within 0.4%.

Katta and Gauvin [127, 128] and Gauvin et. al., [129] developed a quasi-one dimensional model to predict the movement and drying of droplets in a co-current spray drier. For this purpose the drying chamber was divided into a nozzle zone, where the droplets decelerate from their initial release velocity, and a free-entrainment zone where they are conveyed by the drying gas. The boundary between the two zones was established using empirical data. In the nozzle zone the air velocity was computed from empirical correlations applicable to jets; in the free-entrainment zone, experimentally-determined velocity profiles were used [130]. An energy balance for each region was used to predict gas temperature and it was assumed that no radial variations existed at any given cross-section. Empirical data was used to predict the air entrainment rate at the jet boundary. Droplet trajectories were calculated numerically by integrating the equations of motion through the prescribed flow field. Simultaneously heat and mass transfer equations were solved to yield the drying history of the droplets. The model was tested by making comparisons with experimental observations of the effect of a number of variables upon the maximum evaporative capacity of a 1.22m diameter co-current drier. This was defined upon the basis of the maximum feed rate obtainable without wall accumulation. For two different sets of drier operating conditions, corresponding to the maximum evaporative capacity of the drier, the model showed that the largest droplet in the spray should become almost dry by the time it reached the chamber wall. For a slightly larger feed rate, or droplet size, wet particles were predicted to hit the chamber wall and this was in agreement with experimental observation. This was used to establish validity of the model.

5.6 TWO-WAY COUPLING, AXISYMETRIC MODELS

Baltas and Gauvin [131] presented a step-wise procedure for predicting evaporation of droplets falling at their terminal velocity in the spray drier. The cross section of the drier was considered as a number of concentric zones consisting of a central core and nine annuli. A turbulent radial diffusivity was determined equal to that of the air and was used to quantify the effect of interchange of vapour and drops between annuli. Equations were developed for the prediction of changes in droplet water content and changes in the

humidity of the air in each annulus. The latter was determined by taking into account the amount of water evaporated in the annulus and the vapour transfer between annuli. The local air temperature was determined as a function of the humidity. The radial variation in properties was hence established. The model was applied to the drying of a salt solution but was not completely successful in describing the spray evaporation; the predicted evaporation rate being as much as 3.5 times the experimental. This discrepancy was attributed, in part, to the difficulty in establishing accurate experimental data for input to the model.

More recently Crowe et.al., [132, 133] proposed a model which incorporated complete coupling and accounted for property changes in both the radial and axial directions. In this model, the flow field is divided into a network of computational cells. Mass, energy and momentum balances over each cell are solved to give the local pressure, temperature and velocity. The use of this type of model, would however, be limited to relatively simple types of drier because of its extreme complexity.

In conclusion, it is apparent from the literature summarised in this chapter that there is a severe limitation to the applications of models to predict:

a) the progress of drying following the commencement of formation of a solid crust on the surface of a single drop;

b) the drying of swarms of droplets with a distribution of drop sizes and the occurrence of possible inter-particle impingement and agglomeration; and

c) droplet drying and motion in the more complex counter-current spray drier configuration.

Another feature highlighted by the review is the lack of models that are sufficiently detailed to serve as a useful tool during spray drier design and optimisation but which are not so complex as to be of little practical use. It was also clear that, as in some other areas of drying research, many studies did not include even rudimentary experimentation to validate the models proposed.

In this study a new mathematical model has therefore been developed which:

a) can predict the drying progress of a single droplet in the falling rate period;

b) is applicable to droplets with a distribution of sizes;

c) can be applied to both co-current and counter-current drying; and

d) is flexible such that it can be easily applied to a variety of spray drying situations and at the same time is believed to predict drier performance with reasonable accuracy.

A detailed description follows in the next chapter.

Chapter 6

A Mathematical Model for the Spray Drying of Slurry Droplets

The majority of the models published in the literature deal with evaporation from liquid drops or with the drying of slurry or solution droplets during the constant rate period, when the saturated-surface evaporation mechanism is similar to that of liquid drops. Calculations based upon liquid drops are only useful, however, to illustrate the general trends. For rigourous spray drier design and optimisation, the mechanism of the drying of slurry droplets after crust formation, or, if possible, in appropriate cases the different mechanisms applicable to non-porous crust, porous film or non-porous film forming materials, need to be modelled and incorporated into an overall simulation of the drier.

In this study a mathematical model has been developed for the case of the drying of rigid, porous crust-forming materials. Materials which fall into this category include inorganic salts such as sodium sulphate and sodium chloride [94, 134]. Air flow pattern studies in counter-current driers [135] have illustrated the existence of a well-mixed zone in the vicinity of the nozzle and in the vicinity of the air inlet ports. The central section of the tower is believed to comprise a plug flow zone [83]. Hence in the region of the nozzle and air inlet ports, the properties of the air will be uniform, and so far as gas properties are concerned, a two-dimensional modelling approach is not warranted. Furthermore in the plug flow zone the assumption of uniform gas properties over a cross section does not appear to be unreasonable. Thus for counter-current drying, a one dimensional approach to gas properties would appear to be totally justifiable.

However, steep radial temperature and humidity gradients have been reported in the vicinity of the atomising nozzle in a co-current drier [136]. This arises because the air inside

the spray effectively brings about the evaporation and the surrounding air makes a minimal contribution. Theoretically it is possible to incorporate this phenomena into a model, by dividing the drier into two regions, viz: an upper region within which only the air inside the spray envelope contributes to evaporation, and a lower region where the total air flow participates in the process. However, empirical data is required in order to establish the transition between the two regions. In the absence of such data a one dimensional approach must be adopted. Furthermore, the operation of multi-nozzle driers, which are commonplace in industry, will promote turbulence in the vicinity of the atomiser and tend to unify the air properties at any given cross section. This further supports the application of a one-dimensional approach to gas properties.

The movement of droplets following release from a centrifugal pressure nozzle is two-dimensional in parallel air flow, or three-dimensional in rotary air flow. On this basis, a model has been developed which attempts to predict the two or three-dimensional motion of droplets in a spray drier, whilst the variation in air properties is considered in one dimension only. The model is fully-coupled in terms of mass, heat and momentum transfer between the gas and liquid phases.

Because of the complexity of the spray-air contact situation, certain simplifying assumptions are necessary to facilitate the modelling of the drying process. The following assumptions were used in the development of the model:

a) A rigid, porous crust forms on the surface of the droplet immediately upon commencement of drying, (i.e., no constant rate period). This situation would be expected when drying a non-skin forming solid from a slurry.

b) Heat transfer between the droplet surface and the surrounding air is by forced convection (i.e., radiation can be ignored).

c) Following crust formation, heat is transferred from the surface of the drop to the core by conduction through the crust.

d) Evaporation occurs only at the evaporation interface, which is at the boundary of the solid crust and the wet core, and this interface recedes into the core as evaporation proceeds.

This assumption implies vaporisation of the core does not occur, and that upon completion of drying a solid particle results. If the driving force for heat transfer is great enough or if vapour cannot escape from within the particle, then this assumption will be invalidated and a hollow particle will result.

e) The moisture is transferred from the evaporation interface by vapour diffusion through the pores, and this is represented by an effective diffusivity, D_{eff}. For this purpose the pores are assumed to permeate through the crust, whereas in practice blocked pores do occur, and no cracks are considered.

This mechanism of mass transfer would apply only for a rigid porous crust. Non-porous materials exhibit fractures and blow holes whereby jets of steam are released, and non-rigid crusts tend to expand, burst and collapse, or in some cases to shrink.

f) The droplets constituting the spray are spherical and experience no change of shape or size during drying. Thus shrivelling particles, or those which by intent puff-up, e.g. detergents, are not strictly included.

g) There is no droplet coalescence or break-up during droplet travel. There are no data in the literature relating to these phenomena. However if the drying mechanism deviated from that assumed in (d) and (e), and if particles explode, this assumption could be invalidated. For example particles with satellites adhering to them are

commonly found in spray dried products; indeed some with internal satellites have also been observed.

6.1 THE GENERAL MODELLING APPROACH

The approach adopted is to consider changes in the properties of solution and air contained in an increment of column of height, dz, as it proceeds down the spray drier. Since there is a distribution of drop sizes it follows that the residence time of the droplets at any position or plane in the tower will obviously differ. For example the time taken for a droplet to travel the length of an increment is given by:

$$dt_i = \frac{dz}{V_{zi}} \qquad 6.1$$

where V_{zi} is the instantaneous vertical component of the velocity of any droplet of general size D_i. As the value of V_{zi} changes during travel of a particular size of droplet, the time increment will also change. This, together with the fact that dt_i depends on drop size, renders it necessary to follow the drying history of each size of droplet in the distribution independently. However, it is necessary to combine the rates of heat and mass transfer for each droplet size, in order to ascertain the incremental change in the air properties. These points are considered in greater detail in subsequent sections.

6.2 DEVELOPMENT OF EQUATIONS OF MOTION

Consider the two-dimensional motion of a single droplet as shown in Figure 6.1, together with the forces acting upon it. The drag force is made up from skin friction and form drag as described in Chapter 3, and is assumed to act in the opposite direction to the relative velocity. As mentioned earlier, the drag force is only proportional to the relative velocity in laminar motion; hence only in this case will the drag force inevitably act in the direction of relative velocity.

With the aid of such Force-Velocity diagrams, equations can be developed to describe the two or three dimensional trajectories of droplets within a spray drier. The form of these equations will depend upon the air flow pattern to which the droplets will be exposed, which can broadly be classified into two types:

i) Droplet motion in a uniform, linear flow field.

Such flow is typical for co-current driers incorporating perforated plate, or straightening vane-type air dispersers, as in the drying of instant coffee [17].

ii) Droplet motion in rotating air flow.

Such flow is used with both co-current and counter-current driers, e.g, in the detergent industry [76].

These are considered below.

6.2.1 Droplet Motion in Uniform Air Flow

Referring to Figure 6.1, consider the motion of a single droplet released from a nozzle with a velocity Vm/s and at an angle of θ degrees to the vertical, i.e. a cone angle of 2θ. The drag force that will be exerted on the decelerating drop is given by equation 3.3, which from Chapter 3 for decelerating motion within a gas , i.e. a positive V_R, reduces to:

$$F_D = - C_D A \rho_a \frac{V_R^2}{2} \qquad 6.2$$

where

$$V_R = V - V_a = (V_{xR}^2 + V_{zR}^2)^{0.5} = ((V_x - V_{ax})^2 + (V_z - V_{az})^2)^{0.5}$$

From the force diagram in Figure 6.1., if the mass of the droplet is m, resolution of the forces acting on the droplet gives for the horizontal direction:

$$m \frac{dV_x}{dt} = F_x = F_D \cos\alpha = - C_D A \rho_a \frac{V_R^2}{2} \cos\alpha \qquad 6.3$$

and for the vertical direction:

$$m\frac{dV_z}{dt} = F_z + mg = F_D \sin\alpha + mg$$

$$= - C_D A \rho_a \frac{V_R^2}{2} \sin\alpha + mg \qquad 6.4$$

Now from the velocity diagram in Figure 6.1:

$$V_{xR} = V_R \cos\alpha \qquad 6.5$$

$$V_{zR} = V_R \sin\alpha \qquad 6.6$$

Substituting equations 6.5 and 6.6 into equations 6.3 and 6.4 and rearranging yields the equations of motion:

$$\frac{dV_x}{dt} = \frac{-C_D A \rho_a V_R V_{xR}}{2m} \qquad 6.7$$

$$\frac{dV_z}{dt} = \frac{-C_D A \rho_a V_R V_{zR}}{2m} + g \qquad 6.8$$

From Figure 6.1:

$$V_{xR} = V_x - V_a \sin\psi \qquad 6.9$$

$$V_{zR} = V_z - V_a \cos\psi \qquad 6.10$$

Substituting equations 6.9 and 6.10 into equations 6.7 and 6.8:

$$\frac{dV_x}{dt} = \frac{- C_D A \rho_a (V - V_a)(V_x - V_a \sin\psi)}{2m} \qquad 6.11$$

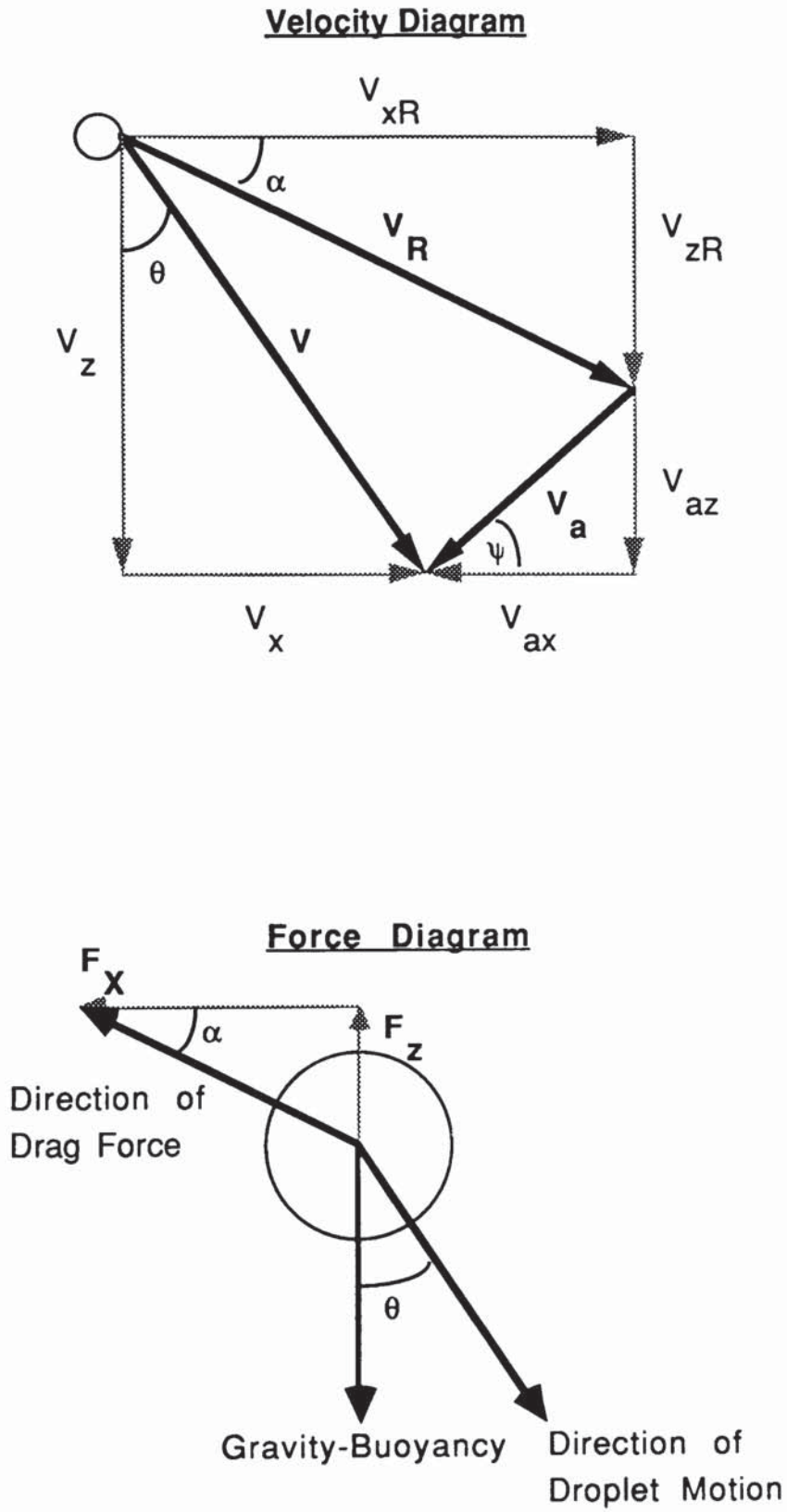

Figure 6.1 *Droplet Motion in a Linear Flow Field*

$$\frac{dV_z}{dt} = \frac{-C_D A \rho_a (V - V_a)(V_z - V_a \cos\psi)}{2m} + g \qquad 6.12$$

These equations are applicable to any uniform air flow field. For the particular case of parallel flow

$$\psi = 0$$

and equations 6.11 and 6.12 become:

$$\frac{dV_x}{dt} = \frac{-C_D A \rho_a (V - V_a) V_x}{2m} \qquad 6.13$$

$$\frac{dV_z}{dt} = \frac{-C_D A \rho_a (V - V_a)(V_z - V_a)}{2m} + g \qquad 6.14$$

where $V = \sqrt{V_x^2 + V_z^2}$

Equations 6.13 and 6.14 thus define droplet motion for a drier operating with parallel streamline air flow, which is either co-current or counter-current to droplet flow.

6.2.2 Droplet Motion in Rotary Air Flow

A droplet which is exposed to a rotating flow of air will exhibit three-dimensional motion, possessing velocities in the radial, tangential and vertical directions. For such flow the equations of particulate motion can be developed in either Cartesian or Cylindrical coordinate systems.

In the following analysis equations will be developed for two-dimensional motion only, as the equation of motion for the vertical direction will be identical to equation 6.8 developed for the linear flow field.

Consider a droplet whose instantaneous position in the horizontal plane in Cartesian coordinates is x, y and in cylindrical coordinates is r, Θ. The droplet will

possess velocities in the radial and tangential directions as shown in Figure 6.2. The droplet relative velocity can be established by assuming the air velocity in rotary flow to act perpendicularly to the radial direction as shown in Figure 6.2. Again assuming the drag force acts in the opposite direction to the relative velocity, gives:

$$F_D = - C_D A \rho_a \frac{V_R^2}{2}$$

where $V_R = V - V_a \equiv (V_{xR}^2 + V_{yR}^{2\,0.5}) \equiv (V_{rR}^2 + V_{tR}^{2\,0.5})$

Resolving the drag force into Cartesian components and summing forces gives:

For the X direction:

$$m \frac{dV_x}{dt} = F_x = F_D \text{Cos}\beta = - C_D A \rho_a \frac{V_R^2}{2} \text{Cos}\beta$$

$$\frac{dV_x}{dt} = \frac{-C_D A \rho_a V_R V_{xR}}{2 m} \qquad 6.15$$

Similarly, for the Y direction:

$$\frac{dV_y}{dt} = \frac{-C_D A \rho_a V_R V_{yR}}{2 m} \qquad 6.16$$

These are the equations of two-dimensional motion in a rotating air flow. However, the equations are difficult to solve in this form because, as the air flow is not uniform, the components of air velocity in the x and y directions will continually change.

Referring back to Figure 6.2, the angle subtended by the tangential air velocity to the Y direction is, by similar triangles, Θ. In Cartesian co-ordinates the tangential velocity of the air is therefore given by:

$$V_{ax} = - V_{at} \text{Sin}\Theta \qquad 6.17$$

$$V_{ay} = V_{at} \text{Cos}\Theta \qquad 6.18$$

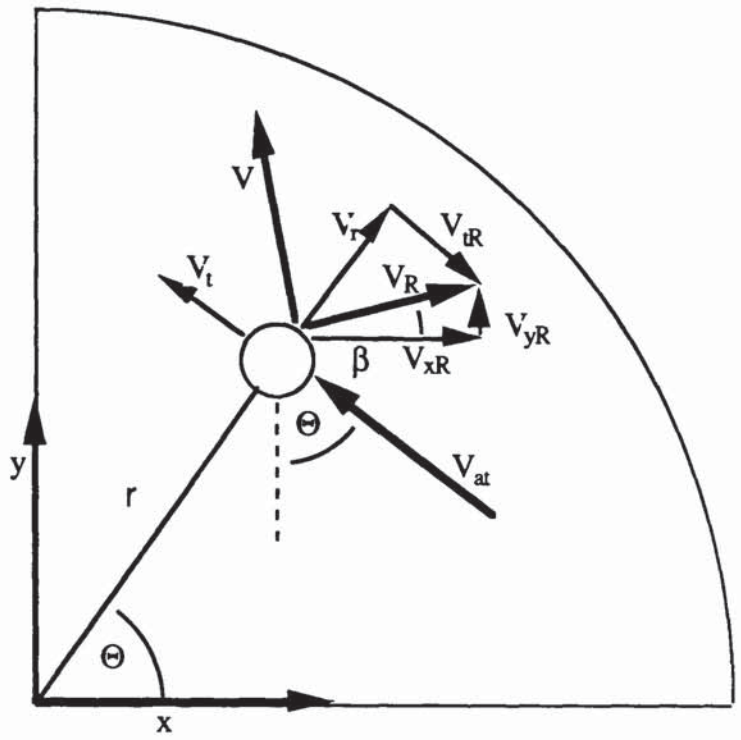

Figure 6.2 *Droplet Motion in Rotating Air Flow*

In addition,

$$\text{Sin}\Theta = \frac{y}{\left(x^2 + y^2\right)^{0.5}} \qquad 6.19$$

and,

$$\text{Cos}\Theta = \frac{x}{\left(x^2 + y^2\right)^{0.5}} \qquad 6.20$$

Substituting equations 6.19 and 6.20 into 6.17 and 6.18 respectively and then into the equations of motion 6.15 and 6.16 yields:

$$\frac{dV_x}{dt} = \frac{-C_D A \rho_a V_R}{2m}\left[V_x + \frac{yV_{at}}{(x^2 + y^2)^{0.5}}\right] \qquad 6.21$$

and

$$\frac{dV_y}{dt} = \frac{-C_D A \rho_a V_R}{2m}\left[V_y - \frac{xV_{at}}{(x^2 + y^2)^{0.5}}\right] \qquad 6.22$$

The third component of velocity, as mentioned previously is identical to that of the uniform flow field.

$$\frac{dV_z}{dt} = \frac{-C_D A \rho_a V_R}{2m}(V_z - V_{az}) + g \qquad 6.23$$

With the relative velocity for 3-dimensional motion given by

$$V_R = \left(V_{xR}^2 + V_{yR}^2 + V_{zR}^2\right)^{0.5}$$

Equations 6.21 - 6.23 define droplet motion in Cartesian coordinates for driers operating with swirl flow.

However, it may be more convenient to deal with the equations of motion in rotary air flow in cylindrical, rather than Cartesian co-ordinates. The equations can be readily converted to cylindrical by the relationship between velocities.

$$V_x = V_r \cos\Theta - V_t \sin\Theta \qquad 6.24$$

$$V_y = V_r \sin\Theta + V_t \cos\Theta \qquad 6.25$$

Substituting 6.24 and 6.25 into 6.21 and 6.22 and rearranging yields

$$\frac{dV_r}{dt} = \frac{V_t^2}{r} - \frac{C_D A \rho_a V_R V_r}{2m} \qquad 6.26$$

and,

$$\frac{dV_t}{dt} = \frac{-V_t V_r}{r} - \frac{C_D A \rho_a V_R (V_t - V_{at})}{2m} \qquad 6.27$$

These are the equations of motion in cylindrical co-ordinates. From equations 6.26 and 6.27 it can be seen that additional 'effective' forces have arisen as a result of the co-ordinate transformation. The term $\frac{mV_t^2}{r}$ represents the centrifugal force and the term $\frac{m\ V_r\ V_t}{r}$ the Coriolisis force.

Together equations 6.23, 6.26 and 6.27 can now fully define droplet motion for either co-current or counter-current driers operating with a rotational air flow pattern.

6.2.3 Solution of Equations of Motion

The equations of motion for either rotating or uniform air flow fields can be solved numerically and simultaneously with equations that will be subsequently developed for the change in droplet and drying air properties. Hence the incremental change in a droplet's velocity in the various component directions can be established. This, together with the droplet's residence time in the increment enables the trajectory of this particular droplet to be mapped.

To solve the equations of motion, however, information is required on:

i) the drag coefficient for the droplet,

ii) the droplet release velocity from the nozzle,

and iii) the droplet size distribution.

These are considered below.

(a) The Drag Coefficient

The conventional correlation for the drag on a spherical particle in steady motion was given in Chapter 3, Figure 3.3. Many empirical or semi-empirical equations have been proposed to approximate the standard drag curve but none considered all available data. Clift et. al., [49], therefore developed a new correlation based upon a critical examination of available data for spheres, and this was reproduced in Table 3.1.

In this correlation the Reynolds number in the range of 0 - 1.2 x 10^4 was divided into five sub-intervals with a distinct correlation for each interval. Adjacent equations for C_D match within 1% at the boundaries between sub-intervals. The correlation, being based upon by far the most comprehensive review of drag data in the literature, was selected for use in this study.

As discussed in Chapter 3, the drag data upon which Table 3.1 and most other correlations are based are valid only for highly idealised conditions. Hence to apply such data in this analysis of motion within a spray drier, a correction may need to be applied to the standard drag curve.

From section 3.1.3 the following effects are considered:

i) For the effects of unsteady motion, no correction is necessary.

ii) For the effect of mass transfer, the following correction is applied [74]:

$$\frac{C_{DM}}{C_D} = (1 + B_M)^{-0.19Sc - 0.74} (1 + B_M)^{-0.29} \qquad 3.13$$

where

$$B_M = \frac{x_{vs} - x_{vo}}{1 - x_{vs}}$$

and x_{vs} and x_{vo} are the mass fractions of vapour at the droplet surface and in the drying air respectively.

(iii) For the effect of droplet rotation, in the absence of any conclusive data, no correction was applied to the drag force. Lift forces were ignored in view of their magnitude in comparison to the drag force [68].

(b) Prediction of Droplet Release Velocity

The initial velocity of the droplet is the starting point in the calculations for the prediction of droplet motion. In this study only flow from centrifugal pressure nozzles will

be dealt with. Consider the emergence of liquid from the orifice of a centrifugal pressure nozzle as was shown in Figure 2.3. The liquid will possess components of velocity in the vertical and radial directions only, V_z and V_r respectively.

The velocity of the liquid sheet is

$$V = \left(V_z^2 + V_r^2\right)^{0.5} \qquad 6.28$$

It may be assumed that this sheet velocity remains constant, neglecting the effects of aerodynamic drag. Thus as the sheet spreads out its thickness must necessarily diminish.

From the equation of continuity

$$Q_v = \pi (r_o^2 - r_c^2) V_z$$

where

$$V_z = V \cos \theta$$

Thus

$$V = \frac{Q_v}{\pi (r_o^2 - r_c^2) \cos \theta} \qquad 6.29$$

Thus the prediction of the sheet velocity requires knowledge of the extent of the air core. Nelson and Stevens [16] performed a dimensionless analysis on the data of Darnell [14] and McIrvine [15]. They concluded that the ratio of the air core diameter to orifice diameter was independent of the Reynolds number at the orifice, and was a function solely of the spray angle, θ, which in turn depends upon the nozzle dimensions. They presented a plot of D_c/D_o versus θ for θ ranging between 20° and 120°. A linear regression was performed upon the data given by the curve, in the range 40 to 100°, to obtain the following relationship between D_c/D_o and θ:

$$\frac{D_c}{D_o} = 0.0112\ \theta - 0.227 \qquad 6.30$$

A correlation coefficient of 0.99 was obtained. Thus from equation 6.30 the diameter of the air core can be established, and then equation 6.29 can be used to predict the liquid sheet, and hence droplet release velocity.

(c) Droplet Size Distribution Data

In view of the absence of any reliable prediction methods for spray droplet size distribution, coupled with the sophisticated techniques now available for determination of such data, the size distributions required for this study were established entirely by empirical means, as described in Chapter 7.

6.3 PREDICTION OF AIR VELOCITY

Owing to the wide variety of possible configurations for a spray drier, as discussed in Chapter 3, a general description of the velocity distribution is not possible. Instead an approximate division can be made between swirling or rotary air flow and unidirectional air flow.

Regardless of the general air flow pattern,however, the atomisation process will result in large quantities of air being drawn into the spray as a result of momentum transfer. The droplets will then be exposed to a parallel flow of fast-moving air in the vicinity of the nozzle, with the velocity of the entrained air diminishing with increasing axial distance. This entrainment effect assists rapid spray evaporation by creating intimate spray-air contact, and also maintains droplet velocities considerably in excess of droplet terminal velocities. The latter is particularly important in the prediction of droplet-wall impingement, resulting in a faster droplet travel to the wall; if the corresponding residence time is insufficient for adequate drying, wall deposits will result.

In a large drier this air entrainment effect may only be local, i.e. it will not appreciably affect the air flow in the rest of the drier. The drying air flow pattern then

becomes controlling outside the immediate vicinity of the nozzle. However in a smaller drier the entrainment effect is likely to be the dominating feature of the air flow pattern.

In either case the extent of air entrainment must be predicted in order to accurately predict droplet motion.

6.3.1 Air Entrainment Effects

Benatt and Eisenklam [137] developed a simple model relating the mass flowrate of entrained air to axial distance. The model was developed upon the basis of observations that air was entrained into the spray perpendicularly, and that upon entry to the spray its direction was abruptly changed to an axial one. These observations have in fact been confirmed by other workers[137 - 140]. The model also included assumptions of (a) negligible liquid evaporation, (b) spraying into a stationary atmosphere, and (c) an infinitely thin drop sheath.

In the present study, the velocity of air associated with the spray was calculated without need for many of the simplifying and arguably unrealistic assumptions that were required in the model of Benatt and Eisenklam. This was made possible by incorporating a momentum balance on the droplet and gaseous phases within the step-wise scheme used for solving the equations of motion. By inclusion of heat and mass transfer effects, for which equations are developed subsequently, droplet evaporation could also be taken into consideration.

Entrainment Model

Consider a control volume for a single spray in co-current flow as shown in Figure 6.3.

The control volume extends from a level just below the point of liquid disintegration to an axial distance z metres, encompassing the entire spray volume. Conducting a momentum balance in the axial direction gives:

Momentum Input = Momentum Output.

The input is made up of:

a) Momentum of the convective air flow $= \dfrac{G_s^2 \pi x^2}{\rho_a}$

where G_s is the superficial air mass flowrate;

and b) Component of Liquid momentum $= G_{Lo} V_o \cos\theta$

The output consists of

a) Momentum of the air inside the spray $= V_{az} (V_{az} \rho_a \pi x^2)$

and b) Momentum of the spray droplets $= \sum_{i=1}^{n} V_{zi} G_{Li}$

where G_{Li} is the instantaneous mass flowrate of droplets of size-class i, of which there is a total of n classes.

Formulating the momentum balance for the axial direction gives:

$$\frac{G_s^2 \pi x^2}{\rho_a} + G_{Lo} V_o \cos\theta = V_{az}^2 \rho_a \pi x^2 + \sum_{i=1}^{n} V_{zi} G_{Li} \qquad 6.31$$

Rearranging gives the following term for the air velocity within the spray:

$$V_{az} = \left[\frac{G_s^2}{\rho_a^2} + \frac{G_{Lo} V_o \cos\theta}{\pi x^2 \rho_a} - \frac{\sum_{i=1}^{n} V_{zi} G_{Li}}{\pi x^2 \rho_a} \right]^{0.5} \qquad 6.32$$

Hence for the case of a co-current spray drier with a central hollow cone pressure nozzle atomiser, and with parallel air flow, equations, 6.32 can be used to determine the velocity of the air that droplets will be exposed to in the vicinity of the atomiser.. For other configurations, such as counter-current drying, the interaction of the convective air flow with the entrained air flow is, as yet, uncertain. Under these circumstances the following

correlation derived from measurements of the axial velocity of induced air for pressure nozzles spraying into still air can be used [111].

$$\frac{V_{az}}{V_o} = 3.2 \left(\frac{D_o'}{z}\right) \qquad 6.33$$

where $D_o' = D_o \left(\frac{\rho_L}{\rho_a}\right)^{0.5}$

V_o is the droplet release velocity from the nozzle atomiser.

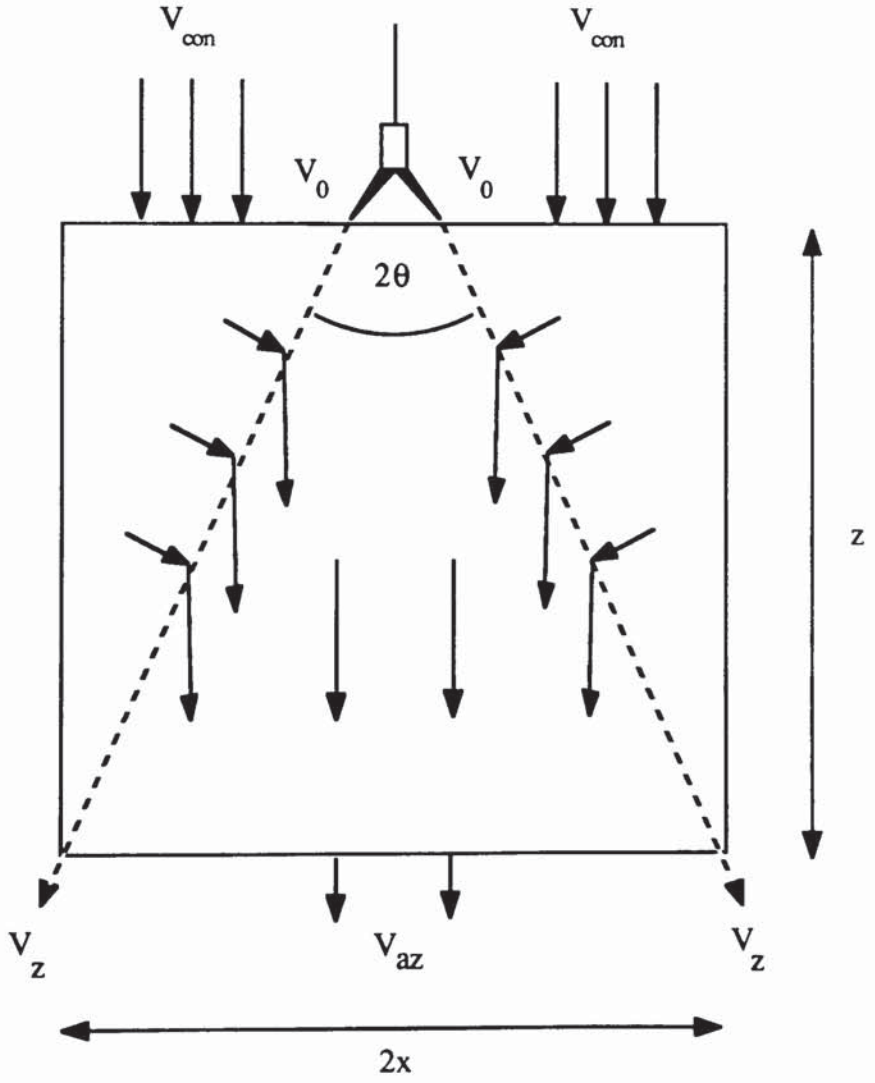

Figure 6.3 *Control Volume for Entrainment Analysis*

However a point that is seldom mentioned in the literature regarding the application of equation 6.33 is that it is only valid for $\frac{z}{D_o}$ values equal or greater to 3.2. If applied to lower values, for example at close proximity to the nozzle, non-sensible values of air velocities result. Hence in the use of equation 6.33, in this study, it will be assumed that for $\frac{z}{D_o}$ values less than 3.2 the ratio $\frac{V_{az}}{V_o}$ remain constant at a value of unity. Examination of the data upon which equation 6.33 is based suggests that this is a valid assumption and unlikely to introduce significant error.

Thus equations have now been identified which will predict the velocity of air induced into the spray from a pressure nozzle. For the case of a co-current drier with parallel streamline flow the prediction is based upon theory, incorporating convective air flow and droplet evaporation effects. For all other configurations the prediction will be based upon empirical induced velocity decay data.

Prediction of Transition to Overall Air Flow Pattern

As the spray descends the tower a stage is reached when the droplets are no longer solely influenced by the entrained air and the air flow pattern within the drier becomes increasingly important. It is difficult to predict when this transition will occur. For the case of a co-current drier, a situation may occur when the flow of air drawn into the spray exceeds the feed flow of air. This will inevitably result in air from a lower level in the drier being drawn outwards from the bottom of the spray, to the walls and recirculating upwards back into the spray as shown in Figure 6.4a. Hence for the case of a co-current drier the transition can be assumed to occur when the situation described above arises.

For a counter-current drier, the transition must be established by empirical methods. In the absence of such data it can be assumed that the air velocity given by equation 6.33 acts throughout the drier. Intuitively, the fast moving flow of air entrained with the spray will have the effect of beating down upon the upward flowing stream of air.

Immense turbulence can be expected to result and a chaotic flow pattern as shown in Figure 6.4b may be established. For large industrial towers, this turbulence may be expected to form only a small part of the overall pattern with much of the drier still under the influence of the drying-air flow pattern. However in smaller driers, e.g. pilot scale, the turbulence could result in well-mixed conditions prevailing in the drier.

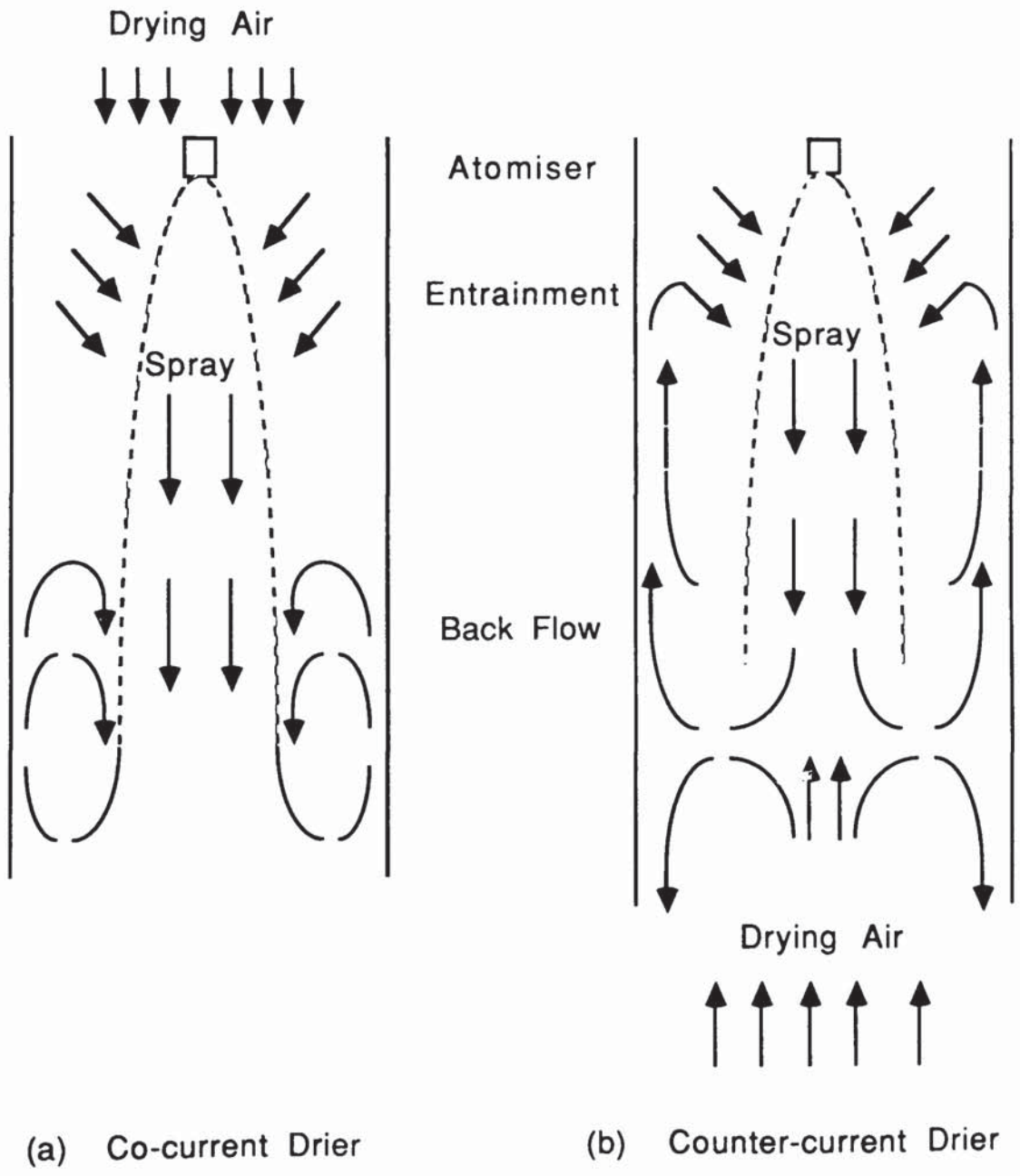

Figure 6.4 *Entrainment Flow Patterns Schematic*

6.3.2 General Air Velocity

Outside the influence of entrainment effects, the velocity of the air in the remainder of the drier can be established as follows.

(a) Parallel,Streamline Air Flow

The equation for the velocity V_{az} of air, for the case of parallel air flow is simply:

$$V_{az} = \frac{G_a}{A_{ch}\,\rho_a} \qquad 6.34$$

(b) Swirling Air Flow

The velocity field in a rotating air flow is similar to that in the cylindrical part of a cyclone. For a non-viscous fluid the ideal tangential velocity distribution would be as shown in Figure 6.5.

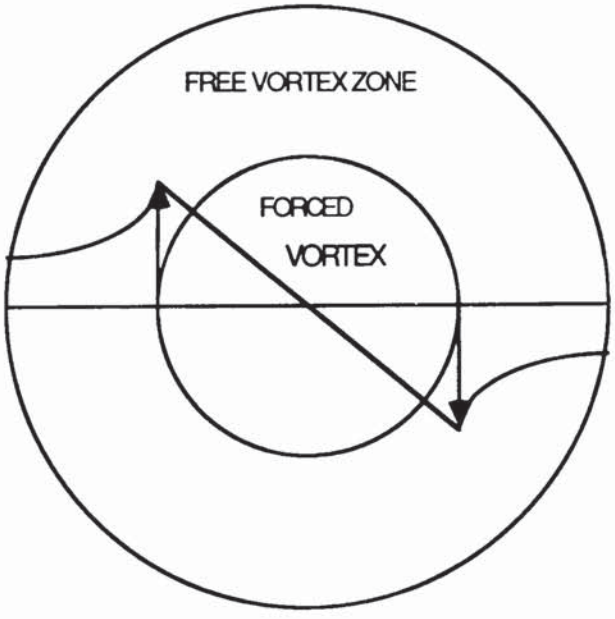

Figure 6.5 *Swirling Air Flow Pattern*

This shows a central forced vortex where the air rotates as a rigid body with zero velocity at the centre, surrounded by a free vortex where the tangential velocity varies inversely with the radius. That is, for the central forced vortex,

$$V_{at}\, r^{-1} = \text{Constant}$$

and for the outer free vortex,

$$V_{at}\, r = \text{Constant}$$

Bailey et. al. [116] assumed the transition between forced and free vortex to occur at a radial distance one fifth of the drier radius.

Thus:

$$V_{at} = k_1 r \qquad r < R_{ch}/5$$

$$V_{at} = \frac{k_2}{r} \qquad r > R_{ch}/5$$

Thus at $r = \frac{R_{ch}}{5}$

$$k_1 \frac{R_{ch}}{5} = \frac{5\, k_2}{R_{ch}}$$

so $$k_1 = \frac{25}{R_{ch}^2}\, k_2$$

Thus the velocity distribution becomes

$$V_{at} = \frac{25}{R_{ch}^2}\, k_2 r \qquad r < R_{ch}/5 \qquad 6.35$$

$$V_{at} = \frac{k_2}{r} \qquad r > R_{ch}/5 \qquad 6.36$$

The value of the proportionality constant k_2 is determined from the air inlet velocity. The axial air velocity in counter-current rotating air flow has been found to be dependent upon

the radial distance from the tower axis [76]. This is believed to be due to a rising core of air in the centre of the drier. However in the absence of any quantitative data a uniform axial air velocity must be assumed.

6.4 DROPLET DRYING MODEL

In the drying of a single slurry droplet, evaporation will initially occur from the wet surface of the drop. The loss of water renders the surface layer of liquid in the drop supersaturated and, if there is no skin formation, solids will be deposited. The core of the droplet will however remain at its initial moisture content and further evaporation is assumed to occur at the interface of the wet core and the dried crust. The core will subsequently recede into the droplet as drying proceeds. The mechanism of moisture transfer from the evaporation interface to the surrounding air will depend upon the nature of the crust that has been deposited and upon the magnitude of the driving force. If the crust is rigid and porous, and the rates of transfer are such as to avoid blow hole formation or 'explosions', the mechanism of moisture transfer will be one of vapour diffusion through the pores in the crust and then convection from the droplet surface to the surrounding air. It is assumed that during drying the droplet does not change in size such that extrusion of liquid as a result of shrinkage, or an increase in the diffusion path as a result of puffing can be ignored.

The energy required for the evaporation process will be supplied by the air, the mechanism of heat transfer being a combination of convection and conduction through the crust. Radiation effects are ignored. The assumed droplet drying scheme is shown in Figure 6.6. Based upon this drying scheme, equations will now be developed to predict the rates of heat and mass transfer between the droplet and the surrounding air.

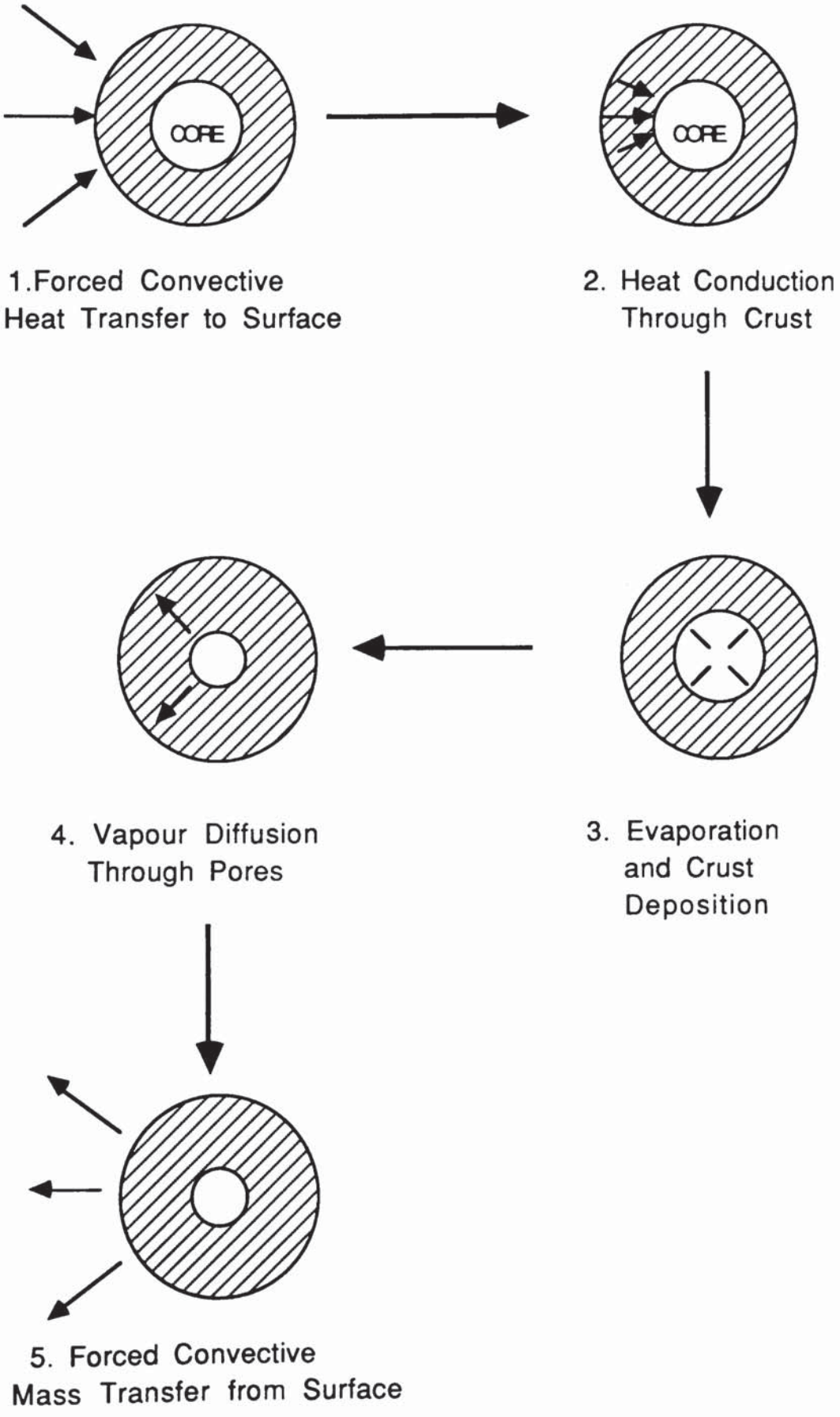

Figure 6.6 *Droplet Drying Scheme*

6.4.1 Heat Transfer to a Droplet

In the process of droplet drying there will be movement of both heat and the boundary of the wet droplet core towards the centre of the drop. The rate of shrinkage of the wet core may be expected to be significantly slower than the rate of conduction of the heat. Thus as far as the temperature profile in the crust at any instant is concerned, the wet core can be assumed to be stationary. A pseudo-steady state model can now be developed.

For the subsequent analysis the assumed droplet drying model is depicted in Figure 6.7. Note, however, that the representation of the temperature and partial pressure gradients is diagrammatic, and in reality it is unlikely that linear gradients will exist over the dried crust.

The rate of heat transfer through the crust at any radius r is given by:

$$Q = 4\pi r^2 k_c \left[\frac{dT}{dr}\right] \qquad 6.37$$

Integrating equation 6.37,

$$\frac{Q}{4\pi k_c} \int \frac{1}{r^2}\, dr = \int dT$$

which gives:

$$T = \frac{Q}{4\pi k_c} \left[-\frac{1}{r}\right] + K_1 \qquad 6.38$$

The boundary conditions applicable are:

(1) At $r = r_s$, $T = T_s$

(2) At $r = r_c$, $T = T_c$

Applying these conditions to equation 6.38 gives:

$$T_s = \frac{Q}{4\pi k_c} \left[-\frac{1}{r_s} \right] + K_1 \qquad 6.39$$

$$T_c = \frac{Q}{4\pi k_c} \left[-\frac{1}{r_c} \right] + K_1 \qquad 6.40$$

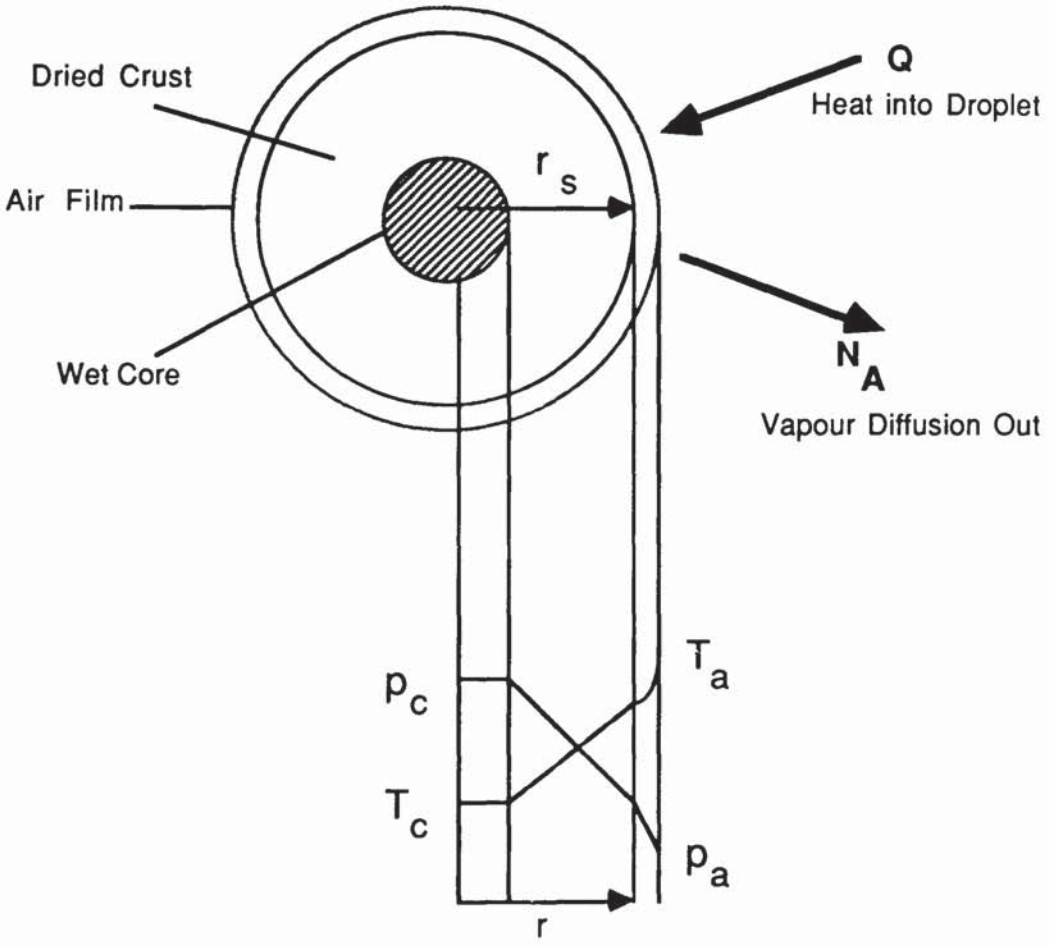

Figure 6.7 *Droplet Heat and Mass Transfer for Shrinking Core Drying Model*

Subtracting equation 6.40 from equation 6.39 gives:

$$T_s - T_c = \frac{Q}{4\pi k_c} \left[\frac{1}{r_c} - \frac{1}{r_s} \right] \qquad 6.41$$

Rearranging gives the rate of heat transfer to the droplet:

$$Q = 4\pi (r_c r_s) k_c \frac{(T_s - T_c)}{(r_s - r_c)} \qquad 6.42$$

In equation 6.42 the temperature at the surface of the droplet, T_s, is unknown. It can, however, be expressed in terms of the gas film heat transfer coefficient and the temperature of the air as follows.

Consider the convective transfer of heat through the gas film surrounding the surface of the droplet. The rate of heat transfer through the film is given by:

$$Q_s = h_g (4\pi r_s^2) (T_a - T_s) = Q$$

or

$$T_s = T_a - \frac{Q}{h_g 4\pi r_s^2} \qquad 6.43$$

Substituting equation 6.43 back into equation 6.42 and rearranging gives:

$$T_a - \frac{Q}{h_g 4\pi r_s^2} - T_c = \frac{Q}{4\pi k_c} \left[\frac{1}{r_c} - \frac{1}{r_s}\right]$$

The rate of heat transfer to the droplet cove can thus be expressed:

$$Q = \frac{4\pi [T_a - T_c]}{\left[\frac{1}{k_c}\left(\frac{1}{r_c} - \frac{1}{r_s}\right) + \frac{1}{h_g r_s^2}\right]} \qquad 6.44$$

To identify the resistances to heat and mass transfer it is useful to express equation 6.44 in terms of an overall heat transfer coefficient.

$$Q = U4\pi r_s^2 [T_a - T_c] \qquad 6.45$$

Thus

$$\frac{1}{U} = \frac{r_s^2}{k_c}\left(\frac{1}{r_c} - \frac{1}{r_s}\right) + \frac{1}{h_g} \qquad 6.46$$

$$\frac{1}{U} = \frac{(r_S - r_c)}{k_c}\frac{r_s}{r_c} + \frac{1}{h_g} \qquad 6.47$$

6.4.2 Mass Transfer from a Droplet

The driving force in any mass transfer process can be expressed as a concentration gradient. Thus for moisture transfer from the saturated surface of the wet core of a droplet, the driving force is the difference between the molar concentration of water vapour at the surface and the molar concentration of water vapour in the air.

From the ideal gas law:

$$PV = nR_gT$$

or
$$C = \frac{n}{V} = \frac{P}{R_gT} \qquad 6.48$$

Thus the driving force can also be expressed as the difference between the water vapour pressure at the temperature of the surface and the partial pressure of water vapour in the surrounding air. Note that a vapour pressure depression at the droplet surface will occur as a result of the presence of dissolved solids and this must be taken into account.

Assuming that the rate of vapour diffusion through the porous crust can be expressed in terms of an effective diffusivity, D_{eff}, then at pseudo steady state, the rate of mass transfer in terms of the molar concentration gradient at any radius r, within a droplet is given by:

$$-N_A = 4\pi r^2 D_{eff}\frac{dC}{dr} = \text{Constant} \qquad 6.49$$

Integrating

$$\frac{-N_A}{4\pi D_{eff}}\int\frac{1}{r^2}\,dr = \int dC$$

gives

$$C = \frac{N_A}{4\pi D_{eff}}\left[\frac{1}{r}\right] + K_2 \qquad 6.50$$

The boundary condition applicable are:

(1) At $r = r_s$, $C = C_s$

(2) At $r = r_c$, $T = T_c$

Applying these conditions:

$$C_s = \frac{N_A}{4\pi D_{eff}} \left[\frac{1}{r_s}\right] + K_2 \qquad 6.51$$

$$C_c = \frac{N_A}{4\pi D_{eff}} \left[\frac{1}{r_c}\right] + K_2 \qquad 6.52$$

Subtracting and rearranging results in the following expression for the rate of moisture transfer by diffusion through the crust:

$$N_A = 4\pi r_c r_s D_{eff} \frac{[C_c - C_s]}{[r_s - r_c]} \qquad 6.53$$

The concentration of water vapour at the surface of the droplet C_s can be expressed in terms of the gas film mass transfer coefficient and the concentration of water vapour in the surrounding air:

$$N_{As} = k_g \, 4\pi r_s^2 [C_s - C_a] = N_A \qquad 6.54$$

Therefore:

$$C_s = \frac{N_A}{k_g 4\pi r_s^2} + C_a \qquad 6.55$$

Substituting equation 6.55 into equation 6.53 gives:

$$C_c - \frac{N_A}{k_g 4\pi r_s^2} - C_a = \frac{N_A}{4\pi D_{eff}} \left[\frac{1}{r_c} - \frac{1}{r_s}\right]$$

The rate of mass transfer by vapour diffusion through the crust can now be expressed:

$$N_A = \frac{4\pi\,[C_c - C_a]}{\left[\frac{1}{D_{eff}}\left(\frac{1}{r_c} - \frac{1}{r_s}\right) + \frac{1}{k_g\, r_s^2}\right]} \qquad 6.56$$

In terms of the partial pressure driving force this becomes:

$$N_A = \frac{4\pi\left[\frac{P_c}{T_c} - \frac{P_a}{T_a}\right]\frac{M_w}{R_g}}{\left[\frac{1}{D_{eff}}\left(\frac{1}{r_c} - \frac{1}{r_s}\right) + \frac{1}{k_g\, r_s^2}\right]} \qquad 6.57$$

In the above expression the effective diffusivity is defined as follows[95]:

$$D_{eff} = D_v\, \varepsilon^{1.5} \qquad 6.58$$

where ε is the porosity of the crust.

The derivation of equation 6.58 is reproduced in Appendix A.

As in the case of heat transfer, it may be useful to express equation 6.57 in terms of an overall mass transfer coefficient, viz:

$$N_A = 4\pi\, r_s^2\, K \left[\frac{P_c}{T_c} - \frac{P_a}{T_a}\right]\frac{M_w}{R_g} \qquad 6.59$$

Thus,

$$\frac{1}{K} = \frac{r_s^2}{D_{eff}}\left(\frac{1}{r_c} - \frac{1}{r_s}\right) + \frac{1}{k_g} = \frac{(r_s - r_c)}{D_{eff}}\frac{r_s}{r_c} + \frac{1}{k_g} \qquad 6.60$$

Equations have thus been developed which can predict the rates of heat and mass transfer between a single droplet and the surrounding air. For the simulation of droplet drying within a spray drier it is necessary to predict the incremental change in droplet properties i.e. changes in droplet mass, droplet moisture content or radius and core temperature. Expressions to describe these changes will now be developed.

6.4.3 Change in Droplet Mass

The change in droplet mass from equation 6.57 is simply given by

$$\frac{dm}{dt} = \frac{4\pi \left[\frac{P_c}{T_c} - \frac{P_a}{T_a}\right] \frac{M_w}{R_g}}{\left[\frac{1}{D_{eff}}\left(\frac{1}{r_c} - \frac{1}{r_s}\right) + \frac{1}{k_g r_s^2}\right]} \qquad 6.61$$

6.4.4 Change in Droplet Core Radius

To predict the change in core radius consider a mass balance over the evaporation interface which can be expressed as

Rate of mass transfer = Rate of vapour diffusion from interface.

Thus,

$$\frac{d}{dt}\left(\frac{4}{3}\pi r^3 \rho_L x_w\right) = - N_A$$

$$- 4\pi r_c^2 \rho_L x_w \frac{dr_c}{dt} = \frac{- 4\pi \left[\frac{P_c}{T_c} - \frac{P_a}{T_a}\right] \frac{M_w}{R_g}}{\left[\frac{1}{D_{eff}}\left(\frac{1}{r_c} - \frac{1}{r_s}\right) + \frac{1}{k_g r_s^2}\right]}$$

Rearranging gives an expression for the rate of change of core radius

$$\frac{dr_c}{dt} = - \frac{\left[\frac{P_c}{T_c} - \frac{P_a}{T_a}\right] M_w}{r_c^2 \rho_L x_w R_g \left[\frac{1}{D_{eff}}\left(\frac{1}{r_c} - \frac{1}{r_s}\right) + \frac{1}{k_g r_s^2}\right]} \qquad 6.62$$

Now the crust thickness is given by

$$\beta = r_s - r_c$$

Thus

$$\frac{d\beta}{dt} = \frac{dr_s}{dt} - \frac{dr_c}{dt} = - \frac{dr_c}{dt}$$

6.4.5 Change in Droplet Core Temperature

To estimate the change in droplet core temperature consider an enthalpy balance on the core of the droplet:

Rate of enthalpy through crust = Rate of enthalpy out of core + Rate of enthalpy to raise vapour to air temperature + Accumulation of enthalpy in the core

The enthalpy loss from the core of the droplet is in two forms. The major loss is the enthalpy of the diffusing vapour comprised mainly of latent heat. However because the core of the droplet recedes as drying proceeds, crust is continuously deposited. This crust possesses sensible heat which must be accounted for.

Now,

Rate of heat transfer through crust = Q

where Q is given by equation 6.45

Rate of enthalpy transfer to raise vapour temperature = $N_A C_{Pv}(T_a - T_c)$

Rate of enthalpy transfer with vapour

$$= N_A (\lambda_D + C_{Pw} (T_c - T_D)) \qquad 6.63$$

where N_A is given by equation 6.59 and T_D is an arbitrary datum temperature.

The enthalpy loss associated with the crust is determined as follows:

Mass of droplet core = $\frac{4}{3}\pi r_c^3 \rho_L$

Rate of change of core mass = $4 \pi r_c^2 \rho_L \frac{dr_c}{dt}$

Now Rate of Change of droplet mass = $4 \pi r_c^2 \rho_L x_w \frac{dr_c}{dt} = N_A$

Hence Rate of Change of core mass = $\frac{N_A}{x_w}$

and

Rate of crust deposition = $\frac{(1 - x_w)}{x_w} N_A$

Thus

Rate of enthalpy loss with crust = $N_A \frac{(1 - x_w)}{x_w} C_{Pc} (T_c - T_D)$ 6.64

where Cp_c is the specific heat capacity of the crust.

Combining equations 6.63 and 6.64 gives:

Total enthalpy out:

$$= N_A \lambda_D + \frac{N_A}{x_w} [x_w Cp_w (T_c - T_D) + (1 - x_w) C_{Pc} (T_c - T_D)]$$

$$= N_A \lambda_D + \frac{N_A}{x_w} C_{PL} [T_c - T_D] \qquad 6.65$$

The enthalpy of the core can be expressed as follows:

$$H_{core} = \frac{4}{3} \pi r_c^3 \rho_L C_{PL} [T_c - T_D] \qquad 6.66$$

Differentiating with respect to time:

$$\frac{dH_{core}}{dt} = [4\pi r_c^2 \rho_L C_{PL} (T_c - T_D)] \frac{dr_c}{dt} + [\frac{4}{3}\pi r_c^3 \rho_L C_{PL}] \frac{dT_c}{dt} \qquad 6.67$$

But

$$\frac{dr_c}{dt} = - \frac{N_A}{4\pi r_c^2 \rho_L x_w} \qquad 6.68$$

Substituting equation 6.68 into equation 6.67 and formulating the overall enthalpy balance:

$$Q = N_A \lambda_D + \frac{N_A}{x_w} C_{PL} (T_c - T_D) - \frac{N_A}{x_w} C_{PL} (T_c - T_D)$$

$$+ \frac{4}{3}\pi r_c^3 \rho_L C_{PL} \frac{dT_c}{dt} + N_A C_{Pv} (T_a - T_c) \qquad 6.69$$

Rearranging gives:

$$\frac{dT_c}{dt} = \frac{3 [Q - N_A (\lambda_D + C_{Pv}) (T_a - T_c)]}{4\pi r_c^3 \rho_L C_{PL}} \qquad 6.70$$

The above equation can be solved simultaneously with equations 6.69 and 6.67 via a numerical method to give the incremental changes in core temperature, core radius and droplet mass. The droplet drying history can thus be established, along the droplet trajectory.

6.5 PREDICTION OF AIR PROPERTIES

The solution of the equations of motion and droplet drying requires a knowledge of the properties of the surrounding air; This will in turn depend upon the type of flow pattern pertinent to the spray drier. Flow patterns can be broadly categorised into:

(a) Plug Flow

(b) Well-Mixed Flow

and in practice, the flow pattern within a drier can be expected to lie somewhere between these two extremes. For the purpose of modelling, the type of flow pattern selected will influence only the temperature and humidity profiles that are established within the drier. Expressions are derived below which facilitate prediction of the variation in air temperature and humidity inside the tower.

(a) Plug Flow

In the analysis it is assumed that there is no axial mixing of air within the tower. However at any cross-section the properties of the air are assumed to be uniform.

Consider an increment of height dz as it descends the drier as shown in Figure 6.8.

At steady state the rate of enthalpy entering into the element is equal to that leaving. An enthalpy balance assuming negligible heat losses can be written:

$$Q_{a1} + Q_{L1} = Q_{a2} + Q_{L2}$$

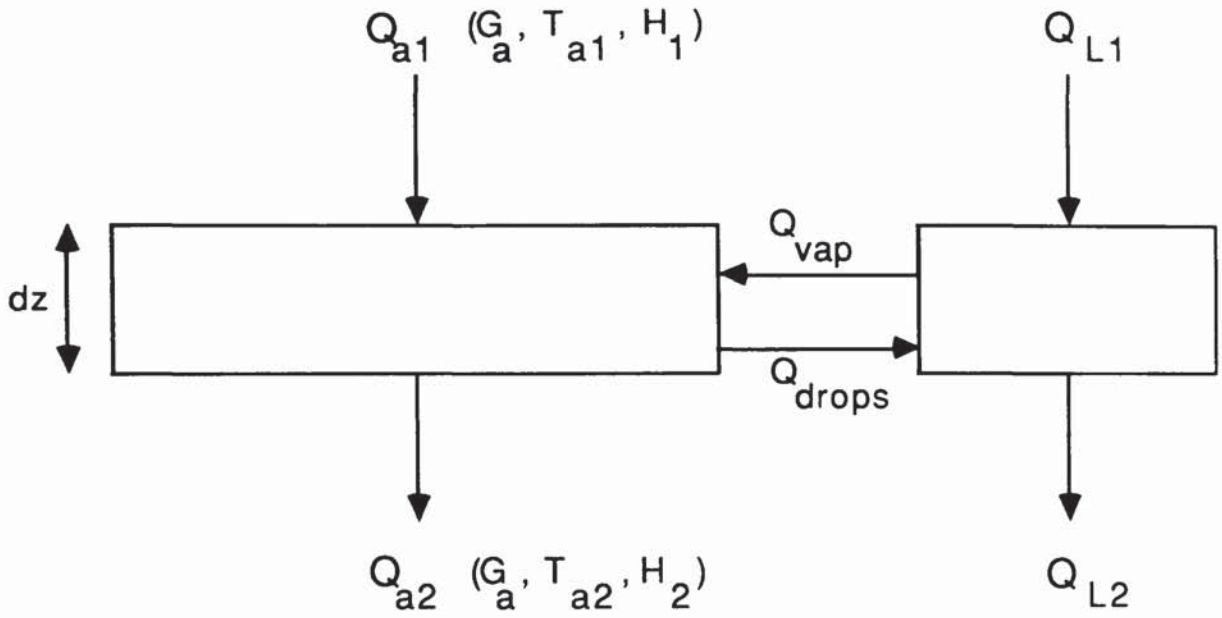

Figure 6.8 *Incremental Mass and Energy Balance*

where the enthalpy of air can be expressed as:

$$Q_{a1} = G_a\, cs_1\, (T_{a1} - T_D) + G_a\, H_1\, \lambda_D \qquad 6.71$$

and

$$Q_{a2} = G_a\, cs_2\, (T_{a2} - T_D) + G_a\, H_2\, \lambda_D \qquad 6.72$$

where cs is the humid heat and is given by:

$$cs = C_P + C_{Pv}\, H \qquad 6.73$$

Now

$$Q_{L2} - Q_{L1} = \text{Change in enthalpy of drops over increment dz.}$$

For a single droplet:

$$Q_{L2} - Q_{L1} = \text{Heat into drop - Heat Output}$$

$$Q_{L2} - Q_{L1} = Q - N_A C_{Pv} (T_a - T_c) - (N_A \lambda_D + N_A C_{Pw} (T_c - T_D))] \quad 6.74$$

However the increment contains drops with a distribution of sizes. Therefore to predict the total change in enthalpy within the liquid phase the number of droplets of each drop-size must be calculated.

As before, if the number of classes of drop-size is designated as n and the subscript i (for i = 1 to n) used to identify a particular class of drop-size then, the residence time of a droplet of diameter D_i in the increment n given by equation 6.1:

$$dt_i = \frac{dz}{v_{zi}}$$

If the weight fraction of droplets of size D_i is W_i and the total liquid mass flowrate into the drier is G_{Lo} then the initial mass flowrate of a particular droplet class is given by:

$$G_{Lio} = G_{Lo} W_i$$

The mass flowrate of a droplet size-class will decrease as the spray descends the tower due to evaporation. Hence let the instantaneous mass flowrate at any position in the tower be designated G_{Li}. The number of droplets of general size D_i associated with an incremental length dz is then given by:

$$N_i = \frac{G_{Li}\, dt_i}{m_i} \quad 6.75$$

The enthalpy change in the liquid phase can now be expressed as:

$$Q_{L2} - Q_{L1} = \sum_{i=1}^{n} N_i [Q_i - N_{Ai} (\lambda_D + C_{Pw} (T_{ci} - T_D) - C_{Pv} (T_a - T_{ci}))] \quad 6.76$$

The enthalpy balance for the increment upon rearrangement then yields the temperature at the exit of the increment:

$$T_{a2} = T_{a1} \frac{cs_1}{cs_2} + T_D \left(1 - \frac{cs_1}{cs_2}\right) + \frac{(H_1 - H_2)\,\lambda_D}{cs_2} - \frac{(Q_{L2} - Q_{L1})}{G_a\, cs_2} \qquad 6.77$$

The humidity change down the tower can be established by conducting an incremental moisture balance:

$$G_a H_1 + G_{L1} = G_a H_2 + G_{L2}$$

Rearranging gives:

$$H_2 = H_1 + \frac{(G_{L1} - G_{L2})}{G_a} \qquad 6.78$$

The term $(G_{L1} - G_{L2})$ is the total evaporation rate within the increment. This can be determined by summing the individual rates of evaporation of all the droplet classes. Thus,

$$G_{L1} - G_{L2} = \sum_{i=1}^{n} N_i\,(N_{Ai}) \qquad 6.79$$

where N_i is given by equation 6.75.

Substituting 6.79 into 6.78 gives:

$$H_2 = H_1 + \frac{\sum_{i=1}^{n} N_i\ N_{A\,i}}{G_a} \qquad 6.80$$

Thus equations 6.80 and 6.77 enable the variation in air humidity and temperature to be established assuming plug flow conditions prevail.

(b) Well-Mixed Flow

If turbulence within the drier is significantly intense, then the flow pattern will approach well-mixed flow and the temperatures and humidity of the air within the drier will be uniform at a value equal to the exit values. In this instance the exit air conditions will be required as a starting point and equations 6.80 and 6.77 can be applied to determine the air temperature and humidity at the inlet to the tower.

6.6 COMPUTER SOLUTION OF THE EQUATIONS OF MOTION AND DRYING

The differential equations developed above were solved by computer using a 4th order Runge-Kutta method. The computer program was written in Fortran 77 and a complete listing is given in Appendix B.

Chapter 7

Experimental Studies

The experimental programme of work followed in this study can be divided into three discrete sections. These are:

(i) Flow Visualisation Study; the objective of this work was to investigate the air flow patterns in a pilot-scale transparent counter-current drier for a variety of air entry configurations.

(ii) Temperature and Humidity Study; this was to provide further insight into the air flow patterns in counter-current drying, and also to provide hard data for validation of the mathematical model.

(iii) Droplet Size Measurements; this work was aimed at generating droplet size distribution data for use in drier simulation, and to include a preliminary study on in-spray droplet agglomeration.

Each of these investigations is described in depth in the following pages.

7.1 FLOW VISUALISATION STUDIES.

The air flow pattern established in a spray drier significantly affects the properties of a spray dried material, in particular the product granulometry and bulk density, and also the thermal efficiency of the process. As discussed in Chapter 3, the movement of air in the drying chamber dictates the rate and degree of drying by influencing the residence time of the droplets, the extent of particle recirculation into the hotter region of the drier and the extent of any hot air by-passing or channelling.

The few experimental air-flow pattern studies reported hitherto have been described in Chapter 3. These suggest the existence of turbulent and streamline zones within the drying chamber, with the possibility of short-circuiting of some of the air as a result of wall-by passing or channelling up the centre of the drier.

The object of the present investigation was to further understand the behaviour of the air flowing through a counter-current spray drier and specifically, to verify the existence of any turbulent, plug-flow or short circuiting zones. This was to be achieved through the deployment of a flow visualisation technique to characterise the various air flows in a transparent spray drying tower.

This flow-visualisation based approach was adopted in this study, since it can provide an accurate, first-hand and detailed qualitative description of air movement in the drying chamber.

Details of the drier and the investigative technique are given below.

7.1.1 The Spray Drier Installation

(a) The Spray Drier

The drier used in this study consisted of a main cylindrical section, 1.2m in diameter and 2.4m in height, onto the bottom of which was mounted a conical base section of maximum diameter 1.75m and height 1.5m, and to the top of which was fitted a dished end section, 0.3m in height. The entire construction was manufactured in 0.5cm thick transparent Poly-Vinyl Chloride. The principal dimensions of the drier, which was a modified version of the tower previously used by Ade-John [83], are given in Figure 7.1.

The air entered the drier via 4 equally spaced cylindrical ducts, 0.11m in diameter and 0.8m in length, situated around the periphery of the top of the base cone. Each duct supplied air to a set of 3 inlet nozzles, i.e. 12 nozzles in total. These nozzles fed air into

the drier through 12 equally spaced rectangular ports, 0.23m in height and 0.15m wide. This multi-chamber air inlet arrangement was preferred over the conventional single plenum chamber design since it enabled a uniform air supply to all 12 air inlet nozzles to be obtained.

The air to each of the four supply ducts was provided by a 37 kW Alfa fan, via a 0.41m x 0.61m x 0.36m box section feeding to four 10.16cm flexible pipes. The flowrate of air to each of the ducts was measured by four 30.5cm pitot tubes, manufactured by Air Flow Developments Ltd. These were positioned in the centre of each of the four air lines. The differential pressures developed across the pitot tubes were measured by four 'Slim Jim'-type manometers, again supplied by Air Flow Developments. These gave a direct reading of the differential pressure in kN/m^2, which was converted to centre-line velocities by application of the following equation [141]:

$$V_{CL} = 1.291\sqrt{\frac{1000}{B}\frac{T_a}{289}P_v} \qquad 7.1$$

B = barometric pressure in mbar

T_a = air temperature

P_v = velocity pressure in Pa ≡ differential pressure

The centre-line velocity was adjusted to give the mean flow velocity using the relationship [51],

$$V_m = 0.82\ V_{CL} \qquad 7.2$$

The air flowrate was then simply calculated by multiplying the mean flow velocity by the cross-sectional area of flow.

The entire spray drier installation is shown in Plate 7.1

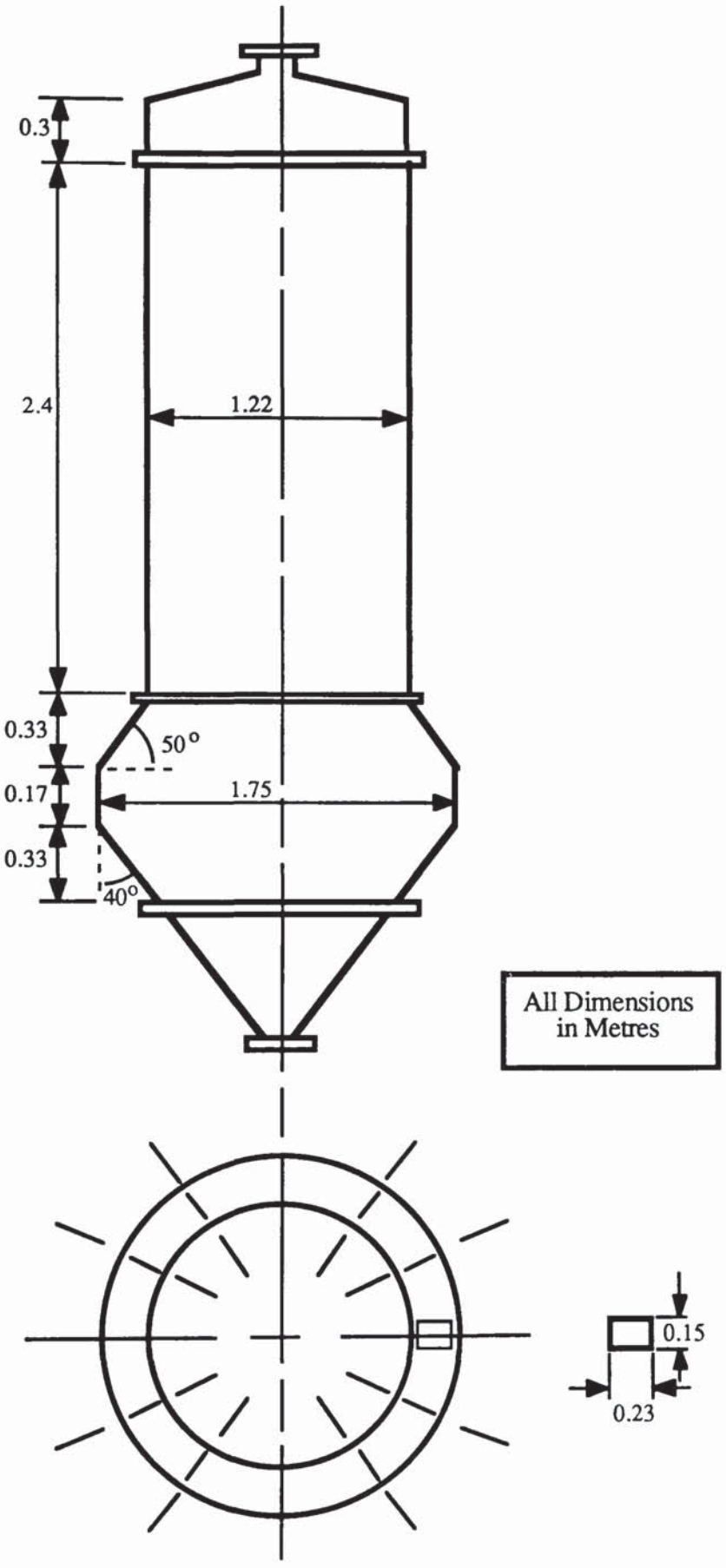

Figure 7.1 *Dimensions of the Transparent Spray Tower*

(b) Air Nozzle Design

The air inlet nozzles fitted to the drier were manufactured in stainless steel and each had a rectangular cross section, 7cm in width and 14cm in height. The length of each nozzle was approximately 15cm. To the face of each nozzle was attached a perforated steel plate designed to provide a uniform flow of air over the nozzle cross-section. The flowrate of air to each nozzle was regulated by means of a ball valve which was installed at the head of the nozzle.

Each nozzle was designed such that by means of a pivotting mechanism the nozzle angle and hence direction of air entry, could be adjusted in both the radial and the horizontal directions. Protractors were fitted to the top and to the side of each nozzle to facilitate the measurement of the swirl, i.e. the radial angle, and the horizontal angle. The angle-range afforded by this mechanism was up to 25° radially and 25° to the horizontal. This facility enabled various drier air-inlet arrangements to be tested, for example, by imparting varying degrees of swirl to the incoming air.

A close up of an inlet nozzle is shown in Plate 7.2.

7.1.2 The Flow Visualisation Technique

The air movement within the transparent drying tower was investigated by using smoke to trace the direction, and gauge the intensities, of air flow in various regions of the drier. The design of the probe and the smoke generating equipment is described below.

The Smoke Generator

To enable effective flow visualisation a highly visible plume of smoke is a necessity, especially in view of the immense turbulence that may be expected in certain areas of the drying chamber. Thus in the flow visualisation studies, a Nutem type NPL smoke generator was employed. In this design, oil was pumped to the tip of a probe of length 26.8cm, where it was heated by an electrical coil, housed in a compact screw-on

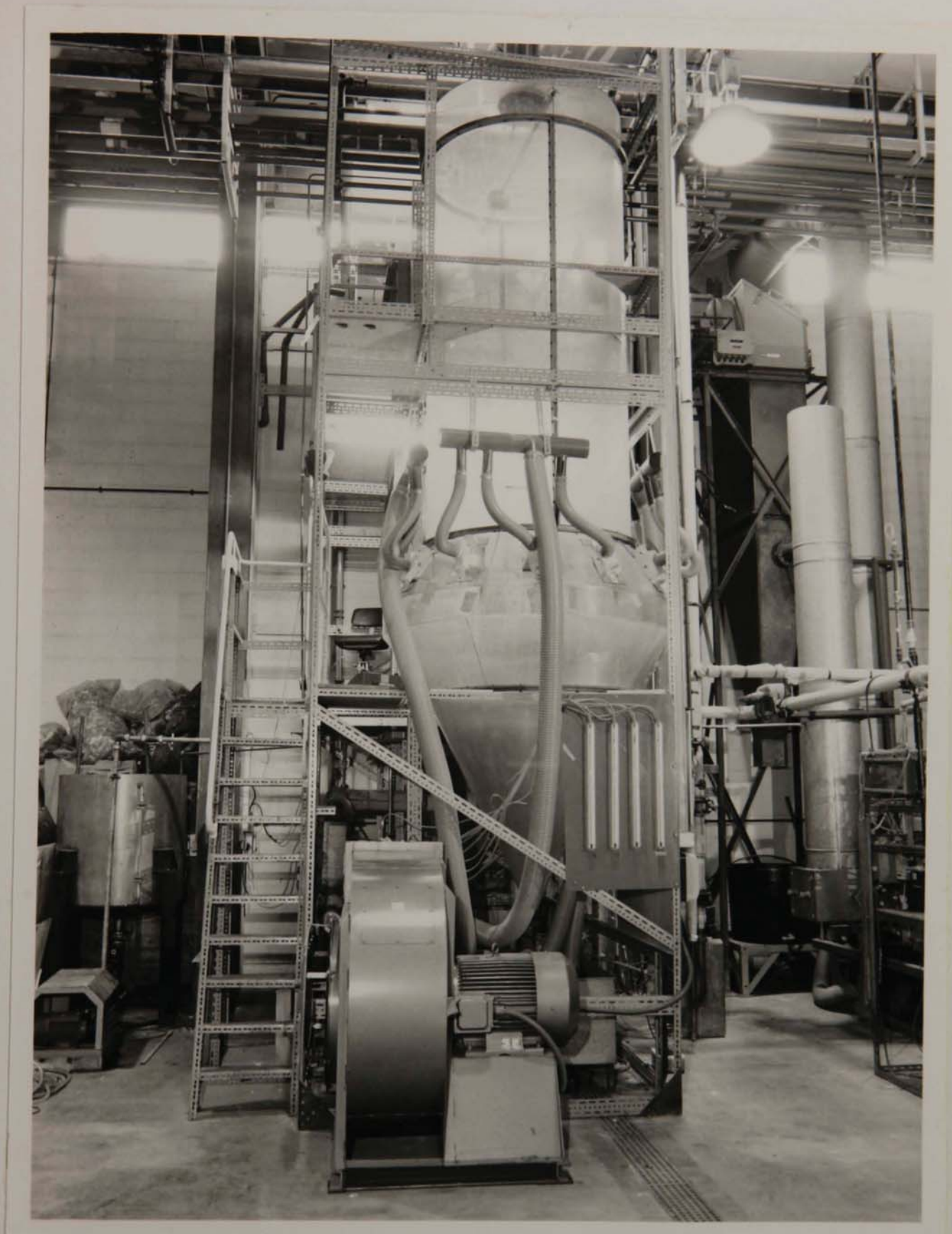

Plate 7.1 *The Transparent Spray Tower*

Plate 7.2 *Variable-Angle Air Inlet Nozzle*

vaporiser, to release a continuous emission of dense smoke directly into the airstream. The end section of the probe was shaped into a 90° bend to minimise wake-generation which could otherwise have invalidated observations. The probe was supplied with control unit type FVSP204 which provided control of both the pumped oil feed and a variable voltage supply for the electrical coil in the vaporiser tip. The combination of oil flowrate and vaporisation temperature could thereby be adjusted to obtain the best emission characteristics under any particular set of flow conditions.

The complete smoke-generating unit is shown in Plate 7.3.

7.1.3 Experimental Conditions

Air dispersers for counter-current driers are generally of the plenum chamber design whereby a peripheral duct feeds a number of air inlet nozzles. The nozzle configuration can either be straight, such that the air enters into the drier radially without swirl and flows upwards in a straight line, or if the nozzles are angled to the radial, the air will enter tangentially and spiral up the tower. In addition the nozzles can optionally be angled to the horizontal to give the air an initial downward movement.

With a plenum chamber-type disperser, the flows to the nozzles are unlikely to be balanced. Maldistribution of the air flow will thus result, with those nozzles nearer the air inlet to the plenum being fed a proportionately greater air flow than those furthest away. Such maldistribution is likely to have some effect on the air flow pattern in the drying chamber.

A further factor complicating the air flow pattern, is the common practice of operating the drier under a negative pressure. This will affect the air flow pattern by causing air from atmosphere to be drawn into the drier.

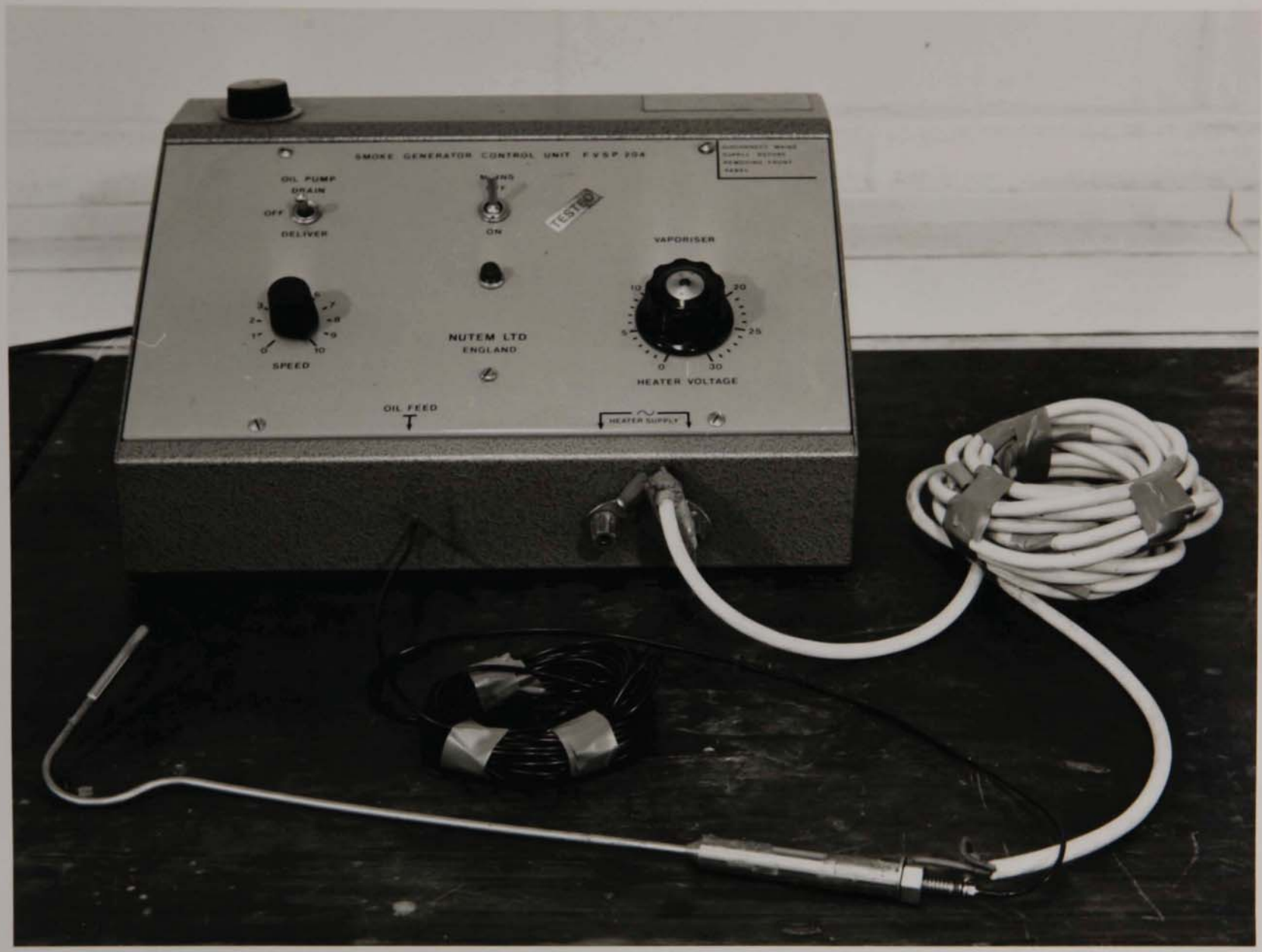

Plate 7.3 *The Smoke Generator*

In view of this diverse operational practice, a comprehensive set of operating conditions and flow arrangements are necessary for any investigation of air-flow patterns to be of practical use. Therefore in this study, operating conditions were selected which considered the effects associated with a number of variables.

These were:

(i) The number of air inlet nozzles operational; drier operation with only 4 nozzles supplying air and with all 12 nozzles functioning was investigated.

(ii) The radial and horizontal angle of the nozzles; the swirl and horizontal angles were varied from 0° to 25°.

(iii) Non-uniform distribution of air to the nozzles; by means of the ball valves on each nozzle the air flow was unevenly distributed so that one side of the drier received approximately 30% less air than the other.

(iv) An additional upward air-flow through the base of the tower to mimic air suction caused by negative pressure operation; this was achieved by coupling the output of a second fan, a 15kW 3-phase Parkinson, to the base of the drier. In this manner up to 13% of the total air-flow rate could be introduced via the base and its impact investigated.

(v) Operation of the Spray. Water was sprayed into the tower at a rate of 0.06kg/s, to determine its influence on the air-flow pattern.

The full range of conditions and flow arrangements are given in Table 7.1.

For each set of conditions the smoke probe was used to establish the directions, and gauge the intensities, of flows in various regions of the drier. This was done by inserting the probe through holes drilled into the tower at 50cm intervals. When probing in this manner the length of the probe was found to be insufficient to fully explore all regions of the drier. Therefore, the effective length of the probe was increased by strapping it, using PVC tape, to a 0.8m length of 0.82cm diameter stainless steel rod.

Case	Nº of Nozzles	Swirl Angle (°)	Horizontal Angle (°)	Total Air Flow (m^3/h)	Secondary Air Flow (% Total)	Maldistribution Split (%)	Spray Flowrate (kg/s)
1	4	0	0	1700	0	-	0
2	4	25	25	1700	0	-	0
3	12	0	0	3700	0	-	0
4	12	25	25	3700	0	-	0
5	4	0	0	1800	0	1050/750	0
6	12	25	0	4111	10	-	0
7	12	25	0	4250	13	-	0
8	12	25	0	3660	11	1850/1400	0
9	12	25	25	4111	10	-	0
10	12	20	25	4111	10	-	0
11	12	15	25	4111	10	-	0
12	12	15	25	3700	0	-	0
13	12	25	25	3700	0	-	0.06

Table 7.1 *Operating Conditions and Nozzle Configurations for Flow Visualisation*

The approximate sizes and locations of the various flows in the drying chamber were estimated for each of the flow arrangements and hence a complete picture of the air flow pattern within the tower was established. Sketches to describe the air flow patterns under the various flow conditions were drawn and these are presented in Chapter 8.

7.2 AIR TEMPERATURE AND HUMIDITY STUDIES.

The temperature and humidity profiles that are set up in a spray drier define the driving force for moisture evaporation and dictate the characteristics of the dried product by influencing the droplet drying mechanism. For example low density, high porosity particles are typical of drying in hot air conditions. Hence an understanding of the temperature and humidity fields should lead to better design of spray driers and improvements in dried product quality.

In addition examination of temperature and humidity profiles can provide fundamental information on the air flow patterns that exist within a drying chamber. For example the approach to either plug-flow or well-mixed conditions can generally be inferred from temperature and humidity data.

Such data, can also, in this instance, be used for comparison with theoretical predictions derived from the mathematical model described earlier. The strengths and weaknesses of the model can thus be identified and its reliability ascertained.

The objective of this work was therefore to develop, and then apply, instrumentation for the accurate measurement of air temperature and air humidity profiles in a counter-current pilot plant drier. Such data could then be interpreted to yield information on the air flow patterns existing in the drying chamber, and also be used to validate the mathematical model.

7.2.1 Previous Experimental Studies

It is appropriate to review previous studies that have dealt with the task of measuring temperature and humidity fields in spray driers. Seltzer and Settlemeyer (36) measured air temperature profiles at several levels along the length of an industrial spray drier whilst spraying water into the chamber. The measurements were obtained by inserting a thermocouple on an aluminium "fishing pole" through various observation ports in the chamber wall. No information is given regarding the thermocouple type, shielding, column dimensions, operating conditions or type of nozzles used. Their data is presented in the form of two drawings of spray driers showing air temperatures at various points inside the drying chamber.

Buckham and Moulton (79) measured air temperatures and humidities in a 1.2m co-current spray drier whilst spraying water and ammonium sulphate solutions through a centrifugal pressure nozzle. Air temperatures were measured using thermocouples located in six thermowells at fixed axial positions. The thermowells were protected from direct contact with the wet spray by inclined trough trays. Humidities were measured at 4 points in the drying chamber by bleeding samples passed a wet and dry bulb thermometer. Since the probes were fixed, no radial probing for temperature and humidity was possible and only one value for temperature and humidity per axial location was reported.

Dloughy and Gauvin (97) measured temperature and humidity profiles in a 20cm diameter co-current drier, whilst spraying water. Air temperatures were measured using a 0.5cm diameter mercury thermometer fitted with a semi-circular shield, 1cm in diameter and 3.8cm long, to prevent droplet impingement. Air humidity was measured using a volumetric technique which consisted of withdrawing an air sample from the drying chamber through an inverted aluminium cup and absorbing any water vapour present with magnesium perchlorate. The corresponding increase in volume enabled determination of the humidity. Only one value of air temperature per axial location was reported.

Hoffman and Gauvin [142] investigated evaporation of water sprays from a pneumatic and a centrifugal pressure nozzle in an atomised suspension reactor. Air temperatures were measured using a shielded platinum-platinum/10% rhodium thermocouple. Three shields were used to prevent droplet impingement on the thermocouple. To increase the convective heat transfer coefficient at the thermocouple junction, the air was aspirated through holes over the inner shields and the thermocouple. Radial temperature profiles were measured, but in all cases the value at the centre-line was the same as at any other radial position. Hence only one temperature at each axial position is reported.

Baltas and Gauvin [98] measured air humidities in a co-current drier whilst spraying water and solutions of sodium nitrate using a pressure nozzle. The technique used for the measurement of air humidity was identical to that of Dloughy and Gauvin. Their data were presented as plots of air humidity versus axial distance from the column top at various radial positions.

Miura et al [120] measured air temperatures and humidities in a square co-current drying chamber whilst spraying water, sodium chloride solution or skim milk through pneumatic and pressure nozzles. Air temperatures were measured using a shielded copper-constantan thermocouple. The description of the shield is not clear. Air humidities were determined by withdrawing air samples from the drier and passing them over a wet and dry-bulb thermometer pair. Only one value of air temperature and humidity per axial location is reported.

Most recently, Papadakis [143] measured air temperature and humidity profiles in a 0.56m diameter co-current spray drier whilst spraying water through a centrifugal pressure nozzle. Air temperatures were measured using ultra-fine copper-constant thermocouples, of 0.013cm diameter. This type of thermocouple was chosen because of its low thermal conductivity which resulted in the lowering of heat conduction errors. Due to its fine

diameter, the thermocouple had to be supported on a wooden dowel fixed to a PTFE base which was fitted in the end of a steel pipe. For probing within the spray a cap made from PTFE tape was used to shield the thermocouple. Air humidities were measured using a wet and dry bulb thermometer. The design consisted of a 0.76m long steel pipe of 2.2cm diameter inside which was placed a thermocouple supported on a wooden rod. Cotton wick was wrapped around the thermocouple tip. The outside of the steel pipe, adjacent to the thermocouple tip was also covered in cotton cloth. Both wick and cotton cloth were wetted before insertion into the drier. Air was then aspirated through the probe, passed the wet bulb, and hence the humidity could be determined. However the presence of a wet saturated surface, i.e. the outer cotton cloth, so near to the vicinity of air sampling would be expected to have a detrimental effect on the accuracy of the humidity measurement. Comprehensive radial and axial air temperature and humidity profiles were nevertheless measured using this technique.

In conclusion , it is apparent from the literature that only very limited experimental studies have previously been carried out to measure air temperatures and humidities within a spray drier, and that all of these have related to co-current drying. It is remarkable that hitherto no experimental investigation of air temperature and humidity fields in a counter-current spray drier has been reported.

7.2.2 Instrumentation Design for Temperature and Humidity Measurement

A novel probe was designed and constructed for this study. This enabled the measurement of both the air temperature and air humidity at any point within the spray drying chamber. The detailed design and dual function of this probe is described in the following section.

7.2.2.1 Temperature Measurement

(a) Temperature Measurement Methods

For measuring the temperature of a gaseous atmosphere as in a spray drying chamber, three groups of methods can be employed. These are:

(i) Contact methods, including thermocouples, expansion thermometers and resistance thermometers.

(ii) Radiation methods, based upon the measurement of the intensity or colour of radiation emitted by the gas; and

(iii) Other gas property-based methods, e.g. density measurement

Of these techniques, the contact method is the most widely employed, although the radiation methods are now also considerably developed.

Additional complications arise when the gas whose temperature is to be measured is laden with droplets of a liquid phase. This is, of course, the situation within a spray drier. Under such circumstances, special consideration must be given to the technique employed, since the presence of the droplets will inevitably interfere with the temperature measurement.

The main difficulty in the application of the contact methods for temperature measurement arise from errors due to radiation and conduction. Consider a sensor, for example a thermocouple situated in a flowing gas stream within a spray drier as shown schematically in Figure 7.2. The sensor is positioned by some sort of support structure, or by its own leads. In such an environment the thermocouple tip will communicate by various paths to several environments, which in general will have different temperatures. These energy transfers are depicted by the dashed lines in Figure 7.2, and are described below.

(i) Radiative heat transfer will take place between the thermocouple tip and the walls of the drying chamber and other gaseous regions in the drier as a

result of temperature differentials. Only if the temperatures of the radiating bodies were identical to that of the gas in the vicinity of the thermocouple would radiation not occur, and the thermocouple tip temperature approach the true local gas temperature.

(ii) Conductive heat transfer will occur along the thermocouple wires from the tip to other parts of the thermocouple system if a temperature gradient exists along the thermocouple length. This would be the case, for example, when attempting to measure the temperature of air in the vicinity of the spray in co-current drying, where steep radial temperature gradients are known to exist.

(iii) The final energy transfer mechanism occurring in the system described in Figure 7.2 is the desirable convective heat transfer from the gas, causing the tip temperature to approach the gas temperature.

The combined effect of the radiative and conductive heat exchanges will be that the temperature of the thermocouple tip, and hence the measured gas temperature will only represent an approximation to the true temperature of the gas. If an accurate temperature measurement is to be obtained, the radiative and conductive errors must be minimised. Guidelines for minimising these errors are developed below.

Guidelines for Minimising Thermocouple Errors

The radiative heat transfer between the thermocouple and a radiating body is given by the following equation:

$$q_{rad} = \sigma e A_{tip} (T_{tip}^4 - T_s^4) \qquad 7.3$$

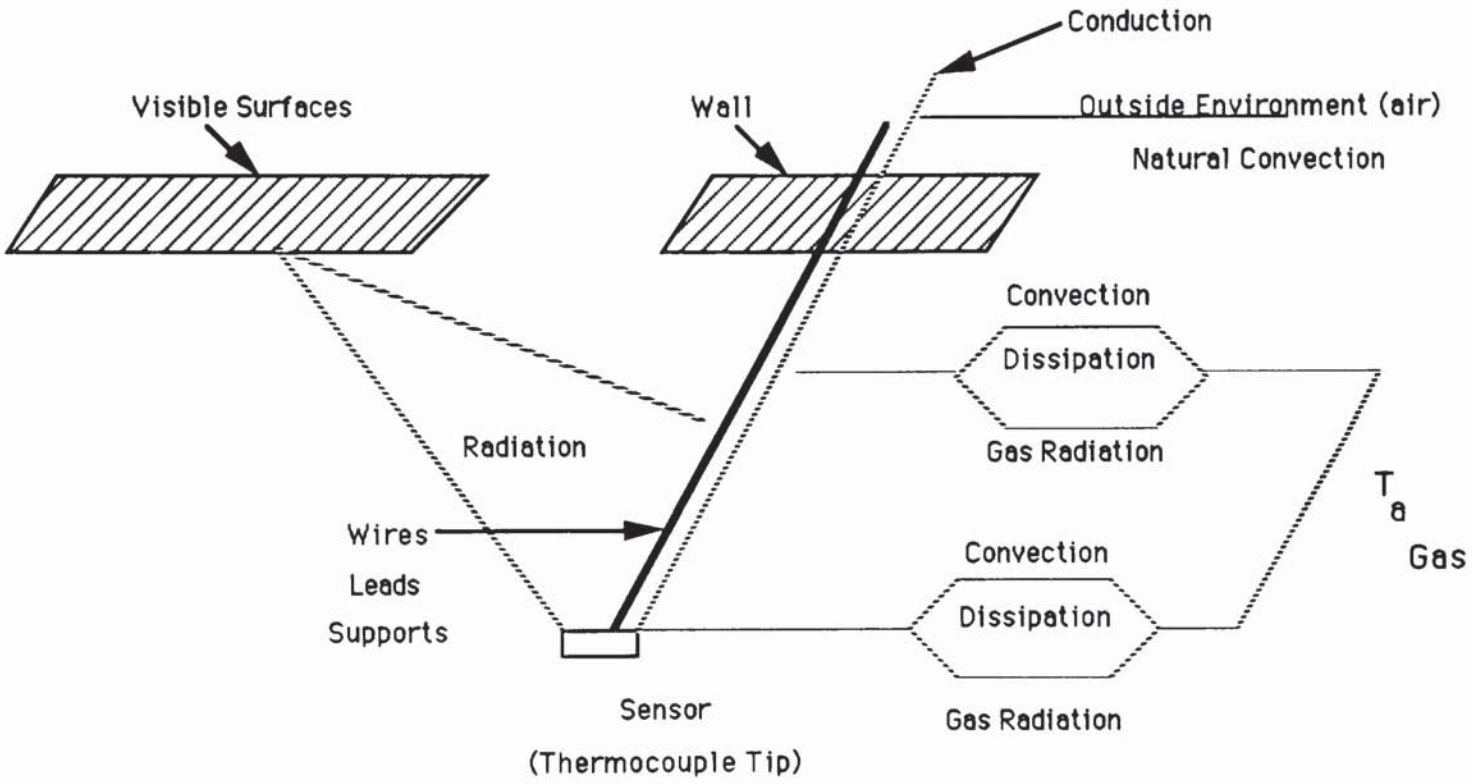

Figure 7.2 *Gas Temperature Measurement Errors*

where σ is the Stefan-Boltzman constant,

e is the emmisivity of the thermocouple,

T_{tip} is the temperature of the thermocouple tip,

and T_s is the temperature of any radiating surface, or body.

Examination of equation 7.3 suggests that the radiative heat transfer error can be minimised by:

(i) Eliminating the temperature differential between any visible, radiating objects and the thermocouple.

(ii) Keeping the emmisivity of the thermocouple wires as low as possible.

(iii) Making the wires of the thermocouple as fine as possible, bearing in mind strength considerations.

(iv) Shielding the thermocouple thereby screening radiation to, or from, the surroundings.

Similarly the heat that is conducted to, or away from, the thermocouple tip through the lead wires is given by,

$$q_{cond} = - k_w \pi r_w^2 \left(\frac{dT}{dx}\right) \qquad 7.4$$

where k_w is the thermal conductivity of the thermocouple wire,

r_w is the radius of the thermocouple wire,

and $\frac{dT}{dx}$ is the temperature gradient

Thus examination of equation 7.4 suggests that the conductive heat transfer error can be minimised by:

(i) Eliminating the temperature gradient along the length of the thermocouple wires.

(ii) Making the thermocouple wires as thin as possible, i.e. keep r_w as low as possible.

(iii) Making the thermal conductivity of the thermocouple wires, k_w , as low as possible.

Once the thermocouple has attained steady state, i.e. a constant tip temperature, the rate of heat transfer to the thermocouple by convection from the surrounding air can be equated to the rate of heat loss by conduction and radiation, viz:

$$q_{conv} = q_{rad} + q_{cond} \qquad 7.5$$

where the convective heat transfer is given by:

$$q_{conv} = h_g A_{tip} [T_a - T_{tip}] \qquad 7.6$$

Substituting equation 7.6 into the equation 7.5 and rearranging gives:

$$T_{tip} = T_a - \frac{q_{rad}}{h_g A_{tip}} - \frac{q_{cond}}{h_g A_{tip}} \qquad 7.7$$

The convective heat transfer coefficient, h_g, assuming the thermocouple tip to be spherical is given by the Ranz Marshall correlation:

$$Nu = 2.0 + 0.6Re^{0.5} Pr^{0.33} \qquad 4.3$$

From equation 7.7, when the convective heat transfer rate is made large, either by increasing the heat transfer coefficient or by increasing the thermocouple tip area, the effects of the radiative and conductive heat transfer errors become less serious and the temperature of the thermocouple approaches that of the true air temperature.

In view of this correlation, it was decided that temperature measurement errors due to radiation and conduction should be attenuated by adopting an approach based upon increasing the convective heat transfer rate to the thermocouple. This could be achieved by raising the velocity of the air-flow, over the tip. This approach was preferred to the alternative of using ultra-fine thermocouples and having to deal with mechanical problems thereby created [143].

The guidelines established earlier for minimising conductive and radiative errors were nevertheless still borne in mind in the subsequent temperature probe design.

(b) Temperature Probe Design

The criteria used in the design of the temperature probe were that it should

(i) Minimise, as far as possible, radiative and conductive errors by maximising the convective heat transfer rate to the thermocouple tip and by generally following the guidelines established previously, and

(ii) In-view of the presence of the droplet phase within the drier, feature some form of shielding to prevent impingement of droplets onto the thermocouple.

High air velocity and effective shielding were combined in the subsequent design of an aspiration-type probe for the measurement of air temperatures in the spray drying chamber.

The principle of operation of the probe was that air could be drawn from any location within the spray drier, and passed over a thermocouple at a very fast rate and hence the temperature of the air established.

The probe was, in total 86cm in length and consisted of a 1.9cm outer diameter stainless steel tube, through which was passed another stainless steel tube, 0.32cm in

diameter, which housed a Chromel-Alumel. i.e. K-type thermocouple. This type of thermocouple was selected because of its common availability and also because of the low thermal conductivities of the wires, which would result in lower conductive heat transfer errors compared to most other types of thermocouple.

The thermocouple, insulated with glass fibre, was 2m in length, with an overall diameter of 1.5mm, wire thickness of 0.315mm, and a tip diameter of 1mm. The thermocouple was manufactured by R.S. Components Ltd.

The stainless steel housing tube was located axially within the probe by support structures at either end. At the exit of the probe the housing was supported by simply exiting it centrally through a rubber stopper which also served to seal the probe. Within the probe the housing was supported by means of a PTFE stand. Essentially this stand was a cylindrical PTFE piece, 38mm long and with a diameter equal to the inside diameter of the probe, i.e. 15mm. From this piece, two side sections had been machined away so that the stand could support the thermocouple housing and at the same time air could by-pass it. The thermocouple housing extended half way into the PTFE stand, whilst the self-supported thermocouple protruded 30mm from the edge of the stand. The thermocouple was permanently fixed by gluing it to the stand. The principal dimensions of the probe are given in Figure 7.3.

In order to ensure that no droplets were entrained with the sampled air flow, special consideration was given to the design of the inlet to the probe. In the final design, a 3.8cm length of 2.9cm outer diameter stainless steel tube was mounted concentrically to the end of the probe to form a cyclone-type arrangement, as shown in Figure 7.3. A 1.6mm hole diameter was drilled tangentially into this shielding cap at an angle of 45° such that air drawn into the probe would be forced to swirl around the probe before entering it and passing over the thermocouple. The swirling motion of the air would endeavour to remove any water droplets that may have been present. As an additional precaution, two stainless

steel plates were fixed to either side of the cap so that any spray hitting the probe would flow down these and not towards the air inlet port. This shielding arrangement prevented droplet impingement and entrainment, and also served to screen the thermocouple from radiation to, or from, the surroundings, thus minimising radiative heat transfer errors. Such errors were further reduced by shrouding the entire shield cap in aluminium foil.

Three tee sections, 1.27cm in diameter, 2.54cm in length were fitted to the rear of the probe. These were used for connection of the vacuum, compressed air and humidity sampling lines. (The purpose of the latter two is described later). For the measurement of air temperature the vacuum line, which was 1.2cm in diameter, was opened fully and air at a rate of 540cm^3/s was drawn passed the thermocouple. This large sampling rate corresponded to an air velocity of approximately 3.0m/s, and ensured a very rapid thermocouple response time. It also minimised any errors that may have occurred as a result of radiation or conduction.

After exiting the probe the thermocouple was connected, via a Comark selector unit, to a digital temperature indicator, Comark type 2502. This featured cold junction compensation and was calibrated for a type K thermocouple to give a direct reading of temperature in degrees Centigrade, with a resolution of 0.1°C.

Conduction and radiation error calculations which are given in Appendix C, confirmed that this probe would enable the accurate measurement of air temperature, with a maximum combined conductive and radiative heat exchange error of just 1°C. This is approximately the same degree of error that can be expected from the use of ultra-fine thermocouples in an immersion-type design [143]. The thermocouple probe is shown in Plate 7.4.

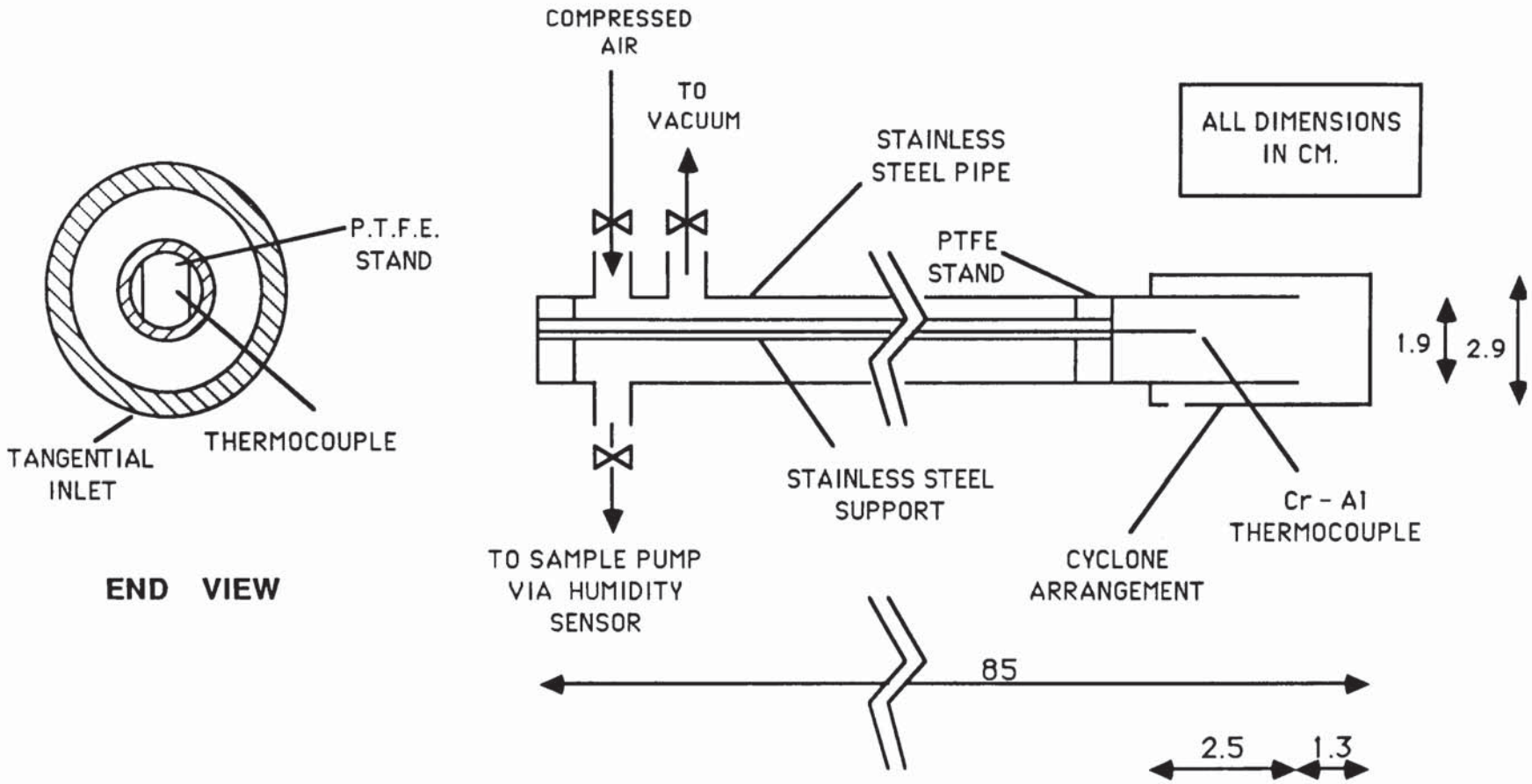

Figure 7.3 *Temperature / Humidity Probe Dimensions*

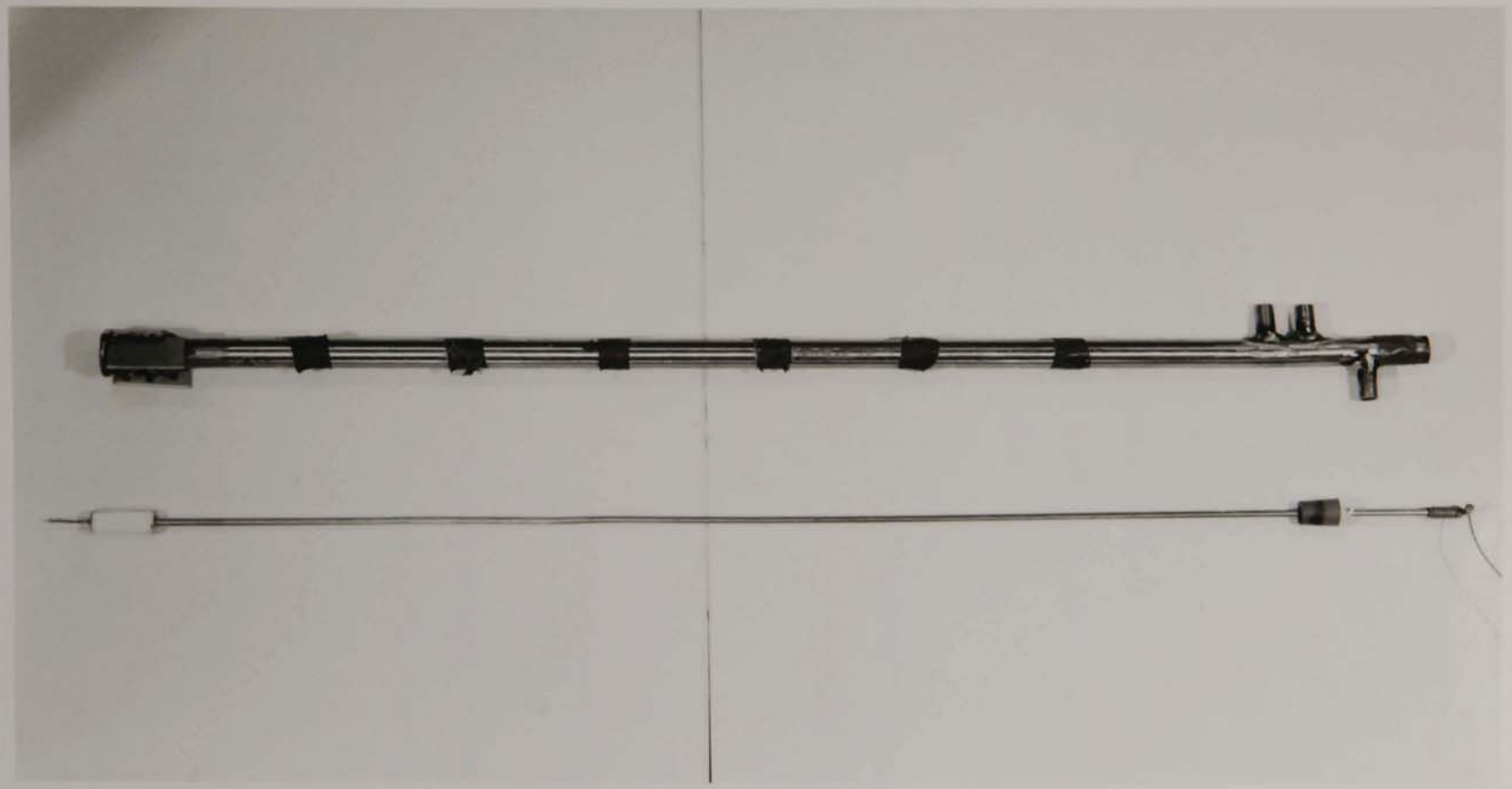

Plate 7.4 *The Thermocouple Probe*

7.2.2.2 Humidity Measurement

(a) Humidity Measurement Methods

Four main methods are commonly employed for the measurement of the humidity of a gas. These are:

(i) Chemical methods, which are based upon passing a known volume of air through a dessicant, such as phosphorous pentoxide or concentrated sulphuric acid, and then measuring either the change in weight of the dessicant or the change in volume of the air.

(ii) Dew-point methods which determine humidity via the measurement of the dew point temperature of the air.

(iii) Wet-bulb temperature methods.

(iv) Porous material methods, which, are based upon the measurement of the change in weight, dimension, or twist of a porous body, e.g. the hair hygrometer.

In the search for a suitable humidity measuring technique for this study, each of the above methods was considered. The chemical method option was discarded because it was judged that extensive sampling of the air would be required to induce the degree of dessicant weight-increase needed to give an accurate measurement. The porous material method was also judged to be unsuitable, because of the poor accuracies typical of this sort of hygrometer.

The possibility of using a wet-bulb temperature method was considered, but eventually rejected in favour of the dew-point method. The reason was that certain conditions would have had to be strictly adhered to, to enable accurate measurements. These were, that the wet-bulb had to maintained saturated with water at all times, and that the air sample had to be passed over the surface of the wet-bulb at a velocity in excess of 5m/s. The latter is necessary for:

(a) the condition of the gas not to be affected appreciably by the evaporation of liquid;

(b) for the heat transfer by convection to be large compared to radiation and conduction from the surroundings and;

(c) for the ratio of coefficients of heat and mass transfer h_g/k_g, to have reached a constant value.

When attempting to measure the humidity within a spray drier, as in this study, compliance with these conditions becomes extremely difficult and accurate measurements cannot be guaranteed. Hence in this study, the alternative, simpler technique of dew-point measurement was selected.

(b) Humidity System Design

For the measurement of air humidity within the drying chamber, the technique chosen involved sampling air from any location within the drier, and passing it through a dew-point sensor, located exterior to the drier.

Sampling of the air from the droplet laden atmosphere required identical consideration as in the design of the temperature probe, since in both instances droplet entrainment with the sampled flow had to be prevented. The same probe designed for temperature measurement was therefore also used to sample the gas for humidity measurement. In this design, provision had already been made for the removal of entrained droplets from the sampled air, and hence no further modifications were necessary. The dimensions of the probe are shown in Figure 7.3.

The dew-point sensor used for determining the humidity of the sampled air, was supplied by Shaw Moisture Measurements Ltd, and was of type 'Normal HT'. The principle of operation of the sensor was based upon the fact that the capacitance varies in direct proportion to the dew point of the gas. The sensing element itself was protected

from dust and moisture by a sintered bronze filter. The sensor and filter are shown in Plate 7.5.

Air flow over the filter resulted in the establishment of dynamic equilibrium between the water vapour pressure outside the layer and the condensed water absorbed in its fine pores. The sensor could then estimate the capacitance of the gas and transmit it via a co-axial cable to a Shaw six-way hygrometer. This meter was scaled from 0 to 100%. The percentage reading could subsequently be converted to dew point by means of a calibration curve supplied by the sensor manufacturer. This calibration is shown in Figure 7.7.

The dew point sensor was housed in a constant temperature unit, which, maintained a constant temperature of gas flowing to the sensing element. It also prevented condensation of the water vapour in the sampled gas, by maintaining the gas at a temperature above its dew point. The unit comprised a brass container into which the dew-point sensor was screwed. A dial switch mounted on the unit controlled a sensitive thermostat, which maintained a constant temperature set by the dial. This temperature could be varied in the range 0-110°C. Heating to the sensor chamber, which was constructed from chrome-plated heavy brass, was supplied by an internal 30W heater. The constant temperature unit was fitted with inlet and outlet ports, each of 0.32cm outer diameter. A constant flow of air through the unit and thus passed the dew point sensor was supplied by a Charles Austen sample pump. This drew air from the drier via the sampling probe at the rate of $8cm^3/s$.

Initially the sample line from the probe to the constant temperature unit was manufactured in 1.27cm diameter PVC. However a preliminary test indicated that a large amount of condensation was occurring within the line, and this was adversely affecting the humidity measurement. Therefore to avoid condensation, the sample line from the probe to the sensor was electrically heated to a temperature above the dew point of the sampled

Plate 7.5 *The Dew-Point Sensor*

air. Because of the poor mechanical quality of PVC tubing at elevated temperature, a 1.27cm diameter Nylon-reinforced-PVC tube of length 1.5m was therefore used to connect the probe to the sensor. A 1.8m length of 80W, rubber-insulated electrical heating tape, of type GW, manufactured by Hotfoil Ltd, was then spirally wrapped round the entire length of the sample line. Heating tape and line were then both covered by an insulating layer of glass fixing tape and then covered by aluminium tape. The temperature of the sample line was controlled by adjusting the voltage supply to the heating tape, by means of a Variac unit. The sample line could thereby be maintained at a temperature of approximately 80°C and hence condensation totally eliminated. The complete humidity measuring apparatus is shown in Plate 7.6. The components of the entire temperature and humidity measurement system developed in this study are shown schematically in Figure 7.4.

7.2.3 Spray Drying Experimental System

A schematic diagram of the entire drier system is shown in Figure 7.5.

(a) The Spray Drying Tower

The spray drying tower used in this investigation was a counter-current stainless steel drier similar in dimensions to the PVC tower used for the Flow Visualisation work described earlier. This was the same tower used previously by Esubiyi [155].

The tower consisted of a main cylindrical section, 1.22m in diameter 2.44m in height, onto the ends of which were bolted a conical base section and a top dished end section. The conical base of the tower was also 1.22m in diameter and had a height of 0.9m. This base terminated into a 5.1cm bore B.S.P flange, to which was fitted a 5.1cm Q.V.F valve. The dimensions of the tower are shown in Figure 7.6.

A 7.5 cm diameter ring main was installed around the base of the tower at a position 0.3m from the bottom. The drying air passed through this main, into four admission ports, equally spaced around the periphery of base cone at 90° to one another.

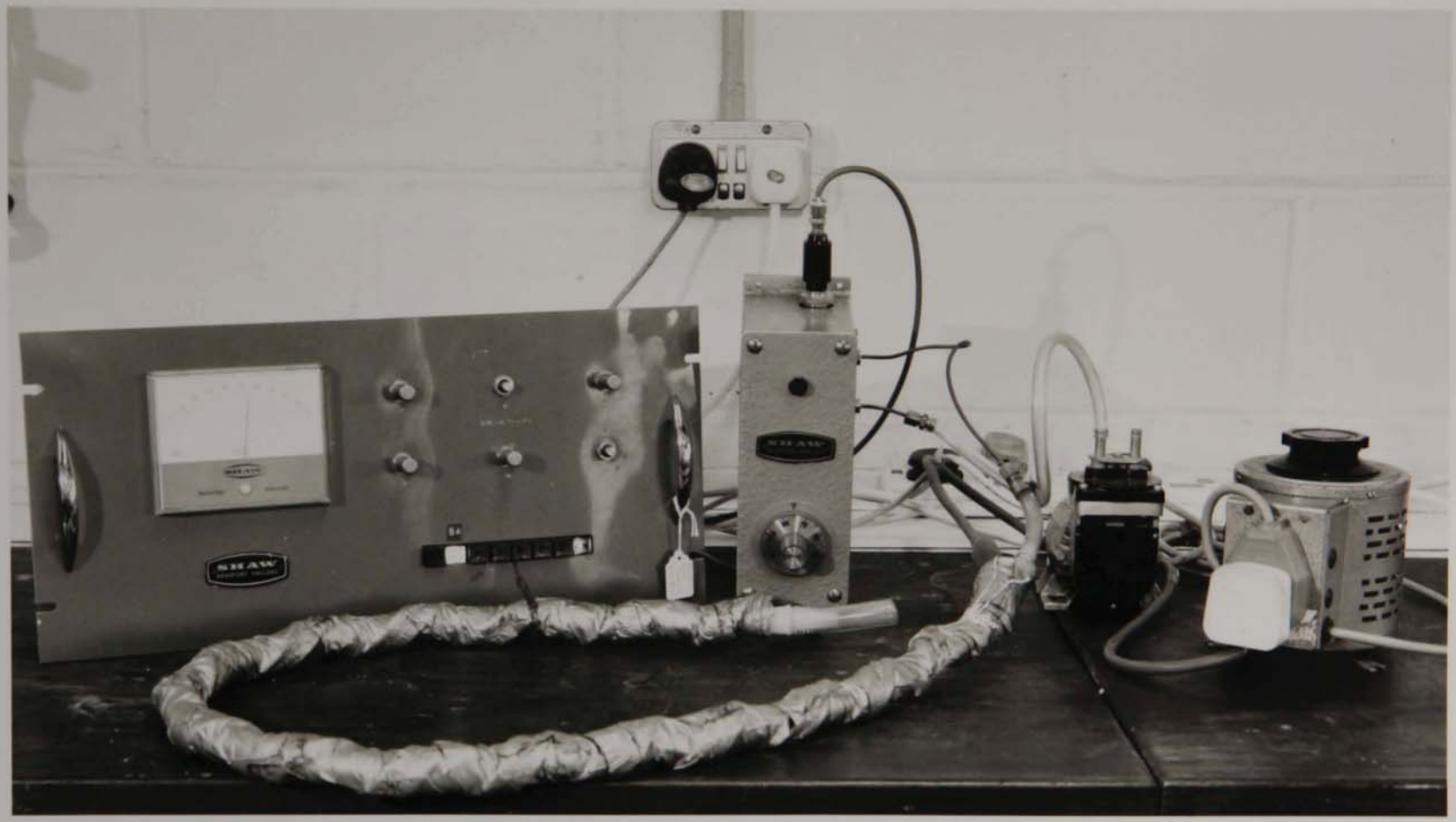

Plate 7.6 *Components of the Humidity Measuring System*

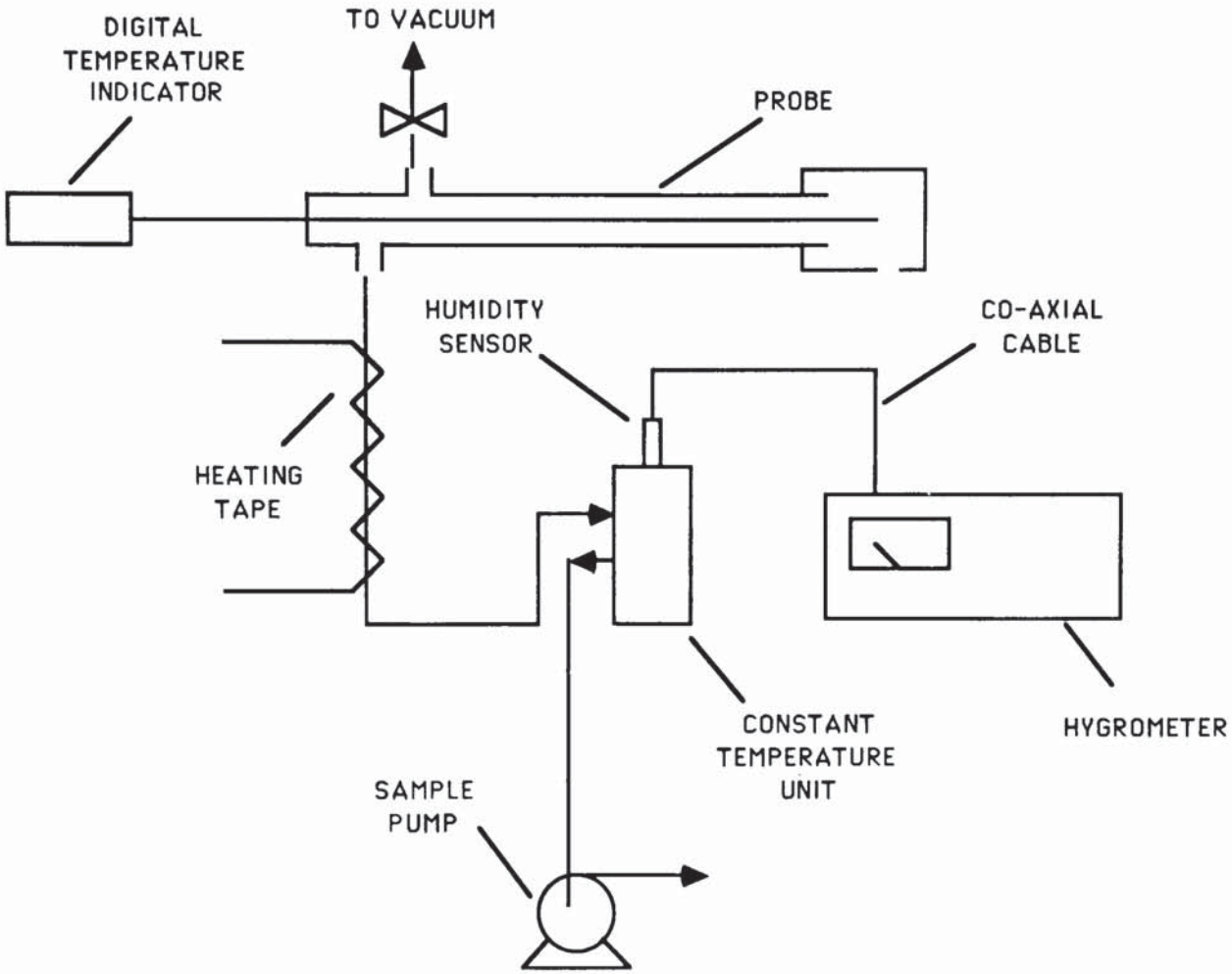

Figure 7.4 *Temperature / Humidity Probe Layout with Accesories*

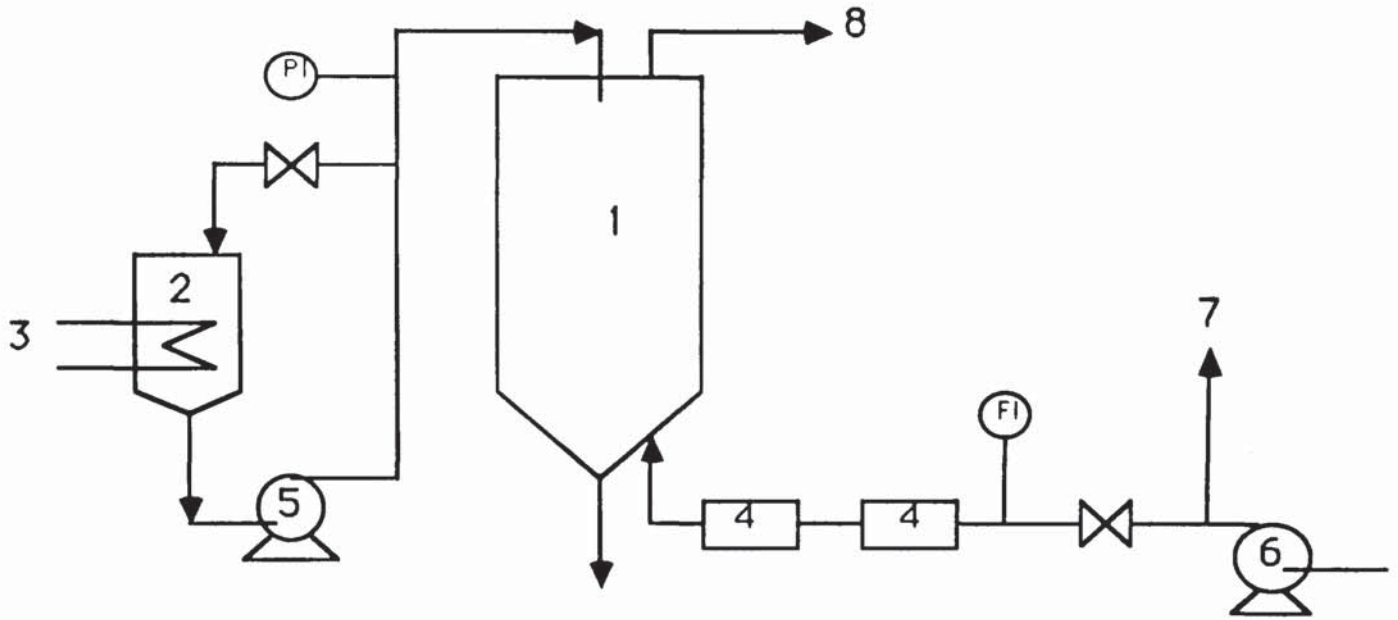

Equipment List

1 Counter-current Spray Drier	5 Liquid Feed Pump
2 Liquid Feed Tank	6 Air Blower
3 Steam Coil	7 Purge
4 Electric Hearters	8 Cyclone Separator

Figure 7.5: *Pilot Spray Drier Installation*

Five sampling ports each of 5.08cm diameter were drilled along the length of the tower at the axial locations of 1m, 2m, 2.5m, 3m and 3.35m from the air entry level. These ports enabled the probe to be inserted into the tower and the air temperatures and humidities at various radial locations to be determined. To provide support for the probe during such measurements, a metallic frame was constructed at the exterior of the drier. Clamps were then attached to this frame-work, which during experimentation, firmly grasped the probe at the desired radial positioning. The complete temperature and humidity measuring system. with the probe in-position inside the drier is shown in Plate 7.7.

(b) Air Supply to the Drier

Air from atmosphere was fed to the ring-main of the drier, through 10.16cm diameter mild steel piping, by a 15kW, 3 phase Parkinson fan. The air flowrate was controlled by a 10.16cm Audco Slim Seal Valve, which simply vented excess air through a purgerator to atmosphere. The flow rate of the air was measured, on-line, by a Dall tube which had a diameter of 10.16cm and a throat bore of 4.6cm. The Dall tube was supplied by George Kent Ltd. The air pressure drop across the tube was measured by an Air Flow Developments 'Slim Jim' manometer which gave a direct reading in N/m^2.

The air was then passed through two Secomak Industrial heaters which were mounted in series. The first was capable of generating 12kW of heat and the second 18kW. Each heater was 0.47m in length and flanged at either end. Due to a large pressure drop in the air feed line, the two heaters could not be used concurrently as excessive heat was generated which would inevitably have resulted in damage to the heater filaments. This was a flaw in the design of the pipework and is discussed further in Chapter 10.

(c) Liquid Feed System

Liquid was pumped to the nozzle atomiser at the top of the tower, through 4.4cm diameter stainless steel piping, from a stainless steel feed tank positioned at the foot of the drier. This feed tank was 0.91m in diameter and 0.91m in height. It was fitted with a

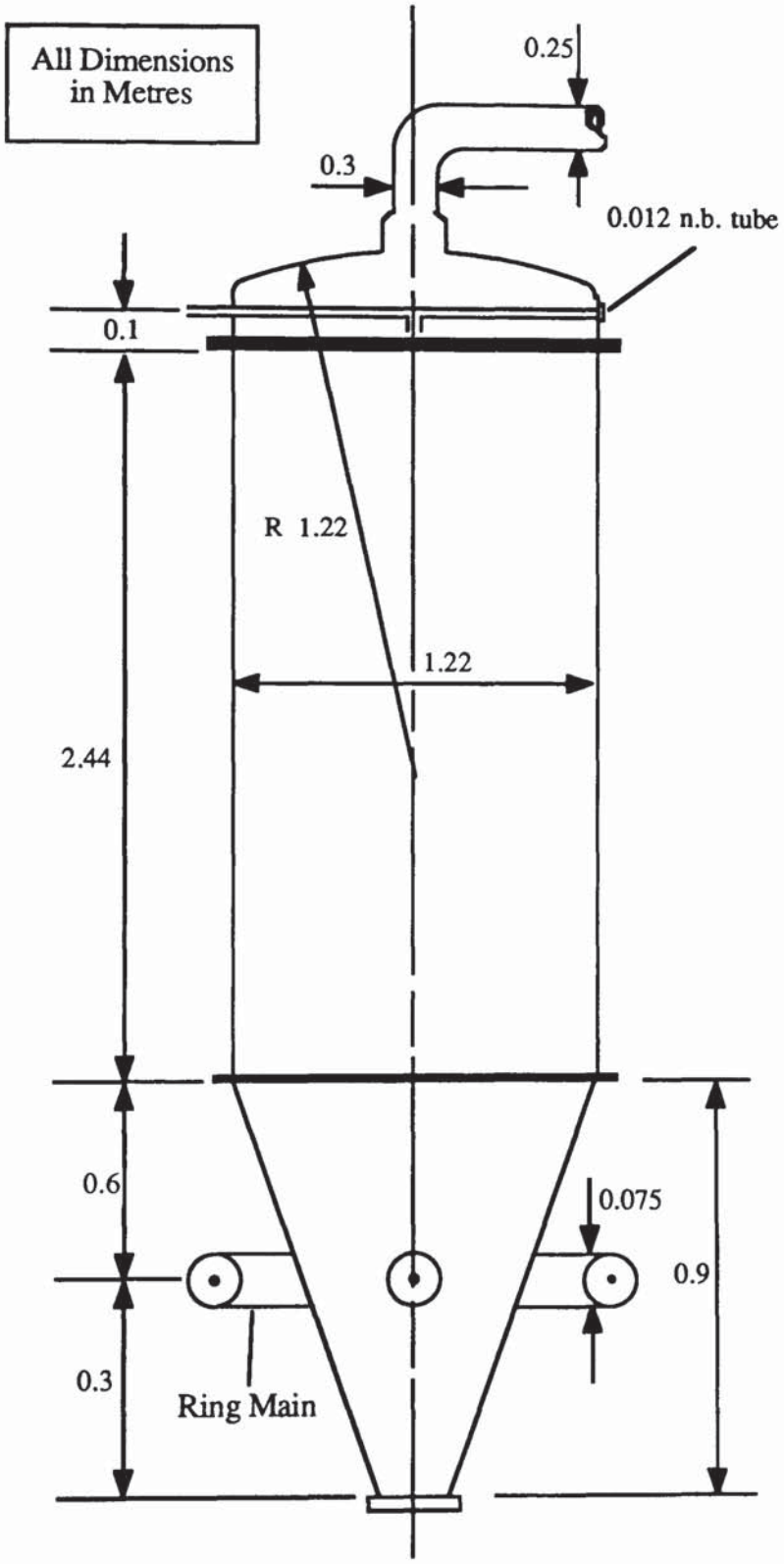

Figure 7.6 *Dimensions of the Stainless Steel Drier*

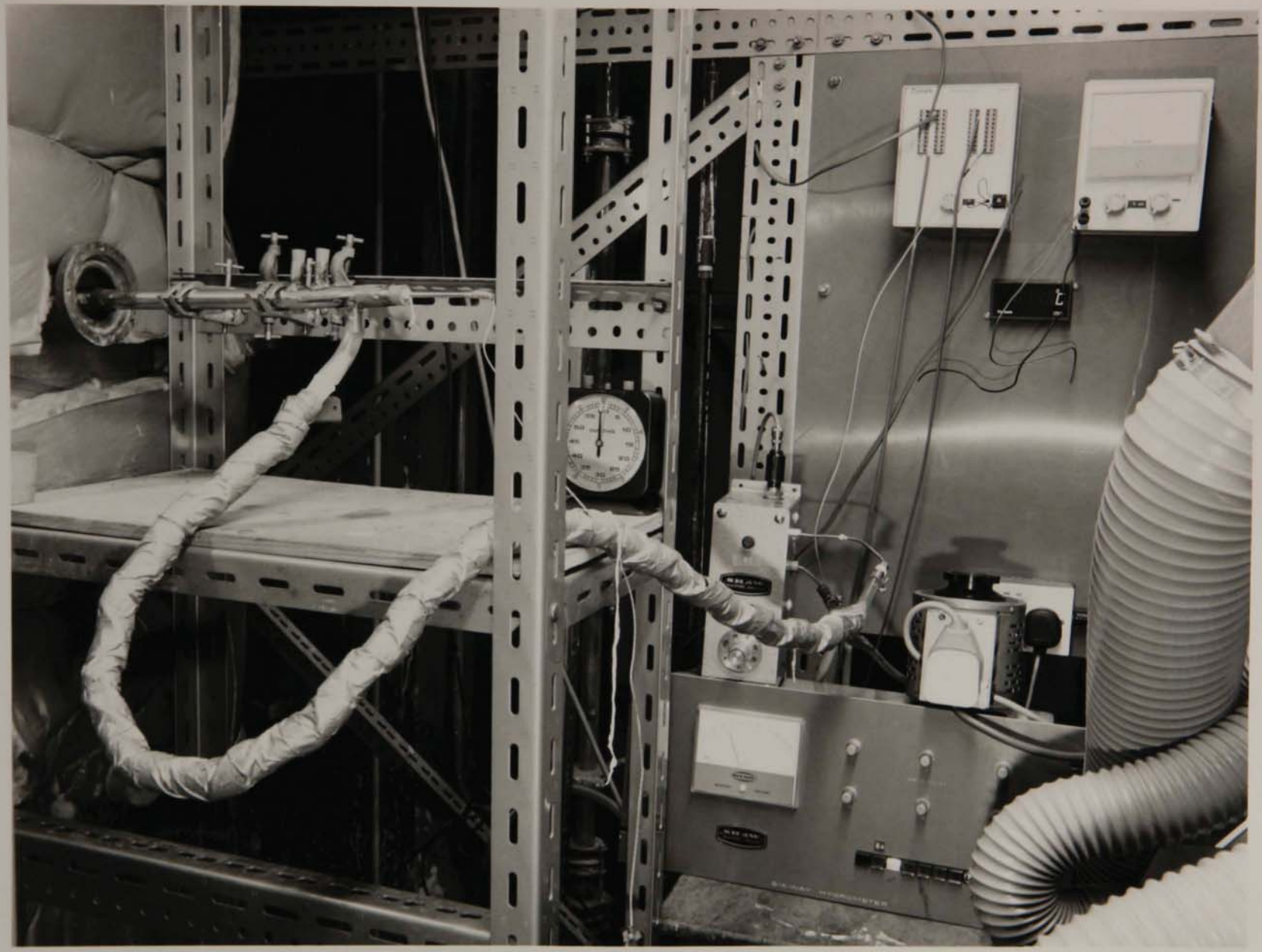

Plate 7.7 *The Temperature and Humidity System*

stirrer, a steam coil and a Spirax-Sarco Type 128 temperature controller. A sight glass was attached to the exterior of the tank to enable easy detection of the feed level. The pump used for transporting the liquid was a fixed speed 3 phase Speck-Kolben piston pump driven by a 3kW Brock-Compton Parkinson motor. Because the pump was of fixed speed, the liquid pressure at the atomiser could only be adjusted by opening or closing a by-pass line recycling back into the liquid feed tank.

The atomisation pressure at the nozzle was measured by a Budenburg diaphragm-type gauge. Preliminary experimentation, however, showed that due to excessive low intensity fluctuation, the life of the pressure gauge was reduced to a few hours. This problem was subsequently overcome by fitting a pressure snubber, also manufactured by Budenburg, directly below the gauge.

Atomisation of the liquid feed within the spray tower was achieved through the use of 2 different centrifugal pressure nozzles, both manufactured by Spraying Systems Co. These were:

(i) A Whirljet $\frac{3}{8}$ BD-5, a stainless steel nozzle of height 32mm and hexagonal diameter 17.5mm, with an inlet diameter of 2.8mm and an orifice diameter of 3.2mm. This type of nozzle provides a hollow cone spray pattern, and a uniform spray distribution.

(ii) A 'SprayDry' $\frac{1}{2}$ AASSTC-6 with a stainless steel body, and a tungsten carbide orifice insert. This nozzle features a six-piece design in which the whirl chamber is held in position with a spring. The nozzle had a height of 58mm with a hexagonal diameter 35mm and an orifice diameter of 3.5mm. This type of nozzle is typically used in the spray drying of detergent and coffee solutions..

The two nozzles are shown in Plate 7.8.

Plate 7.8 *The Centrifugal Pressure Nozzles*

The capacity, pressure and spray angle characteristics of each of these nozzles, as quoted by the manufacturer [144] are given in Table 7.2.

	Pressure (psi)					
	7	20	40	60	80	100
Water Flowrate (kg/s)	0.027	0.044	0.063	0.076	0.088	0.1
Spray Cone Angle (°)	56	67	-	-	76	-

(a) Whirljet $\frac{3}{8}$ BD - 5

	Pressure (psi)					
	40	60	80	100	150	200
Water Flowrate (kg/s)	0.064	0.077	0.089	0.1	0.123	0.142
Spray Cone Angle (°)	89	89	86	83	80	78

(b) Spray Dry $\frac{1}{2}$ AASSTC

Table 7.2: *Pressure Nozzle Spraying Characteristics* [144]

7.2.4 Calibration of Measuring Instruments

(a) Dall Tube

An expression for the mass flowrate of air through a differential pressure meter, such as a Dall tube is given in B.S. 1042 [145]. Rearranging this into SI units gives:

$$G_a = 1.11 \times 10^{-4} C_d Z d_t^2 E \rho_a \Delta P^{0.5} \qquad 7.8$$

where the symbols are as defined in the Nomenclature.

The Dall tube used in this study, had a throat diameter of 4.65cm and a tube diameter of 10.16cm. Assuming a value of 0.98 for the discharge coefficient of the tube [146], equation 7.8 becomes:

$$G_a = 2.40 \times 10^{-3} \rho_a^{0.5} \Delta P^{0.5} \qquad 7.9$$

Thus with the pressure drop measurement across the Dall-tube, equation 7.9 can be used to determine the mass flowrate of air to the spray drier.

(b) The Hygrometry Equipment

The dew point sensor and the six-way hygrometer were calibrated by their manufacturer, Shaw Moisture Meters Ltd. A calibration curve for the dew-point range of 0 to 40°C, corresponding to the percentage reading on the hygrometer was thereby obtained. This is shown in Figure 7.7. A dummy load giving a certain percentage of full-scale deflection, was also provided by the manufacturer to enable the sensitivity adjustment on the hygrometer to be correctly set prior to measurement. Thus, through the use of the sensor calibration curve, the percentage reading from the hygrometer could be directly converted to gas dew point temperature.

The water vapour pressure was then calculated by application of the Antione equation

$$p_v = 133.32\, e^{(18.3036 - (3816.44/T_{dp} - 46.13))} \qquad 7.10$$

The humidity of the air could then finally be calculated by the relationship

$$H = \left(\frac{p_v}{P - p_v}\right)\left(\frac{18}{29}\right) \qquad 7.11$$

Where P is atmospheric pressure.

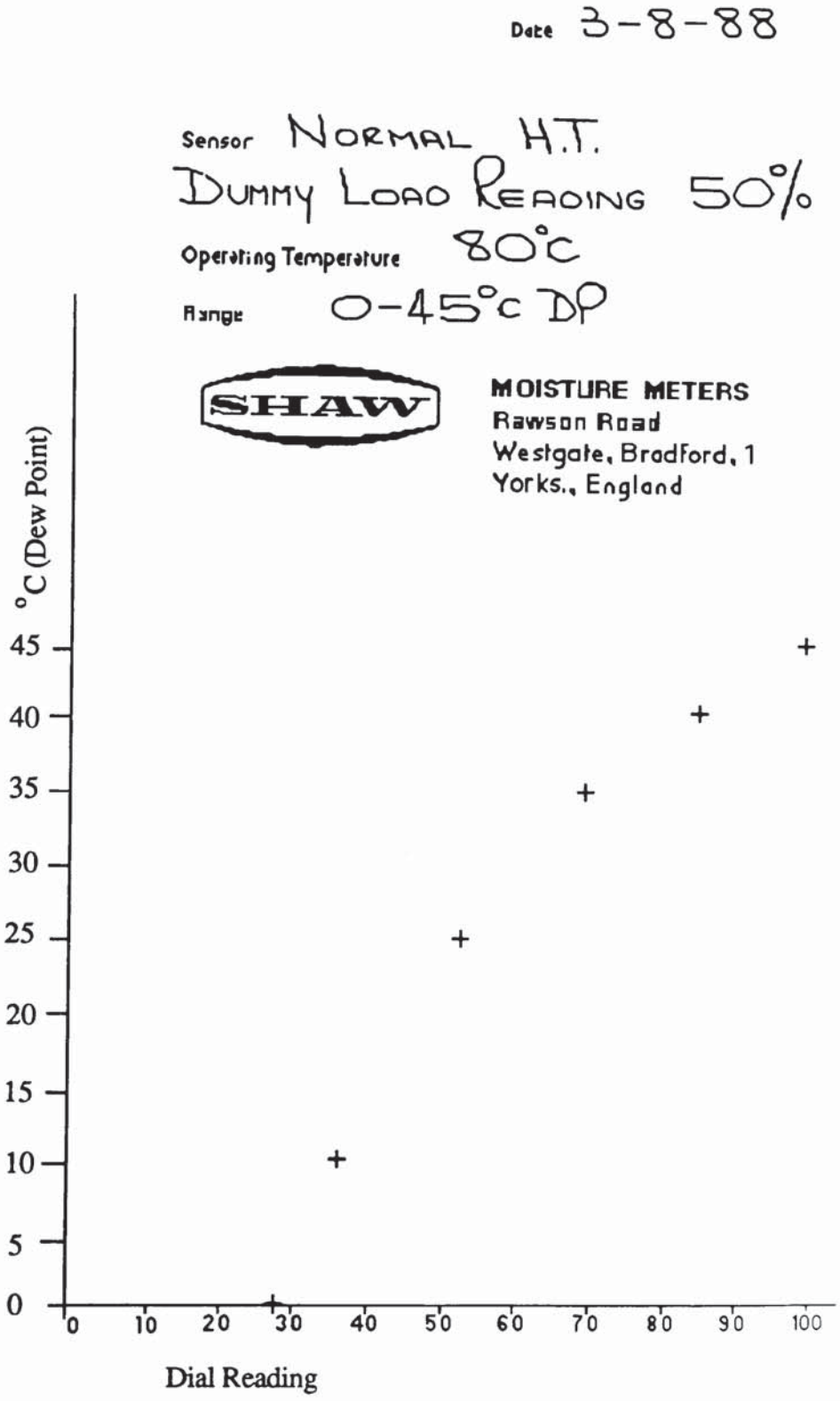

Figure 7.7 *Dew-Point Calibration Curve*

The calibration of the dew-point sensor was checked regularly by sampling ambient air and calculating the humidity from the percentage reading on the meter via the calibration and the equations listed above. This was compared to the humidity determined from the measurements using a Whirling Sling hygrometer. A favourable agreement was always obtained.

7.2.5 Experimental Conditions

The operating parameters likely to have a major influence on the establishment of air temperature and humidity fields within the drying chamber are

(i) the drying air flowrate,

(ii) the drying temperature, and

(iii) the liquid feed rate, which is fixed by the atomisation pressure.

In this study, the drying air flowrate and temperature could not be treated as independent variables, since the only way of controlling the temperature was by altering the air flowrate for a constant heater output. Thus the drying air flowrate was varied between 0.16kg/s and 0.088kg/s with corresponding air temperatures of between 135°C and 190°C.

The liquid atomisation pressure was varied between 50 and 150 psi with corresponding liquid flowrates of between 0.069 and 0.123kg/s In this work it was decided to study the evaporation of only pure water droplets since the trends of temperatures and humidities within the drier will be largely independent of the feed material.

The inlet air humidities for this study depended on atmospheric conditions and varied between 0.0067 and 0.0092kg vapour/kg air.

The complete range of operating conditions for all the experimental runs is given in Table 7.3.

Run	Air Flowrate (kg/s)	Air Temperature (°C)	Air Humidity (kg/kg)	Liquid Flowrate (kg/s)	Atomisation Pressure (psi)	Liquid Temperature (°C)	Nozzle
1	0.16	135	0.0067	0.071	50	19.7	SprayDry
2	0.16	135	0.0077	0.100	100	21.0	SprayDry
3	0.16	136	0.0080	0.123	150	22.7	SprayDry
4	0.135	160	0.0077	0.071	50	25.0	SprayDry
5	0.135	160	0.0092	0.100	100	25.0	SprayDry
6	0.135	160	0.0090	0.123	150	20.9	SprayDry
7	0.135	160	0.0086	0.069	50	22.0	Whirljet
8	0.135	156	0.0077	0.101	100	21.0	Whirljet
9	0.088	190	0.0069	0.101	100	21.0	Whirljet
10	0.088	190	0.0081	0.069	50	20.0	Whirljet

Table 7.3 *Experimental Conditions for Temperature and Humidity Studies*

7.2.6 Experimental Procedure

In total 10 experimental runs were carried out, all using pure water as the feed material. A typical run required approximately 5 hours for completion. The experimental procedure followed in each run is detailed below.

The feed tank was filled with water and the level on the sight tube noted. The feed pump was switched on and the pressure at the atomiser was adjusted by either opening or closing the by-pass line which recycled the water back into the feed tank. In this manner the desired atomisation pressure was obtained.

The air blower was switched on and the desired air flowrate was obtained by adjusting the Audco valve. The pressure differential across the Dall tube, as measured by the manometer was noted. The appropriate electrical heater was then switched on. The inlet and exit air temperatures in the spray tower were monitored until they both reached a constant value, signifying steady state operation had been attained.

Approximately 45 minutes was required to achieve steady state, following which radial and axial probing for temperature and humidity commenced. Initially, radial probing was performed every 10cm starting at a position of 60cm from the column wall and proceeding inwards towards the wall. The exterior of the probe was graduated to facilitate accurate radial positioning. Probing was carried out at each of the five axial locations described earlier. At any axial location, the probe was used exclusively for either temperature or for humidity measurement until radial probing at the particular level had been completed. The procedures for temperature and humidity measurement are described below.

(a) Temperature Measurement

Once the probe had been placed at the desired radial position, it was fastened with clamps to the framework at the exterior of the drier. After ensuring the humidity sample

pump was switched off and the valve in the humidity line was closed, the valve in the vacuum line was opened fully and air from the locality of this particular radial position was drawn into the probe and passed the interior thermocouple. Because of the large air sampling rate, the response of the thermocouple was very rapid and a constant temperature was indicated by the thermocouple after approximately 2 minutes, or slightly longer if the probe had just been inserted into the drier, e.g. at a new axial location. After a steady temperature had been obtained, the vacuum line was closed and the probe moved to the next radial position. Occasionally the temperature indicated by the thermocouple would fluctuate, but this was always within 1°C and eventually a steady temperature would be reached. The maximum time that was needed for establishment of a steady temperature in any of the measurements was of the order of 3.5 minutes.

After probing at a particular axial location had been completed, the probe was taken out of the drier and the thermocouple, together with its housing and supports were removed so that the thermocouple tip could be closely examined. In all cases the thermocouple was found to be completely dry.

(b) Humidity Measurement

For the measurement of air dew-point, and hence humidity, the probe was again inserted into the drier, at the desired radial location and fastened to the framework with clamps. After ensuring the vacuum and compressed air lines were closed, the valve in the humidity sampling line was opened fully and the sample pump was switched on. Sampling continued for approximately 45 seconds, following which the reading on the hygrometer was noted. The sampling duration of 45 seconds was selected on the basis of preliminary work which suggested that this time was sufficient for the humidity of air just outside the probe to be measured and registered on the hygrometer. This time of 45 seconds was also in line with the theoretically calculated sample time based upon the volume of the sampling lines and the sampling flowrate.

When probing at each radial position was complete, the humidity sample pump was switched off, the valve in the humidity line closed and the probe was purged thoroughly with compressed air, for approximately 60 seconds. In this way any condensate within the probe or any water build-up within the cap of the probe, was forced out, thus minimising any adverse effects on the dew-point measurements.

Occasionally after probing at one axial location had been completed, the probe was removed from the drier, purged through with compressed air, and as a check atmospheric air was sampled through the probe. In all cases the dew-point of the air sampled through the probe was within 1°C of air that was sampled directly thus suggesting that any condensate build-up within the probe was insignificant.

The air humidity and temperature profiles within the drying chamber, measured using the procedures described above, are presented in Chapter 8.

7.3 DROPLET SIZE MEASUREMENT STUDIES.

A sequence of experiments were carried out to determine the droplet size distributions of water sprays produced from hollow cone pressure nozzles of the type used in the temperature and humidity study. The objectives of this work were two-fold.

(i) To generate droplet size distribution data for each of the atomisation conditions pertinent to the temperature and humidity study. Such data is required as an input to the mathematical model for the simulation of the experimental runs, and hence assessment of model predictions.

(ii) To carry out an initial investigation on the phenomena of droplet agglomeration within a spray in counter current drying. If present, agglomeration is characterised by a shift in the droplet size distribution towards the coarse end and an increase in the mean drop size, as the spray descends the tower.

To enable accurate determination of droplet size distribution, a Malvern Laser Particle Size Analyser was used. The principle of operation of this equipment is described below.

7.3.1 Malvern Particle Size Analyser

The Malvern laser particle size analyser employs a laser diffraction technique for determination of particulate size distribution. When a beam of light falls on a spherical particle, a diffraction pattern is formed whereby some of the light is diffracted by an amount dependent upon the size of the droplet. If a suitable Fourier Transform lens is placed in the light path behind the droplets and a detector is placed at the focal point of the lens, then the light not diffracted by the droplet is brought to a point on the detector. The light which is diffracted by the drop, forms a light ring concentric to the focal point. If a sample containing different droplet diameters is sampled in the beam then a series of concentric light rings will be generated at various radii each being a function of a particular droplet size . Hence from this diffraction pattern the droplet size distribution can be calculated. The Malvern particle size analyser used in this work was model 2600, and comprised a He/Ne laser emitter, a receiver, a system of lenses and an Olivetti-IBM-Compatible personal computer for data processing. The computer software, version 3.0, was supplied by Malvern Instruments Ltd. The laser diffraction pattern generated by the Malvern was fitted to a Rosin-Rammler distribution model, by computer, to yield the Rosin-Rammler parameters, i.e. the mean and the dispersion coefficient. In addition, it was possible to obtain a hard copy of the measured distribution data by connecting a printer to the Olivetti personal computer. This provided a detailed breakdown of the distribution by giving the % volume of sample that was contained in discrete size bands.

To ensure reliable results with this laser diffraction technique not more than approximately 65% of incident light should be blocked by the particle field. At higher obscuration, the effect is to give distributions which are broader and have a smaller mean size, and in these instances a correction factor may be applied [147].

7.3.2 Droplet Size Data For Drier Simulation

Experimental

The drop size distribution data required for drier simulation studies, was determined on a purpose-built 1.2m diameter perspex spray tower, across which the Malvern particle size analyser was positioned, mounted on an optical bench [148].

Liquid was pumped from a 30cm diameter glass feed tank to the pressure nozzle fitted at the top of the tower using a Compton-Parkinson feed pump driven by a 3kW motor. Baffles were fitted to the interior of the tower to eliminate mist associated with high pressure atomisation, and an adjustable length of PVC tubing extended from both the laser emitter and the receiver into the spray zone. This provided control of the volume of the spray sampled. Both of the above features were designed to minimise obscuration. As a result, drop size distributions of sprays could be measured with obscuration levels of typically less than 50%.

Using this apparatus, the droplet size distributions of water sprays produced from the 'Whirljet $\frac{3}{8}$BD-5' and the 'SprayDry $\frac{1}{2}$AASSTC' nozzles were determined for atomisation pressures of 50, 100 and 150 psi. In addition, a 'typical' droplet size distribution of a commercial solution, spray dried industrially on a large scale using a pressure nozzle, was measured for an atomisation pressure of 1200psi. This data was then used in the simulation of this industrial drying process.

A detailed description of the experimental procedure for operating the Malvern Particle Sizer and the spray tower will be given elsewhere [148].

7.3.3 Droplet Agglomeration Studies

Agglomeration of sprayed droplets within a spray drier will not only affect droplet motion and drying rate, but will also modify the dried product physical characteristics. For

example a significant increase in product granulometry will reduce the product bulk density. In such instances, excessive agglomeration must obviously be prevented.

Droplet coalescence or agglomeration can occur as the result of inter-droplet impingement between two or more sprays, e.g. in multi-nozzle drier operation, or may occur as the result of droplet collisions within a single spray, e.g. fast-moving large droplets impacting on the slower velocity smaller particles.

In this study, it was the latter case that was investigated, through measurement of the change in droplet size distribution as the spray descends the tower.

Experimental

The change in droplet size distribution during the descent of a water spray was measured using the Malvern Laser Particle Size Analyser in conjunction with the 1.2m counter current stainless steel drier. This drier, in addition to having sampling ports fitted to facilitate temperature and humidity measurements, had a second set of identical ports fitted diametrically opposite to and at precisely the same axial locations as the first set. This enabled the Malvern laser emitter and receiver to be mounted across the diameter of the drier.

With this arrangement droplet size distributions of a water spray produced from the 'SprayDry' nozzle spraying at a pressure of 100psi were measured at two axial locations, 0.35m and 1.35m from the nozzle. From the change in droplet size distribution down the tower, the extent of agglomeration could be assessed. These measurements were carried out for conditions of no drying air flow and also with air flowing at ambient temperature at a rate of 0.16kg/s. This was to assess the impact of the upward air flow on droplet agglomeration, bearing in mind that due to spray evaporation there may be a tendency for the distribution to shift downwards. The drier operating conditions are given in Table 7.4.

	No Air	With Air
Liquid Feed	Water	Water
Liquid Temperature (°C)	21·7	21·7
Atomisation Pressure (psi)	100	100
Liquid Flowrate (kg/s)	0·1	0·1
Nozzle	SS - $\frac{1}{2}$AASSTC	SS - $\frac{1}{2}$AASSTC
Air Flowrate (kg/s)	-	0·16
Air Temperature (°C)	-	30·7
Air Humidity (kg/kg)	-	0·0081

Table 7.4 *Drier Operating Conditions For Droplet Agglomeration Studies*

In these measurements, because there was no provision to limit laser obscuration, coupled with the large volume of spray that was sampled, obscuration levels were, in instances, greater than the 65% threshold for reliability. In these circumstances, correction factors had to be applied to the Rosin-Rammler parameters which characterised the spray.

These correction factors were defined as follows [147].

$$C_R = D_{Ro}/D_R \qquad 7.12$$

$$C_q = q_o/q \qquad 7.13$$

$$C_R = 1.0 + (0.036 + 0.4947\ OB^{8.997})\ q^{(1.9 - 3.437\ OB)} \qquad 7.14$$

$$C_q = 1.0 + (0.035 + 0.1099\ OB^{8.65})\ q^{(0.35 + 1.45\ OB)} \qquad 7.15$$

where q_o and q are the corrected and uncorrected dispersion coefficients,

D_{Ro} and D_R are the corrected and uncorrected Rosin-Rammler means, and,

OB is the obscuration level.

The droplet size distributions measured from the above work are presented in Chapter 8.

Chapter 8

Presentation of Experimental and Model Results

The results presented in this Chapter are divided into two sections. These are:

(i) Results obtained from the experimental investigations; and

(ii) Results obtained from the application of the spray drier mathematical model.

These are considered below.

8.1 EXPERIMENTAL RESULTS

In this section results are presented for:

(a) the air flow-pattern visualisation study;

(b) the spray drier temperature and humidity study; and

(c) the in-spray droplet agglomeration study.

8.1.1 Air Flow-Pattern Visualisation Study

The air flow patterns set-up in the transparent spray tower were established via smoke visualisation for each of the air inlet nozzle configurations and drier operating conditions given in Table 7.1. Sketches depicting the general flow patterns observed together with a description of the key characteristics of the flow are presented in Figures 8.1 - 8.13.

Figures 8.1 - 8.13

Observed Air Flow Patterns via Smoke Visualisation

Figure 8.1 *Air Flow Patterns Case 1*

- 4 Nozzles Open
- Straight
- Total Air Flowrate = 1700 m^3/h
- No Spray

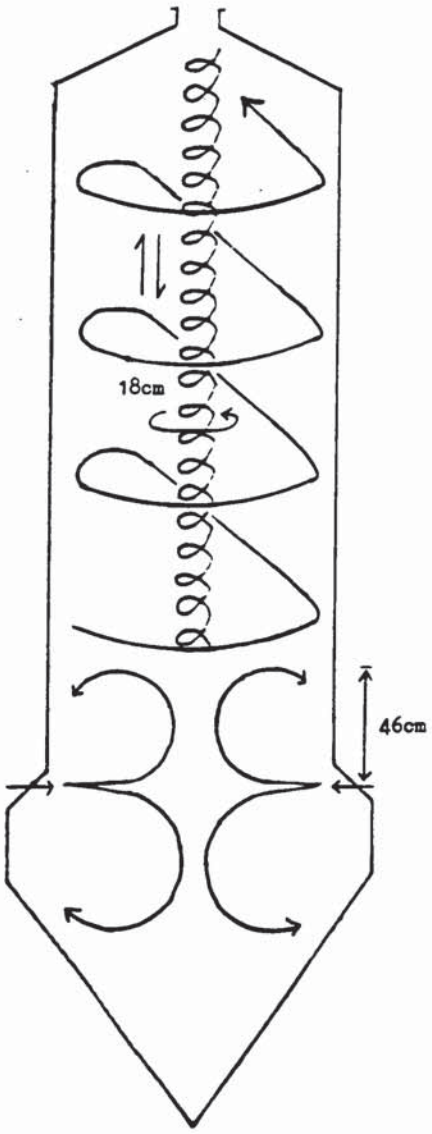

Observations

There was a well mixed zone at the base of the tower which extended approximately 46cm above the nozzle section. Above this, swirl was evident which was predominantly in the upward direction. Towards the centre of the swirl there was a core of higher rotational and axial velocity. Smoke injected here was rapidly taken upward. The core was not stable. Flow was predominantly upward but frequently downward. The core was not stationary but rotated about an axis at the centre of the tower. The diameter of the circular path was about 18cm. Above the well mixed section the air appeared to approach plug flow as it ascended the tower. At the top very little axial mixing was evident.

No wall by-pass was evident.

Figure 8.2 *Air Flow Patterns Case 2*

- 4 Nozzles Open
- 25° To Radial
- 25° To Horizontal
- Total Air Flowrate = 1700 m^3/h
- No Spray

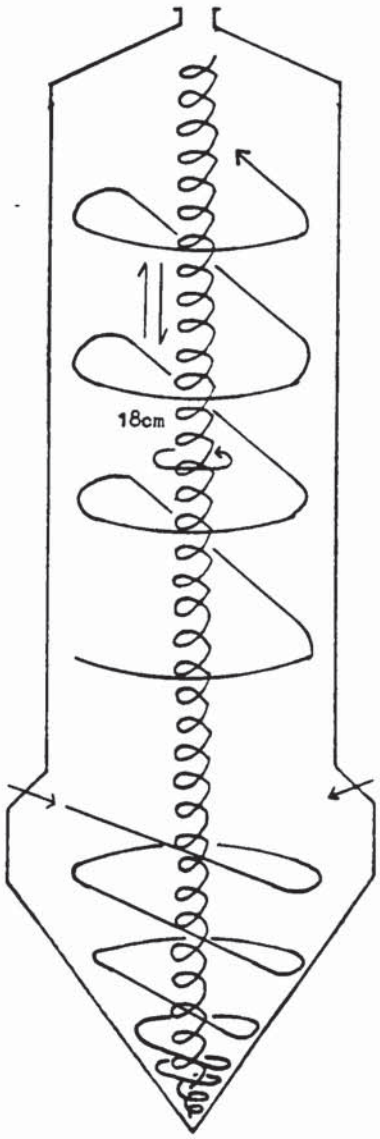

Observations

At the base of the tower there were two zones: An outer zone where flow was swirling downwards towards the apex of the cone and an inner core where flow was swirling upward.

Above the conical base swirl was upward and as the air ascended the tower, the flow pattern increasingly approached a swirling plug flow.

Again a higher rotational and axial velocity core was evident. The core seemed more intense than in Case 1 but was still unstable. Its direction was predominantly upward but fluctuated. The core still rotated and with increased velocity. The diameter of the circular path was about 18cm.

No wall by-pass was evident.

Figure 8.3 *Air Flow Patterns Case 3*

- 12 Nozzles Open
- Straight
- Total Air Flowrate = 3700 m^3/h
- No Spray

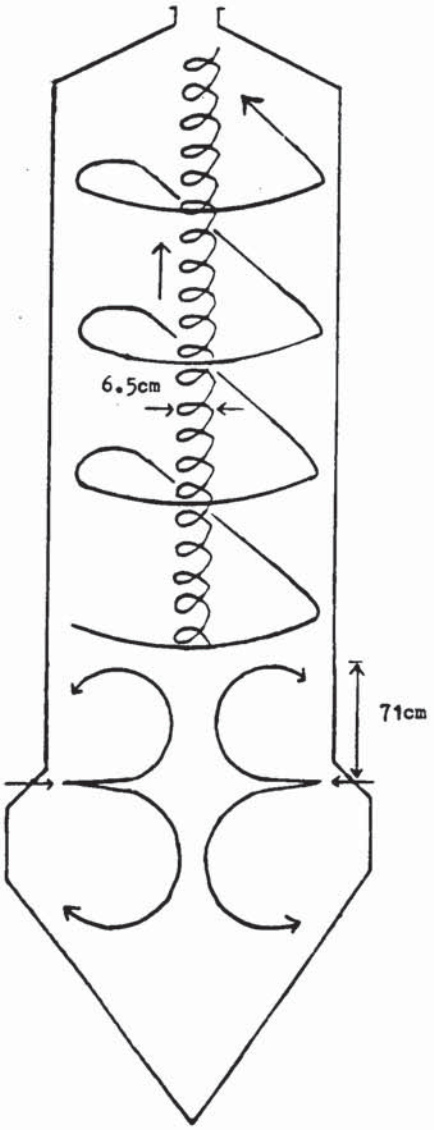

Observations

Increasing air flowrate increased the extent of the well mixed section to approx 70cm above the nozzle section. Significant swirl was still evident above this level. The central core was now more intense and stable, with flow almost exclusively in the upward direction. The core was now stationary at the axis of the tower. The diameter of the core was approximately 6cm.

No wall by-pass was evident.

Figure 8.4 *Air Flow Patterns Case 4*

- 12 Nozzles Open
- 25° To Radial
- 25° To Horizontal
- Total Air Flowrate = 3700 m^3/h
- No Spray

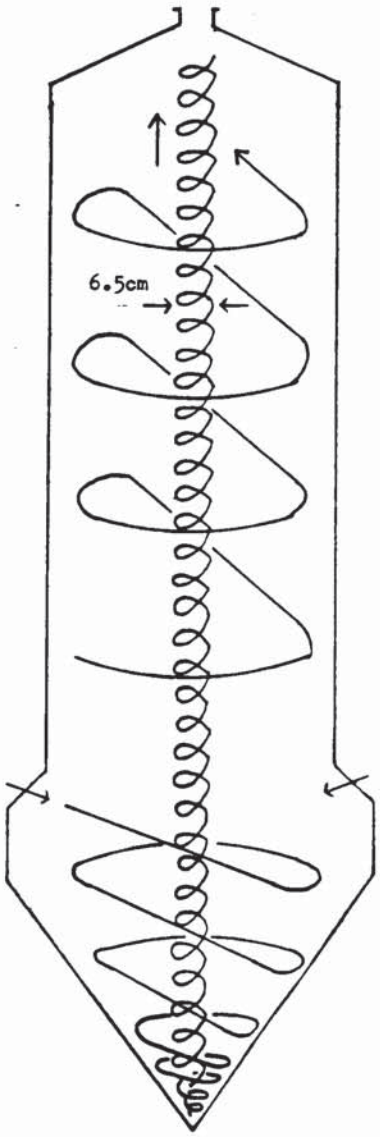

Observations

Increasing air flowrate greatly increased tangential velocities. The central core was more intense than with Case 3 and was stable. Flow was almost exclusively upward and the core was stationary at the axis of the tower. The diameter of the core was approximately 6cm.

No wall by-pass was evident.

Figure 8.5 *Air Flow Patterns Case 5*

- 4 Nozzles Open
- Straight
- Total Air Flowrate = 1800 m^3/h
- Maldistributed 1050 : 750 m^3/h
- No Spray

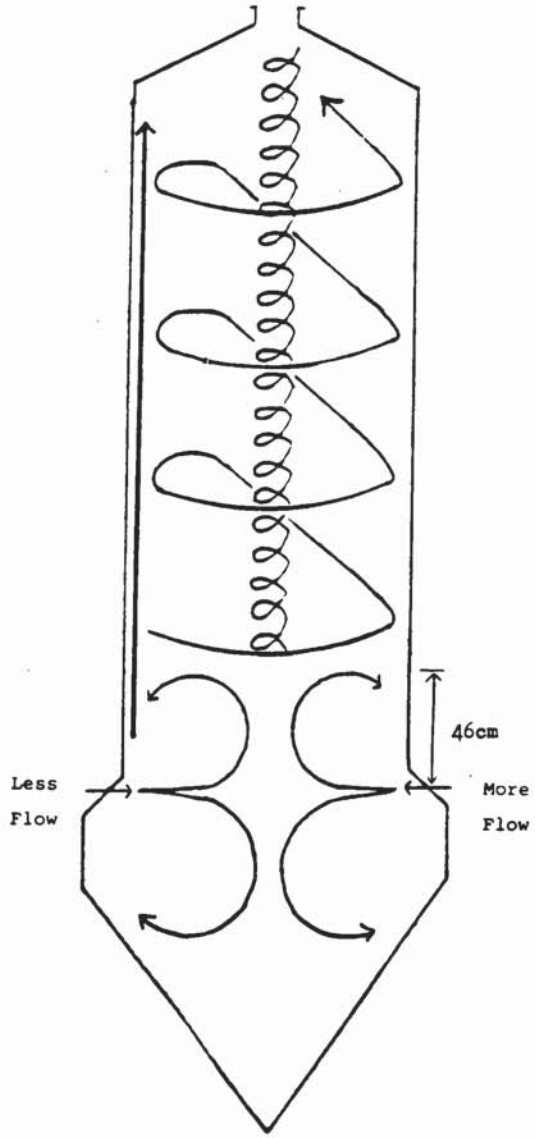

Observations

Maldistribution resulted in significantly less swirl within the tower. The base was still a well-mixed zone extending to about 46cm above the nozzle section.

A core of higher rotational and axial velocity was still evident, but this was much more difficult to locate since its position was not fixed. It tended to rotate around the axis of the tower. The velocities in the core were much less intense than for previous cases. There was a definite wall by-pass but only to one side of the tower - that with the less air flow. The by-pass extended the length of the tower, but at the top it was difficult to detect. The thickness of the by-pass was around 1-2cm.

Figure 8.6 *Air Flow Patterns Case 6*

- 12 Nozzles Open
- 25° To Radial
- 0° To Horizontal
- Total Air Flowrate = 4100 m^3/h with 10% of this total entering at the bottom
- No Spray

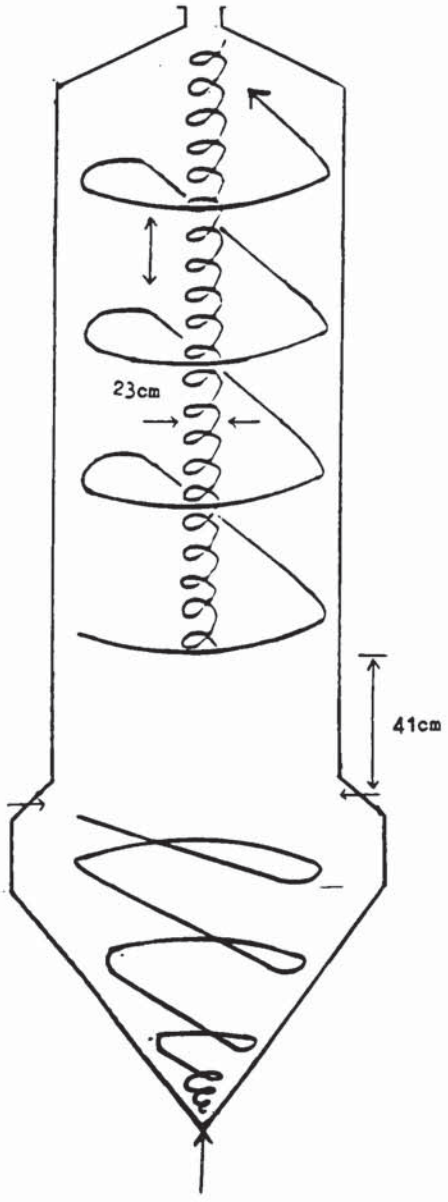

Observations

A central core of 23cm diameter was detected approximately 41cm above the nozzle section. The core was not stable. The flow was predominantly upward but frequently downward. No core was detected at the base of the tower where the flow appeared to be predominantly swirling downward.

No wall by-pass was evident.

Figure 8.7 *Air Flow Patterns Case 7*

- 12 Nozzles Open
- 25° To Radial
- 0° To Horizontal
- Total Air Flowrate = 4250 m^3/h with 13% of this total entering at the bottom
- No Spray

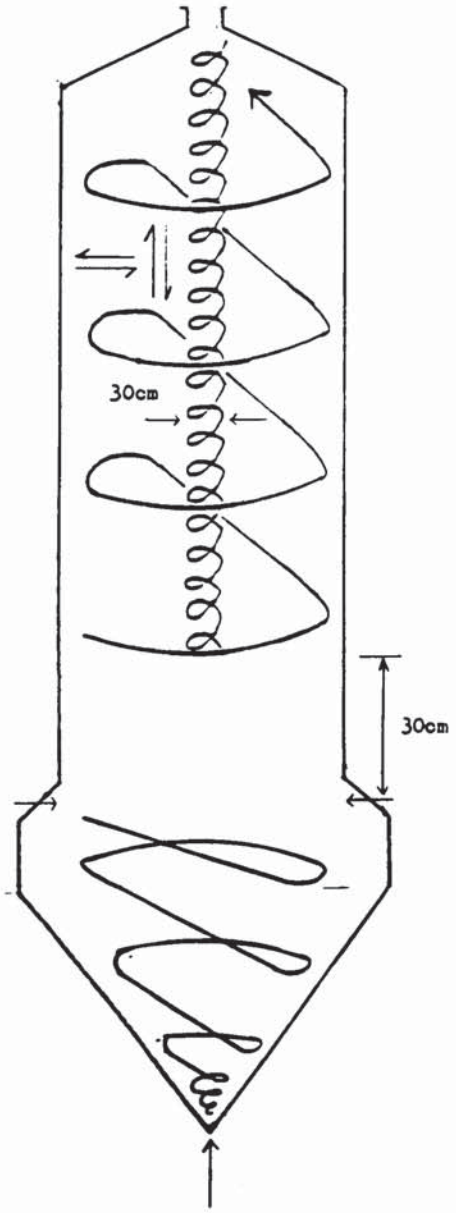

Observations

A central core of 30cm diameter was detected approximately 30cm above the nozzle section. The core was less stable than in Case 6 and moved randomly both up and down the tower as well as towards the sides. No detectable differences were observed below the nozzle section.

No wall by-pass was evident.

Figure 8.8 *Air Flow Patterns Case 8*

- 12 Nozzles Open
- 25° To Radial
- 0° To Horizontal
- Total Air Flowrate = 3660 m^3/h
- Maldistributed 1850 : 1400 m^3/h
- 11% of total air entered at the bottom
- No Spray

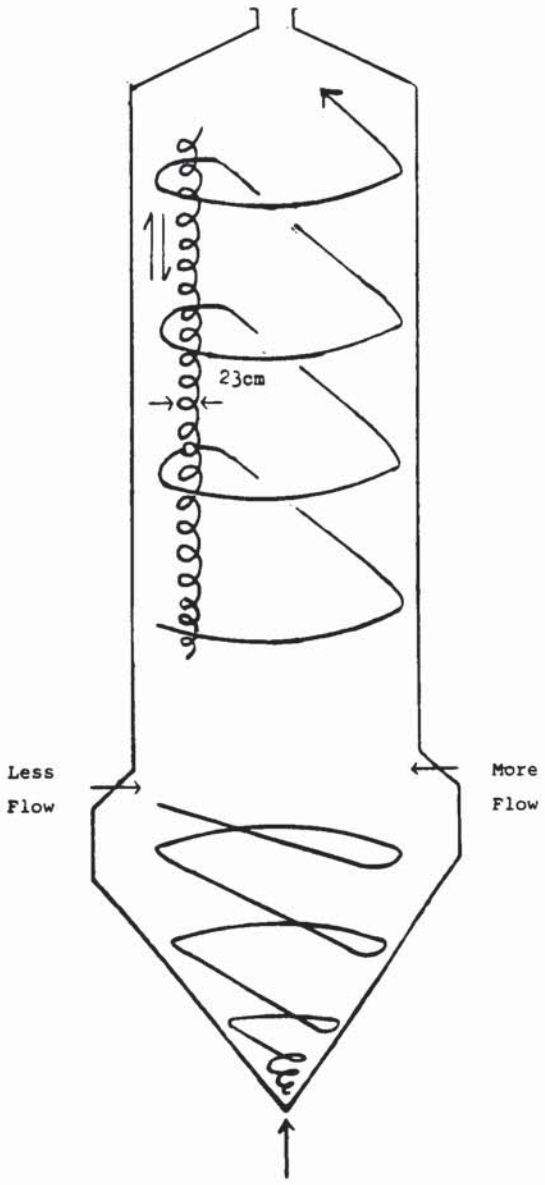

Observations

A central core of 23cm diameter was detected. The core was less intense than in the previous two cases and was more difficult to detect. It had a tendency to be shifted towards the side with less flow. No differences were detected in the region below the nozzles.

No wall by-pass was evident.

Figure 8.9 *Air Flow Patterns Case 9*

- 12 Nozzles Open
- 25° To Radial
- 25° To Horizontal
- Total Air Flowrate = 4111 m^3/h with 10% entering at the bottom
- No Spray

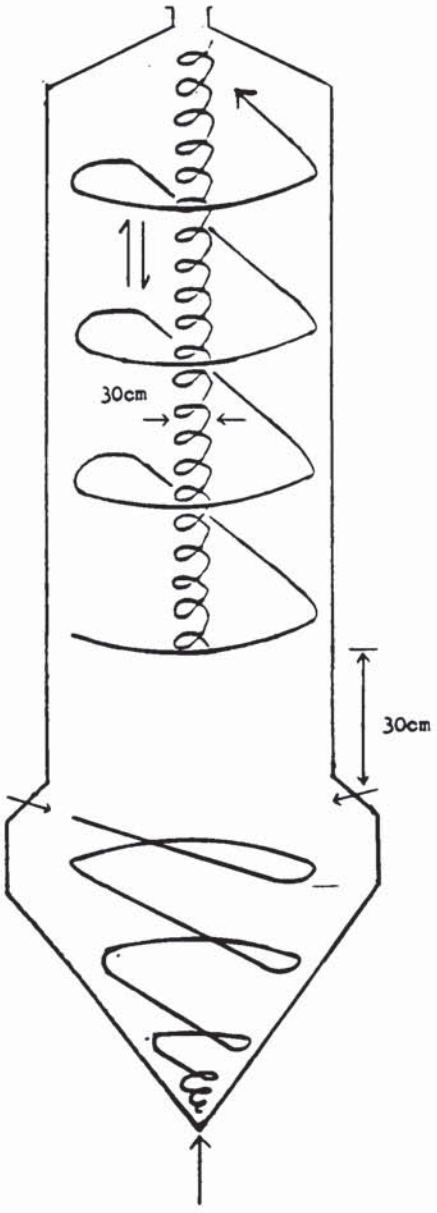

Observations

A core of 30cm diameter was detected approximately 30cm above the nozzle section. The core was slightly off-centre but was stable; very slight fluctuations were detected. No differences were detected below the nozzle section.

No wall by-pass was evident.

Figure 8.10 *Air Flow Patterns Case 10*

- 12 Nozzles Open
- 20° To Radial
- 25° To Horizontal
- Total Air Flowrate = 4111 m^3/h with 10% entering at the bottom
- No Spray

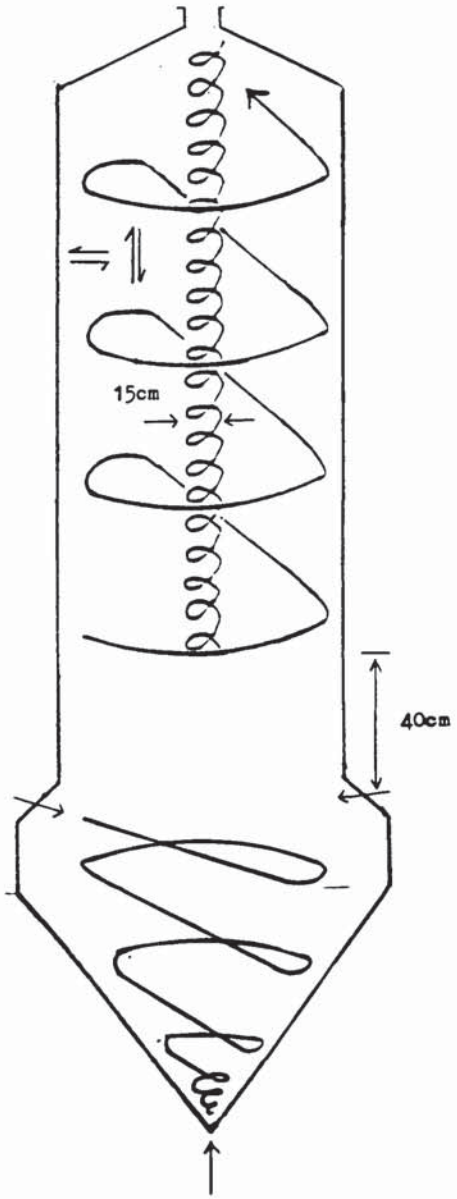

Observations

A core of 15cm diameter was detected 40cm above the nozzle section. The core was less intense and very difficult to detect. It was very unstable moving from side to side and up and down.

No differences were detected below the nozzle section.

No wall by-pass was evident.

Figure 8.11 *Air Flow Patterns Case 11*

- 12 Nozzles Open
- 15° To Radial
- 25° To Horizontal
- Total Air Flowrate = 4111 m^3/h with 10% entering at the bottom
- No Spray

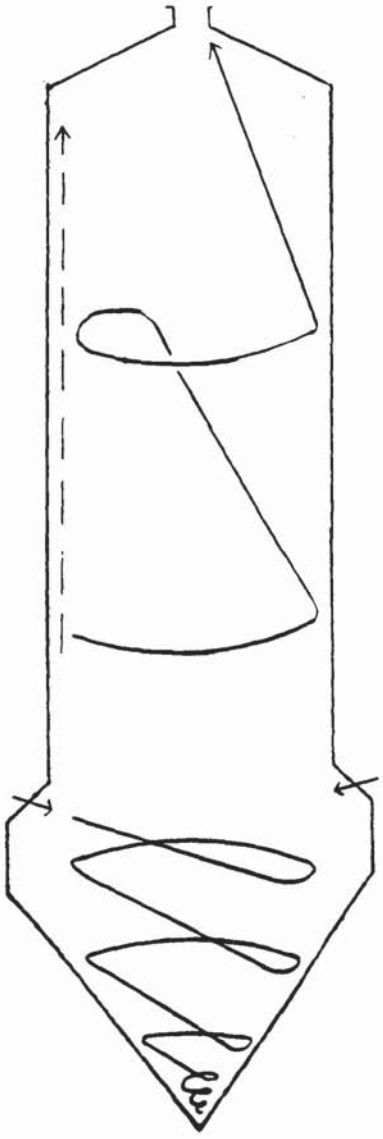

Observations

No core was detected. Very little swirl was detected in the tower. There was a slight by-pass at one side of the tower.

Figure 8.12 *Air Flow Patterns Case 12*

- 12 Nozzles Open
- 15° To Radial
- 25° To Horizontal
- Total Air Flowrate = 3700 m^3/h
- No air in at the bottom
- No Spray

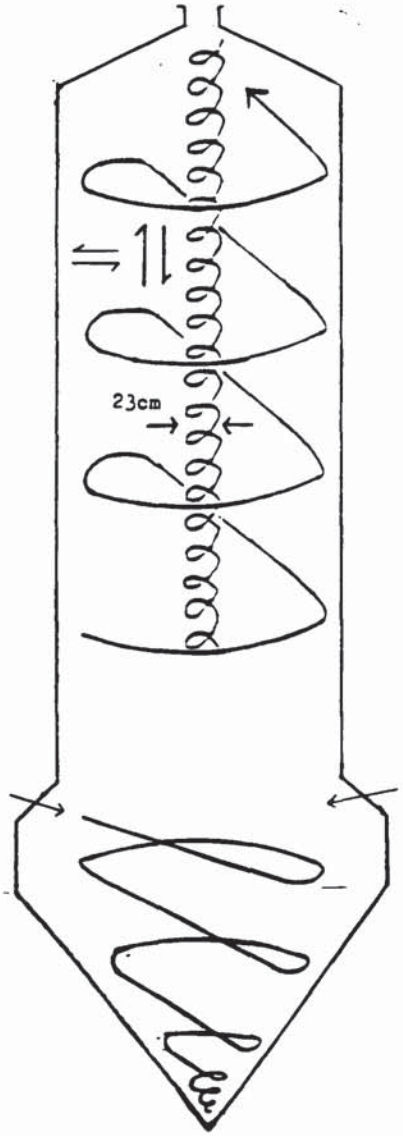

Observations

A core of 23cm diameter was detected. The core was unstable moving from side to side and up and down the tower.

No wall by-pass was evident.

Figure 8.13 *Air Flow Patterns Case 13*

- 12 Nozzles Open
- 25° To Radial
- 25° To Horizontal
- Total Air Flowrate = 3700 m^3/h
- No air at the bottom
- Water Spray on

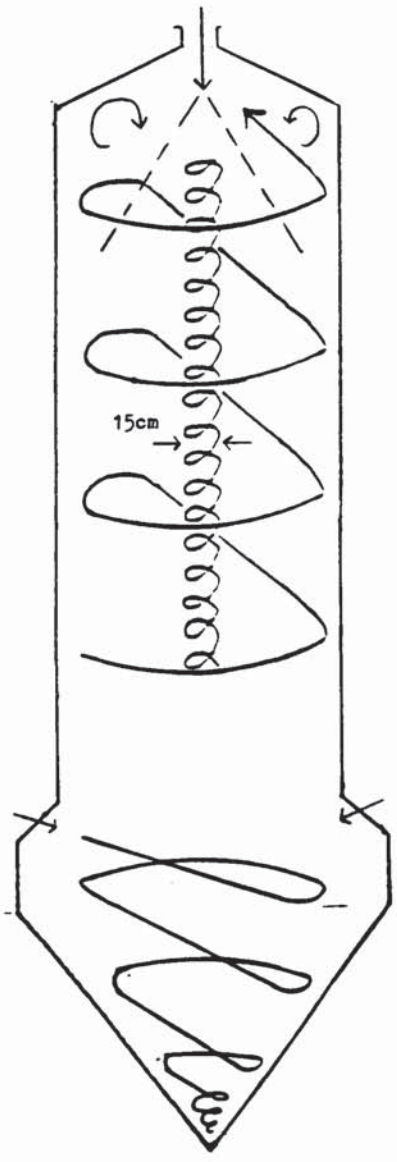

Observations

A strong central core of 15cm diameter was detected. The core moved randomly up and down the axis of the tower.

There was a large degree of turbulence around the atomiser section.

No wall by-pass was evident.

8.1.2 Spray Drier Temperature and Humidity Profile Measurements

Air temperatures and humidities were initially measured at 10cm intervals from the tower wall for each of the five axial planes, i.e. 6 radial measurements per plane. However, it soon became evident that the radial profiles for both temperature and humidity were practically flat, with only a minor variation from one radial measurement to the next. This was exemplified in Figure 8.14 which shows, for a typical run, the radial temperature profiles for the different axial planes. In view of this uniformity, it was considered justified to average the radial measurements at any one axial plane and thereby establish the axial variation in temperature and humidity. For the last five runs, i.e. Runs 5 - 10, measurements were therefore only made at 3 radial positions per plane and the mean of these was taken to be the plane-average.

Full experimental data, including all radial and axial measurements are given in Appendix D. Note that the humidity data are as calculated and do not imply a higher degree of accuracy than justified by the experimental method. The drier operating conditions relating to each run were given in Table 7.3. The axial air temperature and humidity profiles for each of the experimental runs are presented in Figures 8.15 - 8.24 and Figures 8.25 - 8.35 respectively.

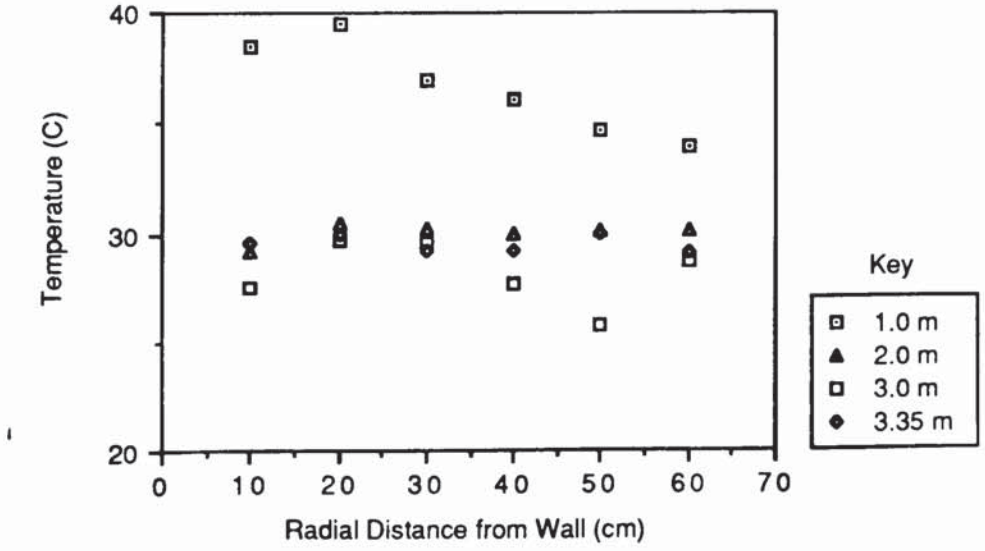

Figure 8.14 *Radial Variation in Air Temperature - Run 2*

Figures 8.15 - 8.24

Axial Air Temperature Profiles

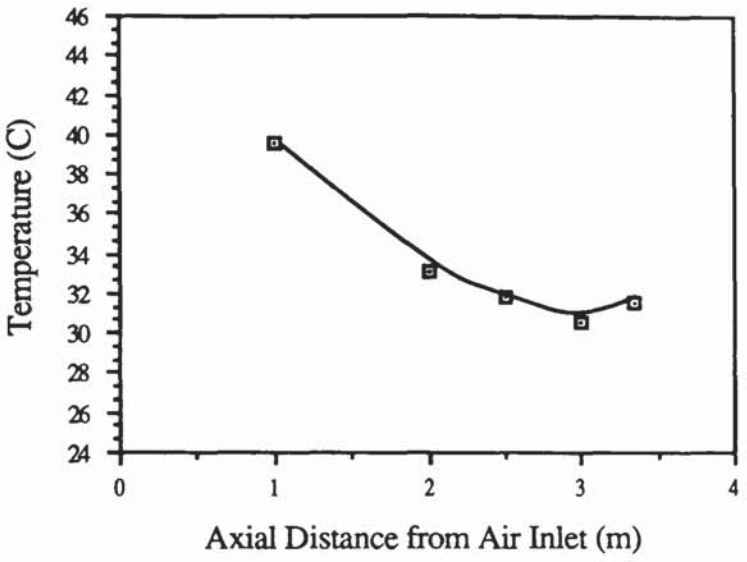

Figure 8.15 *Axial Variation in Air Temperature - Run 1*

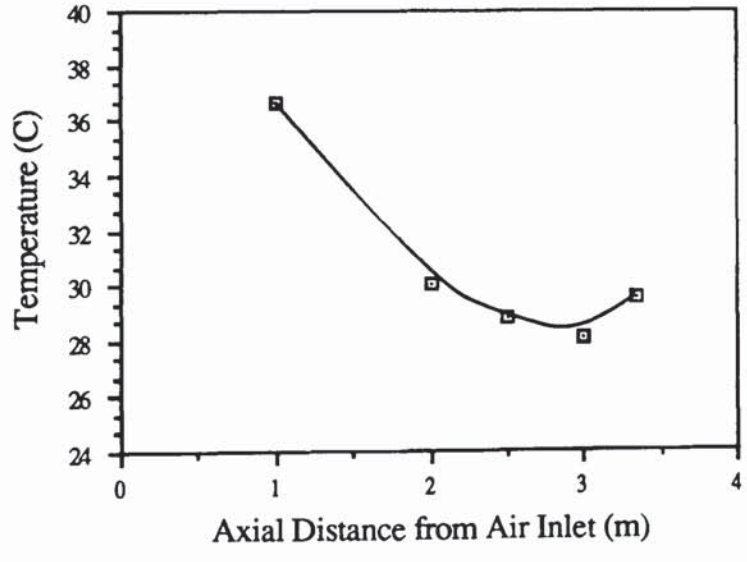

Figure 8.16 *Axial Variation in Air Temperature - Run 2*

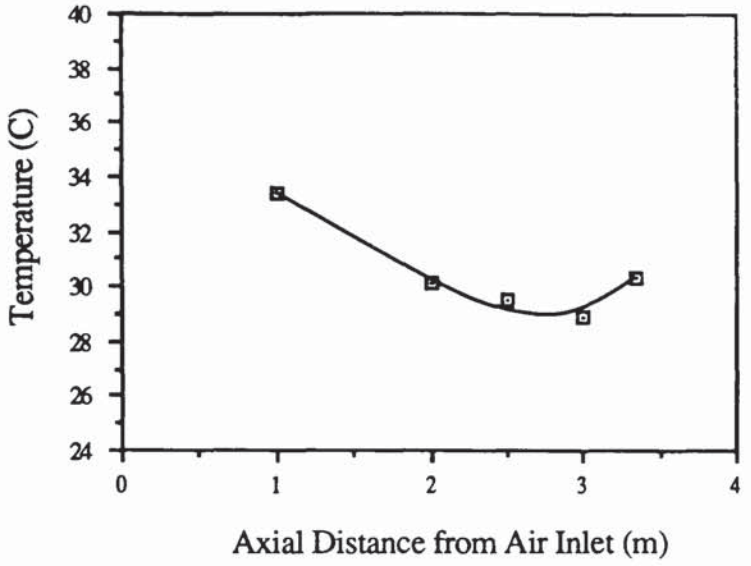

Figure 8.17 *Axial Variation in Air Temperature - Run 3*

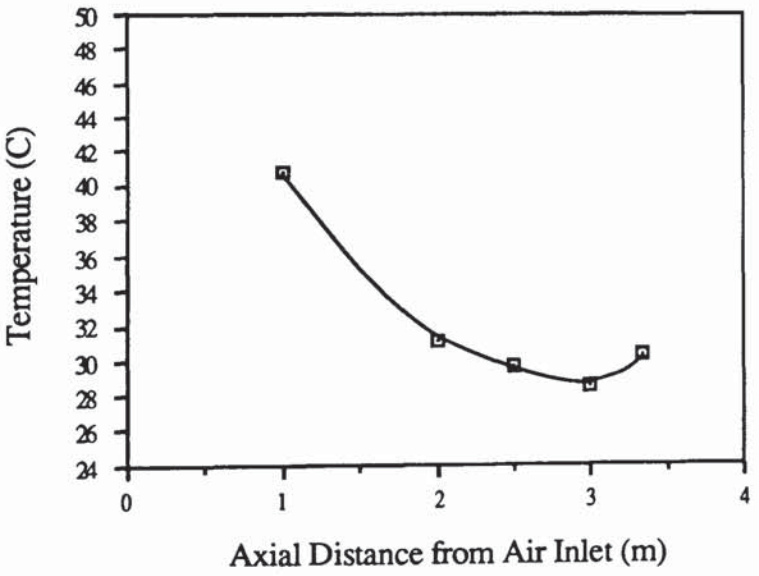

Figure 8.18 *Axial Variation in Air Temperature - Run 4*

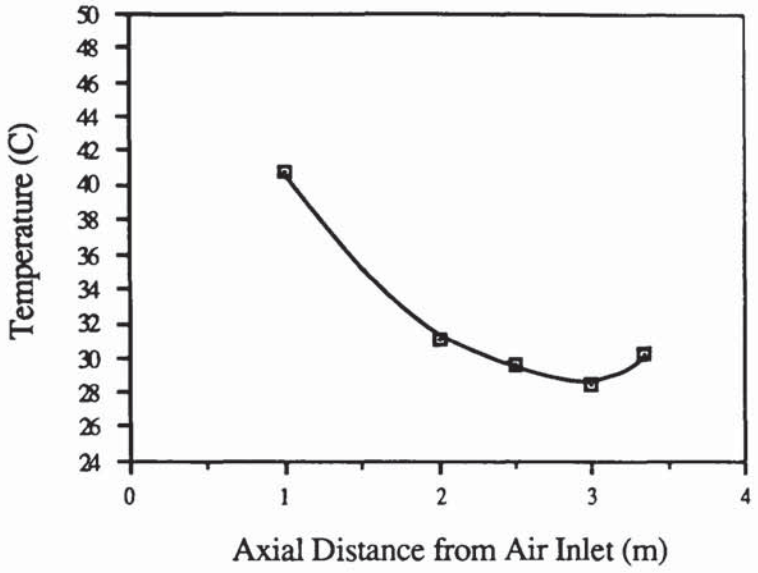

Figure 8.19 *Axial Variation in Air Temperature - Run 5*

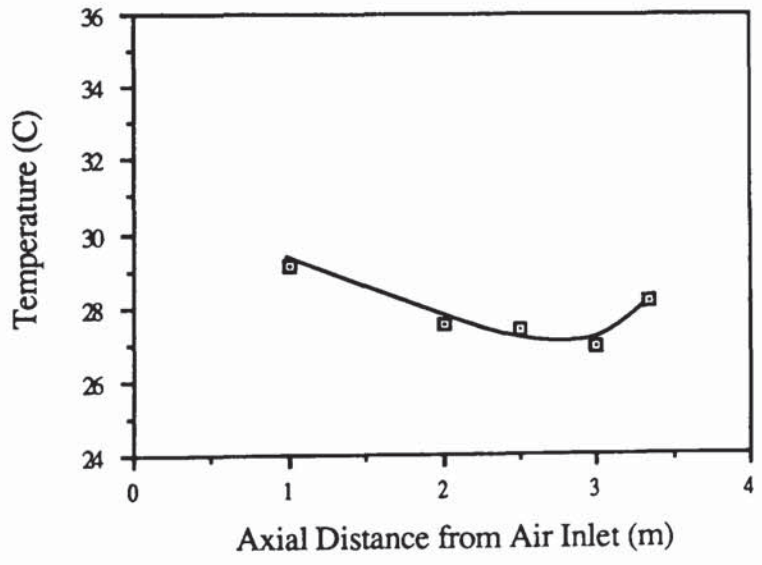

Figure 8.20 *Axial Variation in Air Temperature - Run 6*

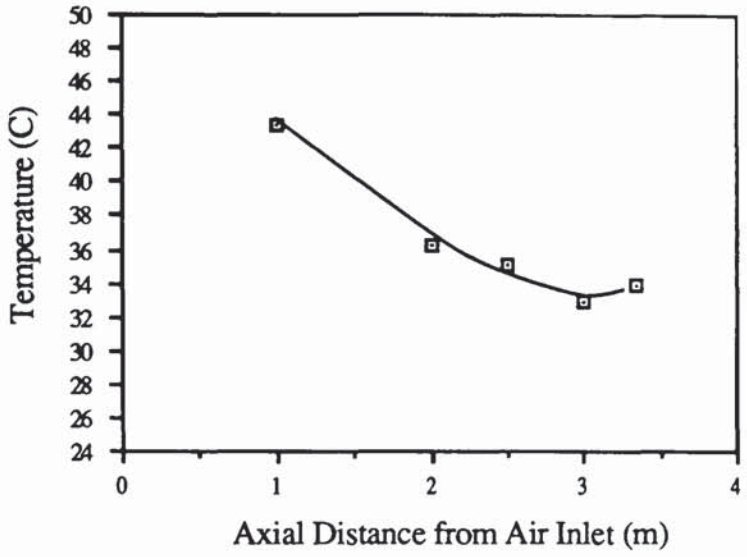

Figure 8.21 *Axial Variation in Air Temperature - Run 7*

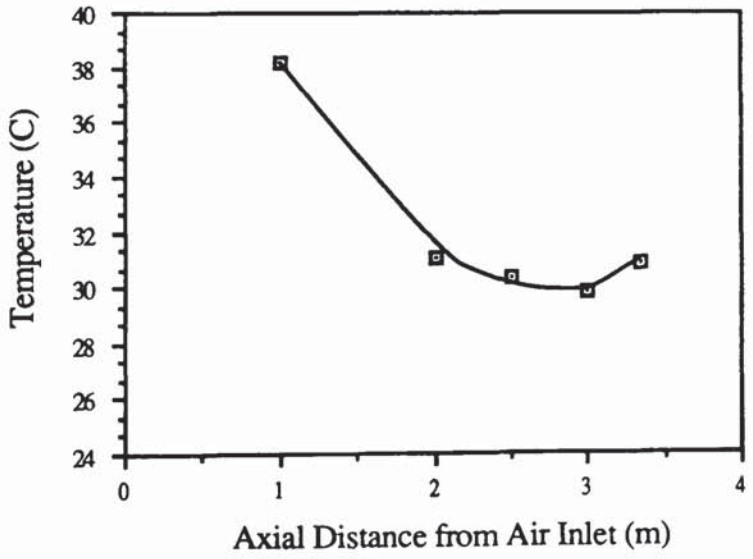

Figure 8.22 *Axial Variation in Air Temperature - Run 8*

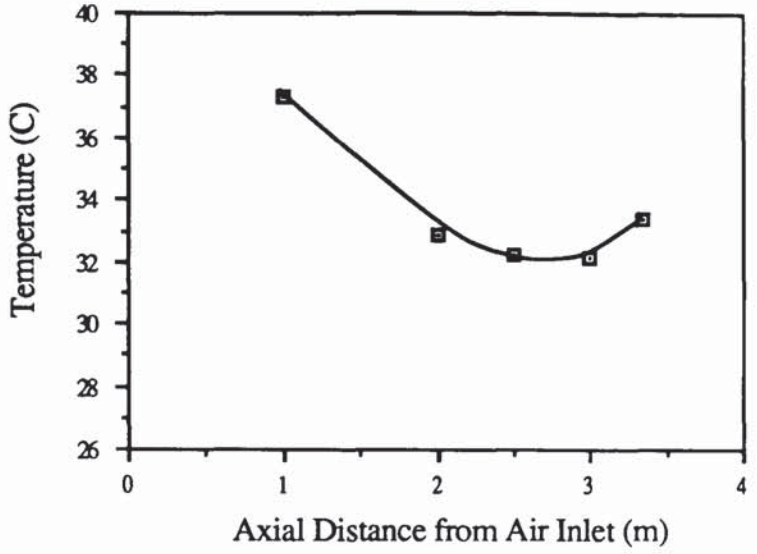

Figure 8.23 *Axial Variation in Air Temperature - Run 9*

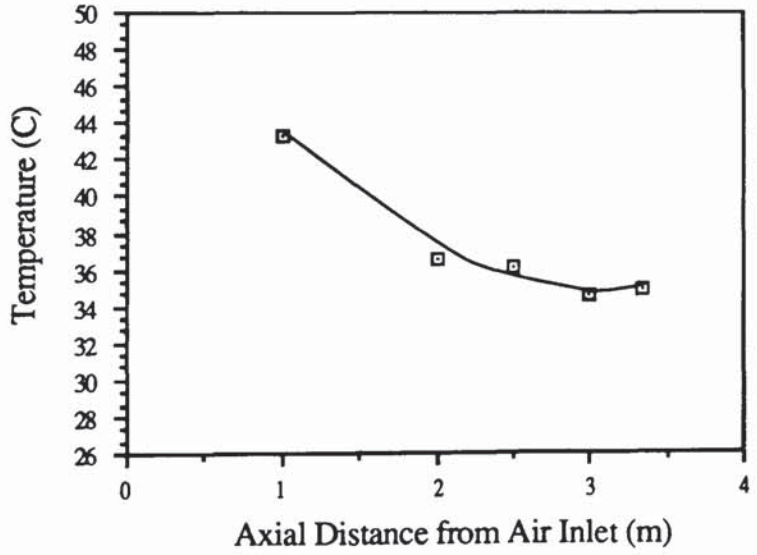

Figure 8.24 *Axial Variation in Air Temperature - Run 10*

Figures 8.25 - 8.34

Axial Air Humidity Profiles

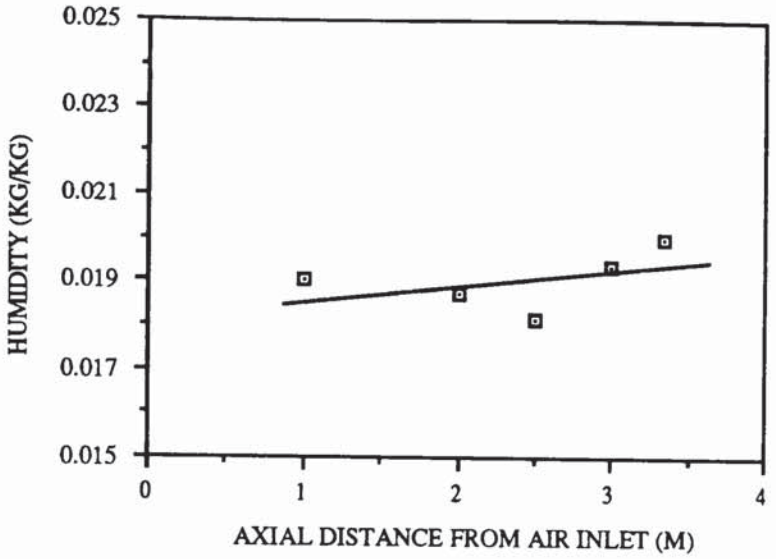

Figure 8.25 *Axial Variation in Air Humidity - Run 1*

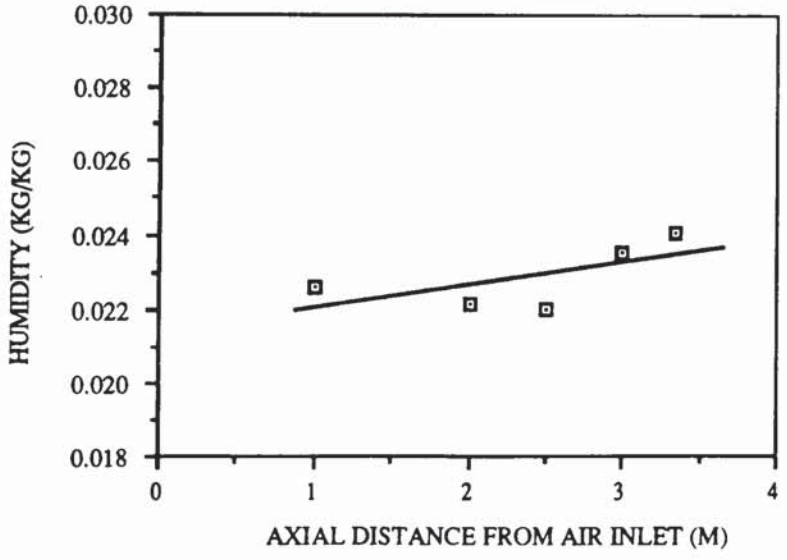

Figure 8.26 *Axial Variation in Air Humidity - Run 2*

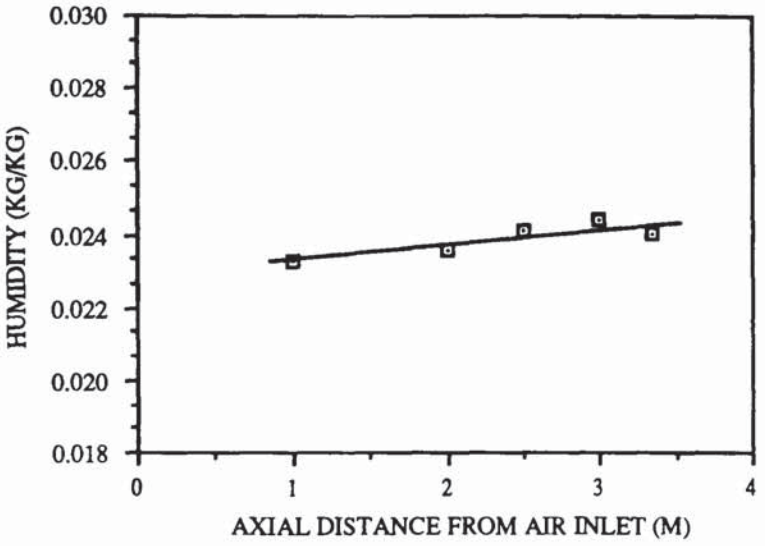

Figure 8.27 *Axial Variation in Air Humidity - Run 3*

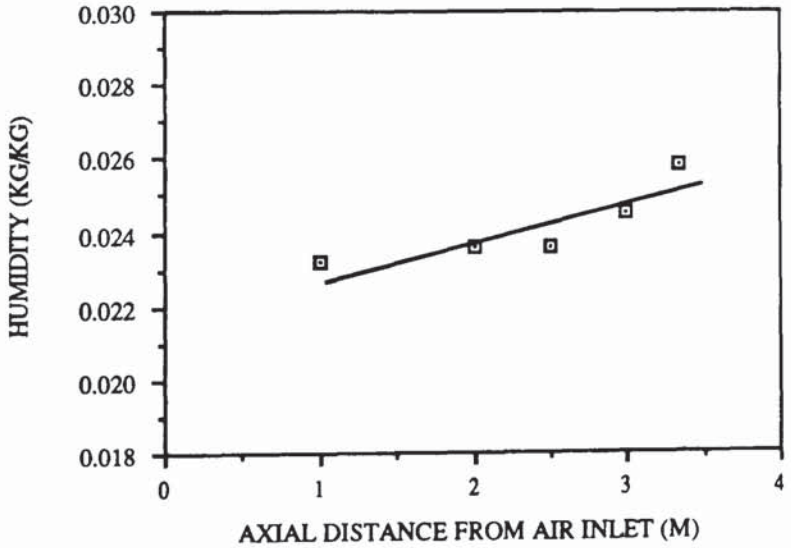

Figure 8.28 *Axial Variation in Air Humidity - Run 4*

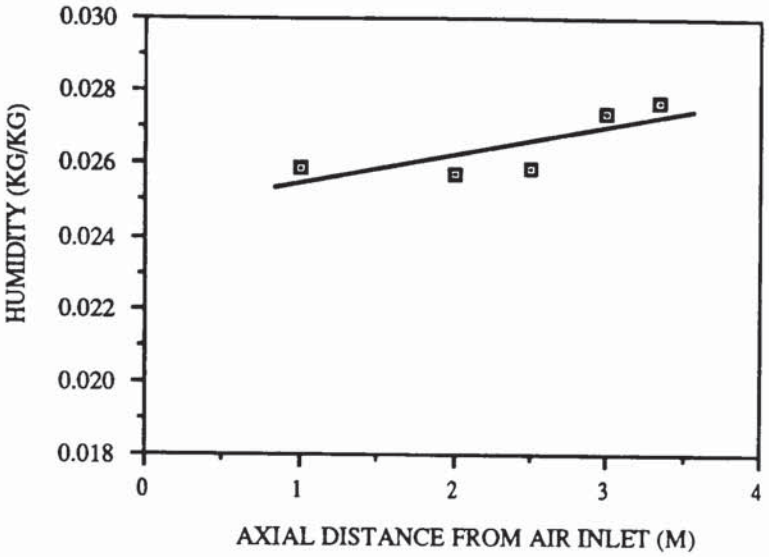

Figure 8.29 *Axial Variation in Air Humidity - Run 5*

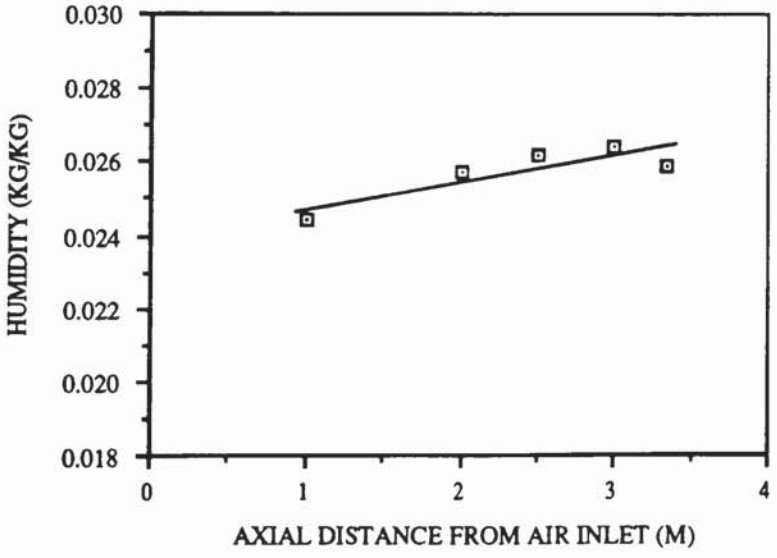

Figure 8.30 *Axial Variation in Air Humidity - Run 6*

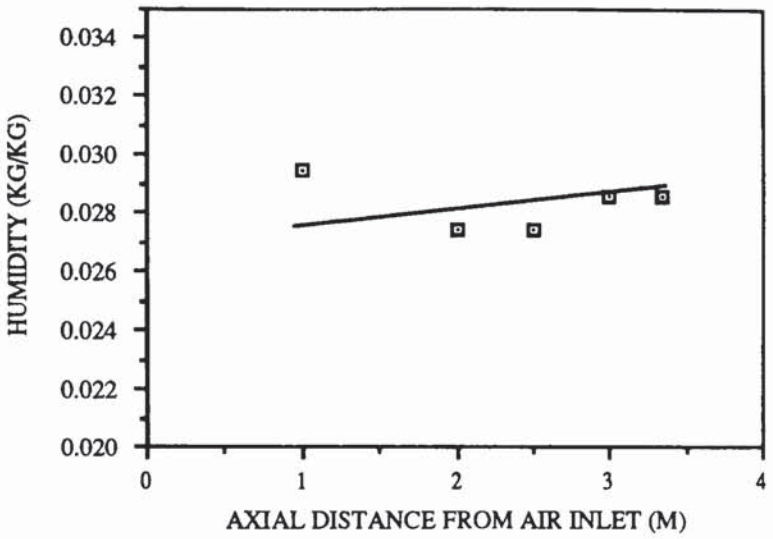

Figure 8.31 *Axial Variation in Air Humidity - Run 7*

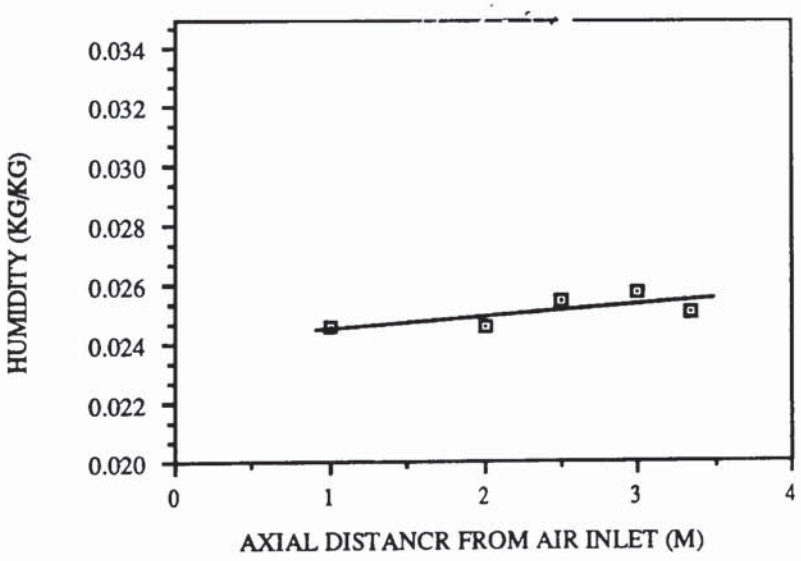

Figure 8.32 *Axial Variation in Air Humidity - Run 8*

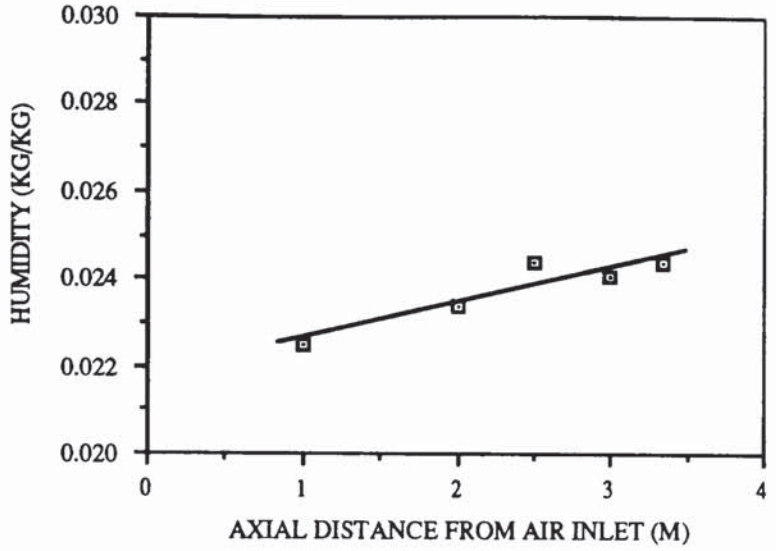

Figure 8.33 *Axial Variation in Air Humidity - Run 9*

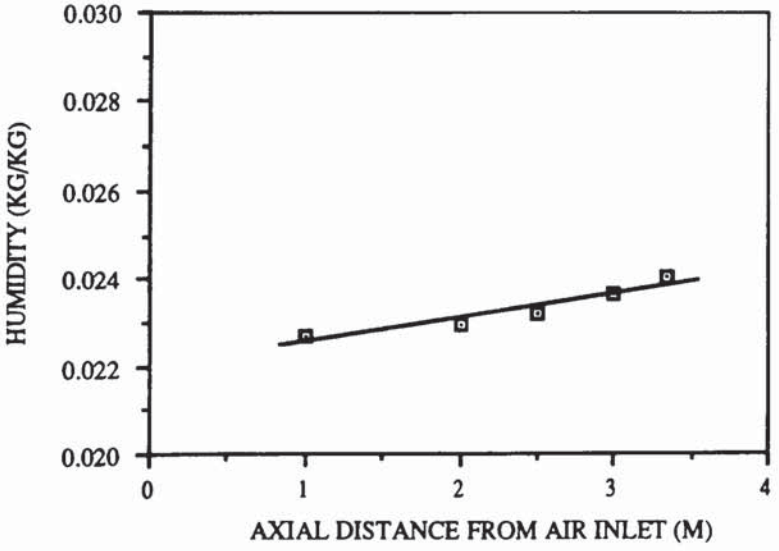

Figure 8.34 *Axial Variation in Air Humidity - Run 10*

8.1.3 In-Spray Droplet Agglomeration Study

In-spray droplet agglomeration was assessed by the measurement of spray droplet-size distribution at levels 0.35m and 1.35m from the nozzle atomiser. The measured droplet size - distributions, as output from the Malvern analyser are presented in Appendix D. These data are presented graphically in Figures 8.35 - 8.38 which show:

(a) the change in drop size-distribution which occurred during descent of the water spray in a stationary atmosphere;

(b) the effect of operating with a counter-current air flow of 0.16 kg/s on this drop-size profile;

(c) the effect of a counter-current air flow on spray drop size-distribution at the 0.35m level; and

(d) the effect of the counter-current air flow on spray drop size-distribution at the 1.35m level.

Full drier operating conditions pertaining to this experimental study were presented in Table 7.4

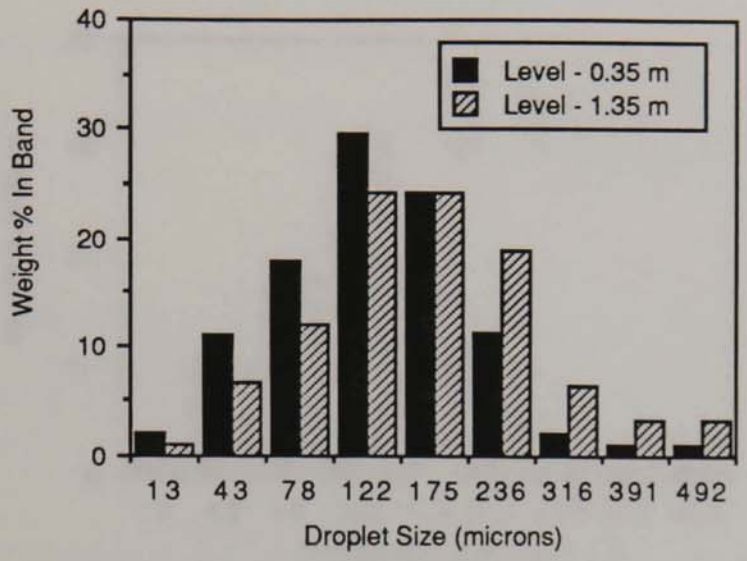

Figure 8.35 *Droplet Size-Distribution Profile - No Air Flow*

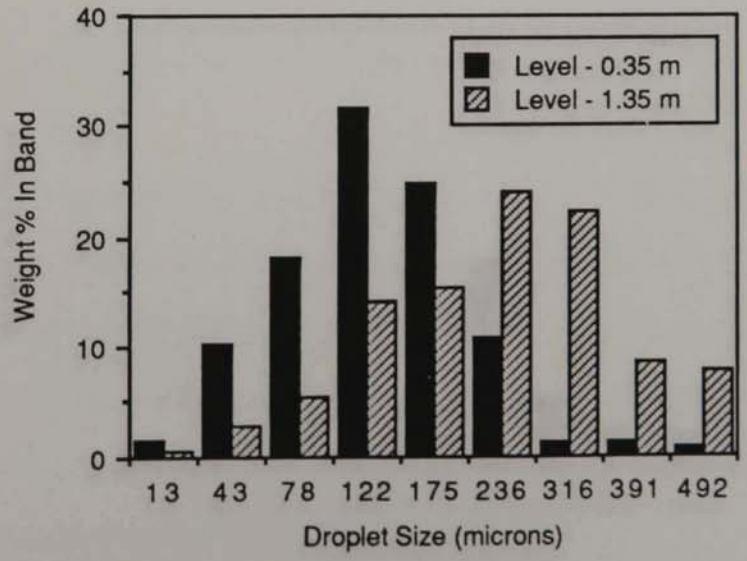

Figure 8.36 *Droplet Size-Distribution Profile - With Air Flow*

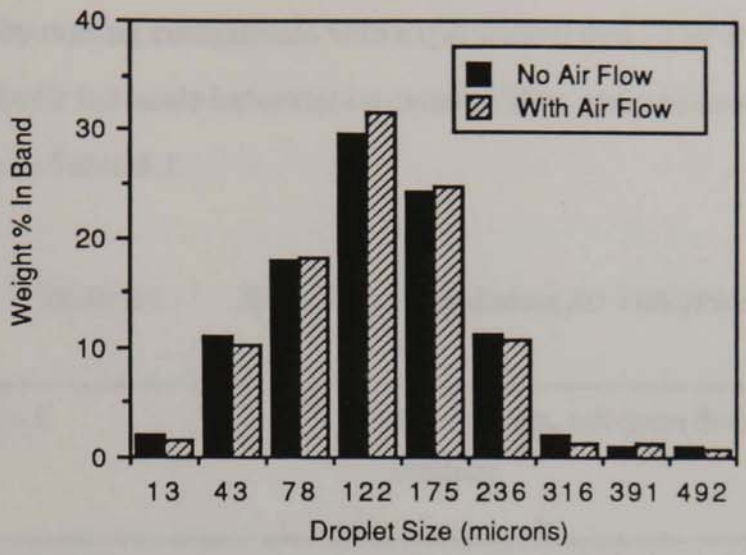

Figure 8.37 *Effect of Air Flow on Droplet Size-Distribution (0.35m from Nozzle)*

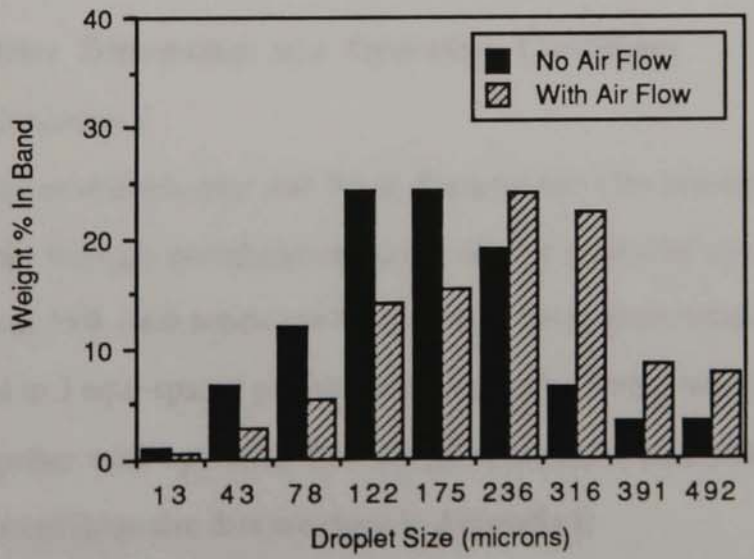

Figure 8.38 *Effect of Air Flow on Droplet Size-Distribution (1.35m from Nozzle)*

8.2 MODEL RESULTS

The validity of the mathematical model developed in Chapter 6 was established by applying it to 3 different fully-operational spray driers. Model predictions were then assessed by making comparisons with experimental data. The driers simulated in this way consisted of 2 full-scale industrial co-current driers and a pilot-scale counter-current drier as shown in Table 8.1.

Table 8.1 : *Spray Drier Simulations for Validation of the Model*

Simulation 1	-	A co-current, tall-form drier for a commercially dried solution.
Simulation 2	-	A co-current tall form drier for the drying of skimmed-milk concentrate [18].
Simulation 3	-	The counter-current pilot scale drier used for studying water evaporation in the temperature and humidity study detailed previously.

8.2.1 Drier Dimensions and Operating Conditions

(a) Simulation 1

The co-current drier was 7m in diameter and 13m in length. Air entered at the top of the drier through straightening vanes, to give a parallel streamline flow of air. The liquid feed, 55% total solids, entered through a ring main located at the top of the drier, which fed to 3 equi-spaced pressure nozzles, each of 3mm orifice diameter. Details of the drier, together with operating data are given in Table 8.2, whilst key product physical properties and drop-size data are given in Appendix E

(b) Simulation 2

The drier was 7m in diameter, and comprised a main cylindrical section of length 15m and a conical base of length 7m, i.e. a total drier length of 22m. Air entered at the top of the drier, to give a parallel flow of air within the drying chamber. The feed, concentrated skimmed-milk of 43% total solids, entered through a single custom-made pressure nozzle of orifice diameter 10mm located centrally at the top of the drier. This unusually large orifice diameter permitted high feed rates without need for nozzle duplication and hence resulted in reduced agglomeration. Drier details and operating data are given in Table 8.3 whilst feed physical properties and drop-size data are given in Appendix E.

For this simulation all data pertaining to the spray drier was obtained from the work of Hayashi [18] whilst the physical properties were obtained from various authorities on skimmed milk [149, 150].

(c) Simulation 3

The pilot-scale spray drier was described previously in Chapter 7. Operating data was given in Table 7.3. From this three runs were selected for model simulation, namely Runs 2, 5 and 10.

8.2.2 Model Predictions

Results obtained from the running of the computer model for each of the simulations are presented in Appendix E. These model predictions are presented in Figures 8.39 - 8.44, Figure 8.45 - 8.50 and Figures 8.51 - 8.56 for Simulations 1, 2 and 3 respectively. For Simulation 2, predicted air temperature and humidity profiles, and the average spray moisture profile are compared with experimentally determined values as reported by Hayashi [18]. For Simulation 3, predicted air temperature and humidity profiles are compared with those determined experimentally in the temperature and humidity study reported earlier.

Table 8.2 : *Simulation 1 - Drier Details and Operating Data*

Tower Details		
Type	:	Co-current, Tall-Form
Diameter	:	7.0m
Length	:	13.0m
Air Flow	:	Parallel, Streamline
Atomiser Details		
Type	:	Pressure Nozzle
Orifice	:	3×10^{-3}m diameter
Configuration	:	3 nozzles; equally fed
Spray Angle	:	65°
Spray Pressure	:	1200 psi
Feed Details		
Inlet Rate	:	approx 1 kg/s
Inlet Temp	:	80°C
Inlet Solids	:	55%
Outlet Rate	:	0.55 kg/s
Outlet Solids	:	97.5%
Air Details		
Inlet Flow	:	approx 11 kg/s
Inlet Temp	:	220°C
Inlet Humidity	:	0.008 kg/kg
Outlet Temp	:	113°C
Outlet Humidity	:	0.0462 kg/kg

Table 8.3 : *Simulation 2 - Drier Details and Operating Data*

Tower Details		
Type	:	Co-current, Tall-Form
Diameter	:	7.0m
Length	:	22.0m [cylindrical section - 15m + conical section - 7m]
Air Flow	:	Parallel, Streamline
Atomiser Details		
Type	:	Pressure Nozzle
Orifice	:	11mm diameter
Configuration	:	Single, centrally-located
Spray Angle	:	110°
Spray Pressure	:	2100 psi
Feed Details		
Feed	:	Concentrated Skimmed Milk
Inlet Rate	:	1.7 kg/s
Inlet Temp	:	80°C
Inlet Solids	:	43%
Outlet Rate	:	0.769 kg/s
Outlet Solids	:	95%
Air Details		
Inlet Flow	:	29.4 kg/s
Inlet Temp	:	175°C
Inlet Humidity	:	0.007 kg/kg
Outlet Temp	:	93°C
Outlet Humidity	:	0.039 kg/kg

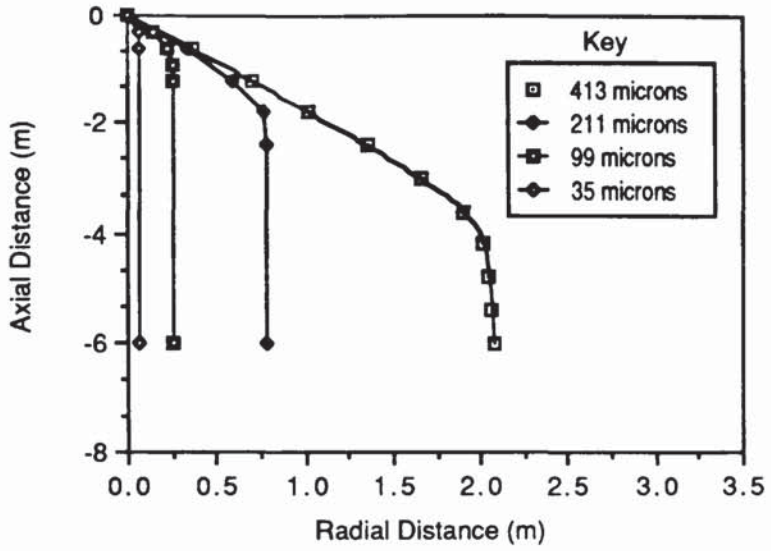

Figure 8.39 *Simulation 1 - Droplet Trajectories*

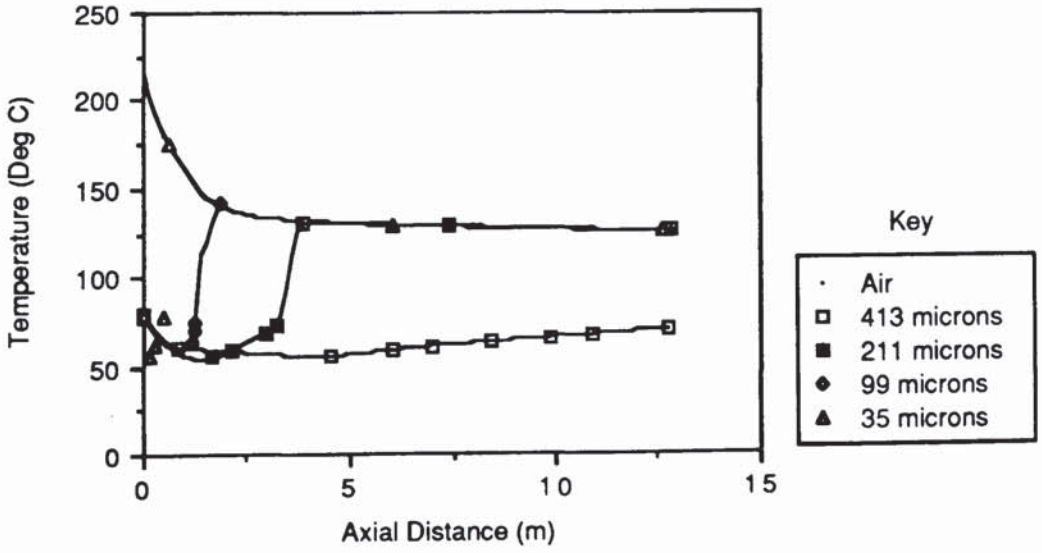

Figure 8.40 *Simulation 1 - Droplet Temperature Profiles*

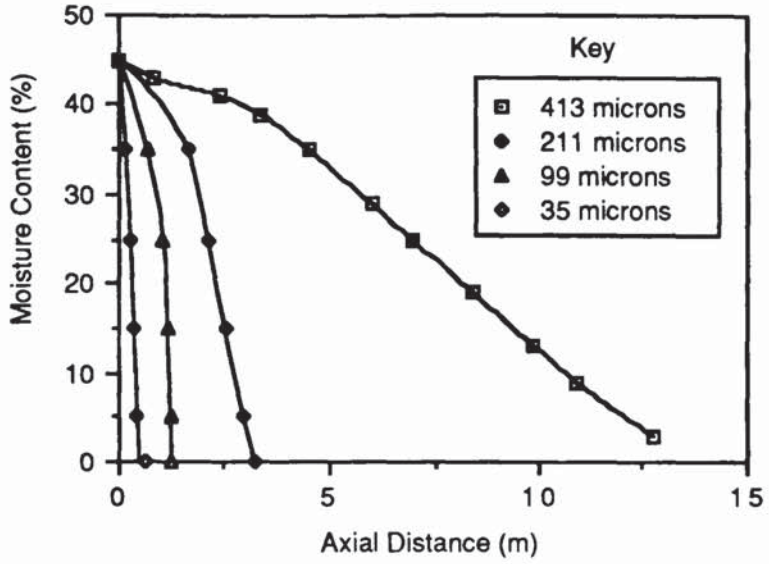

Figure 8.41 *Simulation 1 - Droplet Drying Profiles*

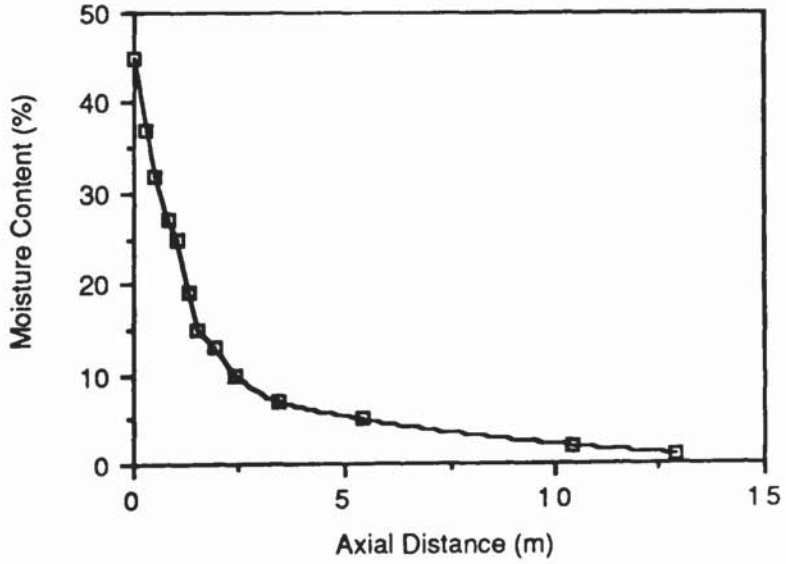

Figure 8.42 *Simulation 1 - Average Spray Moisture Profile*

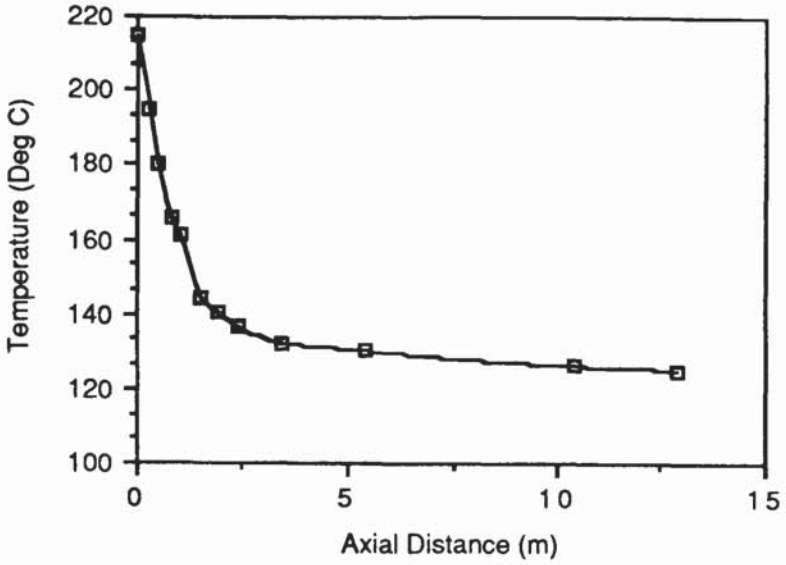

Figure 8.43 *Simulation 1 - Air Temperature Profile*

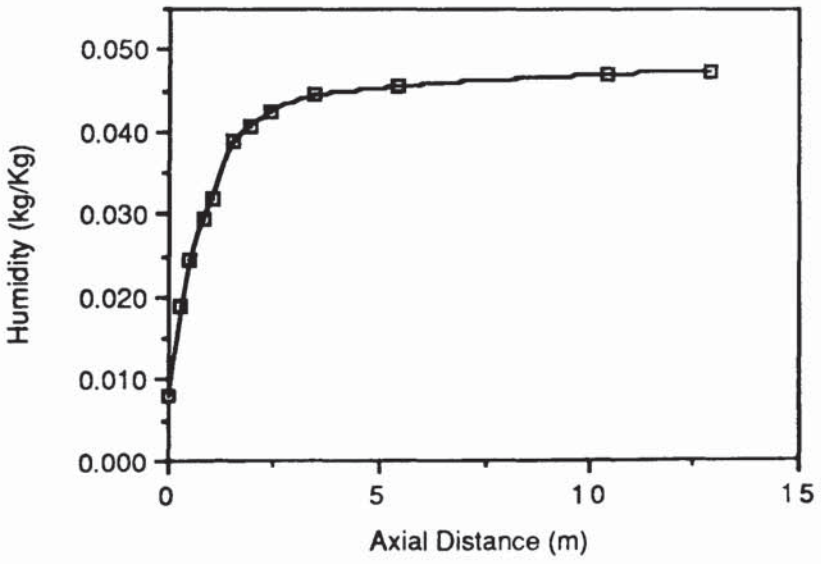

Figure 8.44 *Simulation 1 - Air Humidity Profile*

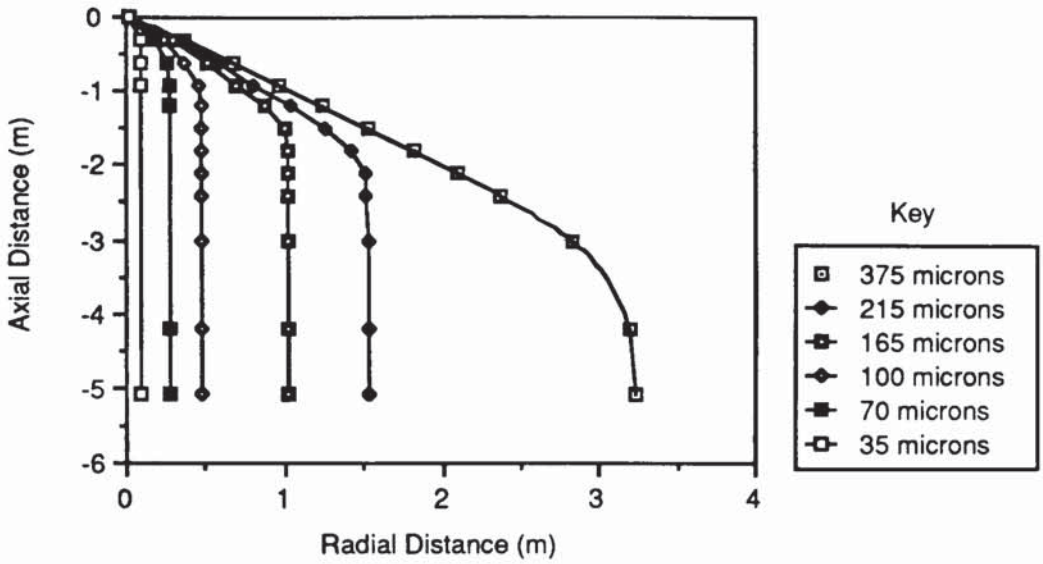

Figure 8.45 *Simulation 2 - Skim Milk: Droplet Trajectories*

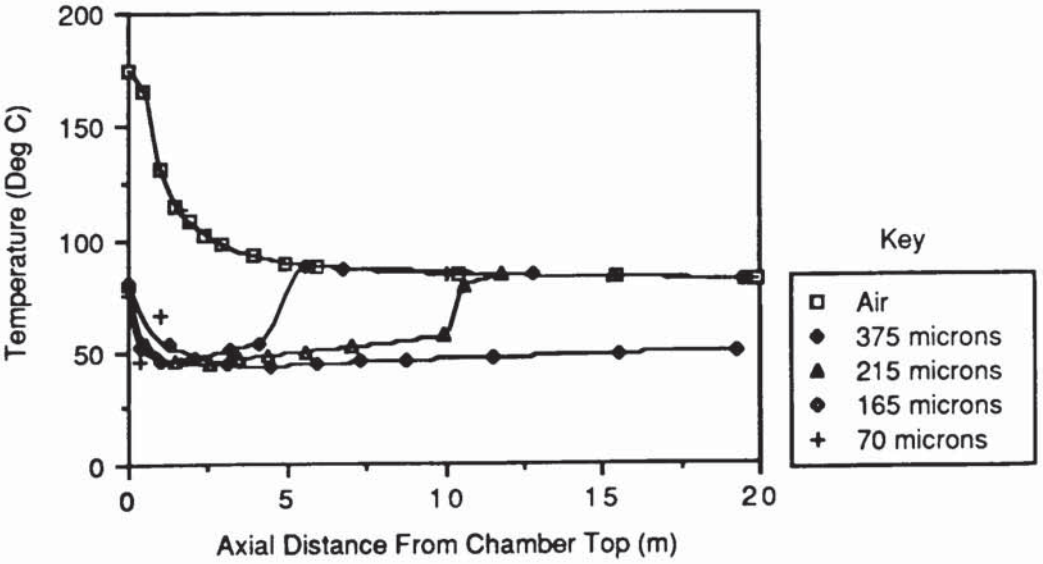

Figure 8.46 *Simulation 2 - Skim Milk: Droplet Temperature Profiles*

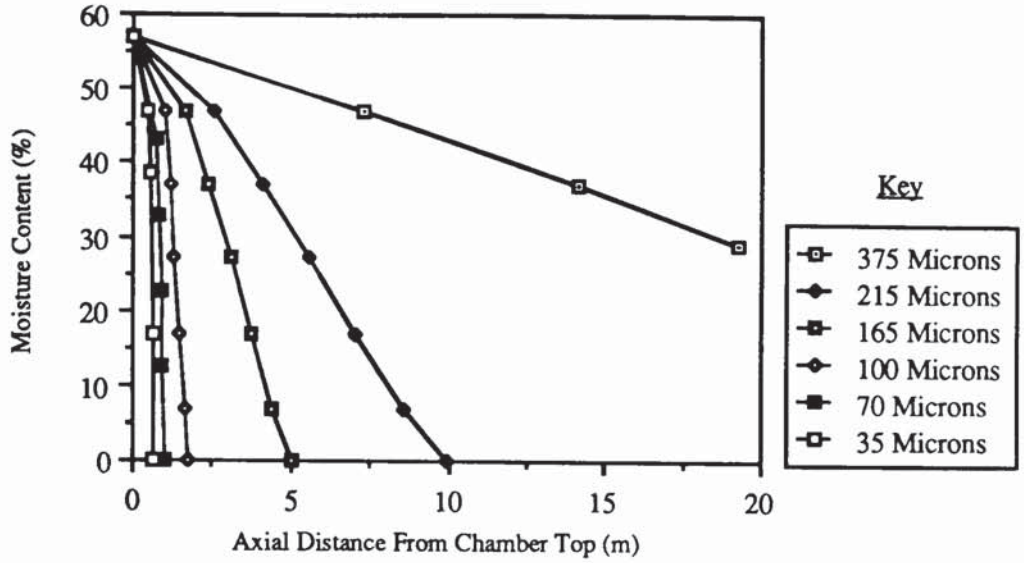

Figure 8.47 *Simulation 2 - Skim Milk: Droplet Drying Profiles*

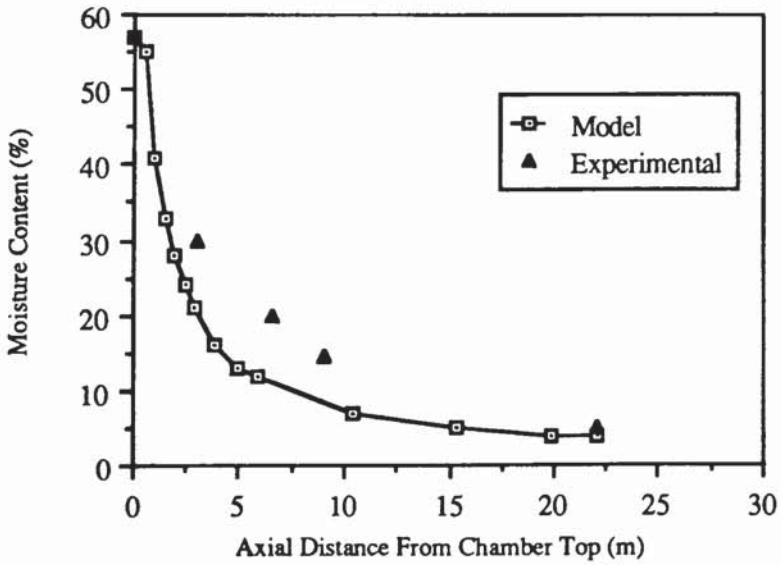

Figure 8.48 *Simulation 2 - Skim Milk: Average Spray Moisture Profile*

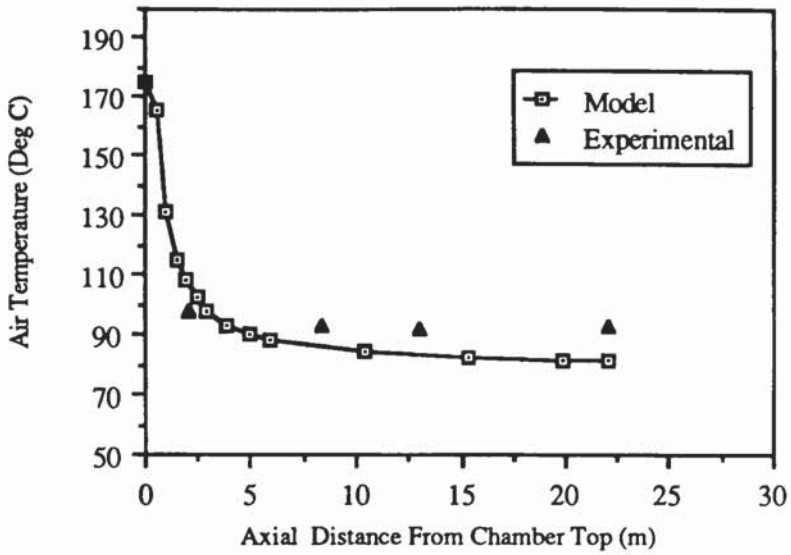

Figure 8.49 *Simulation 2 - Skim Milk: Air Temperature Profile*

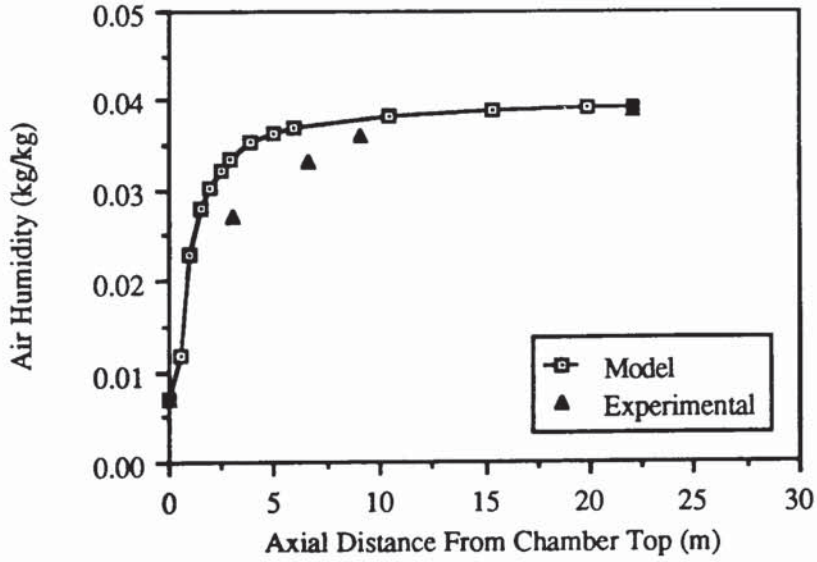

Figure 8.50 *Simulation 2 - Skim Milk: Air Humidity Profile*

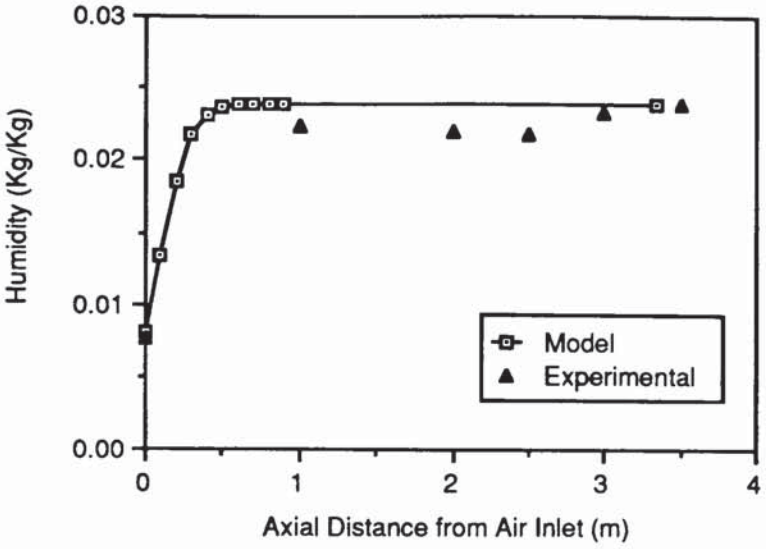

Figure 8.51 *Model versus Experimental Air Humidity Profile - Run 2*

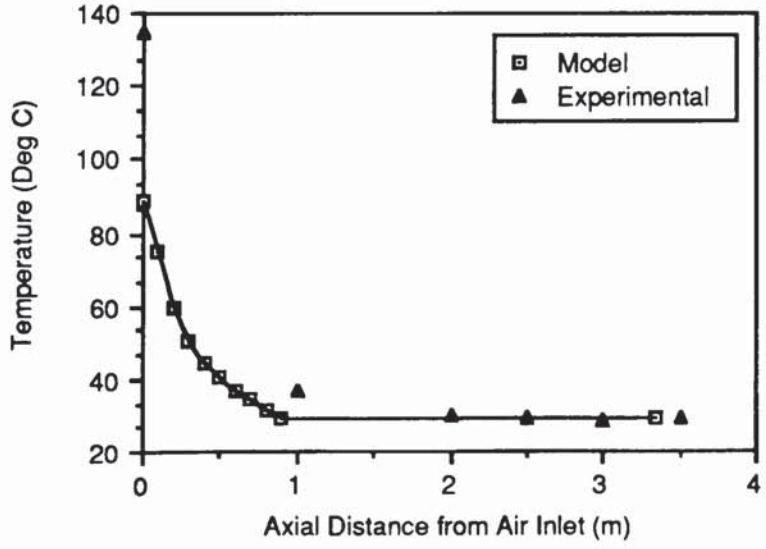

Figure 8.52 *Model versus Experimental Air Temperature Profile - Run 2*

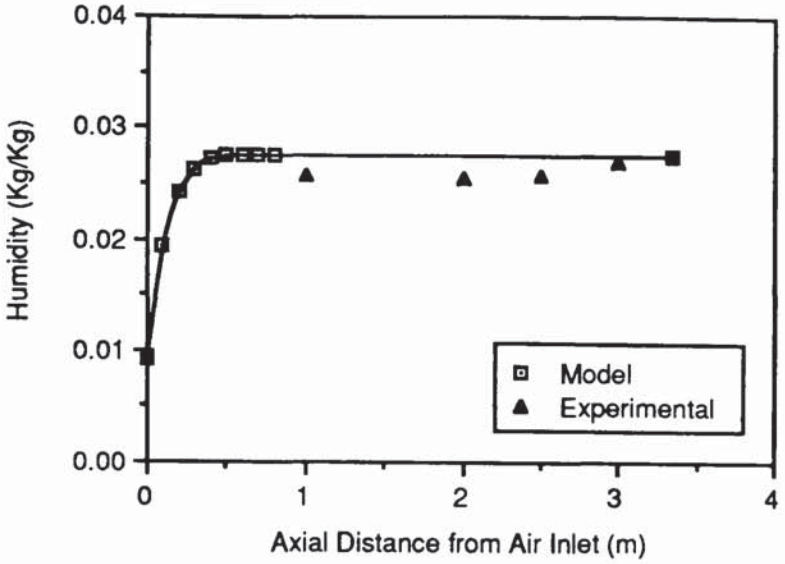

Figure 8.53 *Model versus Experimental Air Humidity Profile - Run 5*

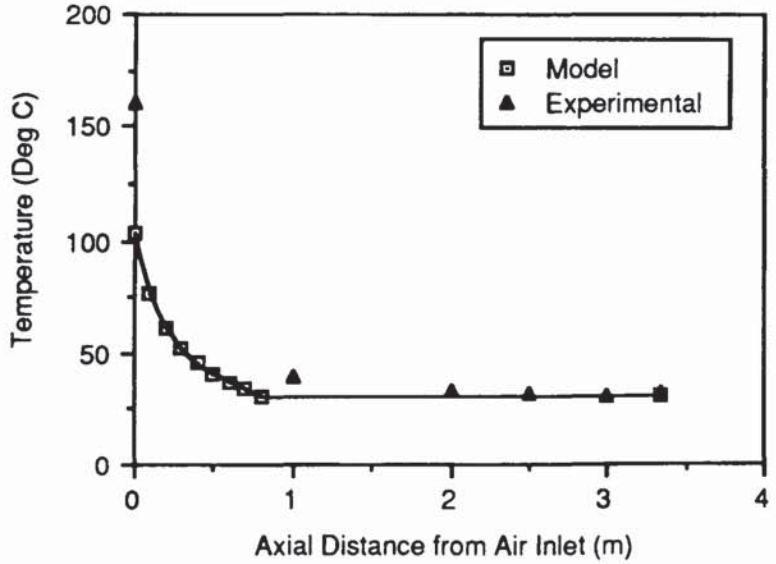

Figure 8.54 *Model versus Experimental Air Temperature Profile - Run 5*

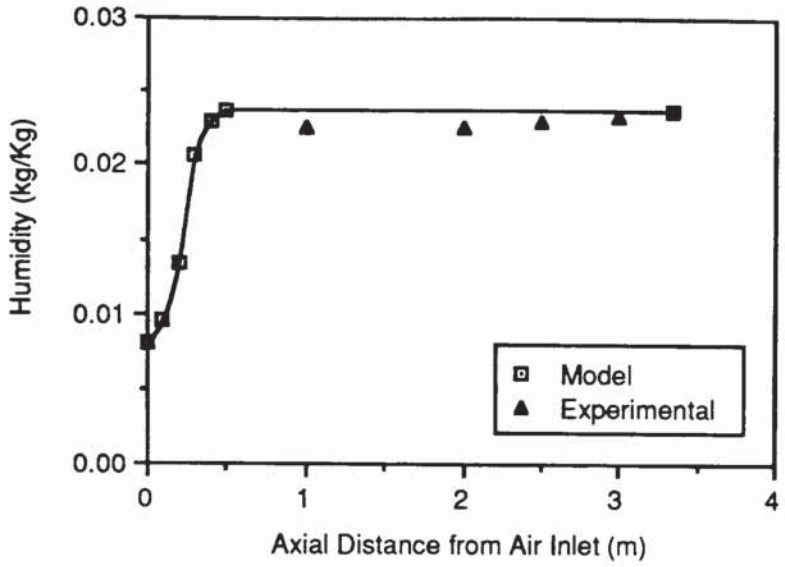

Figure 8.55 *Model versus Experimental Air Humidity Profile - Run 10*

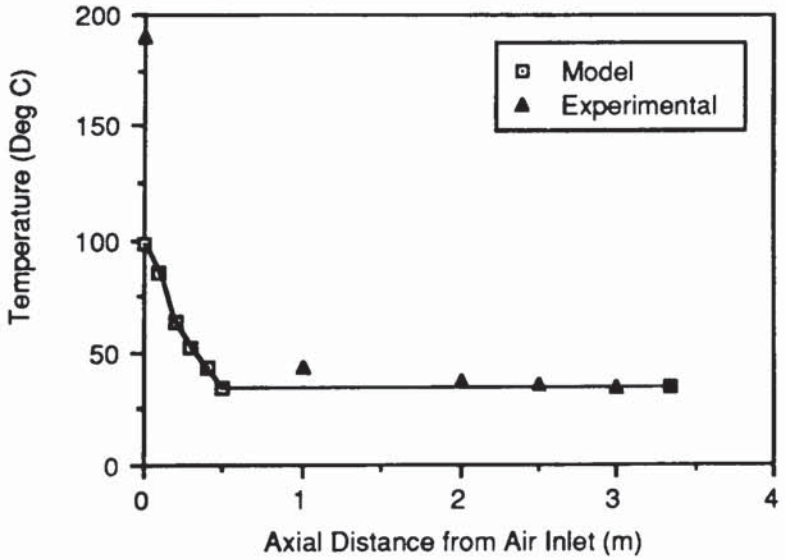

Figure 8.56 *Model versus Experimental Air Temperature Profile - Run 10*

Chapter 9

Discussion

This chapter is divided into two sections in which the following aspects are discussed:

(i) the experimental studies,

(ii) the spray drier mathematical model.

9.1 EXPERIMENTAL STUDIES

9.1.1 Air Flow Pattern Visualisation

The sketches presented in Figures 8.1 - 8.14 show how the air flow pattern within the drier was affected by various operating parameters. As outlined in Chapter 7 the specific parameters of interest in this study were:

(a) air flow rate (controlled by the number of inlet nozzles);

(b) the presence of a secondary air flow at the tower base (to simulate negative pressure operation);

(c) non-uniform distribution of the inlet air to the nozzles;

(d) nozzle swirl angle; and

(e) the operation of a water spray.

In the following discussion, the general flow pattern established in the tower is first described and following this, the effects of the above parameters on the flow pattern are considered.

General Flow Pattern

From the visualisation tests, it can be seen that swirling air flow within the drying chamber was present in all cases. Although swirl is obviously to be expected for angled

inlet nozzles, the fact that it persisted, albeit to a lesser degree, for the straight nozzle configuration (i.e. zero swirl angle) was unexpected.

Associated with the swirl, in practically all cases, there was a core of high rotational and axial velocity channelling along the axis of the tower; smoke injected here was rapidly carried away at several times the mean vertical velocity of flow within the drier. This constitutes an important discovery confirming earlier speculation on the existence of such a core [76, 81, 82]. The significance of this core is that it could result in a proportion of air leaving the drier unduly hot, not having fully participated in the drying process, and it may also tend to entrain fine particles out of the tower.

This bi-zonal flow pattern of an outer region of placid swirl together with an inner high velocity core probably reflects a zone of free-vortex flow surrounding a zone of forced-vortex (i.e. solid body rotation), as is found in natural cyclones and as previously reported for spray driers [151, 152].

It should be stressed that the flows observed in these zones were by no means stable. Although the outer swirl was predominantly flowing upward, it would occasionally reverse direction and momentarily flow towards the tower base. However, this is distinct from a specific zone of reversed flow which has been suggested by studies on similar towers in the past [81, 82]. The existence of such a zone, which, incidentally, has been postulated to be the main mechanism of back-mixing in the tower, could not be confirmed.

Similarly, unlike in previous studies, the central core was found to be generally unstable with a 'surging' effect being commonly observed: at any one time the proportion of the smoke introduced into the core that was moving upwards or downwards varied substantially. Furthermore, under certain flow conditions the core was not stationary, as hitherto reported, but rotated in a circular path around the axis of the tower or shifted

haphazardly from side to side. These, and other characteristics of the flow affected by the various operating conditions are described below.

Effect of Operating Conditions on the Air Flow Pattern

(a) Effect of Air Flow Rate/Number of Nozzles

For drier operation with only 4 inlet nozzles open, as shown in Figures 8.1 and 8.7, the core was found to be least stable. Flow frequently changed direction and the core tended to rotate about the axis of the tower. The effect of opening up all 12 nozzles and thereby increasing the air flow rate from 1700 m^3/h to 3700 m^3/h, was to increase the intensity and stability of the core; the flow direction became exclusively upward and the position of the core remained fixed at the axis of the tower. This is shown in Figures 8.3 and 8.4.

(b) Effect of Secondary Air Flow

To simulate a production tower operating under a negative pressure (i.e. in which airflow was by suction), an additional flow of air was introduced at the tower base. The effect of such a secondary flow, initially at a 10% level on a total flow basis, was to give rise to a wider diameter, less stable core as shown in Figure 8.6. Increasing the proportion of air fed in at the bottom from 10% to 13% caused the core diameter to increase from 23cm to 30cm as shown in Figure 8.7. At the same time, the stability of the core was further reduced and in addition to the frequent axial-direction changes, the core also began to randomly shift from side to side.

(c) Effect of Air Maldistribution

In production towers, the ring-main or plenum chamber is typically fed by a single air line. This would result in the air nozzles attached to the ring main receiving varying proportions of the total air. To simulate this, the air into the tower was deliberately maldistributed such that one side of the drier was fed with more air than the other. For operation with nozzles at a zero swirl angle, the effect of this was quite dramatic. The

degree of swirl was noticeably reduced, as was the intensity of the core which as a consequence became far more difficult to locate. The most striking feature, however, was the development of a wall by-pass for the first time. This appeared to extend the length of the drier but was present along the side of the tower which was receiving less air. This is shown in Figure 8.5.

A similar pattern was observed for operation with 12 angled nozzles. In this instance, maldistribution also resulted in a less-intense, less easily-detectable core which was now located towards the side of the drier with less air flow. This is shown in Figure 8.8.

(d) Effect of Swirl Angle

With the nozzles set at a 25° swirl angle, a very stable, core was detected as shown in Figure 8.9. Decrease in the swirl angle resulted in break-up of the core as shown in Figures 8.10 and 8.11. At a final setting of 15° swirl, no core was detected and a slight wall-by-pass became evident. Keeping this setting but reducing the secondary air input from 10% to 0% led to re-establishment of the core and no wall by pass, as shown in Figure 8.12.

(e) Effect of Water Spray

The tests run with the operation of a single water spray suggested that it had no significant effect on the flow pattern. As expected, turbulence was observed at the top of the tower in the vicinity of the atomiser, and a strong central-core was still evident. In all other aspects the flow behaviour was similar to that described above. However it should be stressed that operation of a single, centrally-located nozzle as used here, does not represent conditions in multi-nozzle towers; with correct positioning a multi-nozzle arrangement may be expected to significantly disrupt any core that existed.

From the wealth of information brought to light by this study, the benefits of employing a flow visualisation technique in combination with a transparent spray tower are clear. For the first time detailed aspects of the flow pattern, such as the stability and positioning of the core under various flow conditions could be established. Previous workers [76, 81, 82, 127] were only able to observe conditions in the spray tower through small sight glasses or postulate flow models embodying the different aspects of flow from the analysis of the responses to tracer injection.

The flow visualisation technique established in this study therefore offers considerable potential for accurate assessment of flow patterns and should continue to be an invaluable tool in future studies on air movement in spray driers.

9.1.2 Temperature and Humidity Study

(a) Radial Profiles

As mentioned previously, temperatures and humidities were initially measured at six points across the cross section of the drier at each of the five levels. However, these detailed profiles, for which the data are presented in Appendix D, did not show the existence of any steep radial gradients, apart from the axial location closest to the air entry ports. Here, the temperature measured nearer to the wall of the drying chamber was several degrees higher than that measured in the centre of the drier as shown in Figure 9.1. This would at first sight, suggest the existence of a hot-air wall by-pass. However the temperature or humidity profiles for the upper regions of the drier did not confirm this. Temperature measurements from the level 1.0m from the air entry ports upwards, were in most cases marginally lower closest to the drier wall, than towards the centre of the drier. This was most probably due to heat losses through the wall.

As far as humidity measurements are concerned, there were no detectable differences in air humidity across the drier cross section. However, this is judged to be a result of the accuracy of the measurement technique as will be discussed subsequently.

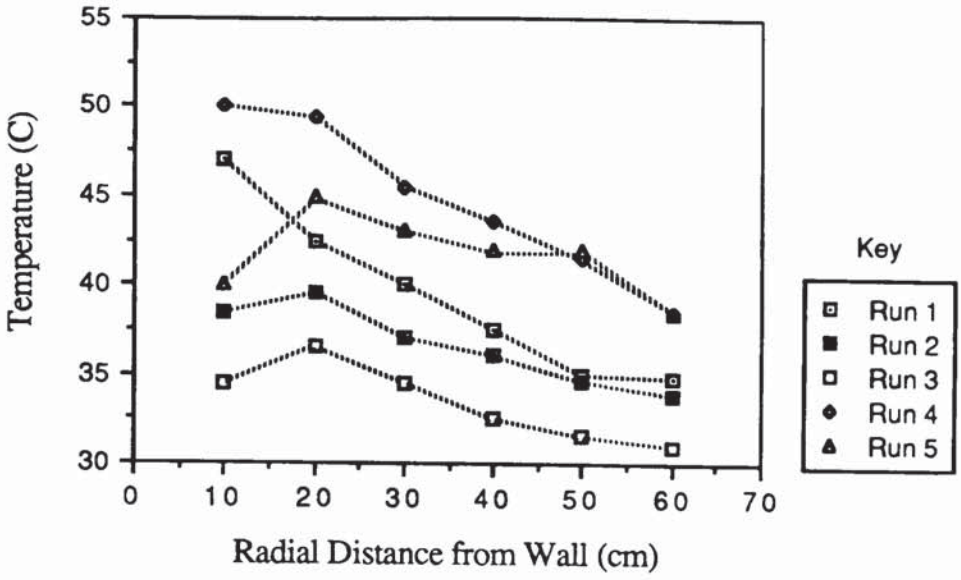

Figure 9.1 *Radial Air Temperature Profiles - 1m Level*

So, having discounted the theory that the steep temperature gradient at the drier base is simply due to a wall by-pass, the following explanation is proposed. At the base of the tower, it is possible to consider the cross-section to be divided into two regions: an inner region where the spray cloud consisting primarily of fine droplets, is concentrated, and an outer annular region where there is only a dilute concentration of larger droplets. It follows then that the incoming hot air at the centre of the drier will immediately contact the fine-spray. The large droplet surface area will result in a high evaporation rate with a corresponding rapid decrease in air temperature. However the air that does not enter the central spray region will only be exposed to a dilute concentration of larger droplets of lower surface area to volume ratios. Hence in this outer region evaporation will not be as rapid and the air temperature will not fall as markedly. The combined result will be the establishment of a temperature gradient over the drier cross-section as was detected. Subsequently, as the air ascends the tower, any swirl or turbulence within the chamber may be expected to unify the radial temperature profiles, again as was noted during the experiments.

In co-current driers, steep temperature and humidity gradients have been found to exist in the vicinity of the atomiser [136]. This was not observed for the counter-current drier in this study. Although the temperatures measured within the spray envelope at a level just below the atomiser were lower than the temperatures outside, the difference was only slight, typically 2-5°C. The steep gradients that are evident in co-current driers arise from the fact that the air stream just outside the spray envelope would have had little or no interaction with the droplets and hence would still be at high temperature and low humidity, close to its inlet value; this would be in contrast to the air within the spray. However in counter-current driers, the air just outside the spray envelope, in the vicinity of the atomiser, would have travelled the length of the drier and hence already participated in the drying process. This, together with the higher degree of turbulence within the drier, would result in the air temperature and humidity being close to their exit values. Hence in this instance the difference in air properties inside and outside the spray would not be so extreme, as demonstrated in this study.

(b) Axial Profiles

Because of the general uniformity of the radial temperature and humidity profiles, the data was averaged to give one value per axial location. In this way the axial variation in air properties could be investigated. These axial profiles are presented in Figures 8.15 - 8.34.

A striking feature of the axial profiles is the very rapid change in air properties that occurs almost instantaneously upon the entry of the air. Typically within 1m of the air entry ports, the fall in air temperature was of the order of 90% of the total drop.

A similar trend was observed for the humidity measurements but the data were more scattered and unlike the temperature profiles, the humidity profiles did not exhibit any characteristic shape. This was probably because the humidity measurements were more likely to suffer from inaccuracies arising from errors in the experimental technique such as

condensation in sample lines and air leakages. The accuracy of the sensor itself is quoted as ± 2°C dew-point and in fact the variation in dew point over the drier length was in many cases of the order of 2°C dew-point. Hence with hindsight it is not surprising that the humidity measurements could not detect the trends picked-up by the temperature measurements. In future work a greater degree of accuracy could perhaps be obtained by adopting an alternative humidity sensor or an alternative measuring technique, for example a gravimetric, dessicant-based method as outlined briefly in Chapter 7.

Concentrating on the temperature profiles, Figures 8.15 - 8.24, it is clear that after the initial rapid fall, there was a more gradual decrease in air temperature in the central length of the drier, i.e. between the 1m and 3m levels from the air entry ports. Hence in this region of the drier it appears that the air may predominantly be in plug flow. In addition it can be seen from the temperature profiles that there was a consistent rise in air temperature at the top of the tower at the level of the atomiser, i.e. 3.35m from the air entry ports. This may be attributed to a by-pass stream of hotter air ascending the tower and being mixed with the bulk of the air in a well-mixed zone in the vicinity of the atomiser.

This would tie-in with observations made during smoke visualisation tests on the transparent tower. These suggested that for maldistributed air entry, a by-pass did exist but only in the region directly opposite the air inlet to the ring-main. Unfortunately, due to the inaccessibility of this region in the current installation, temperature measurements could not be made to confirm this. As discussed earlier, the smoke tests also suggested the existence of a core of high rotational and axial velocity and this could also contribute to the by-passing of hotter air.

Thus on the basis of the temperature measurements, the existence of a central plug-flow zone, an upper well-mixed zone and some degree of hot air channelling can be inferred. However, it was not possible to establish the flow pattern at the base of the tower within a 1m distance from the air entry ports. No measurements could be made in this

region due to practical difficulties related to the lack of working space around the vicinity of the base cone. However, a previous study [135] on the same drier, via residence time distribution analysis, considered the base of the tower to be a well mixed zone and the central length of the drier was suggested to be in plug-flow, with a second well-mixed zone at the top of the tower. A by-pass was also assumed to exist.

It is evident that the findings of the present investigation are in general agreement with this flow arrangement, confirming the existence of the plug-flow zone, the upper well-mixed zone and the by-pass.

9.1.3 Agglomeration Study

As described in Chapter 7, the extent of agglomeration occurring during the descent of a water spray was assessed by the measurement of drop-size distribution at two levels in a spray drying tower. The results were presented in Figures 8.35 - 8.38. From these, the following general inferences can be made:

(i) In the absence of a counter-current air flow, some degree of in-spray agglomeration does occur, characterised by a shift in the drop size distribution to the coarse end, as the spray descends the tower. This is shown in Figure 8.35. The mechanism of agglomeration is most probably one of large fast moving droplets catching-up and colliding with smaller droplets travelling at their terminal velocities.

(ii) With the introduction of a counter-current, upward air flow, the agglomeration effect was amplified as shown in Figure 8.36. The mechanism of agglomeration in this instance is probably a combination of the 'catching-up' effect and of smaller droplets that have been entrained with the upward air flow impacting on the falling spray. This latter phenomena is commonly encountered in counter-current driers and results in the formation of dried particles which have smaller satellite drops adhered to them.

(iii) At a level close to the atomiser, the effect of an upward air flow on droplet agglomeration is evidently negligible as demonstrated by Figure 8.37. This can be explained by the fact that in the vicinity of the atomiser, large amounts of air may be expected to be entrained into the spray. This entrained air will flow in the same direction as the falling droplets and therefore, initially at least, prevent the droplets from actually being exposed to the upward air flow. Only lower down the tower, when the velocity of the entrained air has been sufficiently diminished by the spreading out of the spray, will droplets experience the drying air flow.Only then would agglomeration be expected to be increased, as discussed further below.

(iv) At a level 1.35m from the atomiser, the effect of the upward air flow on agglomeration does become significant as shown in Figure 8.38. This is probably because by this level, the velocity of the entrained air has been sufficiently reduced, to permit the upward air flow to penetrate the spray.

In summary this preliminary study has shown that agglomeration does occur during the descent of a spray, and that the effect would be considerably exaggerated in the operation of counter-current towers. This may in fact be desirable in certain situations where a dust-free, free-flowing powder is the desired end result. This study will need to be extended to a wider range of materials and operating conditions to fully understand this important phenomena of droplet agglomeration. Only with this knowledge will accurate predictions of final dried particle size and form be possible.

9.2 MATHEMATICAL MODEL

9.2.1 Application to Design and Optimisation

The application of the mathematical model has been amply demonstrated by the simulations presented in Chapter 8; these serve to highlight the quality of data that can be generated from the model, starting from basic information on the drying process.

Computer predictions of the type presented in Figures 8.39 - 8.50 can be used, within the limitations of the assumptions - particularly that of a receding interface, diffusion controlled drying mechanism, to provide information on a number of areas critical to the accurate design and optimum operation of a spray drier. These are described below.

(i) The model can provide information on the likelihood of wall or inter-droplet impingement. For example in Simulation 1, from Figure 8.39 it is evident that the movement of the smaller sized droplets, < 99 μm, in the horizontal direction is very small, with droplet terminal velocities being obtained within 25cm of the atomiser. This is in marked contrast to the movement of the larger drops, e.g. > 200 μm, which from Figure 8.39 may be expected to be quite significant in the horizontal direction. Depending upon the positioning of the atomisers, this could result in inter-spray agglomeration or build-up of product on the drier walls. Thus optimum atomiser positioning could be established with the aid of such information as presented in Figure 8.39.

Of course, the likelihood of a droplet adhering to the wall of another droplet upon impact will depend upon the stickiness of the product which will invariably be related to the moisture content and its temperature. This is discussed below.

(ii) The model can predict the variation in moisture content for the various sized droplets. For example in Simulation 1, from Figure 8.41 drops > 200 μm dry far slower than the smaller drops. Hence it is these drops that are likely to have a sufficiently high moisture and hence 'stickiness' level to adhere to the drier walls or to agglomerate. For a given product, it is possible to experimentally correlate 'stickiness' with moisture content and temperature [153]; skin-formation may be an additional factor, presumably resulting in a reduced tendency to adhere. Hence together with information supplied by the model on droplet trajectories, moisture contents and temperatures (e.g. Figures 8.39 - 8.41), it is possible to quantitatively predict the extent of agglomeration or wall-build-up likely to occur within the spray drier. .

(iii) The model can predict the likelihood of thermal degradation to heat sensitive materials. For example in Simulation 1, Figure 8.40 suggests that the droplet temperature regardless of size, initially approximates to the wet-bulb temperature of the drying air. As the droplet dries, the thickness of the dried layer increases, and hence the resistance to moisture diffusion also increases; eventually the rate of heat transfer into the droplet exceeds the rate of mass transfer and the droplet begins to heat up. When the droplet is completely dry it experiences rapid heating and the temperature of the droplet quickly approaches the local air temperature. The smallest droplets, < 99 μm, appear to dry very rapidly, i.e. within the first 2 m of travel. Hence it is these droplets which will experience the high air temperature in the vicinity of the atomiser and could become 'over-cooked', 'scorched' or otherwise thermally-degraded.

(iv) The model can predict the effect of operational parameters on final dried product moisture content. For example in Simulation 1, the moisture content of the dried product is approximately 1%. If it was desired to leave more or less moisture in the product, the optimum operating conditions could easily be ascertained by the repeated running of the type shown in Chapter 8. This could then be used to make a judgement on the optimum operating conditions bearing in mind the considerations detailed in points (i) - (iii).

9.2.2 Validation of Model Predictions

The ability of the mathematical model to accurately predict spray drier performance can be assessed by comparing model predictions to data that has been experimentally determined. In this study the performance of two spray driers was simulated for the purpose of model validation.

(i) The co-current drying of skimmed milk (Simulation 2).

(ii) The counter-current evaporation of water droplets (Simulation 3).

For the former, all data pertaining to the operation of the spray drier together with experimental measurements of air temperature, air humidity and spray moisture profiles were obtained from the work of Hayashi [18].

Operating data and experimental air temperature and humidities for the counter-current drier were generated in the temperature and humidity study detailed previously.

(i) Co-Current Drying of Skimmed Milk

Model predictions for the co-currrent drying of skimmed milk were presented in Figures 8.45 - 8.50. Experimental measurements of the axial variation of spray moisture content, air temperature and air humidity within the drier are superimposed upon the model predictions in Figures 8.48, 8.49 and 8.50 respectively. From these, it is clear that the model predicts the performance of the spray drier remarkably well. This is discussed further below.

Temperature Profile

The rapid drop in air temperature in the vicinity of the atomiser predicted by the model was confirmed by the experimental data. As shown in Figure 8.49, after the first 2 m the model predicted an air temperature of approximately 108°C, compared to a measured value of 98°C. Thereafter both the model, and the experimental data show that the air temperature does not change significantly, with a predicted exit air temperature of 83°C compared to the measured temperature of 93°C.

Humidity and Spray Moisture Profiles

Again the model provided an accurate prediction of the axial variation in air humidity. The predicted exit humidity of the air agreed almost exactly with the value quoted by Hayashi, although the model profile was rather steeper than the experimental. As would be expected, the same trends were observed for the spray moisture profile since

this is essentially the inverse of the humidity profile. The predicted exit moisture content of 3.5% agreed favourably with the experimental value of 4.8%.

The accuracy to which the model predicted the performance of the spray drier, at first sight, may appear somewhat surprising in view of the fact that during drying, skimmed milk droplets are known to form a surface - skin prior to the formation of a dried crust. However as detailed in Chapter 6, the droplet drying model was developed upon the assumption that a rigid porous crust was formed upon the surface of the droplet immediately upon commencement of drying. The reason why the model still provides an accurate simulation of the spray drier, irrespective of this, lies in the drying - rate characteristics of skimmed milk.

Previous single droplet studies [134] have shown that because of skin formation, materials like skimmed milk, do not exhibit any constant rate period, and drying occurs solely in a falling rate period which commences as soon as the droplet contacts the drying air. Furthermore this falling-rate period has been shown to be linear; this is also typical of a rigid porous crust forming material. It is the shape of the falling-rate drying curve that dictates how a material will dry, and this can be considered independently of the underlying drying mechanism. For example a rigid porous crust forming material with similar drying-rate characteristics as a skin-forming material will obviously be dried to the same degree, have the same 'drying-profile' and hence establish similar temperature and humidity profiles within the spray drier. Even if the skin was initially impervious the high temperature driving force typical of co-current drying will result in high initial evaporation rates, regardless of whether the mechanism of drying was by repeated violent skin rupturing or by diffusion through a porous crust and the analogy is again valid.

Thus it appears that the shrinking-core drying model which has been developed for application to rigid-porous crust forming materials can be applied to a skin forming material, so long as the drying characteristics of the latter, i.e. the shape of the falling-rate

drying curve, resembles that of the former. This was in-fact confirmed in a separate study which compared model predictions of a shrinking-core type drying model to experimental data obtained from single droplet studies on the drying of skin-forming materials (154).

(ii) Counter-current Evaporation of Water Droplets

The predicted variations in air temperature and air humidity for Runs 2, 5 and 10 are shown together with experimental measurements in Figures 8.51 - 8.56. From these it is clear that the model predicts drier performance with a reasonable accuracy. In particular the rapid change in air properties in the vicinity of the air inlet ports, as noted in the experimental study, has been accurately simulated by the computer model. In all cases within a 1.0m level from the air entry ports the computer predicts the air temperature and humidity to have reached their exit values.

In reality however, the experimental data shows that there is a more gradual approach to the exit conditions in the central part of the drier. The reason for this discrepancy between model and experimental data, probably lies in the fact that, for the purpose of modelling, the drop-size distribution was taken to be as measured near the atomiser. However, as the agglomeration study previously discussed suggested, some degree of agglomeration is likely to occur as the spray descends the tower. Hence the drop size distribution at the base of the tower is, in reality, likely to be coarser than assumed and therefore a lower evaporation rate can be expected. Allowance for this would result in the model predictions approaching the experimental measurements more closely.

Another feature highlighted by the model predictions was the presence of a significant amount of heat loss in the drier system. Based upon enthalpy balances the model predicted the air inlet temperature needed to bring about the same degree of evaporation as observed in the experiments; in all cases the predicted inlet temperature was substantially lower than the actual temperature as shown in Figures 8.52, 8.54 and 8.56.

This discrepancy is attributed to heat losses which are not taken into account in the model. Subsequent calculation of the transfer coefficient for heat loss defined by:

$$Q_{LOSS} = UA\Delta T_M \qquad 9.1$$

where ΔT_M is the log-mean temperature difference, yielded for the various runs values in the range 5×10^{-3} to 8×10^{-3} kW/m^2 K. For comparison, this was in agreement with a value of 6×10^{-3} kW/m^2 K noted in a previous study on the same drier [155].

In future a correction for heat loss from the drier, based upon calculations similar to those above, could readily be incorporated into the computer model to improve further the accuracy of the model predictions.

Chapter 10

Conclusions and Recommendations

10.1 GENERAL CONCLUSIONS

1. Air flow patterns have been studied in a transparent counter-current spray drier via smoke visualisation, for a variety of flow conditions. This has shown the existence of swirling motion within the drying chamber and the existence of a central core of high rotational and axial velocity. The existence of a strongly-swirling upflow may well be critical to drier operation. Thus care will be necessary in selecting the angle of injection, and to adequately balance the flows from each port. The effect of multi-nozzle atomisation, including their location, also requires further study.

2. Air temperature and humidity measurement techniques were developed and employed to determine air temperature and humidity profiles within the drying chamber for counter-current operation. These profiles indicate a rapid approach to the air exit conditions at the base of the tower. This would mean that the majority of moisture evaporation occurs near the gas inlet; this is quite different to previous observations with co-current operation when there is a rapid drop in gas temperature in the vicinity of the atomiser. The existence of plug-flow, well-mixed flow and by-pass zones may also be inferred but more sophisticated flow visualisation/measurement studies are recommended.

3. A technique was developed for assessing droplet agglomeration based upon measurement of drop-size distribution. This suggests inter-droplet agglomeration does occur during the descent of a water spray from a single nozzle, and that the extent of agglomeration is greatly increased in a counter-current air flow.

4. A mathematical model has been developed for cocurrent spray drier operation to predict drop trajectories, gas temperatures and drop dryness profiles. The predictions were compared with two sets of experimental data and, although it was not possible to validate all features, corresponded reasonably well with experimental observations.

Extension of the model to countercurrent operation was more difficult because the situation is more complex, arising from interactions between the drying air flow and the entrained air flow. The experimentally determined gas temperature and humidity profiles suggest that the majority of evaporation occurs well away from the atomiser, which would be consistent with the decreased driving force for mass transfer with position from the bottom gas inlet. Further work is considered necessary to validate the model satisfactorily for countercurrent operation

10.2 SPECIFIC CONCLUSIONS

10.2.1 Air Flow Patterns

The following more specific conclusions can be made regarding the air flow pattern within the drier:

(i) The central core established in the tower was affected by the introduction of a secondary air flow at the tower base to simulate a tower operating under slight vacuum. This tended to increase the diameter of the core and to render it more unstable.

(ii) Maldistribution trials, which simulated operation of a production tower with the flows not adequately balanced, demonstrated that incorrect operation of the nozzles significantly affects the flow pattern. Maldistribution resulted in either a shifting of the core to the side with less flow, or to the establishment of a wall by-pass on the side with less flow, depending upon nozzle configuration.

(iii) Changing the swirl angle demonstrated that a critical angle exists at which the core commences to break-up, leading to a wall by-pass.

(iv) Operation of a single water spray does not have a significant effect on the flow pattern, apart from increased turbulence in the vicinity of the atomiser.

10.2.2 Temperature and Humidity Study

(i) The accuracy of the temperature measurement technique enabled fine trends in the axial air temperature profile to be detected. From these, the existence of a central plug-flow zone, an upper well-mixed zone and some degree of by-pass may be inferred.

(ii) The humidity measurement technique was shown to be unsuitable for determination of detailed profiles. Only general trends could be established. This was due to the limited accuracy of the dew point sensor used.

10.2.3 Mathematical Model

(i) The mathematical model has been partially tested by comparing model predictions to experimentally determined data for two different spray driers. In the case of co-current operation there was reasonable agreement with experimental data for skimmed milk drying. The model showed promise to extension for counter-current operation subject to a better description of interactions between the various flow patterns visualised.

(ii) The model is applicable to co-current driers and is believed to be adaptable to most spray drying operations, given use of an appropriate model - which may be material specific - for single drop drying in the falling rate period. Gas flow patterns may also require better definition.

10.3 RECOMMENDATIONS FOR FURTHER WORK

1. The air feed system to the stainless drier should be modified. Currently with the electrical heaters in series, it is not possible to achieve air inlet temperatures in excess of 190°C. This is due to the heating - filaments burning out because all the generated heat cannot be carried away. It is recommended that the heater configuration be changed such that the heaters operate in parallel.

2. The temperature and humidity study should be extended to other feed materials, e.g. inorganic salts, and also to various liquid/gas ratios, e.g. in the range 1: 10 - 15, to assess whether the profiles measured in the study are typical of industrial drying practice. An alternative humidity sensor, or technique enabling a greater degree of accuracy should be employed e.g. a desiccant-based gravimetric method.

3. The agglomeration study should be extended to other materials and drier operating conditions to understand this phenomena further. Although this preliminary study with a water spray has suggested the existence of in-spray agglomeration, the degree to which it occurs will be a function of the nature of the droplet drying mechanism and, in particular, the 'stickiness' profile of the material being dried. It is also recommended that the phenomena of inter-spray agglomeration in multi-nozzle operation be investigated by the same technique. This could be achieved by assessing in-spray agglomeration with a single nozzle and then, by allowing for this, predicting the agglomeration occuring due to multi-spray impaction.

4. Following from Recommendation 3, agglomeration should be incorporated into the mathematical model to improve further the accuracy of the droplet drying prediction and also to enable predictions of final product form to be made. This could be achieved by the use of an empirical factor, which would be a function of the nozzle type, the cone angle, the particular liquid properties and the drying conditions.

Nomenclature

a	Area ratio for Dall-tube flow equation, $\left(\frac{d_t}{d_T}\right)$	
A	Area, Cross-sectional (drag), or, Surface (Heat and Mass Transfer).	(m^2) (m^2)
A_{ch}	Cross-sectional Area of the drying chamber.	(m^2)
A_{tip}	Surface Area of the thermocouple tip.	(m^2)
b	Height of vane for the rotary atomiser.	(m)
B	Barometric pressure, or, constant in Nukiyama-Tanasawa equation.	(N/m^2)
B_H	Transfer number for evaporation.	
B_M	Mass transfer number.	
C	Vapour concentration, or, constant in Nukiyama-Tanasawa equation.	($moles/m^3$),
C_a	Vapour concentration in air.	($moles/m^3$)
C_A	Empirical coefficient for accelerated motion.	
C_d	Discharge coefficient.	
C_D	Drag coefficient.	
C_{DM}	Drag coefficient corrected for mass transfer.	
C_H	Empirical coefficient for accelerated motion.	
C_N, C_q	Correction factors.	

C_P	Specific heat capacity of air.	(J/kg/K)
C_{Pc}	Specific heat capacity of dried crust.	(J/kg/K)
C_{PL}	Specific heat capacity of liquid phase.	(J/kg/K)
C_{Pv}	Specific heat capacity of water vapour.	(J/kg/K)
C_{Pw}	Specific heat capacity of water.	(J/kg/K)
C_s	Vapour concentration at droplet surface.	(kg/m^3)
cs	Humid heat (C_P+ H C_{Pv}).	(J/kg/K)
C_v	Velocity coefficient.	
d(D)	Size increment.	
d(N)	Number of droplets or droplet fraction.	
d_t	Dall-tube throat diameter.	(m)
d_T	Dall-tube diameter.	(m)
D	Droplet diameter.	(m)
D_c	Diameter of the air core in a pressure nozzle.	(m)
D_{eff}	Effective diffusivity.	(m^2/s)
D_{GM}	Geometric mean diameter.	(m)
D_I	Initial droplet diameter.	(m)
D_{max}	Maximum drop size.	(m)
D_o	Orifice diameter (pressure nozzle), or, disc diameter (rotary atomiser).	(m) (m)

D_o'	Effective orifice diameter.	(m)
D_R	Rosin-Rammler mean diameter.	(m)
D_V	Diffusivity.	(m^2/s)
e	Emmisivity.	
E	$\sqrt{\frac{1}{(1-a^2)}}$	
F_D	Drag force.	(N)
F_g	Gravitational force.	(N)
F_L	Lift force.	(N)
F_x	Component of drag force in x-direction.	(N)
F_z	Component of drag force in z-direction.	(N)
g	Gravitational constant.	(m/s^2)
G_a	Mass flowrate of drying air (vapour-free), or, Mass flowrate of atomising air for pneumatic atomisation.	(kg/s) (kg/s)
G_L	Mass flowrate of the liquid phase.	(kg/s)
G_s	Superficial air mass flowrate.	(kg/m^2s)
h_g	Gas film convective heat transfer coefficient.	($W/m^2/K$)
H	Air humidity.	(kg/kg)
H_{core}	Enthalpy of droplet core.	(J)
k_a	Thermal conductivity of air.	(W/m/K)

k_c	Thermal conductivity of droplet crust.	(W/m/K)
k_g	Gas film convective mass transfer coefficient.	(m/s)
k_w	Thermal conductivity of thermocouple wire.	(W/m/K)
K	Overall mass transfer coefficient.	(m/s)
m	Droplet mass.	(kg)
M_A	Acceleration modulus.	
M_W	Molecular weight of water.	(kg/mole)
n	Number of moles in the ideal gas equation, or, the total number of size classes in a drop size distribution.	
n_v	Number of rotary atomiser vanes.	
N	R.p.m. of rotary atomiser.	
N_A	Rate of mass transfer.	(kg/s)
N_i	Number of droplets in the incremental analysis.	
p	Partial pressure.	(N/m^2)
p_a	Partial pressure of vapour in air.	(N/m^2)
p_c	Partial pressure of vapour at the droplet core.	(N/m^2)
p_v	Water vapour pressure.	(N/m^2)
P	Pressure.	(N/m^2)
Pr	Prandtl number ($C_p \mu_a/k_a$).	
P_o	Atomisation pressure.	(N/m^2)

P_v	Velocity pressure for pipe flow.	(N/m^2)
ΔP	Pressure drop.	(N/m^2)
q	Dispersion coefficient.	
q_m	Maximum heat transfer to a spray.	(W)
q_{cond}	Rate of conductive heat transfer.	(W)
q_{conv}	Rate of convective heat transfer.	(W)
q_{rad}	Rate of radiative heat transfer.	(W)
Q	Rate of heat transfer.	(W)
Q_a	Enthalpy of drying air.	(J)
Q_L	Enthalpy of liquid phase.	(J)
Q_{loss}	Rate of heat loss.	(W)
Q_v	Volumetric flowrate.	(m^3/s)
r	Radial distance from the centre of the disc, or centre of the drop.	(m)
r_c	Radius of air core (pressure nozzle atomisation), or, radius of droplet core (drying).	(m) (m)
r_o	Radius of orifice (pressure nozzle) or disc radius (rotary atomiser).	(m)
r_s	Droplet radius.	(m)
r_w	Radius of thermocouple wire.	(m)
R_{ch}	Radius of drying chamber.	(m)
R_g	Universal gas constant.	(N/m mole K)

S_G	Geometric standard deviation.	
t	Time.	(s)
T	Temperature.	(K)
T_a	Air temperature.	(K)
T_c	Droplet core temperature.	(K)
T_D	Datum temperature.	(K)
T_{dp}	Dew-point temperature.	(K)
T_s	Surface temperature of droplet, or other body (radiation).	(K)
T_{tip}	Temperature of thermocouple tip.	(K)
ΔT	Temperature driving force.	(K)
U	Overall heat transfer coefficient.	($W/m^2/K$)
v	Volume.	(m^3)
V	Droplet velocity.	(m/s)
V_a	Air velocity.	(m/s)
V_{at}	Tangential air velocity.	(m/s)
V_{ax}	Component of air velocity in the x-direction.	(m/s)
V_{ay}	Component of air velocity in the y-direction.	(m/s)
V_{az}	Component of air velocity in the z-direction.	(m/s)
V_{cl}	Centre-line velocity for pipe flow.	(m/s)

V_D	Volume percent oversize.	(%)
V_f	Droplet terminal velocity.	(m/s)
V_m	Mean velocity in pipe flow.	(m/s)
V_o	Droplet release velocity.	(m/s)
V_o'	Liquid velocity up-stream of orifice.	(m/s)
V_R	Droplet velocity relative to air.	(m/s)
V_r	Component of drop velocity in radial direction.	(m/s)
V_{rR}	Component of drop relative velocity in radial direction.	(m/s)
V_t	Component of drop velocity in tangential direction.	(m/s)
V_{tr}	Component of drop relative velocity in tangential direction.	(m/s)
V_{to}	Tangential air velocity at drier wall.	(m/s)
V_x	Component of drop velocity in x-direction.	(m/s)
V_{xR}	Component of drop relative velocity in x-direction.	(m/s)
V_y	Component of drop velocity in y-direction.	(m/s)
V_{yR}	Component of drop relative velocity in y-direction.	(m/s)
V_z	Component of drop velocity in axial direction.	(m/s)
V_{zR}	Component of drop relative velocity in axial direction.	(m/s)
W_i	Weight fraction of drops of size, D_i.	
x	Distance moved in x-direction.	(m)

x_{vo}	Mass fraction of water vapour in air.	
x_{vs}	Mass fraction of water vapour at droplet surface.	
x_w	Mass fraction of water in droplet core.	
y	Distance moved in y-direction.	(m)
z	Axial distance.	(m)
Z	Correction factor for Dall tube flow equation (assumed unity).	
α	Angle of droplet release in rotary atomisation, or, angle of drag force acting on droplet whilst in linear motion.	(°) (°)
β	Crust thickness.	(m)
ε	Porosity of crust.	
λ	Latent heat of vaporization.	(J/kg)
λ_D	Latent heat of vaporization at datum temperature.	(J/kg)
μ_a	Viscosity of air.	(kg/m s)
μ_L	Viscosity of liquid.	(kg/m s)
ρ_a	Density of air.	(kg/m^3)
ρ_L	Density of liquid.	(kg/m^3)
ρ_p	Density of solid particle.	(kg/m^3)
ζ	Stefan-Boltzman constant.	
θ	Half spray cone-angle.	(°)
Θ	Angle in cylindrical co-ordinate analysis.	(°)

ϕ	Correlating parameter	
Ψ	Angle of linear air velocity acting upon droplet.	(°)
γ	Constriction factor	
τ	Tortuosity	

References

1 Dombrowski, N. and Munday, G., in Blakeborough, N. (Ed.), *Biochemical and Biological Engineering Science*, Vol. 2, 209, Academic Press, New York (1968).

2 Upadhaya, R.L., A.I.Ch.E. Meeting Prog., Pachech 77, Denver (1979).

3 Lord Rayleigh (Strutt, J.W.), Proc. *London Math. Soc.*, 10, (1878).

4 Dombrowski, N. and Fraser, R.P., *Phil. Trans.*, 247A, 101, (1953).

5 Clark, C.J. and Dombrowski, N., *Chem. Eng. Sci.*, 26, 1949, (1971).

6 Dombrowski, N. and Hooper, P.C., *Chem. Eng. Sci.*, 17, 291, (1962).

7 Fraser, R.P., Eisenklam, P., Dombrowski, N.and Hasson,D., *A.I.Ch.E.J.*, 8, 672, (1962).

8 Fraser, R.P., Eisenklam, P.,and Dombrowski, N, *Brit. Chem. Eng.*,No.10, 536, (1957).

9 Filkova, I. and Cedik, P., *Adv. in Drying*, Vol. 3, Hemisphere Publ. Corp, 181, (1984).

10 Fraser, R.P., Eisenklam, P.,and Dombrowski, N, *Brit. Chem. Eng.*,No.8, 414, (1957).

11 Dombrowski, N. and Wolfsohn, D.L., *J. Inst. Fuel*, 45, 327, (1972).

12 Dombrowski, N. and Wolfsohn, D.L., *Trans. Inst. Chem. Eng.*, 50, 259, (1972).

13 Dombrowski, N. and Tahir, M.A., *J. Inst. Fuel*, 50, 59, (1977).

14 Darnell, W.H., Ph.D Thesis, University of Wisconsin, Madison (1953).

15 McIrvine, J.S., Ph.D Thesis, University of Wisconsin, Madison (1961).

16 Nelson, P.A. and Stevens, W.F., *A.I.Ch.E.J.*, 7, 80, (1961).

17 Masters, K., *Spray Drying Handbook* , 4th ed., George Godwin Ltd., London, (1985)

18 Hayashi, H. and Takeda, S., *Proc. 4th Int. Dry. Sym.*, Vol. 2, Kyoto, Japan, (1985).

19 Nakamura, M. and Toyoda, S., *Proc. 4th Int. Dry. Sym.*, Vol. 2, Kyoto, Japan, (1985).

20 Marshall, W.R., Chem. Eng. Prog. Monograph Series No. 2, (1954).

21 Fraser, R.P., Eisenklam, P.,and Dombrowski, N, *Brit. Chem. Eng.*, No.9, 496, (1957).

22 Masters, K. and Mohtadi, M.F., *Brit. Chem. Eng.*, No.12, 1890, (1967).

23 Herring, W.M. and Marshall, W.R., *A.I.Ch.E.J.*, 1, 200, (1955).

24 Friedman, S.J., Gluckert, F.A. and Marshall, W.R., *Chem. Eng. Prog.*, 48, 181, (1952).

25 Rosin, R. and Rammler, E.J., *J.Inst. Fuel*, 7, 29, (1933).

26 Nukiyama, S. and Tanasawa, Y., *Trans Soc. Mech. Eng. Japan*, 4, 86, (1937).

27 Tate, R.W. and Marshall, W.R., *Chem. Eng. Prog.*, 49, 169, (1953).

28 Mugele, R.A. and Evans, H.D., *Ind. Eng. Chem.*, 43, 1317, (1951).

29 *User Guide to Fire and Explosion Hazards in the Drying of Particulate Materials*, Inst. Chem. Eng., (1977).

30 Entwhistle, R.E., *Food Eng.*, 8, 82, (1966).

31 Williams-Gardner, A., *Industrial Drying*, Leonard Hill, London, (1971).

32 Lyne, C.W., *Brit. Chem Eng.*, No. 16, 371, (1971).

33 Masters, K., *Ind. Eng. Chem.*, 60, 53, (1968).

34 Belcher, D.W., Smith, D.A. and Cook, E.M., *Chem. Eng.*, 70, 83, (1963); 70' 201, (1963).

35 Charm, S.E., *Fundamentals of Food Engineering*, Avi Publ. Corp, Westport Conn., (1963).

36 Seltzer, E. and Settelmeyer, J.T., *Adv. Food Res.*, 2, 399, (1949).

37 Patsavas, A.C., *Chem. Eng. Prog.*, 59, 65, (1963).

38 Keey, R.B., *Drying Principles and Practice*, Pergamon Press, Oxford, (1972)

39 Schlicting, H., *Boundary Layer Theory*, 6th ed., McGraw-Hill, New York, (1968).

40 Lapple, C.E., *Fluid and Particle Dynamics*, University of Delaware, (1954).

41 Taneda, S., *J. Phys. Soc. Japan*, 11, 1104, (1956).

42 Torobin, L.B. and Gauvin, W.H., *Can. J. Chem. Eng.*, 37, 129, (1959).

43 Torobin, L.B. and Gauvin, W.H., *Can. J. Chem. Eng.*, 37, 167, (1959).

44 Torobin, L.B. and Gauvin, W.H., *Can. J. Chem. Eng.*, 37, 224, (1959).

45 Torobin, L.B. and Gauvin, W.H., *Can. J. Chem. Eng.*, 38, 142, (1960).

46 Torobin, L.B. and Gauvin, W.H., *Can. J. Chem. Eng.*, 37, 189, (1960).

47 Lapple, C.E. and Shepherd, C.B., *Ind. Eng. Chem.*, 32, 605, (1940).

48 Hughes, R.R. and Gilliland, E.R., *Chem. Eng. Prog.*, 48, 497, (1952).

49 Clift, R., Grace, J.R. and Weber, M.E., *Bubbles Drops and Particles*, Academic Press, London (1978).

50 Perry, J.H., *Chemical Engineers Handbook*, 4th ed.,McGraw-Hill, New York.

51 Coulson, J.M. and Richardson, J.F., *Chemical Engineering Vol. 2*, 3rd ed. Pergamon Press, Oxford, (1978).

52 Clift, R. and Gauvin, W.H., *Can. J. Chem. Eng.*, 49, 439, (1971).

53 Lunnon, R.G., *Proc. Royal Soc.*,110A, 302, (1926).

54 Manning, W.P. and Gauvin, W.H., *A.I.Ch.E.J.*, 6, 184, (1960).

55 Basset, A.B., *A Treatise on Hydrodyamics*, Dover, New York, (1961).

56 Tchen, C.M., Ph.D. Thesis, Univ. Delft, (1947).

57 Mockros, L.F. and Lai, R.Y.S., *Proc. Am. Soc. Civ. Eng.*, J. Eng. Mech. Div., 95, 629, (1969).

58 Odar, F. and Hamilton, W.S., *J. Fluid Mech.*, 18, 302, (1964).

59 Odar, F., Res. Rep. 190, Cold Regions Res. and Eng. Lab., U.S. Army Material Command, Hanover, New Hampshire, (1966).

60 Odar, F., *Trans. A.S.M.E.* Ser. E., J. App. Mech., 238, (1968).

61 Odar, F., *Trans. A.S.M.E.* Ser. E., J. App. Mech., 652, (1968).

62 Hines, J.O., *Turbulence*, 2nd ed., McGraw-Hill, New York, (1975).

63 Heywood, H., Paper presented at Symposium on the Interaction of Fluids and Particles, I. Chem. E., London, (1962).

64 Marchildon, E.K., *Shape Turbulence and Acceleration Effects on the Dynamics of Particle-Fluid Systems*, Ph.D.Thesis, McGill University, (1965).

65 Marchildon, E.K. and Gauvin, W.H., *A.I.Ch.E.J.*, 25, 938, (1979).

66 Staffman, P.G., *J. Fluid Mech.*, 22, 385, (1965).

67 Rubinow, S.I. and Keller, J.B., *J. Fluid Mech.*, 11, 447, (1961).

68 Boothroyd, R.G., *Flowing Gas-solid Suspensions*, Chapter 2, Chapman and Hall Ltd., London, (1971).

69 Eisenklam, P., Weston, J.A. and Arunachalam, S.A., 11th Int. Symp. on Combustion 1966, the Combustion Inst., Pittsburgh, Pennsylvania, (1967).

70 Ingebo, P.D., 8th Symp. on Combustion, 104, Williams and Willeins, (1962).

71 Hamielec, A.E.,Ross, L.L. and Hoffman, T.W., *A.I.Ch.E.J.*, 13, 212, (1967).

72 Renksizbulut, M. and Yuen, M.C., *J. Heat Transfer*, 105, 389, (1983).

73 Chuchottaworn, P., Fujinami, A. and Asano, K., *J. Chem. Eng. Japan*, 16, 18, (1983).

74 Chuchottaworn, P. and Asano, K., *J. Chem. Eng. Japan*, 18, 91, (1985).

75 Morimoto, M., Chuchottaworn, P., Fujinami, A. and Asano, K., Proc. 3rd Int. Conf. on Liquid Atomisation and Spray Systems *(ICLASS-85)*, Imperial College, London, (1985).

76 Chaloud, J.H., Martin, J.B. and Baker, J.S., *Chem. Eng. Prog.*, 53, 593, (1957).

77 Thordarson, R., *A Study of Air Flow in Spray Drier Design*, M.Sc. Thesis, University of Wisconsin, Madison, (1952).

78 Thomas, W.R., *A Study of Air Flow and Particle Motion in Vortex Spray Drier Model*, Ph.D. Thesis, University of Wisconsin, Madison, (1956).

79 Buckham, J.R. and Moulton, R.W., *Chem. Eng. Prog.*, 51, 126, (1955).

80 Arni, V.R.S., *The Production, Movement and Evaporation of Sprays in Spray drying*, Ph.D. Thesis, University of Washington, (1959).

81 Place, G., Ridgway, K. and Danckwerts, P.V., *Trans. Inst. Chem. Eng.*, 37,268, (1959).

82 Paris, J.R., Ross, P.N., Dastuv, S.P. and Morris, R.L., *Ind. Eng. Chem.* Proc. Des. Dev.,10,157, (1971).

83 Ade-John, A.O. and Jeffreys, G.V., *Trans. Inst. Chem. Eng.*, 56, 36, (1978).

84 Keey, R.B. and Pham, Q.T., *Chem. Eng. Sci.*, 32, 1219, (1977).

85 Usui, H. and Sano, Y., *J. Chem. Eng. Japan*, 18, 243, (1983).

86 Frossling,N., *Beitr. Geophys.*, 52, 170, (1938).

87 Hassan-Ali, H., Ph.D. Thesis, University of Aston, Birmingham, (1985).

88 Akbar, S., Ph.D. Thesis, University of Aston, Birmingham, (1989).

89 Ranz, W.E.and Marshall, W.R., *Chem. Eng. Prog.*, 48, 141,(1952); 48, 173, (1952).

90 Ranz, W.E., *Trans. A.S.M.E.*, 78, 909, (1956).

91 Dloughy, J. and Gauvin, W.H., *Can. J. Chem. Eng.*, 113, (August 1960).

92 Bose, A.K. and Pei, D.C.T., *Can. J. Chem. Eng.*, 42, 259, (1964).

93 Dickinson, D.R. and Marshall, W.R., *A.I.Ch.E.J.*, 14, 541, (1968).

94 Charlesworth, D.H., and Marshall, W.R., *A.I.Ch.E.J.*, 6, 9, (1960).

95 Audu, T.O.K. and Jeffreys, G.V., *Trans. Inst. Chem. Eng.*, 53, 165, (1975).

96 Cheong, H.W., Jeffreys, G.V. and Mumford, C.J., *A.I.Ch.E.J.*, 32, 1334, (1986).

97 Dloughy, J. and Gauvin, W.H., *A.I.Ch.E.J.*, 6, 29, (1960).

98 Baltas, L. and Gauvin, W.H., *A.I.Ch.E.J.*, 15, 772, (1969).

99 Duffie, J.A. and Marshall, W.R., *Chem. Eng. Prog.*, 49, 480, (1953).

100 Crosby, E.J. and Marshall, W.R., *Chem. Eng. Prog.*, 54, 56, (1958).

101 Wood, W.M.L., Paper presented to Solids Drying Subject Group, Inst. Chem. Eng., (1986).

102 Arnason, G. and Crowe, C.T., *Drying '80*, Vol. 2, 410, Hemisphere Book Corp., (1980).

103 Seltzer, E. and Marshall, W.R., *Chem. Eng. Prog.*, 46, 501, (1950).

104 Seltzer, E. and Marshall, W.R., *Chem. Eng. Prog.*, 46, 575, (1950).

105 Sjenitzer, F., *Chem. Eng. Sci.*, 1, 101, (1952).

106 Duffie, J.A. and Marshall, W.R., *Chem. Eng. Prog.*, 49, 417, (1953).

107 Kerhof, P.J.A.M. and Schoeber, W.J.A.H., in Spicer, A. (Ed.), *Advances in Preconcentration and Dehydration of Foods*, App. Sci. Publ., London, (1974).

108 Holland-Batt, A.B., *Trans. Inst. Chem. Eng.*, 50, 12, (1972).

109 Janda, F., *Int. Chem. Eng.*, 13, 649, (1973).

110 Janda, F., *Int. Chem. Eng.*, 18, 310, (1978.

111 Gluckert, F.A., *A.I.Ch.E.J.*, 8, 461, (1962).

112 Cheng-Yi, X., Proc. 4th Int. Symp. Drying, Vol. 1, 268, Kyoto, Japan, (1985).

113 Edeling, C., *Beihefte. Agnew. Chem.*, No. 57, (1950).

114 Rawson, N.E., Chinn, J.S. and Stevens, W.F., *A.I.Ch.E.J.*, 7, 448, (1961).

115 Holland-Batt, A.B., *Trans. Inst. Chem. Eng.*, 50, 156, (1972).

116 Bailey, G.H., Slater, I.W. and Eisenklam, P., *Brit. Chem. Eng.*, 15, 912, (1970).

117 Marshall, W.R., *Trans. A.S.M.E.*, 77, 1377, (1955).

118 Goffredi, R.A. and Crosby, J.E., *Ind. Eng. Chem. Proc. Des. Dev.*, 22, 665, (1983).

119 Yuan, W., Jufu, F. and Chong, Z., *Proc. 4th Int. Symp. Drying*, Vol. 1, 200, Kyoto, Japan, (1985).

120 Miuara, T., Ohtani, S. and Maeda, S., *Drying '80*, Vol. 1, 351, Hemisphere Book Corp., (1980).

121 Parti, M. and Palancz, B., *Chem. Eng. Sci.*, 29, 355, (1974).

122 Topar, J., *Drying '80*, Vol. 2, 405, Hemisphere Book Corp., (1980).

123 Keey, R.B., Huber, R.A. and Reay, D., Inst. Chem. Eng. Symp. Series, Solid Sep. Processes Int. Symp., No. 59, Dublin, (1980).

124 Pham, Q.T. and Keey, R.B., *Trans. Inst. Chem. Eng.*, 55, 114, (1977).

125 Keey, R.B.and Pham, Q.T., *The Chemical Engineer*, 516, (1976).

126 Troung, H.T., Pham, Q.T. and Keey, R.B., *J. Sep. Proc. Tech.*, 4, 11, (1983).

127 Katta, S. and Gauvin, W.H., *A.I.Ch.E.J.*, 21, 143, (1975).

128 Katta, S. and Gauvin, W.H., *A.I.Ch.E.J.*, 22, 713, (1976).

129 Gauvin, W.H., Katta, S. and Knelman, F.H., *Int. J. Multiphase Flow*, 1, 793, (1975).

130 Pai, S., *Fluid Dynamics of Jets*, Van Nostrand, (1954).

131 Baltas, L. and Gauvin, W.H., *A.I.Ch.E.J.*, 15, 764, (1969).

132 Crowe, C.T., *Adv. Drying*, Vol.1, 63, Hemisphere Publ. Corp., New York, (1980).

133 Crowe, C.T., Sharma, M.P. and Stock, D.E., *J. Fluid Eng.*, Trans. A.S.M.E. Ser. I, 99, (1977).

134 Trommelen, A.M. and Crosby, J.E., *A.I.Ch.E.J.*, 16, 857, (1970).

135 Ade-John, O.E., Ph.D. Thesis, University of Aston, Birmingham, (1976).

136 Papadakis, S.E. and King, C.J., *Ind. Eng. Chem. Res.*, 27, 2111, (1988); 27,2116, (1988).

137 Benatt, F.G.S. and Eisenklam, P., *J.Inst. Fuel*, 309, (August 1969).

138 Ranz, W.E. and Binark, H., A.S.M.E. pre-print No. 58-A-284, (1958).

139 Rothe, P.H. and Block, J.A., *Int. J. Multiphase Flow*, 3, 263, (1977).

140 Tischkoff, J.M., Proc.3rd Int. Conf. Liquid Atomisation and Spray Systems *(ICLASS-85)*, Imperial College, London, (1985).

141 Operating Instructions: Pitot Static Tube, Air Flow Developments Ltd., High Wycombe, England.

142 Hoffman, T.W. and Gauvin, W.H., *Can. J. Chem. Eng.*, 110, (1962).

143 Papadakis, S.E., Ph.D. Thesis, University of California, Berkeley, (1987).

144 Industrial Catalogue, Spraying Systems Co., Illinois, U.S.A.

145 Flow Measurement, BS 1042 (1943), British Standards Institution.

146 Private Communication, Kent Industrials Ltd.

147 Felton, P.G., Aigal, A.K. and Hamidi, A.A., Proc. 3rd Int. Conf. Liquid Atomisation and Spray Systems *(ICLASS-85)*, Imperial College, London, (1985).

148 Sudlow,C.A., Ph.D. Thesis (To be Published), University of Aston, Birmingham, (1990).

149 Hall, C.W. and Hendrick, T.I., *Drying of Milk and Milk Products*, Avi Publ. Co., Westport, Conn., (1971).

150 Webb, B.H. and Johnson, A.H., *Fundamentals of Dairy Chemistry*, Avi Publ. Co., Westport, Conn., (1965).

151 Shepherd, C.B. and Lapple, C.E., *Ind. Eng. Chem.*, 31, 972, (1939); 32, 1246, (1940).

152 Bank, N. and Gauvin, W.H., *Can. J. Chem. Eng.*, 55, 397, (1977).

153 Genskow, L.R., Proc. 5th Int. Drying Symp., Versailles, France, (1988).

154 Bains, G.S., Ph.D. Thesis (To be Published), University of Aston, Birmingham, (1990).

155 Esubiyi, A.O., Ph.D. Thesis, University of Aston, Birmingham, (1980).

156 Bruggeman, D.A.G., *Annln. Phys.*, 24, 636 (1935).

Appendix A: The Effective Diffusivity in Droplet Mass Transfer

An expression for the mass transfer coefficient through the dried crust of a droplet is developed below. The theory was first proposed by Audu [95].

The resistance to mass transfer of water vapour from the wet droplet core to the gas stream is the sum of the resistances through the crust and the gas film, and is expressed by:

$$\frac{1}{K} = \frac{1}{k_g} + \frac{1}{k_c} \qquad A1$$

The coefficient through the crust, k_c, can be expressed in terms of the effective diffusivity, D_{eff}, of the water vapour diffusing through the pores and the crust thickness β, that is:

$$k_c = \frac{D_{eff}}{\beta} \qquad A2$$

The effective diffusivity is a function of the molecular diffusivity, D_v, the porosity ε, the constriction factor, γ, and the tortuosity factor, τ and is related by the expression:

$$\frac{D_{eff}}{D_v} = \frac{\varepsilon \gamma}{\tau} \qquad A3$$

The porosity, ε, accounts for the reduction in area for moisture diffusion at a particular point in the porous crust; the tortuosity factor is a measure of the ratio of the actual distance which a diffusing species must travel, on the average, and the linear distance between the two points in the crust; the constriction factor takes into account the fact that channels are not uniform in cross section and vary with position.

Both the toruosity and constriction factors are functions of the porosity where [156]:

$$\frac{\gamma}{\tau} = \varepsilon^{0.5} \qquad A4$$

Substituting equation A4 into equation A3 gives:

$$D_{eff} = D_v \varepsilon^{1.5} \qquad A5$$

Appendix B Spray Drier Simulation Model

```
*       Spray Drier Simulation Model.
*       -----------------------------
*
*       Written by Sanjeev Sharma
*                       1985 - 1988
*       -------------------------


*       Main Program
*


*       Initialisation of Variables
*       ---------------------------

        REAL PHEATVAP,HEATVAP,PEVAP,PHEAT,HEAT,VV,C,DT
        REAL D,V,SV,SH,SS,LH,LV,DZ,CONE,DW
        REAL PI,CP,DC,MW,RC,CO,PAIR,KC,HC,CA,DS,R,TA,T1
        REAL VOL,PD,WCON,PA,U,VT,RE,PR,SC,X,KA,LT
        REAL VA,DA,DF,VMEAN,CHg,RHc,CMg,RMc,
        REAL ED,Z,CRC,INV,OMTC
        REAL PSAT,AREA,NAM,EVAP,MOMT0,MOMT2
        REAL MF,CC,LOW,PREV,MOIST,NA,M,DRI
        REAL NAOLD,NAMEAN,MAIR,QAIR,QTOT
        REAL CD,HX,TAV,CAV,AVT,AVC
        REAL DROPS,GAIRo,GSOLo,MSOL,VFLOW,MFRAC,HUMID,MS
        REAL DIST,SEC,VCRIT,CPDRY,NATOT
        REAL MCORE,PVFL,HANEW,GAIR,GSOL
        REAL HA,HA1,HA2,HAG,DCORE,CORE,MASS
        INTEGER N,DRIER,TYPE,NI

        CHARACTER*4,CODE


        DIMENSION REN(9),DI(9),WT(9),WC(9),TIME(9)
        DIMENSION XVEL(9),YVEL(9),XDIS(9),YDIS(9),RVEL(9)
```

```
      DIMENSION ZVEL(9),TVEL(9),RDIS(9),ZDIS(9),THETA(9)
      DIMENSION OVEL(9),TSOL(9),B(9),DRY(9),DROP(9)
      DIMENSION PRVEL(9),PZVEL(9),PTVEL(9),PRDIS(9)
      DIMENSION,PZDIS(9),PTHETA(9)
      DIMENSION DLIM(9),WET(9),CENT(9),SOL(9),PCORE(9)
      DIMENSION PSMA(9),PTSOL(9),PDRY(9),PWC(9)
      DIMENSION PSOL(9),PXDIS(9),PYDIS(9),PXVEL(9),PB(9)
      DIMENSION PYVEL(9),POVEL(9),PTIME(9)
      DIMENSION DVY(9),SOLID(9),DDBAS(9)
      DIMENSION RATE(9),TATE(9),DWBAS(9),CRST(9)
      DIMENSION RES1(9),RES2(9),WTEST(9),ZTEST(9)
      DIMENSION Z1TEST(9)

*     Droplet Size Distribution
*     -------------------------

      DATA DI/413E-6,211E-6,137E-6,99E-6,74E-6,57E-6,
     + 45E-6,35E-6/
      DATA WT/0.103,0.159,0.141,0.139,0.104,0.109,
     + 0.073,0.172/
*


*     ***** KEY NOMENCLATURE *****
*     CP=SPECIFIC HEAT OF WATER
*     CPDRY=SPECIFIC HEAT OF CRUST
*     PD=DENSITY OF DROP
*     PS=DENSITY OF SOLIDS
*     MW=MOLECULAR WEIGHT OF WATER
*     RC=GAS CONSTANT
*     CO=PARTIAL PRESSURE OF WATER IN AIR
*     Xw=MASS FRACTION OF WATER IN SLURRY
*     CPa=SPECIFIC HEAT OF AIR
*     KC=THERMAL CONDUCTIVITY OF CRUST
*     T1=CORE TEMPERATURE
*     X=CORE RADIUS
*     KA=THERMAL CONDUCTIVITY OF AIR
*     LT=LATENT HEAT OF VAPORISATION
```

```
*       VA=VISCOSITY OF AIR
*       DA=DENSITY OF AIR
*       DF=MOLECULAR DIFFUSIVITY
*       ED=EFFECTIVE DIIFUSIVITY
*       E=POROSITY
*       PSAT=SATURATED VAPOUR PRESSURE OF WATER
*       CA=SPRAY CONE ANGLE
*

*       SOLUTION:XXX
*       ------------

*       PHYSICAL PROPERTIES OF SOLUTION:
*       --------------------------------
        CS=3036
        CPDRY=2210
        Xw=0.45
        KC=0.07
        PD=1220
        PS=1450
        E=1-((1-Xw)*PD/PS)
*       --------------------------------

*       OTHER DATA:
*       -----------

        NI=8
        PI=3.1415926
        CP=4180
        MW=18
        RC=8.314E+3
        CPa=1036.23

*
*       Input Operating Data
*       ____________________
*
*
```

```
PRINT*,'****************************'
PRINT*,'SPRAY DRIER TRAJECTORY MODEL'
PRINT*,'****************************'
PRINT*,'ENTER  1  FOR CO-CURRENT DRIER'
PRINT*,'       2  FOR COUNTER-CURRENT DRIER'
READ*,DRIER
IF (DRIER.EQ.1) THEN
TYPE=1
ELSE IF (DRIER.EQ.2) THEN
TYPE=-1
END IF
TY=TYPE

PRINT*,'ENTER  1  FOR PARALLEL STREAMLINE FLOW'
PRINT*,'       2  FOR SWIRL FLOW'
PRINT*,'       3  FOR WELL-MIXED FLOW'

READ*,FLOW

PRINT*,'INCREMENT SIZE: '
READ*,DZo
PRINT*,'NOZZLE OPERATING PRESSURE (PSI)'
READ*,PSI
PRINT*,'SPRAY CONE ANGLE (DEG): '
READ*,CA
PRINT*,'NOZZLE ORIFICE DIAMETER (M)'
READ*,OD
IF (FLOW.NE.3) THEN
PRINT*,'RADIAL COMPONENT OF AIR VELOCITY (M/S)'
READ*,UAR
PRINT*,'VERTICAL COMPONENT OF AIR VELOCITY (M/S)'
READ*,UAZ
END IF
IF (DRIER.EQ.1) THEN
PRINT*,'INLET AIR TEMPERATURE (DEGREES KELVIN): '
ELSE
PRINT*,'EXIT AIR TEMPERATURE (DEGREES KELVIN):'
END IF
```

```
      READ*,TA
      PRINT*,'INLET SLURRY TEMPERATURE (DEGREES KELVIN): '
      READ*,T1
      PRINT*,'ABSOLUTE HUMIDITY (KG.MOISTURE/KG.DRY AIR) :
     '
      READ*,HA
      PRINT*,'MASS FLOWRATE OF AIR (KGS/S): '
      READ*,GAIRo
      PRINT*,'MASS FLOWRATE OF SLURRY (KG/S): '
      READ*,GSOLo
      PRINT*,'SIMULATION RECORD CODE :'
      READ*,CODE
*
*
*
*     Calculation of Air Core Radius and Sheet Vel
*     --------------------------------------------

      AC=(0.0112*CA-0.227)*OD
      OAREA=(OD**2-AC**2)*PI/4
      VS=GSOLo/(PD*OAREA)
      CON=CA*(PI/180)
      SLEN=1E-2
      DZ=DZo

*     Calculate Dry-air Flow
*     ----------------------

      Pa=29*HA*101.325E+3/(18*(1+(29*HA/18)))
      MFRAC=HA/(1+HA)
      MFO=MFRAC
      VFLOW=GAIRo*MFRAC
      XAIR=(1-MFRAC)*GAIRo
      XAIRo=XAIR
*
*     Calculate Drop Weights and Solution Flowrate
*     --------------------------------------------
```

```
      DO 8 I=1,NI
      SMA(I)=(PD*PI*DI(I)**3)/6
      WC(I)=SMA(I)*Xw
      SOLID(I)=SMA(I)*(1-Xw)
      DRY(I)=(WC(I)/SMA(I))*100
      DWBAS(I)=SOLID(I)*100/SMA(I)
      SOL(I)=GSOLo*WT(I)
    8 CONTINUE

*     SUBROUTINE PROPS CALCULATES PROPERTIES OF AIR
*
      CALL PROPS(TA,T1,KA,LT,VA,DA,DF,SPHT,HA)
*
      HAO=HA
      TAO=TA
      CPAO=SPHT

*
      CA=CA*PI/(180*2)
*


*     Open Data Storage Files
*     -----------------------
*
      OPEN (UNIT=50,FILE='DATA',STATUS='OLD')
      OPEN (UNIT=1,FILE='ONE',STATUS='OLD')
      OPEN (UNIT=2,FILE='TWO',STATUS='OLD')
      OPEN (UNIT=3,FILE='THREE',STATUS='OLD')
      OPEN (UNIT=4,FILE='FOUR',STATUS='OLD')
      OPEN (UNIT=5,FILE='FIVE',STATUS='OLD')
      OPEN (UNIT=6,FILE='SIX',STATUS='OLD')
      OPEN (UNIT=7,FILE='SEVEN',STATUS='OLD')
      OPEN (UNIT=8,FILE='EIGHT',STATUS='OLD')

      OPEN (UNIT=100,FILE='AIR',STATUS='OLD')
      OPEN (UNIT=11,FILE='VEL1',STATUS='OLD')
```

```
      OPEN (UNIT=12,FILE='VEL2',STATUS='OLD')
      OPEN (UNIT=13,FILE='VEL3',STATUS='OLD')
      OPEN (UNIT=14,FILE='VEL4',STATUS='OLD')
      OPEN (UNIT=15,FILE='VEL5',STATUS='OLD')
      OPEN (UNIT=16,FILE='VEL6',STATUS='OLD')
      OPEN (UNIT=17,FILE='VEL7',STATUS='OLD')
      OPEN (UNIT=18,FILE='VEL8',STATUS='OLD')


      DO 11 I=1,8
      WRITE(I,*)'  '
      WRITE(I,*)'CODE=',CODE,': DROPLET DRYING BEHAVIOUR'
      WRITE(I,*)'  '
      WRITE(I,*)' DROP SIZE =',DI(I)*1E+6,'MICRONS'
      WRITE(I,*)' ------------------------------'
      WRITE (I,100)
11    CONTINUE

      DO 12 I=11,18
      WRITE(I,*)'  '
      WRITE(I,*)'CODE=',CODE,': DROPLET TRAJECTORY'

      WRITE(I,*)'  '
      WRITE(I,*)' DROP SIZE =',DI(I-10)*1E+6,'MICRONS'
      WRITE(I,*)' ---------------------------------'
      WRITE (I,140)
12    CONTINUE
      WRITE(100,*)'CODE=',CODE,' : AIR PROPERTIES'
      WRITE(100,*)' '
      WRITE(100,160)

*

      WRITE(50,*)'SPRAY DRYER OPERATING CONDITIONS'
      WRITE(50,*)'--------------------------------'
      WRITE(50,*)'SPRAY CONE ANGLE:',CONE,'DEGREES'
      WRITE(50,*)'AIR CORE RADIUS :',AC,'METRES'
      WRITE(50,*)'SHEET LENGTH    :',SLEN,'METRES'
```

```
      WRITE(50,*)'VERT.SHEET VEL. :',VS,'M/S'
      WRITE(50,*)'TAN. SHEET VEL. :',VS*TAN(CA)
      WRITE(50,*)'AIR TEMPERATURE :',TA-273,'DEG C'
      WRITE(50,*)'SOLUTION TEMP.  :',T1-273,'DEG C'
      WRITE(50,*)'RADIAL AIR VEL. :',UAR,'M/S'
      WRITE(50,*)'VERT. AIR VEL.  :',UAZ,'M/S'
      IF (FLOW.EQ.2) THEN
      WRITE(50,*)'TANG. AIR VEL.  :'
      WRITE(50,*)'RADIAL DIS.<=R/5:',' Vt=3.51RD**0.5'
      WRITE(50,*)'RADIAL DIS.> R/5:',' Vt=2.57RD**-0.5'
      END IF
      WRITE(50,*)'AIR FLOWRATE    :',GAIRo,'KG/S'
      WRITE(50,*)'SOL.FLOWRATE    :',GSOLo,'KG/S'
      WRITE(50,*)'AIR HUMIDITY    :',HA,'KG/KG'
      WRITE(50,*)'CODE            :',CODE
      WRITE(50,*)'        *****'
      WRITE(50,*)'DROP SIZE DISTRIBUTION:'
      WRITE(50,*)'----------------------'
      WRITE(50,75)
75    FORMAT(1X,'DROP SIZE(uM)',4X,'WT FRACTION(%)',4X,
     +  'TERM VEL(m/s)'/)

      DO 13 I=1,NI
      WRITE(50,80)DI(I)*1E+6,WT(I)*100,TV(I)
13    CONTINUE
80    FORMAT(1X,F13.2,4X,F14.2,4X,F13.2)
      WRITE(5,*)'=========================='

*
*
       VAIR=UAZ

      RCRIT=0.73152
      UR=VS*TAN(CA)
      UZ=VS
      C=((UR-UAR)**2+(UZ-TY*UAZ)**2+(UT-UAT)**2)**0.5
```

```
      COUNT=0

      DO 15 I=1,NI
      RVEL(I)=UR
      ZVEL(I)=UZ
      TVEL(I)=UT
      RES1(I)=(UR**2+UT**2+UZ**2)**0.5
      OVEL(I)=C
      REN(I)=DI(I)*RES1(I)*DA/VA
      RDIS(I)=SLEN*SIN(CA)
      ZDIS(I)=SLEN*COS(CA)
      CDO(I)=1
      WRITE(I+10,300)RVEL(I),TVEL(I),ZVEL(I),RDIS(I)
     +  ZDIS(I),THETA(I),REN(I),TIME(I)

      TSOL(I)=T1
      B(I)=DI(I)/2
      DLIM(I)=99.50
      CENT(I)=SMA(I)
      WET(I)=Xw*100
   15 CONTINUE

      MOMT0=GSOLo*ZVEL(1)
       *
      TA2=TA
      TAG=-10*TY
      HA2=HA
      HAG=10*TY
      N=NI
*                          DO LOOP STARTS HERE
   16 TA1=TA2
      TA2=TA1+TAG*DZ
      HA1=HA2
      HA2=HA1+HAG*DZ
      COUNT=COUNT+1
*
   18 QTOT=0
```

```
      NATOT=0
      AREA=0
      AHEAT=0
      QNAT=0
      MOMT2=0

*
      TA=(TA1+TA2)/2
      HA=(HA1+HA2)/2
      Pa=29*HA*101.325E+3/(18*(1+(29*HA/18)))
      CALL PROPS(TA,T1,KA,LT,VA,DA,DF,SPHT,HA)


       DO 20 I=1,NI
       D=DI(I)
       R=D/2


       C=(RVEL(I)-UAR)**2+(ZVEL(I)-TY*VAIR)**2
     +  +(TVEL(I)-UAT)**2
       C=C**0.5
       UR=RVEL(I)
       UT=TVEL(I)
       UZ=ZVEL(I)

       RD=RDIS(I)
       T1=TSOL(I)
       WCON=WC(I)
       MASS=SMA(I)
       X=B(I)
       DCORE=2*X
       Z=R-X


*
*      PARTICLE TRAJECTORY SEQUENCE
*      ----------------------------
```

```
   19   DT=DZ/UZ


        RE=DI(I)*DA*C/VA

        CALL DRAG(RE,CD)

*       Correct for Mass Transfer:
        CD=CDO(I)*CD


        IF (FLOW.EQ.1) THEN
        CALL MOVE(UR,UZ,UAR,VAIR,SX,SV,C,CD,DT,MASS,
    +   DA,D,TY)
        RD=RD+SX

*
        ELSE  IF (FLOW.EQ.2) THEN
        IF (RDIS(I).GT.RCRIT) THEN
        UAT=2.57*RDIS(I)**-0.5
        ELSE
        UAT=3.51*RDIS(I)**0.5
        END IF
        CALL SWIRL(D,MASS,DA,DTH,RD,C,UT,UAT,UR,UAR,UZ,
    +   UAZ,CD,DT,TY)
        END IF

        PRDIS(I)=RD
        PZDIS(I)=ZDIS(I)+DZ
        PTHETA(I)=THETA(I)+DTH
        POVEL(I)=C
        DVY(I)=(ZVEL(I)-UZ)/DZ
        PRVEL(I)=UR
        PZVEL(I)=UZ
        PTVEL(I)=UT
        RES2(I)=(UR**2+UT**2+UZ**2)**0.5
```

```
*
      MCORE=CENT(I)


      IF (DWBAS(I).LT.DLIM(I).AND.X.NE.0) THEN

      CALL SLURRYCOEF(TA,HA,T1,DT,SOL(I),SMA(I),D,C,Z,
     +  DCORE,ED,E,MCORE,CS,Pa,OMTC,OHTC,NA,CHg,
     +  CHc,CMg,CMc,DWBAS(I),DLIM(I),X,DROP(I),AREA,CDR)

      CDO(I)=CDR
      NAOLD=NA
      A1=OHTC*4*PI*R**2/(MCORE*CS)
      MCORE=CENT(I)

      CALL TEMP(A1,OMTC,R,NA,MCORE,TA,T1,LT,CHg,CMg,
     +  ED,X,Pa,DT)

C     SUBROUTINE TEMP CALCULATES CORE TEMP OF DROP.

      NAMEAN=(NA+NAOLD)/2

      CALL CRUST(DT,Xw,NAMEAN,MCORE,DCORE,WCON,MASS,
     +  PD,Z,R)

      PCORE(I)=MCORE
      PB(I)=DCORE/2

      ELSE

      RE=D*C*DA/VA
      PR=CPa*VA/KA
      CHg=KA/D*(2+(0.6*PR**0.33*RE**0.5))
      OHTC=CHg
      NA=0
      NAMEAN=0
      OMTC=0
      CHc=0
```

```
      CMc=0
      A1=OHTC*4*PI*R**2/(MASS*CPDRY)
      CALL DRYDROP(A1,CPDRY,TA,T1,DT)
      END IF

      DRI=(WCON/MASS)*100

*
*     AIR PROPERTY VARIATION SEQUENCE
*     -------------------------------
*


      CPV=32.243+1.923E-3*T1+1.055E-5*T1**2-3.596E-
     +  9*T1**3
      CPV=CPV*1000/18
      NATOT=NATOT+(NAMEAN*DROP(I))
      PSOL(I)=SOL(I)-(NAMEAN*DROP(I))


      QNA=NAMEAN*DROP(I)*(2.5116E+6+CPV*(TA-273))
      QNAT=QNAT+QNA

*
      QAIR=OHTC*AREA*(TA-TSOL(I))
      QTOT=QTOT+QAIR
*
      PSMA(I)=MASS
      PWC(I)=WCON
      PTSOL(I)=T1
      PDRY(I)=DRI
*
      KGS(I)=NAMEAN
      KHg(I)=CHg
      KHc(I)=CHc
      KMg(I)=CMg
      KMc(I)=CMc
*
```

```
          CRST(I)=Z

          REN(I)=RE
          PTIME(I)=TIME(I)+DT
          MOMT2=MOMT2+(PZVEL(I)*PSOL(I))


*
   20     CONTINUE
*
          XSA=PI*RDIS(1)**2

          IF (XSPRAY.LT.XAIRo.AND.TYPE.EQ.1.AND.FLOW.EQ.1)
     +    THEN
          CALL ENT (MOMT0,MOMT2,XSA,XSPRAY,DA,VAIR)
          ELSE
          VAIR=UAZ
          END IF


          PEVAP=EVAP+NATOT
          PHEATVAP=HEATVAP+QNAT
          PHEAT=HEAT+QTOT


          HUM2=HAO+TY*(PEVAP/XAIRo)
          HANEW=HUM2

          CALL PROPS (TA2,T1,KA,LT,VA,DA,DF,SPHT,HUM2)
          CPA2=SPHT
          CPR=CPAO/CPA2
          HUM3=(HAO-HUM2)*2.5116E+6/CPA2
          XX1=CPR*(TAO-273)
          XX2=(PHEATVAP-PHEAT)/(XAIRo*CPA2)
          TANEW=XX1+HUM3+(TY*XX2)+273
*
```

```
      TLIM=ABS(TANEW-TA2)
      HLIM=ABS(HANEW-HA2)
      IF (TLIM.GT.0.01.OR.HLIM.GT.0.01) THEN
      HA2=HANEW
      TA2=TANEW
      GO TO 18
      END IF


*
      DO 35 I=1,NI
      TIME(I)=PTIME(I)
      CENT(I)=PCORE(I)
      SMA(I)=PSMA(I)
      TSOL(I)=PTSOL(I)
      DRY(I)=PDRY(I)
      WC(I)=PWC(I)
      B(I)=PB(I)
      SOL(I)=PSOL(I)

      RES1(I)=RES2(I)
      OVEL(I)=POVEL(I)

      RDIS(I)=PRDIS(I)
      ZDIS(I)=PZDIS(I)
      THETA(I)=PTHETA(I)
      RVEL(I)=PRVEL(I)
      ZVEL(I)=PZVEL(I)
      TVEL(I)=PTVEL(I)
      DDBAS(I)=WC(I)/SOLID(I)
      DDBAS(I)=(1-DDBAS(I))*100
      DWBAS(I)=(SOLID(I)/SMA(I))*100
      IF (DWBAS(I).GT.100) THEN
      DWBAS(I)=100
      END IF
   35 CONTINUE
*
      EVAP=PEVAP
```

```
          HEATVAP=PHEATVAP
          HEAT=PHEAT
          TA2=TANEW
*
          GAIR=GAIRo+EVAP
          GSOL=GSOLo-EVAP
          TOTSOL=((1-Xw)*GSOLo)/GSOL

          VFLOW=PVFL

          HA2=HANEW
          HAG=(HA2-HA1)/DZ
          TAG=(TA2-TA1)/DZ




          IF (DWBAS(N).GE.DLIM(N)) THEN
          N=N-1
          PRINT*,N
          END IF
*

*
          DO 50 I=1,NI
          IF(DWBAS(I).LE.DLIM(I).AND.(DWBAS(I)-WTEST(I))
     + .GE.2) THEN
          WTEST(I)=DWBAS(I)
          VALUE=1
          END IF

          IF (ZDIS(I)-ZTEST(I).GE.0.3) THEN
          ZTEST(I)=ZDIS(I)
          VALUE2=1

          END IF
          IF (DWBAS(I).GE.DLIM(I).AND.(ZDIS(I)-Z1TEST(I))
```

```
     +  GE.0.6) THEN
        Z1TEST(I)=ZDIS(I)
        VALUE3=1
        END IF

        IF (VALUE.EQ.1.OR.(DWBAS(I).GE.DLIM(I)
     + .AND.VALUE3.EQ.1)) THEN
        VALUE=0
        VALUE3=0
        J=I
        WRITE(J,200)ZDIS(I),DWBAS(I),TSOL(I)-273,KGS(I)
     + ,INT(KHg(I)),INT(KHc(I)),KMg(I),KMc(I)
        END IF
        IF (VALUE2.EQ.1) THEN
        VALUE2=0

        K=10+I
        WRITE(K,300)RVEL(I),TVEL(I),ZVEL(I),RDIS(I),
     +  THETA(I),ZDIS(I),REN(I),TIME(I)
        END IF

  50    CONTINUE
        IF (ZDIS(1).LT.2.0) THEN
        TESTAIR=0.1
        ELSE
        TESTAIR=0.5
        END IF
        IF ((ZDIS(1)-ATEST).GT.TESTAIR) THEN
        WRITE(100,400)ZDIS(1),TA2-273,HA2,GAIR,VAIR,TOTSOL
        ATEST=ZDIS(1)
        END IF

 100    FORMAT(1X,'ZDIS(M)',2X,'%SOLID',2X,'TEMP(C)'
     + ,2X,'NA kg/s',2x'hg(m/s)',2X,'hc(m/s)',2X,'kg(m/s)'
     + ,2X,'kc(m/s)'/)

 140    FORMAT(1X,'Rvel(m/s)',2X,'Tvel(m/s)',2X,
     +  'Zvel(m/s)',2X,'RDIS(M)',2X,'THETA(0)',2X,
```

```
     +   'ZDIS(M)',2X,'REN NO.',2x,'TIME(S)'//)
*
  160    FORMAT(1X,'ZDIS(M)',2X,'TEMP(C)',2X,'HUMID(kg/kg)'
     + ,2X,'GAIR(kg/s)',2X,'VEL(M/S)',2X,'SOLID(%)'/)
  200    FORMAT(1X,F7.2,2X,F6.2,2X,F7.2,2X,E7.2,2X,I7,2X,I7,
     +   2X,F7.2,2X,F7.2)
  300    FORMAT(1X,F9.2,2X,F9.2,2X,F9.2,2X,F7.2,2X,F8.2,2X,
     +   F7.2,2X,F7.2,2X,F7.2)
  400    FORMAT(1X,F7.2,2X,F7.2,2X,F12.5,2X,F10.2,2X,F7.2,
     +   2X,F7.2)

*
*        VARIABLE STEP SIZE SEQUENCE
*        ---------------------------
*



         DZ=DZo



         IF (TYPE.EQ.1) THEN
         CALL STEPSWIRL (DWBAS(N),N,DZ)
         ELSE
         CALL STEPCOUNT(DWBAS(N),N,DZ)
         END IF

    52   CONTINUE
*
         IF (ZDIS(1).LT.20.AND.DWBAS(1).LT.DLIM(1)) THEN
         GOTO 16
         END IF
*
*        ******************************
*
*
         PRINT*,'THE END'
         CLOSE (UNIT=20)
```

```
      CLOSE (UNIT=30)
      CLOSE (UNIT=40)
      CLOSE (UNIT=50)
      CLOSE (UNIT=60)
      CLOSE (UNIT=70)
      CLOSE (UNIT=80)
      CLOSE (UNIT=90)
      CLOSE (UNIT=10)
      CLOSE (UNIT=100)
      END
*
*
*       SUBROUTINES
*

      SUBROUTINE SWIRL(D,M,DA,DTH,RD,C,UT,UAT,UR,UAR,UZ,
     +  UAZ,CD,DT,TY)
      REAL DTH,RD,C,UT,UAT,UR,UAR,UZ,UAZ,CD,DT,DVR,
      REAL DVT,DVZ,VR,VZ,VT,AREA,M
      REAL KR,KR1,KR2,KR3,KT,KT1,KT2,KT3,KZ,KZ1,KZ2,KZ3

      IF (RD.EQ.0) THEN
      RD=0.0001
      END IF
      G=9.816
      PI=3.1415926
      AREA=(PI*D**2)/4
      R=RD
      DVR=UT**2/R-(CD*AREA*DA*C*(UR-UAR)/(2*M))
      DVT=-UT*UR/R-(CD*AREA*DA*C*(UT-UAT)/(2*M))
      DVZ=G-(CD*AREA*DA*C*(UZ-TY*UAZ)/(2*M))
      KR=DVR*DT
      KT=DVT*DT
      KZ=DVZ*DT
      VR=UR+0.5*KR
      VT=UT+0.5*KT
      VZ=UZ+0.5*KZ
      C=((VR-UAR)**2+(VT-UAT)**2+(VZ-TY*UAZ)**2)**0.5
```

```
DVR=VT**2/R-(CD*AREA*DA*C*(VR-UAR)/(2*M))
DVT=-VT*VR/R-(CD*AREA*DA*C*(VT-UAT)/(2*M))
DVZ=G-(CD*AREA*DA*C*(VZ-TY*UAZ)/(2*M))
KR1=DVR*DT
KT1=DVT*DT
KZ1=DVZ*DT
VR=UR+0.5*KR1
VT=UT+0.5*KT1
VZ=UZ+0.5*KZ1
C=((VR-UAR)**2+(VT-UAT)**2+(VZ-TY*UAZ)**2)**0.5
DVR=VT**2/R-(CD*AREA*DA*C*(VR-UAR)/(2*M))
DVT=-VT*VR/R-(CD*AREA*DA*C*(VT-UAT)/(2*M))
DVZ=G-(CD*AREA*DA*C*(VZ-TY*UAZ)/(2*M))
KR2=DVR*DT
KT2=DVT*DT
KZ2=DVZ*DT
VR=UR+KR2
VT=UT+KT2
VZ=UZ+KZ2
C=((VR-UAR)**2+(VT-UAT)**2+(VZ-TY*UAZ)**2)**0.5
DVR=VT**2/R-(CD*AREA*DA*C*(VR-UAR)/(2*M))
DVT=-VT*VR/R-(CD*AREA*DA*C*(VT-UAT)/(2*M))
DVZ=G-(CD*AREA*DA*C*(VZ-TY*UAZ)/(2*M))
KR3=DVR*DT
KT3=DVT*DT
KZ3=DVZ*DT
C=((VR-UAR)**2+(VT-UAT)**2+(VZ-TY*UAZ)**2)**0.5
URNEW=UR+(KR+(2*KR1)+(2*KR2)+KR3)/6
UTNEW=UT+(KT+(2*KT1)+(2*KT2)+KT3)/6
UZNEW=UZ+(KZ+(2*KZ1)+(2*KZ2)+KZ3)/6
DR=(URNEW+UR)*DT/2
DTAN=(UTNEW+UT)*DT/2
RD=((RD+DR)**2+DTAN**2)**0.5
DTH=ASIN(DTAN/RD)
DTH=DTH*180/PI
UR=URNEW
UT=UTNEW
UZ=UZNEW
```

```
      RETURN
      END
*
*

      SUBROUTINE ENT (M0,M2,XSA,XSPRAY,DA,VAIR)
      REAL M0,M2,XSA,DA,VAIR,PI,A,B,C
      PI=3.1415926

      A=0.2672**2/DA**2
      B=M0/(XSA*DA)
      C=M2/(XSA*DA)

      VAIR=(A+B-C)**0.5
      XSPRAY=VAIR*XSA*DA

      RETURN
      END
*
*

      SUBROUTINE MOVE(UX,UV,UAX,UAZ,SX,SV,C,CD,DT,M,PA,
     +  D,TY)
      REAL UX,UV,SX,SV,C,CD,DT,A,PA,M,D
      REAL DV,DX,KV,KX,KV1,KX1,KV2,KX2,KV3,KX3,VX,VV
      A=3.1415926*(D**2)/4
      C=((UX-UAX)**2+(UV-TY*UAZ)**2)**0.5
      DVX=-CD*A*PA*C*(UX-UAX)/(2*M)
      DVY=9.816-(CD*A*PA*C*(UV-TY*UAZ)/(2*M))
      KX=DVX*DT
      KV=DVY*DT
      C=(((UX+0.5*KX)-UAX)**2+((UV+0.5*KV)-TY*UAZ)**2)
     +  **0.5
      DVX=-CD*A*PA*C*((UX+0.5*KX)-UAX)/(2*M)
      DVY=9.816-(CD*PA*A*C*((UV+0.5*KV)-TY*UAZ)/(2*M))
      KX1=DVX*DT
      KV1=DVY*DT
      C=(((UX+0.5*KX1)-UAX)**2+((UV+0.5*KV1)-TY*UAZ)**2)
     +  **0.5
```

```
      DVX=-CD*A*PA*C*((UX+0.5*KX1)-UAX)/(2*M)
      DVY=9.816-(CD*A*PA*C*((UV+0.5*KV1)-TY*UAZ)/(2*M))
      KX2=DVX*DT
      KV2=DVY*DT
      C=(((UX+KX2)-UAX)**2+((UV+KV2)-TY*UAZ)**2)**0.5
      DVX=-CD*A*PA*C*((UX+KX2)-UAX)/(2*M)
      DVY=9.816-(CD*A*PA*C*((UV+KV2)-TY*UAZ)/(2*M))
      KX3=DVX*DT
      KV3=DVY*DT
      VX=UX+(KX+(2*KX1)+(2*KX2)+KX3)/6
      VV=UV+(KV+(2*KV1)+(2*KV2)+KV3)/6
      SX=DT*(UX+VX)/2
      SV=DT*(UV+VV)/2
      C=((VX-UAX)**2+(VV-TY*UAZ)**2)**0.5
      UX=VX
      UV=VV
      RETURN
      END
*
      SUBROUTINE PROPS(TA,T1,KA,LT,VA,DA,DF,SPHT,HUMID)
      REAL TA,T1,KA,LT,VA,DA,DF
      REAL HUMID,CPV
      TM=((TA-273.15)+(T1-273.15))/2
      KA=(4.2956E-5*TM+0.014)*1.7307
      LT=(1075.95-1.0246*(T1-273.15))*2326.0
      VA=4.568E-8*TM+1.7199E-5
      DA=(1.2929*273.15)/(T1+TA)*2
      DF=0.22*(((TA+T1)/(2*273.15))**1.75)/1E+4
      CPV=32.243+1.923E-3*TA+1.055E-5*TA**2-3.596E-
     +  9*TA**3
      CPV=CPV*1000/18
      SPHT=1035+(CPV*HUMID)
      RETURN
      END
*
      SUBROUTINE SLURRYCOEF(TA,HA,T1,DT,SOL,SMA,D,C,Z,
```

```
     +   DCORE,ED,E,MCORE,CS,Pa,OMTC,OHTC,NA,CHg,CHc,CMg,
     +   CMc,DWBAS,DLIM,X,DROP,AREA,CDR)
         REAL TA,HA,T1,DT,SOL,SMA,PI,D,C,Z,DCORE,MCORE
         REAL CS,Pa,OMTC,OHTC,NA,DROP,AREA,AHEAT,PD,PSAT,KC
         REAL RE,PR,SC,KA,LT,VA,DA,DF,SPHT,CHc,CHg,CMc,CMg
         REAL E,ED,DWBAS,DLIM,X,MW,RC,R,CA,BM,CDR,Xvs,Xvo,Ps
         MW=18
         RC=8.314E+3
         R=D/2
         PI=3.1415926
         CA=1036.23
         PSAT=133.32*EXP(18.3036-(3816.44/(T1-46.13)))


         CALL PROPS(TA,T1,KA,LT,VA,DA,DF,SPHT,HA)

         KC=0.07*(1-E)+(KA*E)

         DROP=SOL*DT/SMA
         AREA=DROP*PI*D**2
         AHEAT=AREA
*
*
         PD=1221+((80-T1+273)/5.6*0.002)


         RE=D*C*DA/VA
         PR=(CA*VA)/KA
         CHg=KA/D*(2+(0.6*PR**0.33*RE**0.50))
         DW=(D+DCORE)/2
         IF (Z.NE.0.AND.DCORE.NE.0) THEN
         CHc=((Z/KC)*D/DCORE)**-1
         END IF
*
         OHTC=((1/CHg)+((Z/KC)*(D/DCORE)))**-1
         A1=OHTC*4*PI*R**2/(MCORE*CS)

         SC=VA/(DA*DF)
```

```
      CMg=DF/D*(2+(0.6*SC**0.33*RE**0.50))
      ED=(E**1.5)*DF
      IF (Z.NE.0.AND.DCORE.NE.0) THEN
      CMc=((Z/ED)*D/DCORE)**-1
      END IF
      OMTC=((1/CMg)+((Z/ED)*(D/DCORE)))**-1
      NA=OMTC*4*PI*R**2*MW/(RC)*((PSAT/T1)-(Pa/TA))
      Ps=(NA/(CMg*4*PI*R**2))+(Pa/(RC*Ta))*RC*T1
      Xvs=(Ps/101.325E+3)*18/29
      Xvo=(Pa/101.325E+3)*18/29
      BM=(Xvs-Xvo)/(1-Xvs)
      CDR=(1+BM)**(-0.19*(SC**-0.74)*(1+BM)**-0.29)
*
      RETURN
      END

      SUBROUTINE CRUST(DT,Xw,NAMEAN,MCORE,DCORE,WCON,
     +  MASS,PD,Z,R)
      REAL H,Xw,NAMEAN,MCORE,DCORE,WCON,MASS,
      REAL PD,Z,X1,X2,XX,PI
      PI=3.1415926
      X1=1
      X2=3
      XX=X1/X2
      MCORE=MCORE-(NAMEAN*H/Xw)
      IF (MCORE.LT.0) THEN
      MCORE=0
      END IF
      DCORE=(MCORE*6/(PD*PI))**XX
      WCON=WCON-(NAMEAN*H)
      IF (WCON.LT.0) THEN
      WCON=0
      END IF
      MASS=MASS-(NAMEAN*H)
      IF (MASS.LT.0) THEN
      MASS=0
      END IF
*
```

```
      Z=R-(DCORE/2)
      RETURN
      END
*
*
*
*
*
*
*
*
      SUBROUTINE TEMP(A1,OMTC,X1,NA,M,TA,T1,LT,CH,CM,ED,
     +  X,CO,H)
      REAL DT,DT1,DT2,DT3,KT1,KT2,KT3,KT4,G,NA
      REAL OHTC,X1,NA1,M,CP,TA,T1,LT,CC,H,CO
      REAL PI,MW,A1
      REAL CPV,CS,KC
      KC=0.070
      PI=3.1415926
      MW=18
      CPV=32.243+1.923E-3*T1+1.055E-5*T1**2-3.596E-
     +  9*T1**3
      CPV=CPV*1000/18
      CS=3036
      RC=8.314E+3
      DT=((A1*(TA-T1))-((NA/(M*CS))*(LT+CPV*(TA-T1))))
      KT1=H*DT
      TR=T1+KT1/2
      CALL TEMPUP (G,NA,OMTC,X1,CO,TA,TR,CPV,LT)
      DT1=((A1*(TA-(T1+KT1/2)))-((NA/(M*CS))*
     + (LT+CPV*(TA-(T1+KT1/2)))))
      KT2=H*DT1
      TR=T1+KT2/2
      CALL TEMPUP (G,NA,OMTC,X1,CO,TA,TR,CPV,LT)
      DT2=((A1*(TA-(T1+KT2/2)))-((NA/(M*CS))*
     +  (LT+CPV*(TA-(T1+KT2/2)))))
      KT3=H*DT2
```

```
      TR=T1+KT3
      CALL TEMPUP (G,NA,OMTC,X1,CO,TA,TR,CPV,LT)
      DT3=((A1*(TA-(T1+KT3)))-((NA/(M*CS))*
     +  (LT+CPV*(TA-(T1+KT3)))))
      KT4=H*DT3
*
*
      T1=T1+(KT1+(2*KT2)+(2*KT3)+KT4)/6
      NA=OMTC*4*PI*X1**2*((G/T1)-(CO/TA))*MW/RC
      RETURN
      END
*
      SUBROUTINE TEMPUP(G,NA,OMTC,R,CO,TA,TR,CPV,LT)
      DOUBLE PRECISION NA,G
      REAL OMTC,R,CO,TA,TR,CPV,LT,PI,MW,RG
      PI=3.1415926
      MW=18
      RG=8.314E+3
      TM=(TR+TA)/2
      G=133.32*EXP(18.3036-(3816.44/(TR-46.13)))
      NA=OMTC*4*PI*R**2*((G/TR)-(CO/TA))*MW/RG
      CPV=32.243+1.923E-3*TM+1.055E-5*TM**2-3.596E-
     +  9*TM**3
      CPV=CPV*1000/18
      LT=(1075.95-1.0246*(TR-273.15))*2326
      RETURN
      END
*
*
      SUBROUTINE DRYDROP(A1,CP,TA,T1,H)
      REAL A1,CP,TA,T1,H,DT,DT1,DT2,DT3,KT1,KT2,KT3,KT4
      DT=A1*(TA-T1)
      KT1=H*DT
      DT1=A1*(TA-(T1+KT1/2))
      KT2=H*DT1
      DT2=A1*(TA-(T1+KT2/2))
      KT3=H*DT2
      DT3=A1*(TA-(T1+KT3))
```

```
      KT4=H*DT3
*
      T1=T1+(KT1+(2*KT2)+(2*KT3)+KT4)/6
      RETURN
      END
*
      SUBROUTINE DRAG(RE,CD)
      REAL RE,CD
      IF (RE.LT.0.01) THEN
      CD=(3/16)+(24/RE)
      ELSE IF (RE.GT.001.AND.RE.LE.20) THEN
      CD=(24/RE)*(1+0.1315*RE**(0.82-(0.05*LOG10(RE))))
      ELSE IF (RE.GT.20.AND.RE.LT.260) THEN
      CD=(24/RE)*(1+(0.1935*RE**0.6305))
      ELSE IF (RE.GT.260.AND.RE.LT.1500) THEN
      W=LOG10(RE)
      CD=10**(1.6435-(1.1242*W)+(0.1558*W**2))
      ELSE IF (RE.GT.1500.AND.RE.LT.1.2E+4) THEN
      W=LOG10(RE)
      CD=10**(-1.9181+0.637*W-0.9295*W**2+0.1049*W**3)
      END IF
      RETURN
      END
*
      SUBROUTINE STEPSWIRL (DRI,N,DZ)
      REAL DRI,DZ
      IF (DRI.GT.99.AND.N.GE.5) THEN
      DZ=1E-6
      ELSE IF (DRI.GT.90.AND.N.GE.5) THEN
      DZ=5E-6
      ELSE IF (DRI.GT.75.AND.N.GE.5) THEN
      DZ=5E-5
      ELSE IF (DRI.GT.99.95.AND.N.LE.5.AND.N.GT.2) THEN
      DZ=5E-6
      ELSE IF (DRI.GT.99.9.AND.N.LE.5.AND.N.GT.2) THEN
      DZ=5E-6
      ELSE IF (DRI.GT.75.AND.N.LE.5.AND.N.GT.2) THEN
```

```
      DZ=5E-5
      END IF
      RETURN
      END


      SUBROUTINE STEPCOUNT (DRI,N,DZ)
      REAL DRI,DZ
      IF (DRI.GT.99.AND.N.GE.1) THEN
      DZ=1E-6
      ELSE IF (DRI.GT.90.AND.N.GE.1) THEN
      DZ=5E-6
      ELSE IF (DRI.GT.75.AND.N.GE.1) THEN
      DZ=1E-5
      ELSE IF (DRI.GT.60.AND.N.GE.1) THEN
      DZ=5E-5
      ELSE IF (DRI.GT.99.95.AND.N.LT.4.AND.N.GT.2) THEN
      DZ=5E-6
      ELSE IF (DRI.GT.99.9.AND.N.LT.4.AND.N.GT.2) THEN
      DZ=5E-6
      ELSE IF (DRI.GT.75.AND.N.LT.4.AND.N.GT.2) THEN
      DZ=5E-5
      END IF
      RETURN
      END
*
```

Appendix C: Temperature Errors of the Probe.

In this analysis, in view of the likely common temperatures of the thermocouple tip and the probe wall, radiation will be neglected, and only conduction errors will be calculated. For simplicity it is assumed that the temperature gradient to which the thermocouple is exposed is linear in the radial direction, i.e.

$$\frac{dT_a}{dx} = \text{Constant} \qquad \text{C1}$$

Let the temperature of the thermocouple tip be designated, T_{tip}, and the true air temperature at the tip, T_a. The analytical approach is to calculate T_{tip} and the difference $(T_{tip}-T_a)$ is then the conduction error.

For the purpose of the analysis, the two bare wires originating from the thermocouple tip can be treated as being one wire of radius and thermal conductivity, where

$$r'_w = \sqrt{2}\, r_w \qquad \text{C2}$$

and,

$$k_w = \frac{k_{chromel} + k_{alumel}}{2} \qquad \text{C3}$$

For the thermocouple used in this study:

$r_w = 0.22$ mm

and, $k_w = 24$ W/mK

Apply a steady state energy balance on the thermocouple tip, ignoring radiative heat transfer, which gives

$$h_g A_{tip}(T_a - T_{tip}) = -k_w A_w\left(\frac{dT}{dx}\right) \qquad \text{C4}$$

where the convective heat transfer coefficient can be calculated by applying the Ranz-Marshall correlation,

$$Nu = 2.0 + 0.6\, Re^{0.5} Pr^{0.33} \qquad \text{C5}$$

the conduction error can now be calculated by rearrangement of equation (C 4),

$$T_a - T_{tip} = -\frac{k_w A_w}{h_g A_{tip}}\frac{dT}{dx} \qquad \text{C6}$$

For the present case of a tip of diameter 1mm and air velocity at the tip of 3m/s, this becomes,

$$T_a - T_{tip} = 5.32 \times 10^{-3} \frac{dT}{dx} \qquad C\,7$$

As a worst case assuming a 30°C temperature difference between the inside of the tower and ambient and assuming the change to occur over a 15cm length, eg for probing near the tower walls,

$$\frac{dT}{dx} = -200\ ^{\circ}C/m$$

and,

$$T_a - T_{tip} \equiv \text{Conduction Error} = -1.06\ ^{\circ}C$$

For comparison, the conduction error for a thermocouple employing ultra-fine wires as described by Papadakis [143], calculated in the same manner is 0.93°C.

Appendix D: Experimental Data

Tables D1 - D8	Air Temperature Measurements
Tables D9 - D16	Air Humidity Measurements
Tables D17 - D18	Drop Size Distribution Measurements

Table D1: *Run 1 - Temperature Measurements (°C)*

Axial Distance from Air Inlet (m)	Radial Distance from Wall (cm) 10	20	30	40	50	60	Average
1.00	47.00	42.50	40.00	37.50	34.90	34.80	39.45
2.00	30.80	32.10	35.00	33.00	33.90	33.50	33.05
2.50	28.60	31.50	32.50	33.00	32.30	33.70	31.93
3.00	31.80	31.60	31.30	28.80	28.90	30.90	30.55
3.35	31.80	31.70	31.50	32.40	30.10	31.90	31.57

Table D2: *Run 2 - Temperature Measurements (°C)*

Axial Distance from Air Inlet (m)	Radial Distance from Wall (cm) 10	20	30	40	50	60	Average
1.00	38.50	39.50	37.00	36.00	34.60	33.90	36.60
2.00	29.20	30.50	30.20	29.90	30.10	30.10	30.00
2.50	27.80	29.10	29.00	29.20	28.70	29.20	28.80
3.00	27.50	29.70	29.50	27.70	25.70	28.70	28.10
3.35	29.50	29.90	29.20	29.20	29.90	29.10	29.50

Table D3: *Run 3 - Temperature Measurements (°C)*

Axial Distance from Air Inlet (m)	Radial Distance from Wall (cm) 10	20	30	40	50	60	Average
1.00	34.50	36.50	34.50	32.50	31.60	30.90	33.40
2.00	29.20	30.60	30.30	30.40	29.60	30.10	30.10
2.50	29.00	29.70	29.70	29.80	29.70	29.40	29.50
3.00	29.60	26.70	30.30	28.50	28.30	29.80	28.90
3.35	30.70	30.40	30.70	30.80	30.40	29.00	30.30

Table D4: *Run 4 - Temperature Measurements (°C)*

Axial Distance from Air Inlet (m)	Radial Distance from Wall (cm) 10	20	30	40	50	60	Average
1.00	50.00	49.50	45.50	43.50	41.50	38.50	44.75
2.00	33.10	33.00	34.00	34.40	35.50	34.50	34.08
2.50	30.80	32.50	32.50	33.50	33.50	33.30	32.70
3.00	32.30	32.50	32.70	30.50	27.30	32.10	31.20
3.35	33.50	33.60	33.80	33.70	34.00	34.20	32.80

Table D5: *Run 5 - Temperature Measurements (°C)*

Axial Distance from Air Inlet (m)	Radial Distance from Wall (cm) 10	20	30	40	50	60	Average
1.00	40.00	45.00	43.00	42.00	42.00	38.50	41.70
2.00	30.60	31.00	32.00	31.10	31.00	30.90	31.10
2.50	28.50	29.00	29.80	29.90	30.00	30.40	29.60
3.00	28.10	29.20	30.00	28.00	26.50	29.40	28.50
3.35	30.30	30.40	30.50	30.70	30.10	30.00	30.30

Table D6: *Runs 6/7 - Temperature Measurements (°C)*

	Run 6				Run 7			
Axial Distance (m)	Radial Distance(cm) 10	30	50	Average	Radial Distance(cm) 10	30	50	Average
1.00	28.90	30.00	28.50	29.13	46.50	43.50	40.00	43.30
2.00	26.90	28.10	27.50	27.50	36.20	37.50	35.20	36.30
2.50	26.10	27.90	28.20	27.40	34.50	36.00	34.90	35.10
3.00	28.00	27.20	25.50	26.90	33.50	32.00	33.20	32.90
3.35	28.10	28.40	27.50	28.10	33.30	34.40	33.90	33.90

Table D7: *Runs 8/9 - Temperature Measurements (°C)*

Axial Distance (m)	Run 8 Radial Distance(cm) 10	30	50	Average	Run 9 Radial Distance(cm) 10	30	50	Average
1.00	39.50	39.00	36.00	38.20	37.50	36.50	38.00	37.30
2.00	30.70	31.50	30.90	31.00	32.70	32.90	33.00	32.90
2.50	30.50	30.50	29.80	30.30	32.10	32.20	32.30	32.20
3.00	30.10	29.00	30.30	29.80	31.60	32.00	32.90	32.20
3.35	30.50	30.90	31.00	30.80	34.20	34.30	34.80	34.40

Table D8: *Run 10 - Temperature Measurements (°C)*

Axial Distance (m)	Radial Distance(cm) 10	30	50	Average
1.00	49.00	42.00	39.00	43.30
2.00	36.50	36.10	37.20	36.60
2.50	35.80	36.00	36.50	36.10
3.00	35.40	33.40	34.90	34.60
3.35	35.60	35.20	33.70	34.80

Table D9: *Run 1 - Dew Point Measurements (°C)*

Axial Distance from Inlet (m)	Radial Distance from Wall (cm) 10	20	30	40	50	60	Ave. D.P.	Ave. H
1.00	24.00	24.00	24.50	24.00	24.50	24.50	24.25	0.0187
2.00	23.50	24.00	24.00	23.50	24.50	24.50	24.00	0.0184
2.50	23.00	23.00	23.00	23.50	24.00	24.50	23.50	0.0179
3.00	23.50	24.50	24.00	24.50	25.50	25.20	24.53	0.0191
3.35	24.50	24.50	25.50	25.00	25.50	26.00	25.16	0.0199

Table D10: *Run 2 - Dew Point Measurements (°C)*

Axial Distance from Inlet (m)	Radial Distance from Wall (cm) 10	20	30	40	50	60	Ave. D.P.	Ave. H
1.00	27.00	27.00	27.50	28.00	28.00	28.00	27.08	0.0224
2.00	27.50	28.00	28.00	28.00	28.00	27.50	26.75	0.0219
2.50	27.50	28.00	28.00	28.50	28.50	28.50	26.67	0.0218
3.00	28.00	28.50	28.50	28.00	28.50	28.50	27.75	0.0233
3.35	27.00	28.00	28.00	28.00	28.50	29.00	28.08	0.0238

Table D11: *Run 3 - Dew Point Measurements (°C)*

Axial Distance from Inlet (m)	Radial Distance from Wall (cm) 10	20	30	40	50	60	Ave. D.P.	Ave. H
1.00	27.00	27.00	27.50	28.00	28.00	28.00	27.58	0.0231
2.00	27.50	28.00	28.00	28.00	28.00	27.50	27.83	0.0234
2.50	27.50	28.00	28.00	28.50	28.50	28.50	28.17	0.0239
3.00	28.00	28.50	28.50	28.00	28.50	28.50	28.33	0.0242
3.35	27.00	28.00	28.00	28.00	28.50	29.00	28.08	0.0238

Table D12: *Run 4 - Dew Point Measurements (°C)*

Axial Distance from Inlet (m)	Radial Distance from Wall (cm) 10	20	30	40	50	60	Ave. D.P.	Ave. H
1.00	26.50	27.00	28.00	27.50	28.00	28.00	27.50	0.0229
2.00	26.50	27.50	28.00	28.00	28.50	28.50	27.83	0.0234
2.50	27.00	27.50	28.00	28.00	28.00	28.50	27.83	0.0234
3.00	28.00	28.50	28.50	28.20	28.00	29.00	28.42	0.0243
3.35	28.50	28.50	29.00	29.50	30.00	30.00	29.25	0.0255

Table D13: *Run 5 - Dew Point Measurements (°C)*

Axial Distance from Inlet (m)	Radial Distance from Wall (cm) 10	20	30	40	50	60	Ave. D.P.	Ave. H
1.00	29.00	29.50	29.50	29.50	29.50	29.00	29.33	0.0257
2.00	29.00	29.50	29.50	30.00	29.50	27.50	29.17	0.0254
2.50	28.00	28.50	29.50	29.50	30.00	30.50	29.33	0.0257
3.00	30.00	30.00	30.00	30.50	30.50	30.50	30.25	0.0271
3.35	30.00	30.00	30.50	30.50	30.50	31.00	30.42	0.0274

Table D14: *Run 6/7 - Dew Point Measurements (°C)*

	Run 6					Run 7				
Axial Distance (m)	Radial Distance (cm) 10	30	50	Ave. D.P.	Ave. H	Radial Distance (cm) 10	30	50	Ave. D.P.	Ave. H
1.00	28.00	28.50	28.50	28.33	0.0242	31.00	31.50	32.00	31.50	0.0292
2.00	28.50	29.00	30.00	29.17	0.0254	31.00	30.00	30.00	30.33	0.0273
2.50	28.50	29.50	30.50	29.50	0.0259	30.00	30.00	31.00	30.33	0.0273
3.00	29.00	30.00	30.00	29.67	0.0262	31.00	31.00	31.00	31.00	0.0284
3.35	29.00	29.50	29.50	29.33	0.0257	30.50	31.00	31.50	31.00	0.0284

Table D15: *Run 8/9 - Dew Point Measurements (°C)*

Axial Distance (m)	Run 8 Radial Distance (cm) 10	30	50	Ave. D.P.	Ave. H	Run 9 Radial Distance (cm) 10	30	50	Ave. D.P.	Ave. H
1.00	28.00	29.00	28.50	28.50	0.0243	27.00	27.00	27.00	27.00	0.0223
2.00	28.00	28.50	29.00	28.50	0.0243	27.50	27.50	28.00	27.67	0.0231
2.50	28.50	29.00	29.50	29.00	0.0252	28.00	28.50	28.50	28.33	0.0242
3.00	28.50	29.00	30.00	29.17	0.0254	27.50	28.50	28.50	28.16	0.0241
3.35	28.00	28.50	30.00	28.83	0.0249	28.00	28.50	28.50	28.33	0.0242

Table D16: *Run 10 - Dew Point Measurements (°C)*

Axial Distance (m)	Radial Distance (cm) 10	30	50	Ave. D.P.	Ave. H
1.00	27.00	27.00	27.50	27.17	0.0225
2.00	27.00	27.30	27.50	27.27	0.0226
2.50	27.00	27.00	28.50	27.50	0.0229
3.00	27.50	28.00	28.00	27.83	0.0234
3.35	27.00	28.50	28.50	28.00	0.0237

Table D17: *Drop Size Distributions with Air Flow*

Malvern Instruments MASTER Particle Sizer M3.0 Date 17-09-88 Time 06-53

Size microns	under	% in band	Size microns	under	% in band
564.0	100.0	0.3	53.1	9.7	2.6
487.0	99.7	0.8	45.8	7.1	1.9
420.0	98.9	1.0	39.5	5.2	1.4
362.0	97.9	1.1	34.1	3.8	1.0
312.0	96.8	0.9	29.4	2.8	0.8
270.0	95.9	3.1	25.4	2.1	0.6
233.0	92.8	8.2	21.9	1.5	0.4
201.0	84.6	11.5	18.9	1.1	0.3
173.0	73.1	12.6	16.3	0.8	0.2
149.0	60.4	11.5	14.1	0.6	0.2
129.0	48.9	9.6	12.1	0.4	0.0
111.0	39.4	8.4	10.5	0.4	0.2
95.9	30.9	7.8	9.0	0.2	0.0
82.7	23.2	5.7	7.8	0.2	0.1
71.4	17.4	4.3	6.7	0.1	0.1
61.6	13.1	3.4	5.8	0.1	0.1

Result source=Sample
Record No. = 0
Focal length = 300 mm.
Experiment type lds
Volume distribution
Beam length =1000.0 mm.
Obscuration =0.5714
Volume Conc. = 0.0027 %
Log. Diff. =5.07
Rosin-Ramm
X= 153.49 , N= 2.15
D(v,0.5) = 130.9 µm
D(v,0.9) = 219.6 µm
D(v,0.1) = 53.9 µm
D(4,3) = 138.5 µm
D(3,2) = 83.4 µm
Span = 1.3
Spec. surf. area
0.03 sq.m./cc.

Sample details:-Spray Drying Tower
Water at 100 psi
Level 3 (Top) No Air Flow

Malvern Instruments MASTER Particle Sizer M3.0 Date 01-01-80 Time 05-27

Size microns	under	% in band	Size microns	under	% in band
564.0	100.0	1.0	53.1	5.6	1.6
487.0	99.0	2.5	45.8	4.0	1.1
420.0	96.6	3.3	39.5	2.9	0.8
362.0	93.3	3.5	34.1	2.1	0.6
312.0	89.8	2.9	29.4	1.5	0.4
270.0	87.0	6.2	25.4	1.1	0.3
233.0	80.8	12.6	21.9	0.8	0.2
201.0	68.1	13.8	18.9	0.6	0.2
173.0	54.4	10.6	16.3	0.4	0.1
149.0	43.8	10.2	14.1	0.3	0.1
129.0	33.6	7.8	12.1	0.2	0.1
111.0	25.8	6.1	10.5	0.2	0.1
95.9	19.7	5.5	9.0	0.1	0.0
82.7	14.2	3.6	7.8	0.1	0.0
71.4	10.4	2.7	6.7	0.1	0.0
61.6	7.7	2.1	5.8	0.0	0.0

Result source=Sample
Record No. = 0
Focal length = 300 mm.
Experiment type lds
Volume distribution
Beam length =1000.0 mm.
Obscuration =0.5321
Volume Conc. = 0.0031 %
Log. Diff. =5.03
Rosin-Ramm
X= 191.85 , N= 2.22
D(v,0.5) = 163.1 µm
D(v,0.9) = 314.4 µm
D(v,0.1) = 70.0 µm
D(4,3) = 177.1 µm
D(3,2) = 115.1 µm
Span = 1.5
Spec. surf. area
0.02 sq.m./cc.

Sample details:-Spray Drying Tower
Water at 100 psi
Level 2 (middle) No air flow

Table D18: *Drop Size Distribution without Air Flow*

Malvern Instruments MASTER Particle Sizer M3.0 Date 17-09-88 Time 21-51

Size microns	under	% in band	Size microns	under	% in band
564.0	100.0	0.2	53.1	8.6	2.4
487.0	99.8	0.5	45.8	6.1	1.7
420.0	99.3	0.7	39.5	4.4	1.2
362.0	98.6	0.7	34.1	3.2	0.9
312.0	97.9	0.6	29.4	2.3	0.6
270.0	97.3	2.8	25.4	1.6	0.5
233.0	94.5	7.9	21.9	1.2	0.3
201.0	86.6	11.6	18.9	0.8	0.3
173.0	75.1	13.3	16.3	0.5	0.1
149.0	61.8	12.5	14.1	0.4	0.1
129.0	49.3	10.3	12.1	0.3	0.1
111.0	39.1	8.9	10.5	0.3	0.1
95.9	30.1	8.1	9.0	0.1	0.0
82.7	22.0	5.9	7.8	0.1	0.0
71.4	16.2	4.3	6.7	0.1	0.0
61.6	11.9	3.3	5.8	0.1	0.0

Result source=Sample
Record No. = 0
Focal length = 300 mm.
Experiment type lds
Volume distribution
Beam length =1000.0 mm.
Obscuration =0.6057
Volume Conc. = 0.0030 %
Log. Diff. =5.62
Rosin-Ramm
X= 150.81 , N= 2.31
D(v,0.5) = 130.1 µm
D(v,0.9) = 212.2 µm
D(v,0.1) = 56.9 µm
D(4,3) = 135.6 µm
D(3,2) = 88.7 µm
Span = 1.2
Spec. surf. area
0.03 sq.m./cc.

Sample details:-Spray Drying Tower
Water at 100 psi
Level 3 (Top) With air flow

Malvern Instruments MASTER Particle Sizer M3.0 Date 01-01-80 Time 05-35

Size microns	under	% in band	Size microns	under	% in band
564.0	100.0	2.0	53.1	2.3	0.7
487.0	98.0	5.6	45.8	1.7	0.5
420.0	92.4	8.4	39.5	1.2	0.3
362.0	84.0	10.6	34.1	0.9	0.3
312.0	73.4	11.6	29.4	0.6	0.2
270.0	61.8	12.4	25.4	0.4	0.0
233.0	49.4	11.6	21.9	0.4	0.2
201.0	37.8	9.2	18.9	0.2	0.0
173.0	28.5	6.0	16.3	0.2	0.1
149.0	22.5	5.7	14.1	0.1	0.0
129.0	16.8	5.0	12.1	0.1	0.0
111.0	11.8	3.3	10.5	0.1	0.0
95.9	8.5	2.3	9.0	0.0	0.0
82.7	6.3	1.7	7.8	0.0	0.0
71.4	4.5	1.3	6.7	0.0	0.0
61.6	3.2	0.9	5.8	0.0	0.0

Result source=Sample
Record No. = 0
Focal length = 300 mm.
Experiment type lds
Volume distribution
Beam length =1000.0 mm.
Obscuration =0.8911
Volume Conc. = 0.0134 %
Log. Diff. =4.91
Rosin-Ramm
X= 275.76 , N= 2.28
D(v,0.5) = 234.7 µm
D(v,0.9) = 400.4 µm
D(v,0.1) = 103.3 µm
D(4,3) = 243.7 µm
D(3,2) = 168.0 µm
Span = 1.3
Spec. surf. area
0.02 sq.m./cc.

Sample details:-Spray Drying Tower
Water at 100 psi
Level 2 (Middle) with air flow

Appendix E: Model Data

Tables E1 - E18	Simulation 1
Tables E19 - E36	Simulation 2
Tables E37 - E39	Simulation 3

Table E1 : *Simulation 1 - Feed Physical Properties and Drop-Size Data*

Physical Properties

Specific Heat of Dried Product	:	2.1kJ/kg °C
Specific Heat of Solution	:	3.0 kJ/kg °C
Density of Solution	:	1200 kg/m^3

Measured Droplet-Size-Distribution

Drop Size (microns) :	413	211	137	99	74	57	45	35
Weight % :	10.3	15.9	14.1	13.9	10.4	10.9	7.3	17.2

Table E2: *Simulation 1*

CODE-1A : AIR PROPERTIES

ZDIS(M)	TEMP(C)	HUMID(kg/kg)	GAIR(kg/s)	VEL(M/S)	SOLID(%)
0.10	209.95	0.01235	11.28	22.76	0.58
0.20	202.50	0.01548	11.31	15.27	0.60
0.30	194.47	0.01875	11.35	11.56	0.63
0.40	186.50	0.02202	11.39	9.33	0.65
0.50	180.02	0.02459	11.41	8.29	0.68
0.60	175.53	0.02638	11.43	7.08	0.69
0.70	171.25	0.02798	11.45	5.98	0.71
0.80	167.58	0.02944	11.47	5.17	0.73
0.90	164.31	0.03077	11.48	4.55	0.74
1.00	161.42	0.03183	11.50	4.07	0.75
1.10	158.48	0.03307	11.51	0.32	0.77
1.20	153.07	0.03535	11.53	0.32	0.80
1.30	149.72	0.03672	11.55	0.32	0.81
1.40	147.05	0.03790	11.56	0.32	0.83
1.50	144.68	0.03895	11.57	0.32	0.85
1.60	143.05	0.03967	11.58	0.32	0.86
1.70	142.19	0.03999	11.59	0.32	0.86
1.80	141.34	0.04036	11.59	0.32	0.87
1.90	140.47	0.04074	11.59	0.32	0.87
2.40	136.55	0.04248	11.61	0.32	0.90
2.90	133.67	0.04378	11.63	0.32	0.92
3.40	132.32	0.04438	11.64	0.32	0.93
3.90	131.82	0.04460	11.64	0.32	0.94
4.40	131.29	0.04483	11.64	0.32	0.94
4.91	130.76	0.04506	11.64	0.32	0.95
5.41	130.26	0.04528	11.65	0.32	0.95
5.91	129.79	0.04549	11.65	0.32	0.95
6.41	129.33	0.04569	11.65	0.32	0.96
6.91	128.90	0.04588	11.65	0.32	0.96
7.41	128.50	0.04606	11.65	0.32	0.97
7.91	128.11	0.04624	11.66	0.32	0.97
8.41	127.75	0.04640	11.66	0.32	0.97
8.91	127.40	0.04656	11.66	0.32	0.98
9.41	127.08	0.04671	11.66	0.32	0.98
9.91	126.78	0.04684	11.66	0.32	0.98
10.41	126.51	0.04697	11.66	0.32	0.98
10.91	126.25	0.04709	11.67	0.32	0.99
11.41	126.02	0.04720	11.67	0.32	0.99
11.91	125.81	0.04729	11.67	0.32	0.99
12.41	125.63	0.04738	11.67	0.32	0.99
12.91	125.47	0.04745	11.67	0.32	0.99

Table E3: *Simulation 1*

CODE-1A : DROPLET TRAJECTORY

DROP SIZE = 413.0000 MICRONS

Rvel(m/s)	Tvel(m/s)	Zvel(m/s)	RDIS(M)	THETA(0)	ZDIS(M)	REN NO.	TIME(S)
32.36	0.00	50.79	0.01	0.00	0.01	871.03	0.00
28.10	0.00	46.70	0.19	0.00	0.30	706.40	0.01
23.82	0.00	41.03	0.36	0.00	0.60	535.53	0.01
20.19	0.00	35.71	0.53	0.00	0.90	500.60	0.02
16.78	0.00	30.14	0.70	0.00	1.20	484.25	0.03
13.60	0.00	24.58	0.87	0.00	1.50	408.07	0.04
10.74	0.00	19.61	1.03	0.00	1.80	328.80	0.05
8.23	0.00	15.24	1.20	0.00	2.10	256.64	0.07
6.06	0.00	11.50	1.36	0.00	2.40	193.49	0.09
4.25	0.00	8.41	1.51	0.00	2.70	140.21	0.13
2.80	0.00	5.99	1.66	0.00	3.00	97.65	0.17
1.71	0.00	4.25	1.79	0.00	3.30	66.47	0.23
0.97	0.00	3.16	1.90	0.00	3.60	46.62	0.31
0.51	0.00	2.59	1.97	0.00	3.90	36.24	0.42
0.26	0.00	2.34	2.02	0.00	4.20	31.74	0.54
0.13	0.00	2.23	2.04	0.00	4.50	29.92	0.67
0.06	0.00	2.18	2.05	0.00	4.80	29.10	0.81
0.03	0.00	2.15	2.06	0.00	5.10	28.63	0.94
0.01	0.00	2.12	2.06	0.00	5.40	28.27	1.09
0.01	0.00	2.10	2.06	0.00	5.70	27.95	1.23
0.00	0.00	2.08	2.07	0.00	6.00	27.65	1.37
0.00	0.00	2.06	2.07	0.00	6.30	27.35	1.52
0.00	0.00	2.04	2.07	0.00	6.60	27.06	1.66
0.00	0.00	2.02	2.07	0.00	6.90	26.78	1.81
0.00	0.00	2.00	2.07	0.00	7.21	26.51	1.96
0.00	0.00	1.98	2.07	0.00	7.51	26.24	2.11
0.00	0.00	1.96	2.07	0.00	7.81	25.97	2.26
0.00	0.00	1.94	2.07	0.00	8.11	25.71	2.42
0.00	0.00	1.93	2.07	0.00	8.41	25.46	2.57
0.00	0.00	1.91	2.07	0.00	8.71	25.22	2.73
0.00	0.00	1.89	2.07	0.00	9.01	24.98	2.89
0.00	0.00	1.88	2.07	0.00	9.31	24.75	3.04
0.00	0.00	1.86	2.07	0.00	9.61	24.52	3.21
0.00	0.00	1.85	2.07	0.00	9.91	24.31	3.37
0.00	0.00	1.83	2.07	0.00	10.21	24.10	3.53
0.00	0.00	1.82	2.07	0.00	10.51	23.90	3.70
0.00	0.00	1.81	2.07	0.00	10.81	23.70	3.86
0.00	0.00	1.79	2.07	0.00	11.11	23.52	4.03
0.00	0.00	1.78	2.07	0.00	11.41	23.35	4.20
0.00	0.00	1.77	2.07	0.00	11.71	23.18	4.37
0.00	0.00	1.76	2.07	0.00	12.01	23.02	4.54
0.00	0.00	1.75	2.07	0.00	12.31	22.88	4.71
0.00	0.00	1.74	2.07	0.00	12.61	22.74	4.88
0.00	0.00	1.73	2.07	0.00	12.91	22.62	5.05

Table E4: *Simulation 1*

CODE=1A : DROPLET TRAJECTORY

DROP SIZE = 211.0000 MICRONS

Rvel(m/s)	Tvel(m/s)	Zvel(m/s)	RDIS(M)	THETA(0)	ZDIS(M)	REN NO.	TIME(S)
32.36	0.00	50.79	0.01	0.00	0.01	445.01	0.00
22.66	0.00	41.33	0.18	0.00	0.30	300.05	0.01
14.37	0.00	29.46	0.33	0.00	0.60	175.44	0.01
8.28	0.00	19.38	0.47	0.00	0.90	116.95	0.03
3.93	0.00	10.32	0.59	0.00	1.20	77.70	0.05
1.14	0.00	3.53	0.70	0.00	1.50	25.56	0.10
0.14	0.00	1.38	0.76	0.00	1.80	8.19	0.25
0.01	0.00	1.19	0.77	0.00	2.10	6.76	0.49
0.00	0.00	1.14	0.78	0.00	2.40	6.37	0.75
0.00	0.00	1.09	0.78	0.00	2.70	6.05	1.02
0.00	0.00	1.05	0.78	0.00	3.00	5.79	1.30
0.00	0.00	1.02	0.78	0.00	3.30	5.59	1.59
0.00	0.00	1.02	0.78	0.00	3.60	5.59	1.89
0.00	0.00	1.02	0.78	0.00	3.90	5.60	2.18
0.00	0.00	1.02	0.78	0.00	4.20	5.61	2.47
0.00	0.00	1.02	0.78	0.00	4.50	5.62	2.77
0.00	0.00	1.02	0.78	0.00	4.80	5.63	3.06
0.00	0.00	1.02	0.78	0.00	5.10	5.64	3.35
0.00	0.00	1.02	0.78	0.00	5.40	5.65	3.65
0.00	0.00	1.02	0.78	0.00	5.70	5.66	3.94
0.00	0.00	1.02	0.78	0.00	6.00	5.67	4.23
0.00	0.00	1.03	0.78	0.00	6.30	5.68	4.52
0.00	0.00	1.03	0.78	0.00	6.60	5.69	4.82
0.00	0.00	1.03	0.78	0.00	6.90	5.70	5.11
0.00	0.00	1.03	0.78	0.00	7.21	5.71	5.40
0.00	0.00	1.03	0.78	0.00	7.51	5.72	5.69
0.00	0.00	1.03	0.78	0.00	7.81	5.73	5.99
0.00	0.00	1.03	0.78	0.00	8.11	5.74	6.28
0.00	0.00	1.03	0.78	0.00	8.41	5.75	6.57
0.00	0.00	1.03	0.78	0.00	8.71	5.75	6.86
0.00	0.00	1.03	0.78	0.00	9.01	5.76	7.16
0.00	0.00	1.03	0.78	0.00	9.31	5.77	7.45
0.00	0.00	1.03	0.78	0.00	9.61	5.77	7.74
0.00	0.00	1.03	0.78	0.00	9.91	5.77	8.03
0.00	0.00	1.03	0.78	0.00	10.21	5.78	8.32
0.00	0.00	1.03	0.78	0.00	10.51	5.78	8.62
0.00	0.00	1.03	0.78	0.00	10.81	5.79	8.91
0.00	0.00	1.03	0.78	0.00	11.11	5.79	9.20
0.00	0.00	1.03	0.78	0.00	11.41	5.79	9.49
0.00	0.00	1.03	0.78	0.00	11.71	5.80	9.79
0.00	0.00	1.03	0.78	0.00	12.01	5.80	10.08
0.00	0.00	1.03	0.78	0.00	12.31	5.80	10.37
0.00	0.00	1.03	0.78	0.00	12.61	5.81	10.66
0.00	0.00	1.03	0.78	0.00	12.91	5.81	10.96

Table E5: *Simulation 1*

CODE-1A : DROPLET TRAJECTORY

DROP SIZE = 137.0000 MICRONS

Rvel(m/s)	Tvel(m/s)	Zvel(m/s)	RDIS(M)	THETA(0)	ZDIS(M)	REN NO.	TIME(S)
32.36	0.00	50.79	0.01	0.00	0.01	288.94	0.00
16.14	0.00	34.57	0.16	0.00	0.30	146.35	0.01
6.16	0.00	18.54	0.28	0.00	0.60	55.69	0.02
1.75	0.00	9.22	0.36	0.00	0.90	22.26	0.04
0.19	0.00	2.09	0.40	0.00	1.20	8.36	0.10
0.00	0.00	0.63	0.41	0.00	1.50	1.54	0.46
0.00	0.00	0.61	0.41	0.00	1.80	1.44	0.96
0.00	0.00	0.61	0.41	0.00	2.10	1.47	1.45
0.00	0.00	0.61	0.41	0.00	2.40	1.49	1.94
0.00	0.00	0.61	0.41	0.00	2.70	1.50	2.43
0.00	0.00	0.61	0.41	0.00	3.00	1.52	2.92
0.00	0.00	0.61	0.41	0.00	3.30	1.53	3.42
0.00	0.00	0.61	0.41	0.00	3.60	1.53	3.91
0.00	0.00	0.61	0.41	0.00	3.90	1.53	4.39
0.00	0.00	0.61	0.41	0.00	4.20	1.54	4.88
0.00	0.00	0.61	0.41	0.00	4.50	1.54	5.37
0.00	0.00	0.61	0.41	0.00	4.80	1.54	5.86
0.00	0.00	0.61	0.41	0.00	5.10	1.54	6.35
0.00	0.00	0.61	0.41	0.00	5.40	1.55	6.84
0.00	0.00	0.61	0.41	0.00	5.70	1.55	7.33
0.00	0.00	0.61	0.41	0.00	6.00	1.55	7.81
0.00	0.00	0.61	0.41	0.00	6.30	1.56	8.30
0.00	0.00	0.62	0.41	0.00	6.60	1.56	8.79
0.00	0.00	0.62	0.41	0.00	6.90	1.56	9.28
0.00	0.00	0.62	0.41	0.00	7.21	1.56	9.76
0.00	0.00	0.62	0.41	0.00	7.51	1.57	10.25
0.00	0.00	0.62	0.41	0.00	7.81	1.57	10.74
0.00	0.00	0.62	0.41	0.00	8.11	1.57	11.23
0.00	0.00	0.62	0.41	0.00	8.41	1.57	11.71
0.00	0.00	0.62	0.41	0.00	8.71	1.57	12.20
0.00	0.00	0.62	0.41	0.00	9.01	1.58	12.69
0.00	0.00	0.62	0.41	0.00	9.31	1.58	13.18
0.00	0.00	0.62	0.41	0.00	9.61	1.58	13.67
0.00	0.00	0.62	0.41	0.00	9.91	1.58	14.15
0.00	0.00	0.62	0.41	0.00	10.21	1.58	14.64
0.00	0.00	0.62	0.41	0.00	10.51	1.59	15.13
0.00	0.00	0.62	0.41	0.00	10.81	1.59	15.61
0.00	0.00	0.62	0.41	0.00	11.11	1.59	16.10
0.00	0.00	0.62	0.41	0.00	11.41	1.59	16.59
0.00	0.00	0.62	0.41	0.00	11.71	1.59	17.08
0.00	0.00	0.62	0.41	0.00	12.01	1.59	17.56
0.00	0.00	0.62	0.41	0.00	12.31	1.59	18.05
0.00	0.00	0.62	0.41	0.00	12.61	1.60	18.54
0.00	0.00	0.62	0.41	0.00	12.91	1.60	19.02

Table E6: *Simulation 1*

CODE-1A : DROPLET TRAJECTORY

DROP SIZE = 99.00000 MICRONS

Rvel(m/s)	Tvel(m/s)	Zvel(m/s)	RDIS(M)	THETA(0)	ZDIS(M)	REN NO.	TIME(S)
32.36	0.00	50.79	0.01	0.00	0.01	208.79	0.00
10.23	0.00	28.03	0.15	0.00	0.30	72.93	0.01
1.94	0.00	12.16	0.22	0.00	0.60	16.80	0.02
0.25	0.00	6.26	0.25	0.00	0.90	5.56	0.06
0.00	0.00	0.48	0.26	0.00	1.20	0.56	0.22
0.00	0.00	0.47	0.26	0.00	1.50	0.53	0.86
0.00	0.00	0.47	0.26	0.00	1.80	0.54	1.50
0.00	0.00	0.47	0.26	0.00	2.10	0.55	2.14
0.00	0.00	0.47	0.26	0.00	2.40	0.56	2.78
0.00	0.00	0.47	0.26	0.00	2.70	0.57	3.42
0.00	0.00	0.47	0.26	0.00	3.00	0.57	4.06
0.00	0.00	0.47	0.26	0.00	3.30	0.58	4.70
0.00	0.00	0.47	0.26	0.00	3.60	0.58	5.34
0.00	0.00	0.47	0.26	0.00	3.90	0.58	5.97
0.00	0.00	0.47	0.26	0.00	4.20	0.58	6.61
0.00	0.00	0.47	0.26	0.00	4.50	0.58	7.25
0.00	0.00	0.47	0.26	0.00	4.80	0.58	7.88
0.00	0.00	0.47	0.26	0.00	5.10	0.58	8.52
0.00	0.00	0.47	0.26	0.00	5.40	0.58	9.15
0.00	0.00	0.47	0.26	0.00	5.70	0.59	9.79
0.00	0.00	0.47	0.26	0.00	6.00	0.59	10.43
0.00	0.00	0.47	0.26	0.00	6.30	0.59	11.06
0.00	0.00	0.47	0.26	0.00	6.60	0.59	11.70
0.00	0.00	0.47	0.26	0.00	6.90	0.59	12.33
0.00	0.00	0.47	0.26	0.00	7.21	0.59	12.97
0.00	0.00	0.47	0.26	0.00	7.51	0.59	13.60
0.00	0.00	0.47	0.26	0.00	7.81	0.59	14.24
0.00	0.00	0.47	0.26	0.00	8.11	0.59	14.87
0.00	0.00	0.47	0.26	0.00	8.41	0.59	15.51
0.00	0.00	0.47	0.26	0.00	8.71	0.59	16.14
0.00	0.00	0.47	0.26	0.00	9.01	0.60	16.78
0.00	0.00	0.47	0.26	0.00	9.31	0.60	17.42
0.00	0.00	0.47	0.26	0.00	9.61	0.60	18.05
0.00	0.00	0.47	0.26	0.00	9.91	0.60	18.69
0.00	0.00	0.47	0.26	0.00	10.21	0.60	19.32
0.00	0.00	0.47	0.26	0.00	10.51	0.60	19.96
0.00	0.00	0.47	0.26	0.00	10.81	0.60	20.59
0.00	0.00	0.47	0.26	0.00	11.11	0.60	21.23
0.00	0.00	0.47	0.26	0.00	11.41	0.60	21.86
0.00	0.00	0.47	0.26	0.00	11.71	0.60	22.50
0.00	0.00	0.47	0.26	0.00	12.01	0.60	23.13
0.00	0.00	0.47	0.26	0.00	12.31	0.60	23.77
0.00	0.00	0.47	0.26	0.00	12.61	0.60	24.40
0.00	0.00	0.47	0.26	0.00	12.91	0.60	25.04

Table E7: *Simulation 1*

CODE-1A : DROPLET TRAJECTORY

DROP SIZE = 74.00000 MICRONS

Rvel(m/s)	Tvel(m/s)	Zvel(m/s)	RDIS(M)	THETA(0)	ZDIS(M)	REN NO.	TIME(S)
32.36	0.00	50.79	0.01	0.00	0.01	156.07	0.00
5.36	0.00	22.14	0.13	0.00	0.30	33.31	0.01
0.43	0.00	9.38	0.16	0.00	0.60	5.40	0.03
0.01	0.00	5.06	0.17	0.00	0.90	1.21	0.08
0.00	0.00	0.40	0.17	0.00	1.20	0.21	0.37
0.00	0.00	0.40	0.17	0.00	1.50	0.22	1.12
0.00	0.00	0.40	0.17	0.00	1.80	0.23	1.86
0.00	0.00	0.40	0.17	0.00	2.10	0.23	2.61
0.00	0.00	0.40	0.17	0.00	2.40	0.23	3.36
0.00	0.00	0.40	0.17	0.00	2.70	0.24	4.11
0.00	0.00	0.40	0.17	0.00	3.00	0.24	4.86
0.00	0.00	0.40	0.17	0.00	3.30	0.24	5.60
0.00	0.00	0.40	0.17	0.00	3.60	0.24	6.35
0.00	0.00	0.40	0.17	0.00	3.90	0.24	7.09
0.00	0.00	0.40	0.17	0.00	4.20	0.24	7.84
0.00	0.00	0.40	0.17	0.00	4.50	0.24	8.58
0.00	0.00	0.40	0.17	0.00	4.80	0.24	9.33
0.00	0.00	0.40	0.17	0.00	5.10	0.24	10.07
0.00	0.00	0.40	0.17	0.00	5.40	0.24	10.82
0.00	0.00	0.40	0.17	0.00	5.70	0.24	11.56
0.00	0.00	0.40	0.17	0.00	6.00	0.24	12.30
0.00	0.00	0.40	0.17	0.00	6.30	0.25	13.05
0.00	0.00	0.40	0.17	0.00	6.60	0.25	13.79
0.00	0.00	0.40	0.17	0.00	6.90	0.25	14.54
0.00	0.00	0.40	0.17	0.00	7.21	0.25	15.28
0.00	0.00	0.40	0.17	0.00	7.51	0.25	16.02
0.00	0.00	0.40	0.17	0.00	7.81	0.25	16.77
0.00	0.00	0.40	0.17	0.00	8.11	0.25	17.51
0.00	0.00	0.40	0.17	0.00	8.41	0.25	18.26
0.00	0.00	0.40	0.17	0.00	8.71	0.25	19.00
0.00	0.00	0.40	0.17	0.00	9.01	0.25	19.75
0.00	0.00	0.40	0.17	0.00	9.31	0.25	20.49
0.00	0.00	0.40	0.17	0.00	9.61	0.25	21.24
0.00	0.00	0.40	0.17	0.00	9.91	0.25	21.98
0.00	0.00	0.40	0.17	0.00	10.21	0.25	22.72
0.00	0.00	0.40	0.17	0.00	10.51	0.25	23.47
0.00	0.00	0.40	0.17	0.00	10.81	0.25	24.21
0.00	0.00	0.40	0.17	0.00	11.11	0.25	24.96
0.00	0.00	0.40	0.17	0.00	11.41	0.25	25.70
0.00	0.00	0.40	0.17	0.00	11.71	0.25	26.44
0.00	0.00	0.40	0.17	0.00	12.01	0.25	27.19
0.00	0.00	0.40	0.17	0.00	12.31	0.25	27.93
0.00	0.00	0.40	0.17	0.00	12.61	0.25	28.67
0.00	0.00	0.40	0.17	0.00	12.91	0.25	29.42

Table E8: *Simulation 1*

CODE-1A : DROPLET TRAJECTORY

DROP SIZE = 57.00000 MICRONS

Rvel(m/s)	Tvel(m/s)	Zvel(m/s)	RDIS(M)	THETA(0)	ZDIS(M)	REN NO.	TIME(S)
32.36	0.00	50.79	0.01	0.00	0.01	120.22	0.00
2.32	0.00	17.91	0.10	0.00	0.30	14.61	0.01
0.03	0.00	7.93	0.12	0.00	0.60	1.50	0.04
0.00	0.00	4.75	0.12	0.00	0.90	0.35	0.09
0.00	0.00	0.37	0.12	0.00	1.20	0.10	0.44
0.00	0.00	0.37	0.12	0.00	1.50	0.10	1.26
0.00	0.00	0.37	0.12	0.00	1.80	0.10	2.08
0.00	0.00	0.37	0.12	0.00	2.10	0.11	2.90
0.00	0.00	0.37	0.12	0.00	2.40	0.11	3.72
0.00	0.00	0.37	0.12	0.00	2.70	0.11	4.54
0.00	0.00	0.37	0.12	0.00	3.00	0.11	5.35
0.00	0.00	0.37	0.12	0.00	3.30	0.11	6.17
0.00	0.00	0.37	0.12	0.00	3.60	0.11	6.99
0.00	0.00	0.37	0.12	0.00	3.90	0.11	7.81
0.00	0.00	0.37	0.12	0.00	4.20	0.11	8.62
0.00	0.00	0.37	0.12	0.00	4.50	0.11	9.44
0.00	0.00	0.37	0.12	0.00	4.80	0.11	10.26
0.00	0.00	0.37	0.12	0.00	5.10	0.11	11.07
0.00	0.00	0.37	0.12	0.00	5.40	0.11	11.89
0.00	0.00	0.37	0.12	0.00	5.70	0.11	12.70
0.00	0.00	0.37	0.12	0.00	6.00	0.11	13.52
0.00	0.00	0.37	0.12	0.00	6.30	0.11	14.33
0.00	0.00	0.37	0.12	0.00	6.60	0.11	15.15
0.00	0.00	0.37	0.12	0.00	6.90	0.11	15.97
0.00	0.00	0.37	0.12	0.00	7.21	0.11	16.78
0.00	0.00	0.37	0.12	0.00	7.51	0.11	17.60
0.00	0.00	0.37	0.12	0.00	7.81	0.11	18.41
0.00	0.00	0.37	0.12	0.00	8.11	0.11	19.23
0.00	0.00	0.37	0.12	0.00	8.41	0.11	20.05
0.00	0.00	0.37	0.12	0.00	8.71	0.11	20.86
0.00	0.00	0.37	0.12	0.00	9.01	0.11	21.68
0.00	0.00	0.37	0.12	0.00	9.31	0.11	22.50
0.00	0.00	0.37	0.12	0.00	9.61	0.11	23.31
0.00	0.00	0.37	0.12	0.00	9.91	0.11	24.13
0.00	0.00	0.37	0.12	0.00	10.21	0.11	24.94
0.00	0.00	0.37	0.12	0.00	10.51	0.11	25.76
0.00	0.00	0.37	0.12	0.00	10.81	0.11	26.58
0.00	0.00	0.37	0.12	0.00	11.11	0.11	27.39
0.00	0.00	0.37	0.12	0.00	11.41	0.11	28.21
0.00	0.00	0.37	0.12	0.00	11.71	0.11	29.03
0.00	0.00	0.37	0.12	0.00	12.01	0.11	29.84
0.00	0.00	0.37	0.12	0.00	12.31	0.11	30.66
0.00	0.00	0.37	0.12	0.00	12.61	0.11	31.47
0.00	0.00	0.37	0.12	0.00	12.91	0.11	32.29

Table E9: *Simulation 1*

CODE-1A : DROPLET TRAJECTORY

DROP SIZE = 45.00000 MICRONS

Rvel(m/s)	Tvel(m/s)	Zvel(m/s)	RDIS(M)	THETA(0)	ZDIS(M)	REN NO.	TIME(S)
32.36	0.00	50.79	0.01	0.00	0.01	94.91	0.00
0.84	0.00	15.38	0.08	0.00	0.30	6.65	0.01
0.00	0.00	7.45	0.08	0.00	0.60	0.50	0.04
0.00	0.00	4.67	0.08	0.00	0.90	0.16	0.09
0.00	0.00	0.35	0.08	0.00	1.20	0.05	0.48
0.00	0.00	0.35	0.08	0.00	1.50	0.05	1.35
0.00	0.00	0.35	0.08	0.00	1.80	0.05	2.21
0.00	0.00	0.35	0.08	0.00	2.10	0.05	3.07
0.00	0.00	0.35	0.08	0.00	2.40	0.05	3.94
0.00	0.00	0.35	0.08	0.00	2.70	0.05	4.80
0.00	0.00	0.35	0.08	0.00	3.00	0.05	5.67
0.00	0.00	0.35	0.08	0.00	3.30	0.05	6.53
0.00	0.00	0.35	0.08	0.00	3.60	0.05	7.39
0.00	0.00	0.35	0.08	0.00	3.90	0.05	8.26
0.00	0.00	0.35	0.08	0.00	4.20	0.05	9.12
0.00	0.00	0.35	0.08	0.00	4.50	0.05	9.98
0.00	0.00	0.35	0.08	0.00	4.80	0.05	10.84
0.00	0.00	0.35	0.08	0.00	5.10	0.05	11.70
0.00	0.00	0.35	0.08	0.00	5.40	0.05	12.57
0.00	0.00	0.35	0.08	0.00	5.70	0.05	13.43
0.00	0.00	0.35	0.08	0.00	6.00	0.06	14.29
0.00	0.00	0.35	0.08	0.00	6.30	0.06	15.15
0.00	0.00	0.35	0.08	0.00	6.60	0.06	16.01
0.00	0.00	0.35	0.08	0.00	6.90	0.06	16.87
0.00	0.00	0.35	0.08	0.00	7.21	0.06	17.73
0.00	0.00	0.35	0.08	0.00	7.51	0.06	18.60
0.00	0.00	0.35	0.08	0.00	7.81	0.06	19.46
0.00	0.00	0.35	0.08	0.00	8.11	0.06	20.32
0.00	0.00	0.35	0.08	0.00	8.41	0.06	21.18
0.00	0.00	0.35	0.08	0.00	8.71	0.06	22.04
0.00	0.00	0.35	0.08	0.00	9.01	0.06	22.91
0.00	0.00	0.35	0.08	0.00	9.31	0.06	23.77
0.00	0.00	0.35	0.08	0.00	9.61	0.06	24.63
0.00	0.00	0.35	0.08	0.00	9.91	0.06	25.49
0.00	0.00	0.35	0.08	0.00	10.21	0.06	26.36
0.00	0.00	0.35	0.08	0.00	10.51	0.06	27.22
0.00	0.00	0.35	0.08	0.00	10.81	0.06	28.08
0.00	0.00	0.35	0.08	0.00	11.11	0.06	28.94
0.00	0.00	0.35	0.08	0.00	11.41	0.06	29.80
0.00	0.00	0.35	0.08	0.00	11.71	0.06	30.67
0.00	0.00	0.35	0.08	0.00	12.01	0.06	31.53
0.00	0.00	0.35	0.08	0.00	12.31	0.06	32.39
0.00	0.00	0.35	0.08	0.00	12.61	0.06	33.25
0.00	0.00	0.35	0.08	0.00	12.91	0.06	34.11

Table E10: *Simulation 1*

CODE-1A : DROPLET TRAJECTORY

DROP SIZE = 35.00000 MICRONS

Rvel(m/s)	Tvel(m/s)	Zvel(m/s)	RDIS(M)	THETA(0)	ZDIS(M)	REN NO.	TIME(S)
32.36	0.00	50.79	0.01	0.00	0.01	73.82	0.00
0.14	0.00	13.31	0.06	0.00	0.30	2.31	0.01
0.00	0.00	7.29	0.06	0.00	0.60	0.21	0.04
0.00	0.00	4.63	0.06	0.00	0.90	0.08	0.10
0.00	0.00	0.33	0.06	0.00	1.20	0.02	0.51
0.00	0.00	0.33	0.06	0.00	1.50	0.02	1.41
0.00	0.00	0.34	0.06	0.00	1.80	0.02	2.30
0.00	0.00	0.34	0.06	0.00	2.10	0.02	3.20
0.00	0.00	0.34	0.06	0.00	2.40	0.02	4.10
0.00	0.00	0.34	0.06	0.00	2.70	0.03	4.99
0.00	0.00	0.34	0.06	0.00	3.00	0.03	5.89
0.00	0.00	0.34	0.06	0.00	3.30	0.03	6.79
0.00	0.00	0.34	0.06	0.00	3.60	0.03	7.68
0.00	0.00	0.34	0.06	0.00	3.90	0.03	8.58
0.00	0.00	0.34	0.06	0.00	4.20	0.03	9.47
0.00	0.00	0.34	0.06	0.00	4.50	0.03	10.37
0.00	0.00	0.34	0.06	0.00	4.80	0.03	11.26
0.00	0.00	0.34	0.06	0.00	5.10	0.03	12.15
0.00	0.00	0.34	0.06	0.00	5.40	0.03	13.05
0.00	0.00	0.34	0.06	0.00	5.70	0.03	13.94
0.00	0.00	0.34	0.06	0.00	6.00	0.03	14.84
0.00	0.00	0.34	0.06	0.00	6.30	0.03	15.73
0.00	0.00	0.34	0.06	0.00	6.60	0.03	16.63
0.00	0.00	0.34	0.06	0.00	6.90	0.03	17.52
0.00	0.00	0.34	0.06	0.00	7.21	0.03	18.41
0.00	0.00	0.34	0.06	0.00	7.51	0.03	19.31
0.00	0.00	0.34	0.06	0.00	7.81	0.03	20.20
0.00	0.00	0.34	0.06	0.00	8.11	0.03	21.10
0.00	0.00	0.34	0.06	0.00	8.41	0.03	21.99
0.00	0.00	0.34	0.06	0.00	8.71	0.03	22.89
0.00	0.00	0.34	0.06	0.00	9.01	0.03	23.78
0.00	0.00	0.34	0.06	0.00	9.31	0.03	24.68
0.00	0.00	0.34	0.06	0.00	9.61	0.03	25.57
0.00	0.00	0.34	0.06	0.00	9.91	0.03	26.47
0.00	0.00	0.34	0.06	0.00	10.21	0.03	27.36
0.00	0.00	0.34	0.06	0.00	10.51	0.03	28.26
0.00	0.00	0.34	0.06	0.00	10.81	0.03	29.15
0.00	0.00	0.34	0.06	0.00	11.11	0.03	30.05
0.00	0.00	0.34	0.06	0.00	11.41	0.03	30.94
0.00	0.00	0.34	0.06	0.00	11.71	0.03	31.84
0.00	0.00	0.34	0.06	0.00	12.01	0.03	32.73
0.00	0.00	0.34	0.06	0.00	12.31	0.03	33.63
0.00	0.00	0.34	0.06	0.00	12.61	0.03	34.52
0.00	0.00	0.34	0.06	0.00	12.91	0.03	35.42

Table E11: *Simulation 1*

CODE-1A : DROPLET DRYING BEHAVIOUR

DROP SIZE = 413.0000 MICRONS

ZDIS(M)	%SOLID	TEMP(C)	NA kg/s	hg(m/s)	hc(m/s)	kg(m/s)	kc(m/s)
0.01	55.00	79.95	.29E-06	1512	0	1.93	0.00
0.85	57.00	61.00	.39E-07	1229	10530	1.45	1.19
2.43	59.00	55.39	.12E-07	765	5017	0.87	0.53
3.39	61.00	54.36	.73E-08	493	3278	0.56	0.34
4.00	63.01	54.65	.57E-08	410	2406	0.47	0.25
4.52	65.01	55.73	.51E-08	392	1880	0.45	0.19
5.03	67.01	56.99	.47E-08	387	1527	0.44	0.16
5.53	69.01	58.19	.45E-08	385	1273	0.44	0.13
6.02	71.01	59.29	.42E-08	382	1080	0.44	0.11
6.50	73.01	60.31	.39E-08	380	929	0.44	0.10
6.98	75.01	61.25	.37E-08	378	807	0.43	0.08
7.46	77.01	62.13	.35E-08	376	705	0.43	0.07
7.94	79.02	62.97	.33E-08	374	619	0.43	0.06
8.41	81.02	63.77	.31E-08	373	545	0.43	0.06
8.89	83.02	64.55	.28E-08	371	479	0.43	0.05
9.37	85.02	65.31	.26E-08	369	421	0.43	0.04
9.86	87.02	66.06	.24E-08	367	369	0.42	0.04
10.37	89.02	66.83	.22E-08	366	320	0.42	0.03
10.89	91.02	67.61	.20E-08	364	274	0.42	0.03
11.45	93.02	68.43	.18E-08	363	231	0.42	0.02
12.04	95.02	69.34	.15E-08	361	187	0.42	0.02
12.72	97.02	70.43	.12E-08	360	140	0.42	0.01

Table E12: *Simulation 1*

CODE=1A : DROPLET DRYING BEHAVIOUR

DROP SIZE = 211.0000 MICRONS

ZDIS(M)	%SOLID	TEMP(C)	NA kg/s	hg(m/s)	hc(m/s)	kg(m/s)	kc(m/s)
0.01	55.01	79.87	.11E-06	2211	0	2.83	0.00
0.29	57.01	60.05	.19E-07	1813	20324	2.22	2.43
0.82	59.01	55.53	.76E-08	1377	9926	1.63	1.11
1.26	61.01	55.29	.47E-08	1023	6459	1.19	0.70
1.50	63.01	54.95	.32E-08	745	4731	0.87	0.50
1.65	65.01	54.99	.25E-08	616	3697	0.72	0.39
1.76	67.02	55.57	.22E-08	563	3001	0.66	0.32
1.85	69.02	56.45	.20E-08	542	2501	0.63	0.27
1.94	71.02	57.46	.19E-08	534	2123	0.62	0.23
2.02	73.03	58.47	.18E-08	530	1825	0.62	0.19
2.11	75.04	59.46	.17E-08	527	1584	0.62	0.17
2.19	77.05	60.41	.16E-08	525	1384	0.61	0.15
2.27	79.06	61.33	.15E-08	523	1214	0.61	0.13
2.35	81.06	62.22	.14E-08	521	1068	0.61	0.11
2.43	83.06	63.09	.14E-08	519	940	0.61	0.10
2.51	85.07	63.96	.13E-08	518	826	0.61	0.09
2.59	87.08	64.84	.12E-08	516	722	0.61	0.08
2.68	89.08	65.74	.11E-08	515	627	0.60	0.07
2.76	91.08	66.67	.99E-09	513	538	0.60	0.06
2.85	93.09	67.68	.89E-09	512	452	0.60	0.05
2.95	95.10	68.81	.78E-09	510	366	0.60	0.04
3.05	97.11	70.20	.63E-09	509	274	0.60	0.03
3.19	99.11	72.33	.41E-09	507	157	0.60	0.02
3.22	99.50	73.06	.33E-09	507	122	0.60	0.01
3.82	99.50	130.73	.00E+00	339	0	0	0.00
4.42	99.50	131.40	.00E+00	339	0	0	0.00
5.02	99.50	130.80	.00E+00	338	0	0	0.00
5.62	99.50	130.21	.00E+00	338	0	0	0.00
6.23	99.50	129.64	.00E+00	337	0	0	0.00
6.83	99.50	129.11	.00E+00	337	0	0	0.00
7.43	99.50	128.61	.00E+00	337	0	0	0.00
8.03	99.50	128.14	.00E+00	336	0	0	0.00
8.63	99.50	127.71	.00E+00	336	0	0	0.00
9.23	99.50	127.30	.00E+00	336	0	0	0.00
9.83	99.50	126.93	.00E+00	336	0	0	0.00
10.43	99.50	126.59	.00E+00	335	0	0	0.00
11.03	99.50	126.28	.00E+00	335	0	0	0.00
11.63	99.50	126.00	.00E+00	335	0	0	0.00
12.23	99.50	125.76	.00E+00	335	0	0	0.00
12.83	99.50	125.55	.00E+00	335	0	0	0.00

Table E13: *Simulation 1*

CODE=1A : DROPLET DRYING BEHAVIOUR

DROP SIZE = 137.0000 MICRONS

ZDIS(M)	%SOLID	TEMP(C)	NA kg/s	hg(m/s)	hc(m/s)	kg(m/s)	kc(m/s)
0.01	55.02	79.74	.60E-07	2843	0	3.64	0.00
0.15	57.02	59.53	.11E-07	2289	31241	2.84	3.82
0.42	59.02	54.80	.50E-08	1885	15280	2.28	1.77
0.68	61.02	54.99	.33E-08	1452	9975	1.74	1.13
0.88	63.02	55.53	.25E-08	1173	7303	1.40	0.81
1.04	65.02	56.01	.20E-08	997	5693	1.19	0.63
1.15	67.02	57.50	.19E-08	1005	4618	1.19	0.51
1.21	69.03	57.61	.15E-08	857	3848	1.02	0.42
1.25	71.04	57.88	.13E-08	776	3268	0.92	0.36
1.28	73.07	58.39	.12E-08	724	2807	0.86	0.30
1.31	75.07	59.05	.11E-08	691	2432	0.82	0.26
1.33	77.08	59.82	.10E-08	671	2125	0.80	0.23
1.35	79.08	60.67	.98E-09	660	1866	0.79	0.20
1.37	81.08	61.57	.92E-09	653	1642	0.78	0.18
1.40	83.09	62.50	.87E-09	649	1445	0.78	0.16
1.42	85.09	63.46	.82E-09	646	1269	0.77	0.14
1.44	87.09	64.44	.77E-09	644	1110	0.77	0.12
1.46	89.09	65.46	.72E-09	642	964	0.77	0.11
1.48	91.09	66.54	.66E-09	640	826	0.77	0.09
1.50	93.10	67.72	.60E-09	639	693	0.77	0.08
1.52	95.10	69.06	.53E-09	637	561	0.77	0.06
1.55	97.10	70.74	.44E-09	636	419	0.77	0.05
1.58	99.10	73.41	.29E-09	635	236	0.77	0.03
1.59	99.50	74.40	.23E-09	635	178	0.77	0.02
2.19	99.50	138.44	.00E+00	517	0	0	0.00
2.79	99.50	134.45	.00E+00	513	0	0	0.00
3.39	99.50	132.38	.00E+00	510	0	0	0.00
3.99	99.50	131.77	.00E+00	510	0	0	0.00
4.59	99.50	131.14	.00E+00	509	0	0	0.00
5.19	99.50	130.52	.00E+00	508	0	0	0.00
5.79	99.50	129.93	.00E+00	508	0	0	0.00
6.39	99.50	129.38	.00E+00	507	0	0	0.00
6.99	99.50	128.87	.00E+00	507	0	0	0.00
7.59	99.50	128.38	.00E+00	506	0	0	0.00
8.19	99.50	127.93	.00E+00	506	0	0	0.00
8.79	99.50	127.51	.00E+00	505	0	0	0.00
9.39	99.50	127.12	.00E+00	505	0	0	0.00
9.99	99.50	126.76	.00E+00	504	0	0	0.00
10.59	99.50	126.43	.00E+00	504	0	0	0.00
11.19	99.50	126.14	.00E+00	504	0	0	0.00
11.79	99.50	125.88	.00E+00	504	0	0	0.00
12.39	99.50	125.65	.00E+00	503	0	0	0.00
12.99	99.50	125.46	.00E+00	503	0	0	0.00

Table E14: *Simulation 1*

CODE=1A : DROPLET DRYING BEHAVIOUR

DROP SIZE = 99.00000 MICRONS

ZDIS(M)	%SOLID	TEMP(C)	NA kg/s	hg(m/s)	hc(m/s)	kg(m/s)	kc(m/s)
0.01	55.03	79.56	.38E-07	3450	0	4.42	0.00
0.09	57.04	59.11	.74E-08	2727	43019	3.41	5.29
0.25	59.04	54.13	.36E-08	2364	21134	2.90	2.51
0.42	61.04	54.86	.25E-08	1917	13778	2.33	1.60
0.55	63.04	55.63	.19E-08	1574	10099	1.90	1.15
0.66	65.04	56.27	.16E-08	1393	7912	1.68	0.90
0.76	67.04	57.08	.14E-08	1263	6425	1.52	0.72
0.85	69.04	57.85	.12E-08	1170	5354	1.41	0.60
0.93	71.04	58.55	.11E-08	1101	4539	1.33	0.51
1.00	73.04	59.28	.10E-08	1042	3903	1.26	0.43
1.06	75.04	60.00	.91E-09	993	3390	1.20	0.38
1.10	77.04	62.59	.97E-09	1186	2965	1.42	0.33
1.13	79.05	62.69	.86E-09	1051	2603	1.26	0.29
1.15	81.05	62.83	.76E-09	953	2290	1.15	0.25
1.16	83.06	63.16	.69E-09	885	2016	1.07	0.22
1.17	85.07	63.73	.63E-09	843	1771	1.02	0.20
1.18	87.07	64.51	.58E-09	820	1550	1.00	0.17
1.18	89.07	65.48	.54E-09	808	1346	0.98	0.15
1.19	91.08	66.59	.50E-09	802	1155	0.98	0.13
1.20	93.08	67.84	.45E-09	799	971	0.97	0.11
1.21	95.09	69.30	.40E-09	798	787	0.97	0.09
1.22	97.09	71.12	.34E-09	797	593	0.97	0.07
1.23	99.09	73.97	.23E-09	797	346	0.98	0.04
1.23	99.50	75.01	.19E-09	797	270	0.98	0.03
1.83	99.50	141.21	.00E+00	712	0	0	0.00
2.43	99.50	136.46	.00E+00	705	0	0	0.00
3.03	99.50	133.18	.00E+00	700	0	0	0.00
3.63	99.50	132.11	.00E+00	699	0	0	0.00
4.23	99.50	131.49	.00E+00	698	0	0	0.00
4.84	99.50	130.85	.00E+00	697	0	0	0.00
5.44	99.50	130.25	.00E+00	696	0	0	0.00
6.04	99.50	129.68	.00E+00	695	0	0	0.00
6.64	99.50	129.15	.00E+00	694	0	0	0.00
7.24	99.50	128.64	.00E+00	694	0	0	0.00
7.84	99.50	128.18	.00E+00	693	0	0	0.00
8.44	99.50	127.74	.00E+00	692	0	0	0.00
9.04	99.50	127.33	.00E+00	692	0	0	0.00
9.64	99.50	126.95	.00E+00	691	0	0	0.00
10.24	99.50	126.61	.00E+00	691	0	0	0.00
10.84	99.50	126.30	.00E+00	690	0	0	0.00
11.44	99.50	126.02	.00E+00	690	0	0	0.00
12.04	99.50	125.77	.00E+00	689	0	0	0.00
12.64	99.50	125.56	.00E+00	689	0	0	0.00

Table E15: *Simulation 1*

CODE-1A : DROPLET DRYING BEHAVIOUR

DROP SIZE = 74.00000 MICRONS

ZDIS(M)	%SOLID	TEMP(C)	NA kg/s	hg(m/s)	hc(m/s)	kg(m/s)	kc(m/s)
0.01	55.05	79.30	.25E-07	4118	0	5.29	0.00
0.06	57.06	58.72	.50E-08	3201	57116	4.01	7.05
0.16	59.06	53.50	.26E-08	2866	28187	3.55	3.39
0.27	61.06	54.49	.19E-08	2431	18429	2.99	2.19
0.36	63.06	55.73	.15E-08	2089	13530	2.56	1.59
0.44	65.06	56.69	.13E-08	1846	10568	2.26	1.23
0.51	67.06	57.36	.11E-08	1638	8589	2.00	0.99
0.57	69.07	58.16	.98E-09	1547	7157	1.89	0.82
0.63	71.07	59.14	.89E-09	1483	6076	1.81	0.70
0.68	73.07	59.98	.82E-09	1416	5215	1.73	0.59
0.73	75.07	60.72	.75E-09	1353	4528	1.65	0.52
0.78	77.07	61.45	.69E-09	1295	3957	1.58	0.45
0.82	79.07	62.19	.64E-09	1247	3472	1.52	0.39
0.86	81.07	62.92	.59E-09	1207	3059	1.48	0.35
0.90	83.07	63.69	.55E-09	1174	2693	1.44	0.30
0.94	85.07	64.50	.51E-09	1149	2367	1.41	0.27
0.97	87.07	65.40	.47E-09	1128	2071	1.38	0.23
1.01	89.07	66.38	.44E-09	1112	1798	1.36	0.20
1.05	91.07	67.45	.40E-09	1098	1541	1.35	0.17
1.08	93.07	71.11	.42E-09	1555	1296	1.89	0.15
1.10	95.07	71.57	.35E-09	1313	1050	1.60	0.12
1.11	97.07	72.40	.28E-09	1147	789	1.41	0.09
1.11	99.07	74.81	.18E-09	1049	456	1.30	0.05
1.11	99.50	75.92	.15E-09	1036	348	1.28	0.04
1.71	99.50	142.15	.00E+00	950	0	0	0.00
2.31	99.50	137.23	.00E+00	940	0	0	0.00
2.92	99.50	133.65	.00E+00	933	0	0	0.00
3.52	99.50	132.22	.00E+00	930	0	0	0.00
4.12	99.50	131.60	.00E+00	929	0	0	0.00
4.72	99.50	130.97	.00E+00	927	0	0	0.00
5.32	99.50	130.36	.00E+00	926	0	0	0.00
5.92	99.50	129.78	.00E+00	925	0	0	0.00
6.52	99.50	129.24	.00E+00	924	0	0	0.00
7.12	99.50	128.73	.00E+00	923	0	0	0.00
7.72	99.50	128.26	.00E+00	922	0	0	0.00
8.32	99.50	127.81	.00E+00	921	0	0	0.00
8.92	99.50	127.40	.00E+00	920	0	0	0.00
9.52	99.50	127.02	.00E+00	919	0	0	0.00
10.12	99.50	126.67	.00E+00	919	0	0	0.00
10.72	99.50	126.35	.00E+00	918	0	0	0.00
11.32	99.50	126.06	.00E+00	918	0	0	0.00
11.92	99.50	125.81	.00E+00	917	0	0	0.00
12.52	99.50	125.59	.00E+00	917	0	0	0.00

Table E16: *Simulation 1*

CODE=1A : DROPLET DRYING BEHAVIOUR

DROP SIZE = 57.00000 MICRONS

ZDIS(M)	%SOLID	TEMP(C)	MA kg/s	hg(m/s)	hc(m/s)	kg(m/s)	kc(m/s)
0.01	55.08	78.94	.18E-07	4840	0	6.22	0.00
0.04	57.09	58.32	.35E-08	3716	73368	4.67	9.07
0.11	59.09	52.91	.19E-08	3390	36375	4.22	4.41
0.19	61.10	54.03	.14E-08	2964	23836	3.68	2.86
0.25	63.11	55.54	.12E-08	2619	17517	3.25	2.09
0.31	65.11	56.77	.10E-08	2365	13678	2.93	1.62
0.35	67.11	57.79	.91E-09	2176	11116	2.69	1.31
0.40	69.11	58.72	.82E-09	2037	9268	2.52	1.09
0.44	71.11	59.61	.74E-09	1930	7871	2.38	0.92
0.48	73.12	60.45	.67E-09	1813	6777	2.24	0.79
0.51	75.12	60.90	.60E-09	1684	5885	2.08	0.68
0.55	77.12	61.66	.56E-09	1635	5144	2.02	0.60
0.58	79.12	62.60	.52E-09	1605	4518	1.98	0.52
0.62	81.12	63.54	.49E-09	1575	3975	1.95	0.46
0.65	83.12	64.46	.46E-09	1544	3499	1.91	0.40
0.68	85.12	65.35	.43E-09	1514	3074	1.87	0.35
0.70	87.12	66.27	.40E-09	1487	2690	1.84	0.31
0.73	89.12	67.26	.37E-09	1462	2336	1.81	0.27
0.76	91.12	68.36	.34E-09	1440	2002	1.78	0.23
0.79	93.12	69.58	.30E-09	1421	1682	1.76	0.19
0.81	95.12	71.02	.27E-09	1404	1363	1.74	0.16
0.84	97.12	72.85	.22E-09	1389	1023	1.73	0.12
0.88	99.12	75.82	.15E-09	1375	589	1.71	0.07
0.89	99.50	76.86	.12E-09	1371	464	1.71	0.05
1.49	99.50	145.03	.00E+00	1236	0	0.77	0.00
2.09	99.50	138.93	.00E+00	1220	0	0	0.00
2.69	99.50	134.79	.00E+00	1210	0	0	0.00
3.29	99.50	132.44	.00E+00	1204	0	0	0.00
3.89	99.50	131.84	.00E+00	1202	0	0	0.00
4.49	99.50	131.20	.00E+00	1200	0	0	0.00
5.09	99.50	130.58	.00E+00	1199	0	0	0.00
5.69	99.50	129.99	.00E+00	1197	0	0	0.00
6.29	99.50	129.44	.00E+00	1196	0	0	0.00
6.89	99.50	128.92	.00E+00	1194	0	0	0.00
7.49	99.50	128.43	.00E+00	1193	0	0	0.00
8.09	99.50	127.98	.00E+00	1192	0	0	0.00
8.69	99.50	127.55	.00E+00	1191	0	0	0.00
9.29	99.50	127.16	.00E+00	1190	0	0	0.00
9.89	99.50	126.80	.00E+00	1189	0	0	0.00
10.49	99.50	126.46	.00E+00	1188	0	0	0.00
11.09	99.50	126.17	.00E+00	1187	0	0	0.00
11.69	99.50	125.90	.00E+00	1187	0	0	0.00
12.29	99.50	125.67	.00E+00	1186	0	0	0.00
12.89	99.50	125.48	.00E+00	1186	0	0	0.00

Table E17: *Simulation 1*

CODE=1A : DROPLET DRYING BEHAVIOUR

DROP SIZE = 45.00000 MICRONS

ZDIS(M)	%SOLID	TEMP(C)	NA kg/s	hg(m/s)	hc(m/s)	kg(m/s)	kc(m/s)
0.01	55.12	78.46	.13E-07	5618	0	7.23	0.00
0.03	57.13	57.89	.26E-08	4286	91509	5.40	11.32
0.08	59.13	52.39	.14E-08	3940	45679	4.92	5.55
0.13	61.14	53.55	.11E-08	3529	30070	4.40	3.64
0.18	63.14	55.24	.95E-09	3187	22148	3.98	2.67
0.22	65.15	56.66	.84E-09	2924	17314	3.65	2.08
0.26	67.16	57.87	.75E-09	2724	14069	3.40	1.68
0.29	69.17	58.97	.68E-09	2574	11711	3.21	1.40
0.32	71.17	59.98	.62E-09	2453	9950	3.06	1.18
0.35	73.17	60.92	.57E-09	2348	8562	2.93	1.02
0.38	75.17	61.78	.53E-09	2250	7435	2.81	0.88
0.40	77.17	62.59	.48E-09	2162	6501	2.70	0.77
0.42	79.17	63.40	.45E-09	2083	5709	2.60	0.67
0.45	81.17	64.22	.42E-09	2016	5025	2.52	0.59
0.47	83.17	65.00	.38E-09	1958	4420	2.45	0.52
0.49	85.18	65.55	.35E-09	1812	3883	2.27	0.46
0.51	87.18	66.37	.32E-09	1776	3396	2.22	0.40
0.54	89.18	67.61	.30E-09	1789	2947	2.24	0.35
0.56	91.18	68.97	.28E-09	1803	2525	2.26	0.30
0.58	93.18	70.41	.26E-09	1806	2119	2.26	0.25
0.60	95.18	71.99	.23E-09	1798	1713	2.26	0.20
0.63	97.18	73.93	.19E-09	1785	1280	2.24	0.15
0.66	99.18	77.10	.12E-09	1767	718	2.23	0.09
0.66	99.50	78.01	.11E-09	1763	584	2.22	0.07
1.26	99.50	150.75	.00E+00	1582	0	0	0.00
1.86	99.50	140.84	.00E+00	1549	0	0	0.00
2.46	99.50	136.17	.00E+00	1534	0	0	0.00
3.06	99.50	133.01	.00E+00	1523	0	0	0.00
3.66	99.50	132.06	.00E+00	1520	0	0	0.00
4.26	99.50	131.44	.00E+00	1518	0	0	0.00
4.86	99.50	130.81	.00E+00	1516	0	0	0.00
5.46	99.50	130.21	.00E+00	1514	0	0	0.00
6.06	99.50	129.64	.00E+00	1512	0	0	0.00
6.66	99.50	129.11	.00E+00	1510	0	0	0.00
7.27	99.50	128.61	.00E+00	1509	0	0	0.00
7.87	99.50	128.14	.00E+00	1507	0	0	0.00
8.47	99.50	127.71	.00E+00	1506	0	0	0.00
9.07	99.50	127.30	.00E+00	1504	0	0	0.00
9.67	99.50	126.93	.00E+00	1503	0	0	0.00
10.27	99.50	126.58	.00E+00	1502	0	0	0.00
10.87	99.50	126.27	.00E+00	1501	0	0	0.00
11.47	99.50	126.00	.00E+00	1500	0	0	0.00
12.07	99.50	125.75	.00E+00	1499	0	0	0.00
12.67	99.50	125.54	.00E+00	1499	0	0	0.00

Table E18: *Simulation 1*

CODE=1A : DROPLET DRYING BEHAVIOUR

DROP SIZE = 35.00000 MICRONS

ZDIS(M)	%SOLID	TEMP(C)	NA kg/s	hg(m/s)	hc(m/s)	kg(m/s)	kc(m/s)
0.01	55.18	77.71	.89E-08	6600	0	8.50	0.00
0.03	57.18	57.35	.18E-08	5036	115145	6.35	14.24
0.06	59.19	51.85	.10E-08	4625	58073	5.79	7.07
0.09	61.20	53.05	.82E-09	4226	38281	5.30	4.65
0.13	63.21	54.86	.72E-09	3892	28248	4.88	3.43
0.16	65.23	56.44	.65E-09	3627	22113	4.56	2.68
0.18	67.25	57.81	.59E-09	3420	17983	4.30	2.18
0.21	69.25	59.02	.54E-09	3258	15017	4.10	1.82
0.23	71.29	60.17	.50E-09	3125	12732	3.93	1.54
0.25	73.34	61.23	.46E-09	2999	10929	3.78	1.32
0.27	75.34	62.20	.43E-09	2893	9468	3.65	1.14
0.29	77.34	63.13	.40E-09	2785	8280	3.51	1.00
0.30	79.35	64.00	.37E-09	2691	7272	3.40	0.87
0.32	81.35	64.88	.35E-09	2610	6400	3.30	0.77
0.34	83.35	65.79	.32E-09	2541	5633	3.21	0.68
0.35	85.36	66.74	.30E-09	2484	4947	3.14	0.59
0.37	87.36	67.75	.28E-09	2435	4324	3.08	0.52
0.38	89.37	68.84	.26E-09	2394	3749	3.03	0.45
0.40	91.37	70.03	.24E-09	2360	3207	2.99	0.38
0.41	93.37	71.37	.21E-09	2330	2685	2.95	0.32
0.43	95.37	72.93	.19E-09	2303	2161	2.92	0.26
0.45	97.37	74.97	.15E-09	2279	1596	2.90	0.19
0.47	99.37	78.53	.96E-10	2255	834	2.87	0.10
0.60	99.50	174.82	.00E+00	2150	0	2.26	0.00
1.20	99.50	153.21	.00E+00	2041	0	0	0.00
1.80	99.50	141.37	.00E+00	1991	0	0	0.00
2.40	99.50	136.58	.00E+00	1971	0	0	0.00
3.00	99.50	133.25	.00E+00	1956	0	0	0.00
3.60	99.50	132.12	.00E+00	1952	0	0	0.00
4.20	99.50	131.50	.00E+00	1949	0	0	0.00
4.80	99.50	130.87	.00E+00	1946	0	0	0.00
5.40	99.50	130.27	.00E+00	1944	0	0	0.00
6.00	99.50	129.70	.00E+00	1941	0	0	0.00
6.60	99.50	129.16	.00E+00	1939	0	0	0.00
7.20	99.50	128.66	.00E+00	1937	0	0	0.00
7.80	99.50	128.19	.00E+00	1935	0	0	0.00
8.40	99.50	127.75	.00E+00	1933	0	0	0.00
9.00	99.50	127.34	.00E+00	1931	0	0	0.00
9.60	99.50	126.96	.00E+00	1930	0	0	0.00
10.20	99.50	126.62	.00E+00	1928	0	0	0.00
10.80	99.50	126.30	.00E+00	1927	0	0	0.00
11.40	99.50	126.02	.00E+00	1926	0	0	0.00
12.00	99.50	125.78	.00E+00	1925	0	0	0.00
12.60	99.50	125.56	.00E+00	1924	0	0	0.00

Table E19: *Simulation 2 - Feed Physical Properties and Drop-Size Data*

Physical Properties									
Specific Heat of Dried Product	:	3.7 kJ/kg °C							
Specific Heat of Solution	:	3.98 kJ/kg °C							
Density of Solution	:	1253 kg/m^3							
Measured Droplet-Size-Distribution									
Drop Size (microns)	:	375	215	165	137	102	70	45	35
Weight %	:	10	10	15	11	19	15	14	6

Table E20: *Simulation 2*

CODE=1b : AIR PROPERTIES

ZDIS(M)	TEMP(C)	HUMID(kg/kg)	GAIR(kg/s)	VEL(M/S)	SOLID(%)
0.10	173.02	0.00911	29.46	66.45	0.45
0.20	171.22	0.00995	29.49	49.26	0.45
0.30	169.39	0.01064	29.51	40.55	0.46
0.40	167.50	0.01129	29.53	34.90	0.46
0.50	165.56	0.01193	29.54	30.84	0.47
0.60	158.48	0.01412	29.61	0.79	0.49
0.70	146.62	0.01768	29.71	0.79	0.53
0.80	141.55	0.01930	29.76	0.79	0.55
0.90	135.78	0.02118	29.81	0.79	0.57
1.00	130.77	0.02284	29.86	0.79	0.59
1.10	127.02	0.02391	29.89	0.79	0.61
1.20	123.88	0.02495	29.92	0.79	0.62
1.30	120.82	0.02598	29.95	0.79	0.64
1.40	117.90	0.02696	29.98	0.79	0.65
1.50	115.18	0.02787	30.01	0.79	0.67
1.60	112.77	0.02869	30.03	0.79	0.69
1.70	110.74	0.02938	30.05	0.79	0.70
1.80	109.16	0.02986	30.07	0.79	0.71
1.90	107.90	0.03026	30.08	0.79	0.72
2.40	102.49	0.03208	30.13	0.79	0.76
2.90	98.24	0.03353	30.17	0.79	0.79
3.40	95.09	0.03452	30.20	0.79	0.82
3.90	92.93	0.03526	30.23	0.79	0.84
4.40	91.15	0.03588	30.24	0.79	0.85
4.90	89.75	0.03637	30.26	0.79	0.87
5.40	88.82	0.03664	30.27	0.79	0.88
5.90	88.14	0.03687	30.27	0.79	0.88
6.40	87.52	0.03708	30.28	0.79	0.89
6.91	86.94	0.03728	30.28	0.79	0.90
7.41	86.40	0.03747	30.29	0.79	0.90
7.91	85.90	0.03764	30.29	0.79	0.91
8.41	85.45	0.03780	30.30	0.79	0.91
8.91	85.04	0.03794	30.30	0.79	0.92
9.41	84.68	0.03807	30.31	0.79	0.92
9.91	84.38	0.03817	30.31	0.79	0.93
10.41	84.15	0.03823	30.31	0.79	0.93
10.91	83.98	0.03828	30.31	0.79	0.93
11.41	83.82	0.03834	30.31	0.79	0.93
11.91	83.66	0.03839	30.32	0.79	0.93
12.41	83.51	0.03844	30.32	0.79	0.93
12.91	83.37	0.03849	30.32	0.79	0.94
13.41	83.22	0.03854	30.32	0.79	0.94
13.91	83.08	0.03859	30.32	0.79	0.94
14.41	82.94	0.03864	30.32	0.79	0.94
14.91	82.80	0.03869	30.33	0.79	0.94
15.41	82.67	0.03873	30.33	0.79	0.95
15.91	82.54	0.03878	30.33	0.79	0.95
16.41	82.41	0.03882	30.33	0.79	0.95
16.91	82.28	0.03887	30.33	0.79	0.95
17.41	82.16	0.03891	30.33	0.79	0.95
17.91	82.03	0.03895	30.33	0.79	0.95
18.41	81.91	0.03899	30.33	0.79	0.95
18.91	81.80	0.03904	30.34	0.79	0.96
19.41	81.68	0.03908	30.34	0.79	0.96
19.91	81.57	0.03912	30.34	0.79	0.96

Table E21: *Simulation 2*

CODE-1b : DROPLET TRAJECTORY

DROP SIZE = 375.0000 MICRONS

Rvel(m/s)	Tvel(m/s)	Zvel(m/s)	RDIS(M)	THETA(0)	ZDIS(M)	REN NO.	TIME(S)
79.24	0.00	55.48	0.01	0.00	0.01	1389.72	0.00
62.42	0.00	57.75	0.36	0.00	0.30	1019.91	0.01
49.45	0.00	50.33	0.67	0.00	0.60	1093.35	0.01
38.46	0.00	39.38	0.96	0.00	0.90	753.70	0.02
29.66	0.00	30.62	1.25	0.00	1.20	614.13	0.03
22.68	0.00	23.69	1.54	0.00	1.50	489.42	0.04
16.75	0.00	17.83	1.83	0.00	1.80	373.38	0.05
11.79	0.00	12.95	2.10	0.00	2.10	269.18	0.07
7.81	0.00	9.07	2.37	0.00	2.40	183.56	0.10
4.81	0.00	6.20	2.62	0.00	2.70	118.28	0.14
2.74	0.00	4.32	2.83	0.00	3.00	73.75	0.20
1.47	0.00	3.28	2.99	0.00	3.30	48.21	0.28
0.77	0.00	2.82	3.10	0.00	3.60	36.44	0.38
0.40	0.00	2.64	3.16	0.00	3.90	32.03	0.49
0.21	0.00	2.58	3.20	0.00	4.20	30.57	0.60
0.11	0.00	2.55	3.21	0.00	4.50	30.08	0.72
0.05	0.00	2.53	3.22	0.00	4.80	29.88	0.84
0.03	0.00	2.52	3.23	0.00	5.10	29.76	0.96
0.01	0.00	2.51	3.23	0.00	5.40	29.64	1.08
0.01	0.00	2.50	3.23	0.00	5.70	29.53	1.20
0.00	0.00	2.49	3.23	0.00	6.00	29.41	1.32
0.00	0.00	2.48	3.23	0.00	6.30	29.30	1.44
0.00	0.00	2.47	3.23	0.00	6.60	29.19	1.56
0.00	0.00	2.46	3.23	0.00	6.90	29.08	1.68
0.00	0.00	2.45	3.23	0.00	7.20	28.96	1.80
0.00	0.00	2.44	3.23	0.00	7.50	28.85	1.93
0.00	0.00	2.43	3.23	0.00	7.80	28.74	2.05
0.00	0.00	2.42	3.23	0.00	8.10	28.62	2.17
0.00	0.00	2.41	3.23	0.00	8.40	28.51	2.30
0.00	0.00	2.41	3.23	0.00	8.70	28.39	2.42
0.00	0.00	2.40	3.23	0.00	9.00	28.27	2.55
0.00	0.00	2.39	3.23	0.00	9.30	28.16	2.67
0.00	0.00	2.38	3.23	0.00	9.60	28.04	2.80
0.00	0.00	2.37	3.23	0.00	9.90	27.92	2.92
0.00	0.00	2.36	3.23	0.00	10.20	27.79	3.05
0.00	0.00	2.36	3.23	0.00	10.51	27.67	3.18
0.00	0.00	2.35	3.23	0.00	10.81	27.54	3.31
0.00	0.00	2.34	3.23	0.00	11.11	27.42	3.43
0.00	0.00	2.33	3.23	0.00	11.41	27.29	3.56
0.00	0.00	2.32	3.23	0.00	11.71	27.17	3.69
0.00	0.00	2.32	3.23	0.00	12.01	27.04	3.82
0.00	0.00	2.31	3.23	0.00	12.31	26.92	3.95
0.00	0.00	2.30	3.23	0.00	12.61	26.80	4.08
0.00	0.00	2.29	3.23	0.00	12.91	26.68	4.21
0.00	0.00	2.29	3.23	0.00	13.21	26.56	4.34
0.00	0.00	2.28	3.23	0.00	13.51	26.44	4.48
0.00	0.00	2.27	3.23	0.00	13.81	26.32	4.61
0.00	0.00	2.27	3.23	0.00	14.11	26.20	4.74
0.00	0.00	2.26	3.23	0.00	14.41	26.08	4.87
0.00	0.00	2.25	3.23	0.00	14.71	25.97	5.01
0.00	0.00	2.24	3.23	0.00	15.01	25.85	5.14
0.00	0.00	2.24	3.23	0.00	15.31	25.74	5.27
0.00	0.00	2.23	3.23	0.00	15.61	25.62	5.41
0.00	0.00	2.22	3.23	0.00	15.91	25.51	5.54
0.00	0.00	2.22	3.23	0.00	16.21	25.40	5.68
0.00	0.00	2.21	3.23	0.00	16.51	25.29	5.81
0.00	0.00	2.20	3.23	0.00	16.81	25.18	5.95
0.00	0.00	2.20	3.23	0.00	17.11	25.07	6.09

Table E22: *Simulation 2*

CODE=1b : DROPLET TRAJECTORY

DROP SIZE = 215.0000 MICRONS

Rvel(m/s)	Tvel(m/s)	Zvel(m/s)	RDIS(M)	THETA(0)	ZDIS(M)	REN NO.	TIME(S)
79.24	0.00	55.48	0.01	0.00	0.01	796.78	0.00
54.10	0.00	58.79	0.33	0.00	0.30	515.68	0.00
37.21	0.00	47.07	0.58	0.00	0.60	531.84	0.01
22.66	0.00	29.04	0.81	0.00	0.90	287.25	0.02
11.72	0.00	15.50	1.04	0.00	1.20	157.55	0.03
4.56	0.00	6.70	1.26	0.00	1.50	65.00	0.06
1.12	0.00	2.67	1.43	0.00	1.80	19.63	0.14
0.21	0.00	1.85	1.51	0.00	2.10	9.86	0.28
0.04	0.00	1.76	1.52	0.00	2.40	9.00	0.45
0.01	0.00	1.73	1.53	0.00	2.70	8.85	0.62
0.00	0.00	1.71	1.53	0.00	3.00	8.73	0.79
0.00	0.00	1.69	1.53	0.00	3.30	8.61	0.97
0.00	0.00	1.67	1.53	0.00	3.60	8.48	1.15
0.00	0.00	1.65	1.53	0.00	3.90	8.35	1.33
0.00	0.00	1.63	1.53	0.00	4.20	8.21	1.51
0.00	0.00	1.61	1.53	0.00	4.50	8.08	1.70
0.00	0.00	1.60	1.53	0.00	4.80	7.95	1.88
0.00	0.00	1.58	1.53	0.00	5.10	7.82	2.07
0.00	0.00	1.57	1.53	0.00	5.40	7.69	2.26
0.00	0.00	1.55	1.53	0.00	5.70	7.56	2.46
0.00	0.00	1.54	1.53	0.00	6.00	7.43	2.65
0.00	0.00	1.52	1.53	0.00	6.30	7.31	2.85
0.00	0.00	1.51	1.53	0.00	6.60	7.19	3.04
0.00	0.00	1.50	1.53	0.00	6.90	7.08	3.24
0.00	0.00	1.49	1.53	0.00	7.20	6.97	3.44
0.00	0.00	1.47	1.53	0.00	7.50	6.87	3.65
0.00	0.00	1.46	1.53	0.00	7.80	6.77	3.85
0.00	0.00	1.45	1.53	0.00	8.10	6.68	4.06
0.00	0.00	1.44	1.53	0.00	8.40	6.59	4.26
0.00	0.00	1.44	1.53	0.00	8.70	6.52	4.47
0.00	0.00	1.43	1.53	0.00	9.00	6.45	4.68
0.00	0.00	1.42	1.53	0.00	9.30	6.39	4.89
0.00	0.00	1.41	1.53	0.00	9.60	6.33	5.11
0.00	0.00	1.41	1.53	0.00	9.90	6.29	5.32
0.00	0.00	1.41	1.53	0.00	10.20	6.28	5.53
0.00	0.00	1.41	1.53	0.00	10.51	6.28	5.75
0.00	0.00	1.41	1.53	0.00	10.81	6.29	5.96
0.00	0.00	1.41	1.53	0.00	11.11	6.29	6.17
0.00	0.00	1.41	1.53	0.00	11.41	6.29	6.39
0.00	0.00	1.41	1.53	0.00	11.71	6.30	6.60
0.00	0.00	1.41	1.53	0.00	12.01	6.30	6.81
0.00	0.00	1.41	1.53	0.00	12.31	6.30	7.03
0.00	0.00	1.41	1.53	0.00	12.61	6.30	7.24
0.00	0.00	1.41	1.53	0.00	12.91	6.31	7.45
0.00	0.00	1.41	1.53	0.00	13.21	6.31	7.66
0.00	0.00	1.41	1.53	0.00	13.51	6.31	7.88
0.00	0.00	1.41	1.53	0.00	13.81	6.31	8.09
0.00	0.00	1.41	1.53	0.00	14.11	6.32	8.30
0.00	0.00	1.41	1.53	0.00	14.41	6.32	8.52
0.00	0.00	1.41	1.53	0.00	14.71	6.32	8.73
0.00	0.00	1.41	1.53	0.00	15.01	6.32	8.94
0.00	0.00	1.41	1.53	0.00	15.31	6.33	9.16
0.00	0.00	1.41	1.53	0.00	15.61	6.33	9.37
0.00	0.00	1.41	1.53	0.00	15.91	6.33	9.58
0.00	0.00	1.41	1.53	0.00	16.21	6.33	9.80
0.00	0.00	1.41	1.53	0.00	16.51	6.34	10.01
0.00	0.00	1.41	1.53	0.00	16.81	6.34	10.22
0.00	0.00	1.41	1.53	0.00	17.11	6.34	10.44

Table E23: *Simulation 2*

CODE-1b : DROPLET TRAJECTORY

DROP SIZE = 165.0000 MICRONS

Rvel(m/s)	Tvel(m/s)	Zvel(m/s)	RDIS(M)	THETA(0)	ZDIS(M)	REN NO.	TIME(S)
79.24	0.00	55.48	0.01	0.00	0.01	611.48	0.00
47.31	0.00	58.96	0.30	0.00	0.30	351.89	0.00
27.76	0.00	42.99	0.51	0.00	0.60	347.18	0.01
12.35	0.00	19.64	0.70	0.00	0.90	137.21	0.02
3.29	0.00	5.97	0.88	0.00	1.20	39.53	0.05
0.34	0.00	1.79	1.00	0.00	1.50	7.04	0.16
0.02	0.00	1.48	1.02	0.00	1.80	4.75	0.35
0.00	0.00	1.42	1.02	0.00	2.10	4.42	0.55
0.00	0.00	1.38	1.02	0.00	2.40	4.19	0.77
0.00	0.00	1.34	1.02	0.00	2.70	3.98	0.99
0.00	0.00	1.31	1.02	0.00	3.00	3.78	1.22
0.00	0.00	1.28	1.02	0.00	3.30	3.59	1.45
0.00	0.00	1.25	1.02	0.00	3.60	3.42	1.68
0.00	0.00	1.23	1.02	0.00	3.90	3.26	1.93
0.00	0.00	1.20	1.02	0.00	4.20	3.12	2.17
0.00	0.00	1.19	1.02	0.00	4.50	3.00	2.42
0.00	0.00	1.17	1.02	0.00	4.80	2.91	2.68
0.00	0.00	1.17	1.02	0.00	5.10	2.86	2.94
0.00	0.00	1.17	1.02	0.00	5.40	2.87	3.19
0.00	0.00	1.17	1.02	0.00	5.70	2.88	3.45
0.00	0.00	1.17	1.02	0.00	6.00	2.89	3.71
0.00	0.00	1.17	1.02	0.00	6.30	2.89	3.96
0.00	0.00	1.17	1.02	0.00	6.60	2.90	4.22
0.00	0.00	1.17	1.02	0.00	6.90	2.91	4.48
0.00	0.00	1.17	1.02	0.00	7.20	2.91	4.74
0.00	0.00	1.17	1.02	0.00	7.50	2.92	4.99
0.00	0.00	1.17	1.02	0.00	7.80	2.93	5.25
0.00	0.00	1.17	1.02	0.00	8.10	2.93	5.51
0.00	0.00	1.17	1.02	0.00	8.40	2.94	5.76
0.00	0.00	1.17	1.02	0.00	8.70	2.94	6.02
0.00	0.00	1.17	1.02	0.00	9.00	2.95	6.28
0.00	0.00	1.17	1.02	0.00	9.30	2.95	6.53
0.00	0.00	1.17	1.02	0.00	9.60	2.96	6.79
0.00	0.00	1.17	1.02	0.00	9.90	2.96	7.05
0.00	0.00	1.17	1.02	0.00	10.20	2.96	7.31
0.00	0.00	1.17	1.02	0.00	10.51	2.97	7.56
0.00	0.00	1.17	1.02	0.00	10.81	2.97	7.82
0.00	0.00	1.17	1.02	0.00	11.11	2.97	8.08
0.00	0.00	1.17	1.02	0.00	11.41	2.97	8.33
0.00	0.00	1.17	1.02	0.00	11.71	2.98	8.59
0.00	0.00	1.17	1.02	0.00	12.01	2.98	8.85
0.00	0.00	1.17	1.02	0.00	12.31	2.98	9.10
0.00	0.00	1.17	1.02	0.00	12.61	2.98	9.36
0.00	0.00	1.17	1.02	0.00	12.91	2.98	9.62
0.00	0.00	1.17	1.02	0.00	13.21	2.98	9.87
0.00	0.00	1.17	1.02	0.00	13.51	2.99	10.13
0.00	0.00	1.17	1.02	0.00	13.81	2.99	10.39
0.00	0.00	1.17	1.02	0.00	14.11	2.99	10.64
0.00	0.00	1.17	1.02	0.00	14.41	2.99	10.90
0.00	0.00	1.17	1.02	0.00	14.71	2.99	11.16
0.00	0.00	1.17	1.02	0.00	15.01	3.00	11.42
0.00	0.00	1.17	1.02	0.00	15.31	3.00	11.67
0.00	0.00	1.17	1.02	0.00	15.61	3.00	11.93
0.00	0.00	1.17	1.02	0.00	15.91	3.00	12.19
0.00	0.00	1.17	1.02	0.00	16.21	3.00	12.44
0.00	0.00	1.17	1.02	0.00	16.51	3.00	12.70
0.00	0.00	1.17	1.02	0.00	16.81	3.01	12.96
0.00	0.00	1.17	1.02	0.00	17.11	3.01	13.21

Table E24: *Simulation 2*

CODE-1b : DROPLET TRAJECTORY

DROP SIZE = 137.0000 MICRONS

Rvel(m/s)	Tvel(m/s)	Zvel(m/s)	RDIS(M)	THETA(0)	ZDIS(M)	REN NO.	TIME(S)
79.24	0.00	55.48	0.01	0.00	0.01	507.71	0.00
41.44	0.00	59.08	0.28	0.00	0.30	261.30	0.00
20.88	0.00	39.23	0.46	0.00	0.60	249.71	0.01
6.30	0.00	12.46	0.61	0.00	0.90	67.07	0.02
0.53	0.00	2.07	0.74	0.00	1.20	7.45	0.09
0.01	0.00	1.23	0.77	0.00	1.50	2.48	0.30
0.00	0.00	1.18	0.77	0.00	1.80	2.24	0.55
0.00	0.00	1.14	0.77	0.00	2.10	2.03	0.81
0.00	0.00	1.10	0.77	0.00	2.40	1.85	1.08
0.00	0.00	1.07	0.77	0.00	2.70	1.70	1.36
0.00	0.00	1.05	0.77	0.00	3.00	1.60	1.64
0.00	0.00	1.04	0.77	0.00	3.30	1.57	1.92
0.00	0.00	1.04	0.77	0.00	3.60	1.58	2.21
0.00	0.00	1.05	0.77	0.00	3.90	1.60	2.50
0.00	0.00	1.05	0.77	0.00	4.20	1.61	2.79
0.00	0.00	1.05	0.77	0.00	4.50	1.62	3.07
0.00	0.00	1.05	0.77	0.00	4.80	1.63	3.36
0.00	0.00	1.05	0.77	0.00	5.10	1.64	3.64
0.00	0.00	1.05	0.77	0.00	5.40	1.64	3.93
0.00	0.00	1.05	0.77	0.00	5.70	1.65	4.22
0.00	0.00	1.05	0.77	0.00	6.00	1.65	4.50
0.00	0.00	1.05	0.77	0.00	6.30	1.66	4.79
0.00	0.00	1.05	0.77	0.00	6.60	1.66	5.07
0.00	0.00	1.05	0.77	0.00	6.90	1.66	5.36
0.00	0.00	1.05	0.77	0.00	7.20	1.67	5.65
0.00	0.00	1.05	0.77	0.00	7.50	1.67	5.93
0.00	0.00	1.05	0.77	0.00	7.80	1.68	6.22
0.00	0.00	1.05	0.77	0.00	8.10	1.68	6.50
0.00	0.00	1.05	0.77	0.00	8.40	1.68	6.79
0.00	0.00	1.05	0.77	0.00	8.70	1.69	7.08
0.00	0.00	1.05	0.77	0.00	9.00	1.69	7.36
0.00	0.00	1.05	0.77	0.00	9.30	1.69	7.65
0.00	0.00	1.05	0.77	0.00	9.60	1.69	7.93
0.00	0.00	1.05	0.77	0.00	9.90	1.70	8.22
0.00	0.00	1.05	0.77	0.00	10.20	1.70	8.51
0.00	0.00	1.05	0.77	0.00	10.51	1.70	8.79
0.00	0.00	1.05	0.77	0.00	10.81	1.70	9.08
0.00	0.00	1.05	0.77	0.00	11.11	1.70	9.36
0.00	0.00	1.05	0.77	0.00	11.41	1.70	9.65
0.00	0.00	1.05	0.77	0.00	11.71	1.70	9.94
0.00	0.00	1.05	0.77	0.00	12.01	1.70	10.22
0.00	0.00	1.05	0.77	0.00	12.31	1.71	10.51
0.00	0.00	1.05	0.77	0.00	12.61	1.71	10.79
0.00	0.00	1.05	0.77	0.00	12.91	1.71	11.08
0.00	0.00	1.05	0.77	0.00	13.21	1.71	11.37
0.00	0.00	1.05	0.77	0.00	13.51	1.71	11.65
0.00	0.00	1.05	0.77	0.00	13.81	1.71	11.94
0.00	0.00	1.05	0.77	0.00	14.11	1.71	12.22
0.00	0.00	1.05	0.77	0.00	14.41	1.71	12.51
0.00	0.00	1.05	0.77	0.00	14.71	1.71	12.80
0.00	0.00	1.05	0.77	0.00	15.01	1.71	13.08
0.00	0.00	1.05	0.77	0.00	15.31	1.72	13.37
0.00	0.00	1.05	0.77	0.00	15.61	1.72	13.65
0.00	0.00	1.05	0.77	0.00	15.91	1.72	13.94
0.00	0.00	1.05	0.77	0.00	16.21	1.72	14.23
0.00	0.00	1.05	0.77	0.00	16.51	1.72	14.51
0.00	0.00	1.05	0.77	0.00	16.81	1.72	14.80
0.00	0.00	1.05	0.77	0.00	17.11	1.72	15.08

Table E25: *Simulation 2*

CODE-1b : DROPLET TRAJECTORY

DROP SIZE = 102.0000 MICRONS

Rvel(m/s)	Tvel(m/s)	Zvel(m/s)	RDIS(M)	THETA(0)	ZDIS(M)	REN NO.	TIME(S)
79.24	0.00	55.48	0.01	0.00	0.01	378.00	0.00
31.46	0.00	59.14	0.24	0.00	0.30	156.59	0.00
11.26	0.00	31.68	0.36	0.00	0.60	139.71	0.01
0.77	0.00	3.05	0.46	0.00	0.90	9.01	0.04
0.00	0.00	0.99	0.48	0.00	1.20	0.82	0.29
0.00	0.00	0.95	0.48	0.00	1.50	0.66	0.60
0.00	0.00	0.93	0.48	0.00	1.80	0.59	0.92
0.00	0.00	0.93	0.48	0.00	2.10	0.60	1.25
0.00	0.00	0.93	0.48	0.00	2.40	0.62	1.57
0.00	0.00	0.93	0.48	0.00	2.70	0.63	1.89
0.00	0.00	0.93	0.48	0.00	3.00	0.64	2.22
0.00	0.00	0.93	0.48	0.00	3.30	0.65	2.54
0.00	0.00	0.93	0.48	0.00	3.60	0.65	2.86
0.00	0.00	0.93	0.48	0.00	3.90	0.66	3.18
0.00	0.00	0.93	0.48	0.00	4.20	0.66	3.50
0.00	0.00	0.93	0.48	0.00	4.50	0.67	3.83
0.00	0.00	0.93	0.48	0.00	4.80	0.67	4.15
0.00	0.00	0.93	0.48	0.00	5.10	0.68	4.47
0.00	0.00	0.93	0.48	0.00	5.40	0.68	4.79
0.00	0.00	0.93	0.48	0.00	5.70	0.68	5.11
0.00	0.00	0.93	0.48	0.00	6.00	0.68	5.44
0.00	0.00	0.93	0.48	0.00	6.30	0.68	5.76
0.00	0.00	0.93	0.48	0.00	6.60	0.69	6.08
0.00	0.00	0.93	0.48	0.00	6.90	0.69	6.40
0.00	0.00	0.93	0.48	0.00	7.20	0.69	6.72
0.00	0.00	0.93	0.48	0.00	7.50	0.69	7.05
0.00	0.00	0.93	0.48	0.00	7.80	0.69	7.37
0.00	0.00	0.93	0.48	0.00	8.10	0.69	7.69
0.00	0.00	0.93	0.48	0.00	8.40	0.69	8.01
0.00	0.00	0.93	0.48	0.00	8.70	0.70	8.33
0.00	0.00	0.93	0.48	0.00	9.00	0.70	8.66
0.00	0.00	0.93	0.48	0.00	9.30	0.70	8.98
0.00	0.00	0.93	0.48	0.00	9.60	0.70	9.30
0.00	0.00	0.93	0.48	0.00	9.90	0.70	9.62
0.00	0.00	0.93	0.48	0.00	10.20	0.70	9.94
0.00	0.00	0.93	0.48	0.00	10.51	0.70	10.27
0.00	0.00	0.93	0.48	0.00	10.81	0.70	10.59
0.00	0.00	0.93	0.48	0.00	11.11	0.70	10.91
0.00	0.00	0.93	0.48	0.00	11.41	0.70	11.23
0.00	0.00	0.93	0.48	0.00	11.71	0.70	11.55
0.00	0.00	0.93	0.48	0.00	12.01	0.70	11.88
0.00	0.00	0.93	0.48	0.00	12.31	0.70	12.20
0.00	0.00	0.93	0.48	0.00	12.61	0.70	12.52
0.00	0.00	0.93	0.48	0.00	12.91	0.70	12.84
0.00	0.00	0.93	0.48	0.00	13.21	0.71	13.16
0.00	0.00	0.93	0.48	0.00	13.51	0.71	13.49
0.00	0.00	0.93	0.48	0.00	13.81	0.71	13.81
0.00	0.00	0.93	0.48	0.00	14.11	0.71	14.13
0.00	0.00	0.93	0.48	0.00	14.41	0.71	14.45
0.00	0.00	0.93	0.48	0.00	14.71	0.71	14.78
0.00	0.00	0.93	0.48	0.00	15.01	0.71	15.10
0.00	0.00	0.93	0.48	0.00	15.31	0.71	15.42
0.00	0.00	0.93	0.48	0.00	15.61	0.71	15.74
0.00	0.00	0.93	0.48	0.00	15.91	0.71	16.06
0.00	0.00	0.93	0.48	0.00	16.21	0.71	16.39
0.00	0.00	0.93	0.48	0.00	16.51	0.71	16.71
0.00	0.00	0.93	0.48	0.00	16.81	0.71	17.03
0.00	0.00	0.93	0.48	0.00	17.11	0.71	17.35

Table E26: *Simulation 2*

CODE=1b : DROPLET TRAJECTORY

DROP SIZE = 70.00000 MICRONS

Rvel(m/s)	Tvel(m/s)	Zvel(m/s)	RDIS(M)	THETA(0)	ZDIS(M)	REN NO.	TIME(S)
79.24	0.00	55.48	0.01	0.00	0.01	259.42	0.00
19.12	0.00	58.27	0.18	0.00	0.30	76.63	0.00
3.14	0.00	18.72	0.25	0.00	0.60	53.10	0.01
0.00	0.00	0.86	0.27	0.00	0.90	0.20	0.21
0.00	0.00	0.85	0.27	0.00	1.20	0.17	0.56
0.00	0.00	0.85	0.27	0.00	1.50	0.18	0.91
0.00	0.00	0.85	0.27	0.00	1.80	0.19	1.27
0.00	0.00	0.85	0.27	0.00	2.10	0.19	1.62
0.00	0.00	0.85	0.27	0.00	2.40	0.20	1.97
0.00	0.00	0.85	0.27	0.00	2.70	0.20	2.32
0.00	0.00	0.85	0.27	0.00	3.00	0.21	2.67
0.00	0.00	0.85	0.27	0.00	3.30	0.21	3.02
0.00	0.00	0.85	0.27	0.00	3.60	0.21	3.37
0.00	0.00	0.85	0.27	0.00	3.90	0.21	3.72
0.00	0.00	0.85	0.27	0.00	4.20	0.21	4.07
0.00	0.00	0.85	0.27	0.00	4.50	0.22	4.43
0.00	0.00	0.85	0.27	0.00	4.80	0.22	4.78
0.00	0.00	0.86	0.27	0.00	5.10	0.22	5.13
0.00	0.00	0.86	0.27	0.00	5.40	0.22	5.48
0.00	0.00	0.86	0.27	0.00	5.70	0.22	5.83
0.00	0.00	0.86	0.27	0.00	6.00	0.22	6.18
0.00	0.00	0.86	0.27	0.00	6.30	0.22	6.53
0.00	0.00	0.86	0.27	0.00	6.60	0.22	6.88
0.00	0.00	0.86	0.27	0.00	6.90	0.22	7.23
0.00	0.00	0.86	0.27	0.00	7.20	0.22	7.58
0.00	0.00	0.86	0.27	0.00	7.50	0.22	7.94
0.00	0.00	0.86	0.27	0.00	7.80	0.22	8.29
0.00	0.00	0.86	0.27	0.00	8.10	0.22	8.64
0.00	0.00	0.86	0.27	0.00	8.40	0.22	8.99
0.00	0.00	0.86	0.27	0.00	8.70	0.22	9.34
0.00	0.00	0.86	0.27	0.00	9.00	0.23	9.69
0.00	0.00	0.86	0.27	0.00	9.30	0.23	10.04
0.00	0.00	0.86	0.27	0.00	9.60	0.23	10.39
0.00	0.00	0.86	0.27	0.00	9.90	0.23	10.74
0.00	0.00	0.86	0.27	0.00	10.20	0.23	11.10
0.00	0.00	0.86	0.27	0.00	10.51	0.23	11.45
0.00	0.00	0.86	0.27	0.00	10.81	0.23	11.80
0.00	0.00	0.86	0.27	0.00	11.11	0.23	12.15
0.00	0.00	0.86	0.27	0.00	11.41	0.23	12.50
0.00	0.00	0.86	0.27	0.00	11.71	0.23	12.85
0.00	0.00	0.86	0.27	0.00	12.01	0.23	13.20
0.00	0.00	0.86	0.27	0.00	12.31	0.23	13.56
0.00	0.00	0.86	0.27	0.00	12.61	0.23	13.91
0.00	0.00	0.86	0.27	0.00	12.91	0.23	14.26
0.00	0.00	0.86	0.27	0.00	13.21	0.23	14.61
0.00	0.00	0.86	0.27	0.00	13.51	0.23	14.96
0.00	0.00	0.86	0.27	0.00	13.81	0.23	15.31
0.00	0.00	0.86	0.27	0.00	14.11	0.23	15.66
0.00	0.00	0.86	0.27	0.00	14.41	0.23	16.01
0.00	0.00	0.86	0.27	0.00	14.71	0.23	16.36
0.00	0.00	0.86	0.27	0.00	15.01	0.23	16.71
0.00	0.00	0.86	0.27	0.00	15.31	0.23	17.07
0.00	0.00	0.86	0.27	0.00	15.61	0.23	17.42
0.00	0.00	0.86	0.27	0.00	15.91	0.23	17.77
0.00	0.00	0.86	0.27	0.00	16.21	0.23	18.12
0.00	0.00	0.86	0.27	0.00	16.51	0.23	18.47
0.00	0.00	0.86	0.27	0.00	16.81	0.23	18.82
0.00	0.00	0.86	0.27	0.00	17.11	0.23	19.17

Table E27: *Simulation 2*

CODE-1b : DROPLET TRAJECTORY

DROP SIZE = 45.00000 MICRONS

Rvel(m/s)	Tvel(m/s)	Zvel(m/s)	RDIS(M)	THETA(0)	ZDIS(M)	REN NO.	TIME(S)
79.24	0.00	55.48	0.01	0.00	0.01	166.77	0.00
7.76	0.00	54.83	0.12	0.00	0.30	30.66	0.00
0.10	0.00	3.11	0.14	0.00	0.60	4.37	0.02
0.00	0.00	0.81	0.14	0.00	0.90	0.04	0.37
0.00	0.00	0.81	0.14	0.00	1.20	0.05	0.74
0.00	0.00	0.81	0.14	0.00	1.50	0.05	1.11
0.00	0.00	0.81	0.14	0.00	1.80	0.05	1.48
0.00	0.00	0.81	0.14	0.00	2.10	0.05	1.85
0.00	0.00	0.81	0.14	0.00	2.40	0.05	2.22
0.00	0.00	0.81	0.14	0.00	2.70	0.05	2.59
0.00	0.00	0.81	0.14	0.00	3.00	0.05	2.95
0.00	0.00	0.81	0.14	0.00	3.30	0.06	3.32
0.00	0.00	0.81	0.14	0.00	3.60	0.06	3.69
0.00	0.00	0.81	0.14	0.00	3.90	0.06	4.06
0.00	0.00	0.81	0.14	0.00	4.20	0.06	4.42
0.00	0.00	0.82	0.14	0.00	4.50	0.06	4.79
0.00	0.00	0.82	0.14	0.00	4.80	0.06	5.16
0.00	0.00	0.82	0.14	0.00	5.10	0.06	5.53
0.00	0.00	0.82	0.14	0.00	5.40	0.06	5.90
0.00	0.00	0.82	0.14	0.00	5.70	0.06	6.27
0.00	0.00	0.82	0.14	0.00	6.00	0.06	6.63
0.00	0.00	0.82	0.14	0.00	6.30	0.06	7.00
0.00	0.00	0.82	0.14	0.00	6.60	0.06	7.37
0.00	0.00	0.82	0.14	0.00	6.90	0.06	7.74
0.00	0.00	0.82	0.14	0.00	7.20	0.06	8.11
0.00	0.00	0.82	0.14	0.00	7.50	0.06	8.47
0.00	0.00	0.82	0.14	0.00	7.80	0.06	8.84
0.00	0.00	0.82	0.14	0.00	8.10	0.06	9.21
0.00	0.00	0.82	0.14	0.00	8.40	0.06	9.58
0.00	0.00	0.82	0.14	0.00	8.70	0.06	9.95
0.00	0.00	0.82	0.14	0.00	9.00	0.06	10.32
0.00	0.00	0.82	0.14	0.00	9.30	0.06	10.68
0.00	0.00	0.82	0.14	0.00	9.60	0.06	11.05
0.00	0.00	0.82	0.14	0.00	9.90	0.06	11.42
0.00	0.00	0.82	0.14	0.00	10.20	0.06	11.79
0.00	0.00	0.82	0.14	0.00	10.51	0.06	12.16
0.00	0.00	0.82	0.14	0.00	10.81	0.06	12.53
0.00	0.00	0.82	0.14	0.00	11.11	0.06	12.90
0.00	0.00	0.82	0.14	0.00	11.41	0.06	13.26
0.00	0.00	0.82	0.14	0.00	11.71	0.06	13.63
0.00	0.00	0.82	0.14	0.00	12.01	0.06	14.00
0.00	0.00	0.82	0.14	0.00	12.31	0.06	14.37
0.00	0.00	0.82	0.14	0.00	12.61	0.06	14.74
0.00	0.00	0.82	0.14	0.00	12.91	0.06	15.11
0.00	0.00	0.82	0.14	0.00	13.21	0.06	15.47
0.00	0.00	0.82	0.14	0.00	13.51	0.06	15.84
0.00	0.00	0.82	0.14	0.00	13.81	0.06	16.21
0.00	0.00	0.82	0.14	0.00	14.11	0.06	16.58
0.00	0.00	0.82	0.14	0.00	14.41	0.06	16.95
0.00	0.00	0.82	0.14	0.00	14.71	0.06	17.32
0.00	0.00	0.82	0.14	0.00	15.01	0.06	17.68
0.00	0.00	0.82	0.14	0.00	15.31	0.06	18.05
0.00	0.00	0.82	0.14	0.00	15.61	0.06	18.42
0.00	0.00	0.82	0.14	0.00	15.91	0.06	18.79
0.00	0.00	0.82	0.14	0.00	16.21	0.06	19.16
0.00	0.00	0.82	0.14	0.00	16.51	0.06	19.52
0.00	0.00	0.82	0.14	0.00	16.81	0.06	19.89
0.00	0.00	0.82	0.14	0.00	17.11	0.06	20.26

Table E28: *Simulation 2*

CODE-1b : DROPLET TRAJECTORY

DROP SIZE = 35.00000 MICRONS

Rvel(m/s)	Tvel(m/s)	Zvel(m/s)	RDIS(M)	THETA(0)	ZDIS(M)	REN NO.	TIME(S)
79.24	0.00	55.48	0.01	0.00	0.01	129.71	0.00
3.64	0.00	51.80	0.09	0.00	0.30	17.33	0.00
0.00	0.00	0.81	0.10	0.00	0.60	0.03	0.05
0.00	0.00	0.80	0.10	0.00	0.90	0.02	0.42
0.00	0.00	0.80	0.10	0.00	1.20	0.02	0.80
0.00	0.00	0.80	0.10	0.00	1.50	0.02	1.17
0.00	0.00	0.80	0.10	0.00	1.80	0.02	1.54
0.00	0.00	0.80	0.10	0.00	2.10	0.02	1.92
0.00	0.00	0.80	0.10	0.00	2.40	0.02	2.29
0.00	0.00	0.80	0.10	0.00	2.70	0.03	2.66
0.00	0.00	0.80	0.10	0.00	3.00	0.03	3.04
0.00	0.00	0.80	0.10	0.00	3.30	0.03	3.41
0.00	0.00	0.80	0.10	0.00	3.60	0.03	3.78
0.00	0.00	0.80	0.10	0.00	3.90	0.03	4.16
0.00	0.00	0.80	0.10	0.00	4.20	0.03	4.53
0.00	0.00	0.80	0.10	0.00	4.50	0.03	4.90
0.00	0.00	0.80	0.10	0.00	4.80	0.03	5.27
0.00	0.00	0.80	0.10	0.00	5.10	0.03	5.64
0.00	0.00	0.80	0.10	0.00	5.40	0.03	6.01
0.00	0.00	0.80	0.10	0.00	5.70	0.03	6.39
0.00	0.00	0.80	0.10	0.00	6.00	0.03	6.76
0.00	0.00	0.80	0.10	0.00	6.30	0.03	7.13
0.00	0.00	0.80	0.10	0.00	6.60	0.03	7.51
0.00	0.00	0.80	0.10	0.00	6.90	0.03	7.88
0.00	0.00	0.80	0.10	0.00	7.20	0.03	8.25
0.00	0.00	0.80	0.10	0.00	7.50	0.03	8.63
0.00	0.00	0.80	0.10	0.00	7.80	0.03	9.00
0.00	0.00	0.80	0.10	0.00	8.10	0.03	9.37
0.00	0.00	0.80	0.10	0.00	8.40	0.03	9.75
0.00	0.00	0.80	0.10	0.00	8.70	0.03	10.12
0.00	0.00	0.80	0.10	0.00	9.00	0.03	10.49
0.00	0.00	0.80	0.10	0.00	9.30	0.03	10.87
0.00	0.00	0.80	0.10	0.00	9.60	0.03	11.24
0.00	0.00	0.80	0.10	0.00	9.90	0.03	11.61
0.00	0.00	0.80	0.10	0.00	10.20	0.03	11.99
0.00	0.00	0.80	0.10	0.00	10.51	0.03	12.36
0.00	0.00	0.80	0.10	0.00	10.81	0.03	12.74
0.00	0.00	0.80	0.10	0.00	11.11	0.03	13.11
0.00	0.00	0.80	0.10	0.00	11.41	0.03	13.48
0.00	0.00	0.80	0.10	0.00	11.71	0.03	13.86
0.00	0.00	0.80	0.10	0.00	12.01	0.03	14.23
0.00	0.00	0.80	0.10	0.00	12.31	0.03	14.60
0.00	0.00	0.80	0.10	0.00	12.61	0.03	14.98
0.00	0.00	0.80	0.10	0.00	12.91	0.03	15.35
0.00	0.00	0.80	0.10	0.00	13.21	0.03	15.73
0.00	0.00	0.80	0.10	0.00	13.51	0.03	16.10
0.00	0.00	0.80	0.10	0.00	13.81	0.03	16.47
0.00	0.00	0.80	0.10	0.00	14.11	0.03	16.85
0.00	0.00	0.80	0.10	0.00	14.41	0.03	17.22
0.00	0.00	0.80	0.10	0.00	14.71	0.03	17.59
0.00	0.00	0.80	0.10	0.00	15.01	0.03	17.97
0.00	0.00	0.80	0.10	0.00	15.31	0.03	18.34
0.00	0.00	0.80	0.10	0.00	15.61	0.03	18.71
0.00	0.00	0.80	0.10	0.00	15.91	0.03	19.09
0.00	0.00	0.80	0.10	0.00	16.21	0.03	19.46
0.00	0.00	0.80	0.10	0.00	16.51	0.03	19.84
0.00	0.00	0.80	0.10	0.00	16.81	0.03	20.21
0.00	0.00	0.80	0.10	0.00	17.11	0.03	20.58

Table E29: *Simulation 2*

CODE=1b : DROPLET DRYING BEHAVIOUR

DROP SIZE = 375.0000 MICRONS

ZDIS(M)	%SOLID	TEMP(C)	NA kg/s	hg(m/s)	hc(m/s)	kg(m/s)	kc(m/s)
0.01	43.00	79.94	.30E-06	1968	0	2.40	0.00
1.24	45.00	52.91	.20E-07	1330	11231	1.48	1.13
3.14	47.00	44.07	.36E-08	505	5501	0.54	0.51
4.49	49.00	43.65	.23E-08	399	3644	0.43	0.34
5.91	51.00	44.54	.20E-08	395	2701	0.42	0.25
7.33	53.00	45.38	.18E-08	392	2134	0.42	0.19
8.74	55.00	46.09	.17E-08	388	1755	0.41	0.16
10.15	57.01	46.72	.16E-08	386	1481	0.41	0.14
11.53	59.01	47.31	.15E-08	383	1275	0.41	0.12
12.88	61.01	47.86	.14E-08	380	1113	0.41	0.10
14.20	63.01	48.35	.13E-08	378	983	0.40	0.09
15.51	65.01	48.82	.12E-08	376	874	0.40	0.08
16.79	67.01	49.24	.11E-08	373	783	0.40	0.07
18.06	69.01	49.64	.11E-08	371	705	0.40	0.06
19.31	71.01	50.02	.10E-08	369	637	0.39	0.06

Table E30: *Simulation 2*

CODE=1b : DROPLET DRYING BEHAVIOUR

DROP SIZE = 215.0000 MICRONS

ZDIS(M)	%SOLID	TEMP(C)	NA kg/s	hg(m/s)	hc(m/s)	kg(m/s)	kc(m/s)
0.01	43.01	79.86	.13E-06	2675	0	3.26	0.00
0.54	45.01	53.05	.15E-07	2248	19832	2.63	2.19
1.44	47.01	45.49	.32E-08	1014	9784	1.12	0.96
1.89	49.01	43.58	.15E-08	582	6425	0.64	0.61
2.22	51.01	43.95	.12E-08	520	4758	0.57	0.45
2.53	53.01	44.82	.11E-08	513	3756	0.56	0.35
2.85	55.01	45.60	.10E-08	509	3085	0.56	0.29
3.16	57.01	46.29	.93E-09	506	2604	0.55	0.24
3.48	59.01	46.87	.86E-09	502	2240	0.55	0.21
3.79	61.01	47.44	.81E-09	500	1956	0.54	0.18
4.10	63.01	47.96	.76E-09	497	1726	0.54	0.16
4.40	65.01	48.42	.71E-09	494	1536	0.54	0.14
4.71	67.01	48.86	.67E-09	492	1376	0.53	0.13
5.01	69.01	49.29	.63E-09	490	1239	0.53	0.12
5.30	71.01	49.71	.59E-09	487	1119	0.53	0.10
5.60	73.02	50.12	.56E-09	485	1014	0.53	0.09
5.89	75.02	50.53	.53E-09	484	920	0.53	0.09
6.17	77.02	50.93	.51E-09	482	836	0.52	0.08
6.46	79.02	51.32	.48E-09	480	759	0.52	0.07
6.74	81.02	51.71	.45E-09	478	688	0.52	0.06
7.03	83.03	52.09	.42E-09	476	622	0.52	0.06
7.32	85.03	52.49	.39E-09	475	561	0.52	0.05
7.62	87.03	52.89	.37E-09	473	502	0.51	0.05
7.92	89.03	53.31	.34E-09	472	446	0.51	0.04
8.23	91.03	53.75	.31E-09	470	391	0.51	0.04
8.56	93.03	54.24	.28E-09	469	335	0.51	0.03
8.91	95.03	54.79	.24E-09	468	278	0.51	0.03
9.31	97.03	55.48	.20E-09	466	215	0.51	0.02
9.81	99.03	56.53	.13E-09	465	132	0.51	0.01
9.97	99.50	56.95	.11E-09	465	102	0.51	0.01
10.57	99.50	79.61	.00E+00	302	0	0	0.00
11.17	99.50	83.23	.00E+00	302	0	0	0.00
11.77	99.50	83.68	.00E+00	302	0	0	0.00
12.37	99.50	83.60	.00E+00	302	0	0	0.00
12.97	99.50	83.44	.00E+00	301	0	0	0.00
13.57	99.50	83.27	.00E+00	301	0	0	0.00
14.17	99.50	83.10	.00E+00	301	0	0	0.00
14.77	99.50	82.93	.00E+00	301	0	0	0.00
15.37	99.50	82.77	.00E+00	301	0	0	0.00
15.97	99.50	82.61	.00E+00	301	0	0	0.00
16.57	99.50	82.46	.00E+00	301	0	0	0.00
17.17	99.50	82.31	.00E+00	301	0	0	0.00
17.77	99.50	82.16	.00E+00	301	0	0	0.00
18.37	99.50	82.01	.00E+00	300	0	0	0.00
18.97	99.50	81.86	.00E+00	300	0	0	0.00
19.57	99.50	81.72	.00E+00	300	0	0	0.00

Table E31: *Simulation 2*

CODE-1b : DROPLET DRYING BEHAVIOUR

DROP SIZE = 165.0000 MICRONS

ZDIS(M)	%SOLID	TEMP(C)	NA kg/s	hg(m/s)	hc(m/s)	kg(m/s)	kc(m/s)
0.01	43.01	79.79	.91E-07	3104	0	3.79	0.00
0.35	45.01	52.68	.10E-07	2295	25809	2.70	2.88
1.03	47.01	46.20	.30E-08	1401	12761	1.57	1.29
1.35	49.01	44.19	.14E-08	796	8394	0.89	0.83
1.53	51.01	44.04	.10E-08	636	6216	0.71	0.60
1.68	53.01	44.79	.91E-09	602	4911	0.67	0.47
1.83	55.02	45.49	.83E-09	591	4039	0.66	0.39
1.98	57.02	46.26	.77E-09	585	3407	0.65	0.33
2.12	59.02	46.97	.73E-09	581	2931	0.64	0.28
2.26	61.02	47.60	.68E-09	577	2558	0.64	0.24
2.40	63.02	48.19	.64E-09	574	2257	0.64	0.22
2.54	65.02	48.72	.60E-09	570	2008	0.63	0.19
2.67	67.02	49.22	.57E-09	567	1799	0.63	0.17
2.80	69.02	49.70	.54E-09	564	1620	0.62	0.15
2.93	71.03	50.15	.51E-09	561	1464	0.62	0.14
3.06	73.03	50.57	.48E-09	558	1326	0.62	0.13
3.19	75.03	50.99	.45E-09	555	1204	0.61	0.11
3.32	77.03	51.38	.43E-09	553	1093	0.61	0.10
3.45	79.03	51.79	.40E-09	550	993	0.61	0.09
3.58	81.03	52.20	.38E-09	548	901	0.60	0.09
3.71	83.03	52.62	.35E-09	545	815	0.60	0.08
3.84	85.03	53.04	.33E-09	543	734	0.60	0.07
3.97	87.03	53.48	.31E-09	541	658	0.60	0.06
4.10	89.03	53.93	.28E-09	539	585	0.59	0.06
4.24	91.03	54.42	.26E-09	537	513	0.59	0.05
4.39	93.03	54.95	.23E-09	535	441	0.59	0.04
4.54	95.03	55.56	.20E-09	533	367	0.59	0.03
4.72	97.03	56.33	.17E-09	532	285	0.59	0.03
4.94	99.03	57.51	.12E-09	530	179	0.59	0.02
5.00	99.50	57.97	.95E-10	530	142	0.59	0.01
5.60	99.50	87.94	.00E+00	390	0	0	0.00
6.20	99.50	87.95	.00E+00	389	0	0	0.00
6.80	99.50	87.25	.00E+00	388	0	0	0.00
7.40	99.50	86.58	.00E+00	388	0	0	0.00
8.00	99.50	85.97	.00E+00	387	0	0	0.00
8.60	99.50	85.43	.00E+00	387	0	0	0.00
9.20	99.50	84.95	.00E+00	387	0	0	0.00
9.80	99.50	84.54	.00E+00	386	0	0	0.00
10.40	99.50	84.23	.00E+00	386	0	0	0.00
11.00	99.50	84.00	.00E+00	386	0	0	0.00
11.61	99.50	83.81	.00E+00	386	0	0	0.00
12.21	99.50	83.63	.00E+00	385	0	0	0.00
12.81	99.50	83.44	.00E+00	385	0	0	0.00
13.41	99.50	83.27	.00E+00	385	0	0	0.00
14.01	99.50	83.10	.00E+00	385	0	0	0.00
14.61	99.50	82.93	.00E+00	385	0	0	0.00
15.21	99.50	82.77	.00E+00	385	0	0	0.00
15.81	99.50	82.61	.00E+00	385	0	0	0.00
16.41	99.50	82.45	.00E+00	384	0	0	0.00
17.01	99.50	82.30	.00E+00	384	0	0	0.00
17.61	99.50	82.16	.00E+00	384	0	0	0.00
18.21	99.50	82.01	.00E+00	384	0	0	0.00
18.81	99.50	81.86	.00E+00	384	0	0	0.00
19.41	99.50	81.72	.00E+00	384	0	0	0.00

Table E32: *Simulation 2*

CODE=1b : DROPLET DRYING BEHAVIOUR

DROP SIZE = 137.0000 MICRONS

ZDIS(M)	%SOLID	TEMP(C)	NA kg/s	hg(m/s)	hc(m/s)	kg(m/s)	kc(m/s)
0.01	43.02	79.72	.70E-07	3449	0	4.21	0.00
0.27	45.02	52.44	.80E-08	2560	31030	3.02	3.47
0.84	47.02	46.44	.27E-08	1750	15324	1.98	1.58
1.10	49.02	44.67	.14E-08	999	10081	1.12	1.01
1.23	51.03	44.30	.96E-09	763	7467	0.86	0.74
1.33	53.04	44.73	.81E-09	684	5896	0.77	0.58
1.41	55.04	45.42	.72E-09	654	4841	0.74	0.48
1.50	57.04	46.19	.67E-09	644	4086	0.72	0.40
1.58	59.04	46.91	.63E-09	639	3517	0.72	0.34
1.66	61.04	47.59	.59E-09	635	3070	0.71	0.30
1.74	63.05	48.14	.56E-09	631	2706	0.71	0.26
1.81	65.05	48.85	.53E-09	628	2408	0.70	0.23
1.89	67.06	49.44	.51E-09	625	2157	0.70	0.21
1.96	69.06	49.99	.48E-09	622	1941	0.70	0.19
2.04	71.07	50.53	.46E-09	620	1753	0.69	0.17
2.11	73.08	51.04	.43E-09	617	1588	0.69	0.15
2.18	75.08	51.54	.41E-09	615	1440	0.69	0.14
2.25	77.09	52.02	.39E-09	612	1308	0.69	0.13
2.32	79.09	52.50	.37E-09	610	1187	0.68	0.11
2.39	81.09	52.98	.35E-09	608	1076	0.68	0.10
2.46	83.09	53.46	.33E-09	606	973	0.68	0.09
2.53	85.09	53.94	.31E-09	604	876	0.68	0.08
2.60	87.09	54.45	.29E-09	602	784	0.67	0.08
2.68	89.09	54.97	.26E-09	600	695	0.67	0.07
2.75	91.09	55.53	.24E-09	598	609	0.67	0.06
2.83	93.09	56.15	.22E-09	596	521	0.67	0.05
2.92	95.09	56.87	.19E-09	595	430	0.67	0.04
3.02	97.09	57.78	.15E-09	593	329	0.66	0.03
3.14	99.09	59.28	.10E-09	592	192	0.66	0.02
3.17	99.50	59.86	.80E-10	592	147	0.66	0.01
3.77	99.50	93.79	.00E+00	470	0	0	0.00
4.37	99.50	91.59	.00E+00	467	0	0	0.00
4.97	99.50	89.86	.00E+00	466	0	0	0.00
5.57	99.50	88.73	.00E+00	465	0	0	0.00
6.17	99.50	87.93	.00E+00	464	0	0	0.00
6.77	99.50	87.21	.00E+00	463	0	0	0.00
7.37	99.50	86.54	.00E+00	462	0	0	0.00
7.97	99.50	85.94	.00E+00	462	0	0	0.00
8.57	99.50	85.40	.00E+00	461	0	0	0.00
9.17	99.50	84.92	.00E+00	461	0	0	0.00
9.78	99.50	84.52	.00E+00	460	0	0	0.00
10.38	99.50	84.21	.00E+00	460	0	0	0.00
10.98	99.50	83.99	.00E+00	460	0	0	0.00
11.58	99.50	83.80	.00E+00	460	0	0	0.00
12.18	99.50	83.61	.00E+00	459	0	0	0.00
12.78	99.50	83.43	.00E+00	459	0	0	0.00
13.38	99.50	83.26	.00E+00	459	0	0	0.00
13.98	99.50	83.09	.00E+00	459	0	0	0.00
14.58	99.50	82.92	.00E+00	459	0	0	0.00
15.18	99.50	82.76	.00E+00	458	0	0	0.00
15.78	99.50	82.60	.00E+00	458	0	0	0.00
16.38	99.50	82.44	.00E+00	458	0	0	0.00
16.98	99.50	82.29	.00E+00	458	0	0	0.00
17.58	99.50	82.15	.00E+00	458	0	0	0.00
18.18	99.50	82.00	.00E+00	458	0	0	0.00
18.78	99.50	81.85	.00E+00	457	0	0	0.00
19.38	99.50	81.71	.00E+00	457	0	0	0.00
19.98	99.50	81.57	.00E+00	457	0	0	0.00

Table E33: *Simulation 2*

CODE=1b : DROPLET DRYING BEHAVIOUR

DROP SIZE = 102.0000 MICRONS

ZDIS(M)	%SOLID	TEMP(C)	MA kg/s	hg(m/s)	hc(m/s)	kg(m/s)	kc(m/s)
0.01	43.03	79.56	.46E-07	4087	0	5.00	0.00
0.17	45.03	52.07	.55E-08	3049	41494	3.61	4.65
0.61	47.03	46.59	.24E-08	2583	20574	2.99	2.21
0.83	49.03	45.56	.13E-08	1476	13557	1.69	1.40
0.92	51.04	45.00	.85E-09	1078	10041	1.23	1.02
0.98	53.04	45.15	.68E-09	906	7932	1.04	0.80
1.02	55.04	45.48	.59E-09	818	6531	0.94	0.66
1.05	57.06	46.12	.54E-09	784	5505	0.90	0.56
1.09	59.06	46.90	.51E-09	773	4738	0.89	0.48
1.12	61.08	47.71	.49E-09	768	4133	0.88	0.42
1.16	63.10	48.48	.47E-09	764	3644	0.88	0.37
1.19	65.11	49.22	.45E-09	762	3241	0.88	0.33
1.22	67.14	49.92	.43E-09	759	2900	0.87	0.29
1.25	69.15	50.58	.41E-09	757	2610	0.87	0.26
1.28	71.17	51.22	.39E-09	754	2357	0.87	0.24
1.31	73.18	51.83	.37E-09	752	2134	0.86	0.21
1.34	75.18	52.43	.36E-09	750	1934	0.86	0.19
1.37	77.18	53.02	.34E-09	748	1756	0.86	0.18
1.40	79.19	53.60	.32E-09	746	1595	0.86	0.16
1.42	81.19	54.18	.31E-09	744	1445	0.85	0.14
1.45	83.19	54.76	.29E-09	742	1307	0.85	0.13
1.48	85.19	55.35	.27E-09	740	1177	0.85	0.12
1.51	87.19	55.97	.26E-09	739	1053	0.85	0.11
1.54	89.19	56.61	.24E-09	737	934	0.85	0.09
1.57	91.19	57.31	.22E-09	736	817	0.84	0.08
1.60	93.19	58.08	.20E-09	734	699	0.84	0.07
1.64	95.19	58.97	.17E-09	733	577	0.84	0.06
1.67	97.19	60.11	.14E-09	732	440	0.84	0.04
1.72	99.19	62.02	.93E-10	731	254	0.84	0.03
1.73	99.50	62.58	.78E-10	731	207	0.84	0.02
2.33	99.50	103.70	.00E+00	638	0	0	0.00
2.93	99.50	98.42	.00E+00	630	0	0	0.00
3.53	99.50	94.72	.00E+00	625	0	0	0.00
4.13	99.50	92.27	.00E+00	622	0	0	0.00
4.73	99.50	90.32	.00E+00	619	0	0	0.00
5.33	99.50	89.01	.00E+00	617	0	0	0.00
5.93	99.50	88.17	.00E+00	616	0	0	0.00
6.53	99.50	87.43	.00E+00	615	0	0	0.00
7.13	99.50	86.74	.00E+00	614	0	0	0.00
7.73	99.50	86.12	.00E+00	613	0	0	0.00
8.33	99.50	85.56	.00E+00	612	0	0	0.00
8.93	99.50	85.06	.00E+00	612	0	0	0.00
9.54	99.50	84.63	.00E+00	611	0	0	0.00
10.14	99.50	84.29	.00E+00	611	0	0	0.00
10.74	99.50	84.05	.00E+00	610	0	0	0.00
11.34	99.50	83.86	.00E+00	610	0	0	0.00
11.94	99.50	83.67	.00E+00	610	0	0	0.00
12.54	99.50	83.49	.00E+00	609	0	0	0.00
13.14	99.50	83.32	.00E+00	609	0	0	0.00
13.74	99.50	83.14	.00E+00	609	0	0	0.00
14.34	99.50	82.97	.00E+00	609	0	0	0.00
14.94	99.50	82.81	.00E+00	608	0	0	0.00
15.54	99.50	82.65	.00E+00	608	0	0	0.00
16.14	99.50	82.49	.00E+00	608	0	0	0.00
16.74	99.50	82.34	.00E+00	608	0	0	0.00
17.34	99.50	82.19	.00E+00	608	0	0	0.00
17.94	99.50	82.04	.00E+00	607	0	0	0.00
18.54	99.50	81.90	.00E+00	607	0	0	0.00

Table E34: *Simulation 2*

CODE=1b : DROPLET DRYING BEHAVIOUR

DROP SIZE = 70.00000 MICRONS

ZDIS(M)	%SOLID	TEMP(C)	NA kg/s	hg(m/s)	hc(m/s)	kg(m/s)	kc(m/s)
0.01	43.05	79.20	.27E-07	5095	0	6.24	0.00
0.10	45.05	51.56	.34E-08	3838	59870	4.55	6.73
0.38	47.05	45.24	.14E-08	2859	29893	3.36	3.28
0.61	49.05	46.98	.11E-08	2616	19753	3.05	2.13
0.69	51.05	46.32	.74E-09	1791	14642	2.08	1.54
0.73	53.07	46.10	.58E-09	1439	11586	1.68	1.21
0.75	55.12	46.24	.48E-09	1226	9500	1.43	0.99
0.77	57.16	46.56	.43E-09	1107	8008	1.30	0.84
0.78	59.20	47.15	.39E-09	1054	6880	1.24	0.72
0.79	61.24	47.93	.37E-09	1035	5999	1.22	0.63
0.81	63.28	48.77	.36E-09	1028	5286	1.21	0.55
0.82	65.31	49.60	.34E-09	1025	4701	1.21	0.49
0.83	67.31	50.40	.33E-09	1023	4214	1.20	0.44
0.84	69.37	51.20	.32E-09	1021	3785	1.20	0.40
0.85	71.39	51.95	.31E-09	1019	3419	1.20	0.36
0.86	73.46	52.71	.30E-09	1018	3090	1.20	0.32
0.87	75.46	53.44	.28E-09	1016	2793	1.20	0.29
0.88	77.47	54.17	.27E-09	1015	2535	1.20	0.27
0.89	79.48	54.89	.26E-09	1013	2301	1.20	0.24
0.90	81.48	55.61	.25E-09	1012	2086	1.19	0.22
0.91	83.48	56.34	.24E-09	1011	1885	1.19	0.20
0.93	85.49	57.09	.23E-09	1010	1696	1.19	0.18
0.94	87.50	57.87	.21E-09	1009	1515	1.19	0.16
0.95	89.50	58.70	.20E-09	1008	1341	1.19	0.14
0.96	91.50	59.59	.18E-09	1007	1170	1.19	0.12
0.97	93.50	60.58	.17E-09	1006	997	1.19	0.10
0.98	95.50	61.76	.15E-09	1006	817	1.19	0.09
0.99	97.50	63.28	.12E-09	1005	611	1.19	0.06
1.01	99.50	66.08	.72E-10	1006	307	1.20	0.03
1.61	99.50	113.11	.00E+00	942	0	0	0.00
2.21	99.50	104.69	.00E+00	924	0	0	0.00
2.81	99.50	99.14	.00E+00	913	0	0	0.00
3.41	99.50	95.18	.00E+00	904	0	0	0.00
4.01	99.50	92.61	.00E+00	899	0	0	0.00
4.61	99.50	90.59	.00E+00	895	0	0	0.00
5.21	99.50	89.16	.00E+00	892	0	0	0.00
5.81	99.50	88.30	.00E+00	890	0	0	0.00
6.41	99.50	87.54	.00E+00	888	0	0	0.00
7.01	99.50	86.85	.00E+00	887	0	0	0.00
7.61	99.50	86.21	.00E+00	886	0	0	0.00
8.21	99.50	85.64	.00E+00	884	0	0	0.00
8.81	99.50	85.13	.00E+00	883	0	0	0.00
9.41	99.50	84.70	.00E+00	882	0	0	0.00
10.01	99.50	84.34	.00E+00	882	0	0	0.00
10.61	99.50	84.08	.00E+00	881	0	0	0.00
11.21	99.50	83.89	.00E+00	881	0	0	0.00
11.81	99.50	83.70	.00E+00	880	0	0	0.00
12.41	99.50	83.52	.00E+00	880	0	0	0.00
13.01	99.50	83.34	.00E+00	880	0	0	0.00
13.61	99.50	83.17	.00E+00	879	0	0	0.00
14.21	99.50	83.00	.00E+00	879	0	0	0.00
14.81	99.50	82.84	.00E+00	879	0	0	0.00
15.41	99.50	82.67	.00E+00	878	0	0	0.00
16.01	99.50	82.52	.00E+00	878	0	0	0.00
16.61	99.50	82.36	.00E+00	878	0	0	0.00
17.21	99.50	82.21	.00E+00	877	0	0	0.00
17.81	99.50	82.06	.00E+00	877	0	0	0.00
18.41	99.50	81.92	.00E+00	877	0	0	0.00
19.01	99.50	81.78	.00E+00	876	0	0	0.00

Table E35: *Simulation 2*

CODE=1b : DROPLET DRYING BEHAVIOUR

DROP SIZE = 45.00000 MICRONS

ZDIS(M)	%SOLID	TEMP(C)	NA kg/s	hg(m/s)	hc(m/s)	kg(m/s)	kc(m/s)
0.01	43.09	78.40	.14E-07	6642	0	8.15	0.00
0.05	45.10	50.83	.19E-08	5132	91039	6.10	10.23
0.21	47.11	44.44	.85E-09	3944	45915	4.66	5.06
0.38	49.11	45.33	.65E-09	3274	30506	3.87	3.35
0.52	51.11	47.28	.67E-09	4381	22709	5.14	2.49
0.57	53.12	48.92	.54E-09	2949	18004	3.49	1.97
0.59	55.12	48.54	.43E-09	2375	14767	2.82	1.60
0.61	57.12	48.51	.36E-09	2043	12471	2.43	1.35
0.61	59.13	48.61	.31E-09	1810	10855	2.16	1.17
0.62	61.28	48.81	.28E-09	1654	9410	1.98	1.01
0.63	63.44	49.32	.26E-09	1570	8239	1.88	0.89
0.63	65.56	50.03	.24E-09	1534	7296	1.84	0.78
0.63	67.78	50.90	.23E-09	1520	6470	1.83	0.70
0.64	69.81	51.73	.23E-09	1516	5823	1.82	0.63
0.64	71.91	52.58	.22E-09	1514	5244	1.82	0.56
0.65	74.06	53.45	.21E-09	1512	4722	1.82	0.51
0.65	76.08	54.30	.20E-09	1512	4233	1.82	0.46
0.65	78.09	55.11	.19E-09	1511	3843	1.82	0.42
0.66	80.10	55.92	.19E-09	1510	3487	1.82	0.38
0.66	82.10	56.73	.18E-09	1510	3159	1.82	0.34
0.66	84.11	57.57	.17E-09	1510	2850	1.82	0.31
0.67	86.13	58.43	.16E-09	1509	2558	1.82	0.28
0.67	88.13	59.33	.15E-09	1509	2281	1.82	0.25
0.67	90.13	60.30	.14E-09	1509	2009	1.82	0.22
0.68	92.14	61.35	.13E-09	1509	1742	1.82	0.19
0.68	94.14	62.55	.12E-09	1510	1470	1.83	0.16
0.69	96.14	63.99	.11E-09	1511	1180	1.83	0.13
0.69	98.14	65.98	.84E-10	1512	835	1.84	0.09
0.70	99.50	68.45	.55E-10	1515	481	1.84	0.05
1.30	99.50	121.31	.00E+00	1485	0	0	0.00
1.90	99.50	108.10	.00E+00	1442	0	0	0.00
2.50	99.50	101.71	.00E+00	1420	0	0	0.00
3.10	99.50	96.99	.00E+00	1405	0	0	0.00
3.70	99.50	93.81	.00E+00	1395	0	0	0.00
4.30	99.50	91.53	.00E+00	1387	0	0	0.00
4.90	99.50	89.79	.00E+00	1381	0	0	0.00
5.50	99.50	88.71	.00E+00	1378	0	0	0.00
6.10	99.50	87.91	.00E+00	1375	0	0	0.00
6.70	99.50	87.18	.00E+00	1373	0	0	0.00
7.30	99.50	86.52	.00E+00	1371	0	0	0.00
7.90	99.50	85.92	.00E+00	1369	0	0	0.00
8.50	99.50	85.38	.00E+00	1367	0	0	0.00
9.10	99.50	84.90	.00E+00	1365	0	0	0.00
9.70	99.50	84.51	.00E+00	1364	0	0	0.00
10.30	99.50	84.20	.00E+00	1363	0	0	0.00
10.90	99.50	83.98	.00E+00	1362	0	0	0.00
11.50	99.50	83.79	.00E+00	1362	0	0	0.00
12.10	99.50	83.61	.00E+00	1361	0	0	0.00
12.70	99.50	83.43	.00E+00	1360	0	0	0.00
13.30	99.50	83.26	.00E+00	1360	0	0	0.00
13.90	99.50	83.08	.00E+00	1359	0	0	0.00
14.50	99.50	82.92	.00E+00	1359	0	0	0.00
15.10	99.50	82.76	.00E+00	1358	0	0	0.00
15.70	99.50	82.59	.00E+00	1358	0	0	0.00
16.30	99.50	82.44	.00E+00	1357	0	0	0.00
16.90	99.50	82.29	.00E+00	1357	0	0	0.00
17.50	99.50	82.14	.00E+00	1356	0	0	0.00
18.10	99.50	81.99	.00E+00	1356	0	0	0.00
18.70	99.50	81.85	.00E+00	1355	0	0	0.00

Table E36: *Simulation 2*

CODE=1b : DROPLET DRYING BEHAVIOUR

DROP SIZE = 35.00000 MICRONS

ZDIS(M)	%SOLID	TEMP(C)	NA kg/s	hg(m/s)	hc(m/s)	kg(m/s)	kc(m/s)
0.01	43.14	77.64	.99E-08	7748	0	9.52	0.00
0.04	45.15	50.29	.14E-08	6138	114760	7.30	12.89
0.15	47.15	43.99	.62E-09	4719	58374	5.58	6.44
0.27	49.16	45.04	.49E-09	4039	38919	4.79	4.28
0.37	51.17	46.31	.42E-09	3582	28992	4.26	3.19
0.47	53.17	47.40	.37E-09	3287	22973	3.91	2.52
0.53	55.20	50.83	.43E-09	4233	18915	5.02	2.08
0.55	57.24	50.75	.35E-09	3261	16005	3.89	1.76
0.56	59.36	50.47	.29E-09	2769	13726	3.32	1.51
0.57	61.55	50.44	.26E-09	2425	11918	2.92	1.31
0.58	63.68	50.60	.23E-09	2206	10511	2.66	1.15
0.58	65.82	50.99	.21E-09	2071	9335	2.51	1.02
0.58	67.89	51.56	.20E-09	1997	8361	2.42	0.92
0.58	70.13	52.34	.19E-09	1957	7455	2.38	0.82
0.59	72.47	53.25	.18E-09	1939	6637	2.36	0.73
0.59	74.90	54.25	.17E-09	1932	5902	2.35	0.65
0.59	76.93	55.20	.17E-09	1930	5240	2.35	0.58
0.59	78.96	56.06	.16E-09	1929	4753	2.35	0.52
0.59	80.96	56.92	.15E-09	1929	4310	2.35	0.48
0.60	82.99	57.81	.15E-09	1929	3895	2.35	0.43
0.60	85.03	58.72	.14E-09	1930	3503	2.36	0.39
0.60	87.07	59.67	.13E-09	1930	3131	2.36	0.35
0.60	89.10	60.67	.13E-09	1930	2775	2.36	0.31
0.60	91.10	61.74	.12E-09	1931	2423	2.36	0.27
0.61	93.10	62.92	.11E-09	1932	2078	2.37	0.23
0.61	95.11	64.29	.98E-10	1933	1719	2.37	0.19
0.61	97.11	66.02	.83E-10	1935	1320	2.38	0.15
0.61	99.11	68.81	.57E-10	1940	784	2.39	0.09
0.61	99.50	69.80	.48E-10	1941	620	2.40	0.07
1.21	99.50	123.68	.00E+00	1916	0	0	0.00
1.81	99.50	109.09	.00E+00	1854	0	0	0.00
2.41	99.50	102.44	.00E+00	1826	0	0	0.00
3.01	99.50	97.50	.00E+00	1805	0	0	0.00
3.61	99.50	94.15	.00E+00	1791	0	0	0.00
4.21	99.50	91.79	.00E+00	1781	0	0	0.00
4.81	99.50	89.98	.00E+00	1773	0	0	0.00
5.41	99.50	88.82	.00E+00	1769	0	0	0.00
6.02	99.50	88.01	.00E+00	1765	0	0	0.00
6.62	99.50	87.27	.00E+00	1762	0	0	0.00
7.22	99.50	86.60	.00E+00	1759	0	0	0.00
7.82	99.50	85.99	.00E+00	1757	0	0	0.00
8.42	99.50	85.44	.00E+00	1754	0	0	0.00
9.02	99.50	84.96	.00E+00	1752	0	0	0.00
9.62	99.50	84.55	.00E+00	1750	0	0	0.00
10.22	99.50	84.23	.00E+00	1749	0	0	0.00
10.82	99.50	84.01	.00E+00	1748	0	0	0.00
11.42	99.50	83.82	.00E+00	1747	0	0	0.00
12.02	99.50	83.63	.00E+00	1747	0	0	0.00
12.62	99.50	83.45	.00E+00	1746	0	0	0.00
13.22	99.50	83.28	.00E+00	1745	0	0	0.00
13.82	99.50	83.11	.00E+00	1744	0	0	0.00
14.42	99.50	82.94	.00E+00	1744	0	0	0.00
15.02	99.50	82.78	.00E+00	1743	0	0	0.00
15.62	99.50	82.61	.00E+00	1742	0	0	0.00
16.22	99.50	82.46	.00E+00	1742	0	0	0.00
16.82	99.50	82.31	.00E+00	1741	0	0	0.00
17.42	99.50	82.16	.00E+00	1740	0	0	0.00
18.02	99.50	82.01	.00E+00	1740	0	0	0.00
18.62	99.50	81.87	.00E+00	1739	0	0	0.00

Table E37: *Simulation 3, Run 2*

CODE=02 : AIR PROPERTIES

ZDIS(M)	TEMP(C)	HUMID(kg/kg)	QAIR(kg/s)	SOL(KG/S)
0.01	29.60	0.02380	0.15240	0.1000
0.02	29.95	0.02380	0.15240	0.1000
0.03	30.29	0.02380	0.15240	0.1000
0.04	30.61	0.02380	0.15240	0.1000
0.05	30.92	0.02380	0.15240	0.1000
0.06	31.23	0.02380	0.15240	0.1000
0.07	31.53	0.02380	0.15240	0.1000
0.08	31.83	0.02380	0.15240	0.1000
0.09	32.12	0.02380	0.15240	0.1000
0.10	32.41	0.02380	0.15240	0.1000
0.11	32.70	0.02380	0.15240	0.1000
0.12	32.99	0.02380	0.15240	0.1000
0.13	33.29	0.02380	0.15240	0.1000
0.14	33.58	0.02380	0.15240	0.1000
0.15	33.88	0.02380	0.15240	0.1000
0.16	34.17	0.02380	0.15240	0.1000
0.17	34.47	0.02380	0.15240	0.1000
0.18	34.76	0.02380	0.15240	0.1000
0.19	35.05	0.02380	0.15240	0.1000
0.21	35.34	0.02380	0.15240	0.1000
0.22	35.63	0.02380	0.15240	0.1000
0.23	35.92	0.02380	0.15240	0.1000
0.24	36.22	0.02380	0.15240	0.1000
0.25	36.51	0.02380	0.15240	0.1000
0.26	36.80	0.02380	0.15240	0.1000
0.27	37.09	0.02380	0.15240	0.1000
0.28	37.38	0.02380	0.15240	0.1000
0.29	37.67	0.02380	0.15240	0.1000
0.30	37.96	0.02380	0.15240	0.1000
0.31	38.27	0.02379	0.15240	0.1000
0.32	38.59	0.02379	0.15239	0.1000
0.33	38.91	0.02377	0.15239	0.1000
0.34	39.25	0.02376	0.15239	0.1000
0.35	39.60	0.02374	0.15239	0.1000
0.36	39.96	0.02371	0.15238	0.1000
0.37	40.33	0.02368	0.15238	0.1000
0.38	40.71	0.02365	0.15237	0.1000
0.39	41.11	0.02361	0.15237	0.1000
0.40	41.52	0.02357	0.15236	0.1000
0.42	41.94	0.02352	0.15236	0.1000
0.43	42.38	0.02347	0.15235	0.1000
0.44	42.84	0.02342	0.15234	0.0999
0.45	43.31	0.02335	0.15233	0.0999
0.46	43.79	0.02328	0.15232	0.0999
0.47	44.30	0.02321	0.15231	0.0999
0.48	44.83	0.02312	0.15230	0.0999
0.49	45.37	0.02303	0.15228	0.0999
0.50	45.94	0.02293	0.15227	0.0999
0.51	46.49	0.02283	0.15225	0.0999
0.52	47.07	0.02272	0.15224	0.0998
0.53	47.68	0.02260	0.15222	0.0998
0.54	48.30	0.02247	0.15220	0.0998
0.55	48.95	0.02232	0.15218	0.0998
0.56	49.63	0.02217	0.15215	0.0998
0.57	50.33	0.02200	0.15213	0.0997
0.58	51.06	0.02183	0.15210	0.0997
0.59	51.83	0.02163	0.15207	0.0997
0.60	52.62	0.02142	0.15204	0.0996
0.61	53.45	0.02120	0.15201	0.0996
0.62	54.32	0.02096	0.15197	0.0996
0.63	55.22	0.02070	0.15193	0.0995
0.64	56.16	0.02042	0.15189	0.0995
0.65	57.15	0.02012	0.15185	0.0995
0.66	58.18	0.01979	0.15180	0.0994
0.67	59.25	0.01945	0.15175	0.0994
0.68	60.38	0.01907	0.15169	0.0993
0.69	61.56	0.01867	0.15163	0.0992
0.70	62.80	0.01825	0.15157	0.0992
0.71	64.10	0.01779	0.15150	0.0991
0.72	65.46	0.01730	0.15143	0.0990
0.73	66.89	0.01678	0.15135	0.0990
0.74	68.39	0.01623	0.15127	0.0989
0.75	69.97	0.01564	0.15118	0.0988
0.76	71.63	0.01501	0.15109	0.0987
0.77	73.37	0.01434	0.15099	0.0986
0.78	75.21	0.01363	0.15088	0.0985
0.79	77.14	0.01287	0.15077	0.0984
0.80	79.18	0.01207	0.15065	0.0983
0.81	81.33	0.01122	0.15052	0.0981
0.82	83.60	0.01032	0.15039	0.0980
0.83	85.99	0.00936	0.15025	0.0979
0.84	88.52	0.00834	0.15010	0.0977

Table E38: *Simulation 3, Run 5*

CODE=05 : AIR PROPERTIES

ZDIS(M)	TEMP(C)	HUMID(kg/kg)	QAIR(kg/s)	SOL(KG/S)
0.01	30.12	0.02740	0.13743	0.1000
0.02	30.53	0.02740	0.13743	0.1000
0.03	30.93	0.02740	0.13743	0.1000
0.04	31.30	0.02740	0.13743	0.1000
0.05	31.67	0.02740	0.13743	0.1000
0.06	32.03	0.02740	0.13743	0.1000
0.07	32.39	0.02740	0.13743	0.1000
0.08	32.74	0.02740	0.13743	0.1000
0.09	33.09	0.02740	0.13743	0.1000
0.10	33.44	0.02740	0.13743	0.1000
0.11	33.79	0.02740	0.13743	0.1000
0.12	34.14	0.02740	0.13743	0.1000
0.13	34.50	0.02740	0.13743	0.1000
0.14	34.86	0.02740	0.13743	0.1000
0.15	35.22	0.02740	0.13743	0.1000
0.16	35.58	0.02740	0.13743	0.1000
0.17	35.94	0.02740	0.13743	0.1000
0.18	36.30	0.02740	0.13743	0.1000
0.19	36.66	0.02740	0.13743	0.1000
0.21	37.01	0.02740	0.13743	0.1000
0.22	37.37	0.02740	0.13743	0.1000
0.23	37.73	0.02740	0.13743	0.1000
0.24	38.09	0.02740	0.13743	0.1000
0.25	38.46	0.02740	0.13743	0.1000
0.26	38.82	0.02740	0.13743	0.1000
0.27	39.18	0.02740	0.13743	0.1000
0.28	39.55	0.02740	0.13743	0.1000
0.29	39.91	0.02740	0.13743	0.1000
0.30	40.29	0.02740	0.13743	0.1000
0.31	40.68	0.02740	0.13743	0.1000
0.32	41.08	0.02740	0.13743	0.1000
0.33	41.49	0.02740	0.13743	0.1000
0.34	41.92	0.02740	0.13743	0.1000
0.35	42.36	0.02740	0.13743	0.1000
0.36	42.81	0.02738	0.13743	0.1000
0.37	43.28	0.02737	0.13743	0.1000
0.38	43.77	0.02734	0.13743	0.1000
0.39	44.27	0.02731	0.13742	0.1000
0.40	44.79	0.02727	0.13742	0.1000
0.42	45.33	0.02722	0.13741	0.1000
0.43	45.89	0.02716	0.13740	0.1000
0.44	46.47	0.02710	0.13739	0.1000
0.45	47.07	0.02703	0.13739	0.1000
0.46	47.69	0.02696	0.13738	0.0999
0.47	48.34	0.02688	0.13736	0.0999
0.48	49.01	0.02678	0.13735	0.0999
0.49	49.72	0.02668	0.13734	0.0999
0.50	50.45	0.02656	0.13732	0.0999
0.51	51.17	0.02644	0.13731	0.0999
0.52	51.93	0.02631	0.13729	0.0999
0.53	52.71	0.02617	0.13727	0.0998
0.54	53.53	0.02602	0.13725	0.0998
0.55	54.38	0.02585	0.13723	0.0998
0.56	55.27	0.02567	0.13720	0.0998
0.57	56.20	0.02547	0.13718	0.0997
0.58	57.17	0.02525	0.13715	0.0997
0.59	58.18	0.02501	0.13711	0.0997
0.60	59.24	0.02475	0.13708	0.0996
0.61	60.35	0.02447	0.13704	0.0996
0.62	61.51	0.02417	0.13700	0.0996
0.63	62.72	0.02384	0.13696	0.0995
0.64	63.99	0.02348	0.13691	0.0995
0.65	65.33	0.02309	0.13686	0.0994
0.66	66.73	0.02267	0.13680	0.0994
0.67	68.21	0.02222	0.13674	0.0993
0.68	69.76	0.02172	0.13668	0.0992
0.69	71.39	0.02119	0.13660	0.0992
0.70	73.10	0.02062	0.13653	0.0991
0.71	74.91	0.02000	0.13644	0.0990
0.72	76.82	0.01933	0.13635	0.0989
0.73	78.83	0.01861	0.13626	0.0988
0.74	80.95	0.01784	0.13616	0.0987
0.75	83.19	0.01701	0.13605	0.0986
0.76	85.56	0.01613	0.13593	0.0985
0.77	88.06	0.01518	0.13580	0.0984
0.78	90.72	0.01417	0.13566	0.0982
0.79	93.53	0.01308	0.13552	0.0981
0.80	96.51	0.01192	0.13536	0.0979
0.81	99.67	0.01068	0.13520	0.0978
0.82	103.02	0.00936	0.13502	0.0976

Table E39: *Simulation 3, Run 10*

CODE=YY : AIR PROPERTIES

ZDIS(M)	TEMP(C)	HUMID(kg/kg)	QAIR(kg/s)	SOL(KG/S)
0.01	35.13	0.02370	0.13201	0.0690
0.02	35.78	0.02370	0.13201	0.0690
0.03	36.40	0.02370	0.13201	0.0690
0.04	36.99	0.02370	0.13201	0.0690
0.05	37.55	0.02370	0.13201	0.0690
0.06	38.11	0.02370	0.13201	0.0690
0.07	38.66	0.02370	0.13201	0.0690
0.08	39.20	0.02370	0.13201	0.0690
0.09	39.73	0.02370	0.13201	0.0690
0.10	40.26	0.02370	0.13201	0.0690
0.11	40.79	0.02370	0.13201	0.0690
0.12	41.31	0.02369	0.13201	0.0690
0.13	41.85	0.02367	0.13201	0.0690
0.14	42.39	0.02363	0.13200	0.0690
0.15	42.93	0.02360	0.13200	0.0690
0.16	43.48	0.02355	0.13199	0.0690
0.17	44.02	0.02350	0.13199	0.0690
0.18	44.57	0.02345	0.13198	0.0690
0.19	45.12	0.02339	0.13197	0.0690
0.21	45.67	0.02332	0.13196	0.0690
0.22	46.23	0.02325	0.13195	0.0689
0.23	46.79	0.02317	0.13194	0.0689
0.24	47.36	0.02309	0.13193	0.0689
0.25	47.93	0.02300	0.13192	0.0689
0.26	48.51	0.02291	0.13191	0.0689
0.27	49.10	0.02281	0.13190	0.0689
0.28	49.69	0.02270	0.13188	0.0689
0.29	50.30	0.02258	0.13187	0.0689
0.30	50.95	0.02245	0.13185	0.0688
0.31	51.64	0.02230	0.13183	0.0688
0.32	52.37	0.02212	0.13181	0.0688
0.33	53.15	0.02194	0.13178	0.0688
0.34	53.96	0.02173	0.13176	0.0687
0.35	54.81	0.02150	0.13173	0.0687
0.36	55.72	0.02125	0.13170	0.0687
0.37	56.67	0.02097	0.13166	0.0686
0.38	57.67	0.02067	0.13162	0.0686
0.39	58.73	0.02034	0.13158	0.0686
0.40	59.84	0.01999	0.13153	0.0685
0.42	61.02	0.01960	0.13148	0.0685
0.43	62.26	0.01918	0.13143	0.0684
0.44	63.58	0.01872	0.13137	0.0684
0.45	64.97	0.01823	0.13131	0.0683
0.46	66.44	0.01769	0.13124	0.0682
0.47	68.00	0.01712	0.13116	0.0682
0.48	69.66	0.01650	0.13108	0.0681
0.49	71.41	0.01583	0.13100	0.0680
0.50	73.28	0.01511	0.13090	0.0679
0.51	75.16	0.01438	0.13081	0.0678
0.52	77.16	0.01359	0.13071	0.0677
0.53	79.28	0.01275	0.13060	0.0676
0.54	81.53	0.01185	0.13048	0.0675
0.55	83.92	0.01089	0.13036	0.0673
0.56	86.47	0.00986	0.13023	0.0672
0.57	89.18	0.00876	0.13008	0.0671